LOW-TEMPERATURE MAGNETISM

Drift of domain walls of the *ab* type in weak ferromagnets

V. S. Gerasimchuk and A. A. Shitov

*Donbass State Academy of Civil Engineering and Architecture, ul. Derzhavina 2, 86123 Makeevka, Ukraine**

(Submitted April 19, 2002; revised July 10, 2002)
Fiz. Nizk. Temp. **28**, 1235–1238 (December 2002)

The drift motion of 180° domain walls of the *ab* type in a weak ferromagnet in an elastic stress field created by a sound wave propagating parallel or perpendicular to the plane of the domain wall is investigated. The dependence of the domain-wall drift velocity on the direction, amplitude, and polarization of the sound wave is found. The conditions for drift of a stripe domain structure are determined. © *2002 American Institute of Physics.*
[DOI: 10.1063/1.1531390]

INTRODUCTION

The study of the dynamics of domain walls (DWs) in weak ferromagnets (WFMs) has been the subject of a large number of both theoretical and experimental works (see, e.g., Refs. 1 and 2). One of the most intensively studied classes of WFMs are rare-earth orthoferrites. The reason for the heightened interest in this class of magnets is the high DW velocities in orthoferrites. The DW velocity in WFMs in a static magnetic field is the highest attainable in magnetically ordered materials. Moreover, DW motion can also be brought about by alternating fields, in particular, by a sound field, the influence of which on DWs has been inadequately studied. The elastic strain due to a sound wave acts on a DW by changing its energy, which leads to motion of the DW.[3]

In rare-earth orthoferrites far from the spin-reorientation region there can exist two types of 180° DWs, which separate domains with opposite orientations of the antiferromagnetic vector **l** and ferromagnetic vector **m**.[1,4,5] DWs of one type (ac) correspond to a rotation of the vectors **l** and **m** in the plane of the DW, while DWs of the second type (ab) correspond to a rotation of the vector **l** with a simultaneous change in the magnitude of the vector **m**. Which of the types of DWs is realized is determined by the sign of the difference of the anisotropy constants of the magnet. This sign changes at the transition through the critical point, and a DW of one type is transformed into a DW of the other type. Such a transition is observed, in particular, in dysprosium orthoferrite $DyFeO_3$ at $T=150$ K,[6] below which a DW of the ab type is realized, and above which, a DW of the ac type.

The majority of theoretical and experimental studies on WFMs have been done for DWs of the ac type. At the same time, as was shown in Ref. 2, the dynamic properties of ac and ab walls are substantially different. A comparative analysis of DWs of the ac and ab types under the influence of an alternating magnetic field was done in Ref. 7. The approach used in that paper was based on a description of the nonlinear dynamics of the magnet by means of an effective Lagrangian. That approach has also been used to study DW dynamics in two-sublattice WFMs and in ferrites.[8,9] The drift of DWs in a ferromagnet in the field of a sound wave was considered in Ref. 10 on the basis of the Slonczewski equations.

In this paper we investigate theoretically the influence of a sound wave on the dynamics of ab DWs in a WFM.

EQUATIONS OF MOTION

For description of the nonlinear dynamics of DWs in a two-sublattice WFM we use the Lagrangian density written in terms of the antiferromagnetic unit vector **l** ($\mathbf{l}^2=1$). We assume that the Cartesian axes x, y, z coincide with the crystal axes a, b, c. To describe the DW dynamics it is convenient to transform to a spherical coordinate system:

$$l_x+il_z=\sin\theta\exp(i\varphi), \quad l_y=\cos\theta. \tag{1}$$

For a WFM of the rare-earth orthoferrite type with characteristic symmetry $2_x^-2_z^-$ the Lagrangian density in angle variables can be written in the form[4,7]

$$\begin{aligned} L(\theta,\varphi)=M_0^2\Bigg\{&\frac{\alpha}{2c^2}[(\dot\theta)^2+(\dot\varphi)^2\sin^2\theta]-\frac{\alpha}{2}\\ &\times[(\nabla\theta)^2+(\nabla\varphi)^2\sin^2\theta]-\frac{\beta_1}{2}\sin^2\theta\sin^2\varphi-\frac{\tilde\beta_2}{2}\\ &\times\cos^2\theta-\gamma[\sin 2\theta(u_{xy}\cos\varphi+u_{yz}\sin\varphi)\\ &+u_{yy}\cos^2\theta+\sin^2\theta(u_{xx}\cos^2\varphi+u_{xz}\sin 2\varphi\\ &+u_{zz}\sin^2\varphi)]\Bigg\}, \end{aligned} \tag{2}$$

where an overdot denotes a time derivative, $M_0^2=(M_1^2+M_2^2)/2$, M_0 is the modulus of the sublattice magnetization vectors, $\mathbf{M}_1$ and $\mathbf{M}_2$ are the sublattice magnetization vectors, $c=gM_0\sqrt{\alpha\delta}/2$ is the minimum spin-wave phase velocity, δ and α are the homogeneous and inhomogeneous exchange interaction constants, respectively, g is the gyromagnetic ratio, β_1 and β_2 are the effective rhombic anisotropy constants, $\tilde\beta_2=\beta_2+d^2/\delta$, d is the Dzyaloshinskiĭ constant, u_{ik} is the elastic strain tensor, and γ is the magnetoelastic con-

stant. From here on we shall treat the sound wave as an external field. We have not included in (2) the term describing the energy of the elastic subsystem, as we are neglecting the influence of the magnetic subsystem on the elastic subsystem. We shall assume that the wavelength of the sound is much larger than the width of a DW, so that we can ignore the internal structure of the DW.

The dynamic drag on a DW due to dissipative processes is taken into account by means of a dissipative function F:

$$F=\frac{\lambda M_0}{2g}\mathbf{i}^2=\frac{\lambda M_0}{2g}(\dot\theta^2+\dot\varphi^2\sin^2\theta), \tag{3}$$

where λ is the Gilbert damping parameter.

The equations of motion in the angle variables with the damping taken into account have the form

$$\begin{aligned}&\alpha\nabla[(\nabla\varphi)\sin^2\theta]-\frac{\alpha}{c^2}\frac{d}{dt}(\dot\varphi\sin^2\theta)\\&\quad-\beta_1\sin^2\theta\sin\varphi\cos\varphi-\gamma\\&\quad\times\{\sin^2\theta[(u_{zz}-u_{xx})\sin 2\varphi+2u_{xz}\cos 2\varphi)\\&\quad+\sin 2\theta(u_{yz}\cos\varphi-u_{xy}\sin\varphi)\}=\frac{\lambda}{gM_0}\dot\varphi\sin^2\theta,\end{aligned} \tag{4}$$

$$\begin{aligned}&\alpha\left(\Delta\theta-\frac{1}{c^2}\ddot\theta\right)+\sin\theta\cos\theta\left[\alpha\left(\frac{1}{c^2}\dot\varphi^2-(\nabla\varphi)^2\right)\right.\\&\quad\left.-\beta_1\sin^2\varphi+\tilde\beta_2\right]-\gamma[\sin 2\theta(u_{xx}\cos^2\varphi\\&\quad+u_{xz}\sin 2\varphi+u_{zz}\sin^2\varphi-u_{yy})\\&\quad+2\cos 2\theta(u_{xy}\cos\varphi+u_{yz}\sin\varphi)]=\frac{\lambda}{gM_0}\dot\theta.\end{aligned} \tag{5}$$

If $\beta_1>\tilde\beta_2>0$, then far from the spin-reorientation region in the WFM and in the absence of external fields the DW of the ab type is stable: the vector $\mathbf{l}$ rotates in the xy plane, and the ferromagnetic vector $\mathbf{m}$ varies only in magnitude ($\mathbf{m}=(\mathbf{M}_1+\mathbf{M}_2)/2M_0=-d\mathbf{e}_z\sin\theta/\delta$, $\mathbf{e}_z$ is the unit vector along the z axis).[4,5] this DW corresponds to a value $\varphi=\varphi_0=0$, and the variable $\theta=\theta_0(y)$ satisfies the equation

$$\alpha\theta_0''+\tilde\beta_2\sin\theta_0\cos\theta_0=0, \tag{6}$$

where a prime denotes differentiation with respect to the variable y. The solution of equation (6), which describes a static 180° DW, has the form

$$\begin{aligned}&\theta_0'=-\frac{R}{y_0}\cos\theta_0(y)=-\frac{R\rho}{y_0}\cosh^{-1}\frac{y}{y_0},\\&\sin\theta_0(y)=-R\tanh\frac{y}{y_0},\end{aligned} \tag{7}$$

where $y_0=\sqrt{\alpha/\tilde\beta_2}$ is the DW thickness, $R=\pm1$ is the topological charge, and $\rho=\pm1$ is a parameter describing the direction of rotation of the vector $\mathbf{l}$ in the DW. In solving equation (6) we have assumed that it satisfies the boundary conditions $\theta_0(\pm\infty)=\pm\pi/2$.

180° DWs separating domains with opposite directions of the magnetization in the stripe domain structure have opposite topological charges R. Rotation of the vector $\mathbf{l}$ in a DW can occur both through the positive and negative z directions, depending on the parameter ρ. Therefore, adjacent DWs making up a stripe domain structure with rotation of the vector $\mathbf{l}$ in the xy plane correspond to values $l_x(y=\pm\infty)=\mp R$ and to one of the two values $l_y(y=0)=\pm\rho$. In the presence of an external field and for a certain matching of the signs of the topological charges R and parameters ρ in adjacent DWs of the ac type in a WFM, translational motion of the stripe domain structure as a whole can occur.[9]

SOUND WAVE PROPAGATING IN THE PLANE OF THE DW

Let us find the solution of system (4) and (5). For this we use a version of perturbation theory for solitons.[7–10] We consider a monochromatic sound wave of frequency ω propagating parallel to the plane of a DW: $\mathbf{u}(\mathbf{r}_\perp,t)=\mathbf{u}_0\exp(i\mathbf{k}_\perp\cdot\mathbf{r}_\perp-i\omega t)$, where $\mathbf{k}_\perp\cdot\mathbf{r}_\perp=k_xx+k_zz$. We introduce the collective variable $Y(\mathbf{r}_\perp,t)$, where $\mathbf{r}_\perp=(x,z)$, as the coordinate of the center of the DW. Assuming that the amplitude of the sound wave is sufficiently small, we seek the solution of the system of equations (4), (5) in the form of an expansion,

$$\begin{aligned}&\theta(\mathbf{r},t)=\theta_0(\xi)+\theta_1(\xi,\mathbf{r}_\perp,t)+\theta_2(\xi,\mathbf{r}_\perp,t)+\ldots,\\&\varphi(\mathbf{r},t)=\varphi_1(\xi,\mathbf{r}_\perp,t)+\varphi_2(\xi,\mathbf{r}_\perp,t)+\ldots,\end{aligned} \tag{8}$$

where $\xi=y-Y(\mathbf{r}_\perp,t)$, and the indices $n=1,2,\ldots$ indicate the order of smallness of the quantities in respect to the amplitude of the sound wave. The function $\theta_0(\xi)$ describes the unperturbed DW and satisfies relations (7). The functions θ_n and φ_n $(n=1,2,\ldots)$ describe the distortions of the shape of the DW due to excitation of spin waves. The drift velocity of a DW is determined as the average of the instantaneous velocity $\overline{V(\mathbf{r}_\perp,t)}=\overline{\dot Y(\mathbf{r}_\perp,t)}$ over the oscillation period, i.e., $V_{\rm dr}=\overline{V(\mathbf{r}_\perp,t)}$ (the overbar denotes averaging over the period of the sound wave).

Representing the derivatives of the collective variable as series in the amplitude of the sound wave, we can obtain the system of equations of the first approximation. It follows from those equations that in the given geometry of the problem, in a linear approximation in the amplitude of the sound wave the wave will not cause motion of the DW but will lead to the excitation of localized and nonlocalized spin waves. Here the spin waves are excited by both the transverse and longitudinal components of the external field.

From the dynamical equations for the magnetization in the second order of perturbation theory one can determine the DW velocity. By averaging the resulting expression over the period of the sound wave, we obtain the DW drift velocity $V_{\rm dr}=\overline{V_2}=\overline{\partial Y_2/\partial t}$:

$$V_{\rm dr}=R\rho\mu_1(\omega)[(k_zu_{0x})(k_zu_{0y})+(k_xu_{0y})(k_zu_{0z})], \tag{9}$$

where the nonlinear DW mobility

$$\mu_1(\omega)=-\mu_0\frac{q^2}{(1+\sigma)^2\sigma^2}, \tag{10}$$

with

$$\mu_0=\frac{\pi y_0 g\gamma^2 M_0}{4\lambda\tilde{\beta}_2},\quad q=\frac{\omega\omega_r}{\omega_1^2},\quad \sigma=\frac{(\beta_1-\tilde{\beta}_2)}{\tilde{\beta}_2},$$

$\omega_1=c/y_0$ is the activation frequency of the lower branch of bulk spin waves, and $\omega_r=\lambda\delta g M_0/4$ is the characteristic relaxation frequency.

If we set $R=-1$ and $\rho=+1$ in formula (9), then that expression describes the drift of a solitary DW. The presence of the factor $R\rho$ in the expression for the drift velocity (9) attests to the possibility of drift of the stripe domain structure as a whole. Adjacent DWs have opposite values of the topological charge R, and for drift of the stripe domain structure it is necessary that the parameters ρ in the adjacent DWs also be different, i.e., the orientation of the vector $\mathbf{l}$ in adjacent DWs should be opposite, while the direction of rotation should be the same. In that case the factors $R\rho$ for adjacent DWs have the same sign, and the DWs move in the same direction, i.e., motion of the domain structure occurs.

SOUND WAVE PROPAGATING PERPENDICULAR TO THE PLANE OF THE DW

Let us consider the equations of motion (4), (5) in the case of a sound wave propagating perpendicular to the plane of the DW: $\mathbf{u}=\mathbf{u}_0\exp[i(k_y y-\omega t)]$. For simplicity we consider the case when there is no z component of the sound field, $\mathbf{u}_0=u_0(1,1,0)$. We introduce the collective coordinate of the center of the DW, $Y(t)$, which here, unlike the case considered above, is independent of $\mathbf{r}_\perp$. In the first order of perturbation theory the sound wave excites spin waves and causes oscillatory motion of the DW with a velocity

$$V_1=-\frac{i\gamma(ky_0)^3\pi\omega_1^2}{2\tilde{\beta}_2(\omega_r-i\omega)}\left[\frac{R\rho u_{0x}}{\mathrm{ch}\dfrac{\pi k y_0}{2}}+\frac{iu_{0y}}{\mathrm{sh}\dfrac{\pi k y_0}{2}}\right]e^{ikY-i\omega t},\tag{11}$$

where $k=k_y$.

From this relation one can determine the amplitude of the displacement, $h=\mathrm{Re}(iV_1/\omega)$, which is equal to 10^{-6} cm for $YFeO_3$ at a frequency $\omega\sim10^6$ s^{-1}. The oscillations of the DW, like the spin waves, are excited by both the transverse and longitudinal components of the sound wave. We note that a DW of the ab type does not oscillate in a sound wave propagating in the plane of the DW. Domain walls of the ac type do not oscillate for either geometry of the problem.[8,9] To describe the oscillations in these cases it is necessary to take into account the internal structure of the DWs, e.g., the presence of Bloch lines in them.

In the second order of perturbation theory the domain structure undergoes drift motion at a velocity

$$V_{\mathrm{dr}}=\mu_{xx}(\omega)(ku_{0x})^2+R\rho u_{xy}(\omega)(ku_{0x})(ku_{0y})+\mu_{yy}(\omega)(ku_{0y})^2,\tag{12}$$

where the nonlinear mobility $\mu_{ij}(\omega)$ in the long-wavelength approximation has the form

$$\mu_{xy}=\eta_1\mu_0(ky_0)^2,\quad \mu_{xx}=-\eta_2\mu_0 k y_0 q,$$
$$\mu_{yy}=\eta_3\mu_0 k y_0 q.\tag{13}$$

The numerical coefficients $\eta_1\sim1$, $\eta_2\sim0.4$, and $\eta_3\sim3$ are obtained by evaluating the expressions for $\mu_{ij}(\omega)$. The main contribution to the drift velocity is from the nonlinear mobility μ_{xy}. To estimate the drift velocity we use the parameters of yttrium orthoferrite:[1] $\mu_0\approx2\times10^{13}$ cm/s, $y_0\approx4\times10^{-6}$ cm, $\sigma\sim2$, $\tilde{\beta}_2\sim1$, $\omega_1\approx4\times10^{11}$ s^{-1}, and $\omega_r\approx6\times10^8$ s^{-1}. The drift velocity associated with the mobility μ_{xy} for $\omega\sim10^9$ s^{-1}, a sound velocity $s=10^5$ cm/s, and a maximum attainable value of the strain tensor $ku_0\sim10^{-5}$ is $V_{\mathrm{dr}}\approx3$ cm/s.

The presence of the factor $R\rho$ in expression (12) indicates that in the field of a sound wave having components u_{0y} and u_{0x} and propagating perpendicular to the plane of the DWs, a drift of the stripe domain structure will occur.

On the basis of the analysis given above, we have established that in a WFM the drift of a solitary DW of the ab type and of the stripe domain structure can occur both in sound waves propagating perpendicular and parallel to the plane of the DW.

In the field of a sound wave propagating in the plane of the DW the drift effect is negligible. The greatest effect on a DW of the ab type should be expected in the field of a sound wave propagating perpendicular to the plane of the DW. The maximum drift velocity in such a sound wave is attained in the simultaneous presence of a longitudinal component u_{0y} and a transverse component u_{0x} of the field. The simultaneous presence of transverse and longitudinal components of the sound wave is also necessary for the drift of a domain structure containing DWs of the ab type.

From the expressions for the drift velocity of DWs of the ab and ac types,[8,9] it is seen that in a sound wave propagating perpendicular to the plane of the DWs the drift velocity of the DWs is determined by those components of the sound wave which lie in the plane of rotation of the antiferromagnetic vector $\mathbf{l}$, i.e., u_{0x} and u_{0z} in a DW of the ac type and u_{0x} and u_{0y} in a DW of the ab type.

*E-mail: vme@dgasa.dn.ua

[1] V. G. Bar'yakhtar, B. A. Ivanov, and M. V. Chetkin, Usp. Fiz. Nauk **146**, 417 (1985) [Sov. Phys. Usp. **28**, 563 (1985)].
[2] E. V. Gomonaĭ, B. A. Ivanov, V. A. L'vov, and G. K. Oksyuk, Zh. Éksp. Teor. Fiz. **97**, 307 (1990) [Sov. Phys. JETP **70**, 174 (1990)].
[3] V. G. Bar'yaktar and B. A. Ivanov, Fiz. Met. Metalloved. **39**, 478 (1975).
[4] V. G. Bar'yakhtar, B. A. Ivanov, and A. L. Sukstanskiĭ, Zh. Éksp. Teor. Fiz. **78**, 1509 (1980) [Sov. Phys. JETP **51**, 757 (1980)].
[5] A. L. Sukstanskiĭ, Fiz. Tverd. Tela (Leningrad) **27**, 3509 (1985) [Sov. Phys. Solid State **27**, 2119 (1985)].
[6] A. V. Zalesskiĭ, A. M. Savvinov, IU. S. Sheludev (I. S. Zheludev), and A. N. Ivashchenko, Zh. Éksp. Teor. Fiz. **68**, 1449 (1985) [Sov. Phys. JETP **41**, 723 (1985)]; N. F. Kharchenko, S. L. Gnatchenko, and R. Szymczak, Acta Phys. Pol. A **68**, 347 (1985).
[7] V. S. Gerasimchuk and A. L. Sukstanskiĭ, Phys. Rev. B **59**, 323 (1999).
[8] V. S. Gerasimchuk and A. L. Sukstanskiĭ, Zh. Éksp. Teor. Fiz. **118**, 1384 (2000) [JETP **91**, 1198 (2000)].
[9] V. S. Gerasimchuk and A. A. Shitov, Fiz. Nizk. Temp. **27**, 170 (2001) [Low Temp. Phys. **27**, 125 (2001)].
[10] S. I. Denisov, Fiz. Tverd. Tela (Leningrad) **31**, 270 (1989) [Sov. Phys. Solid State **31**, 1192 (1989)].

Translated by Steve Torstveit

Influence of Cr concentration on the structural and magnetic properties of the diluted magnetic semiconductor $Hg_{1-x}Cr_xSe$

V. D. Prozorovskiĭ, I. Yu. Reshidova, and A. I. Puzynya

*A. A. Galkin Donetsk Physicotechnical Institute, ul. R. Lyuksemburg 72, 83114 Donetsk, Ukraine**

S. Yu. Paranchych and V. R. Romanyuk

Yu. Fed'kovich Chernovtsy National University, ul. Kotsyubinskogo 2, 68012 Chernovtsy, Ukraine

(Submitted April 23, 2002; revised July 8, 2002)
Fiz. Nizk. Temp. **28**, 1239–1243 (December 2002)

The results of a study of the structural and magnetic properties of single-crystal samples of the diluted magnetic semiconductor $Hg_{1-x}Cr_xSe$ with different concentrations of chromium ions ($0<x\leqslant 0.07$) in the temperature interval 50–300 K are reported. It is found that the boundary of the existence region of the homogeneous solid solution lies at chromium concentrations $x<0.05$. In samples with $x\geqslant 0.05$ the sharp growth of the magnetic susceptibility in the region of the phase transition temperature is due not only to a transition to a phase similar to a spin-glass phase, which is observed in all the samples studied, but also to a ferromagnetic contribution from ferromagnetic inclusions of $HgCr_2Se_4$ and CrSe in those samples. © *2002 American Institute of Physics.* [DOI: 10.1063/1.1531391]

Diluted magnetic semiconductors (DMSs), such as II–VI compounds containing controlled amounts of substituent magnetic ions, are currently the subject of intensive research. The most characteristic feature of DMSs is a large spin splitting of the spectrum of free carriers in a magnetic field as a result of the strong spin-dependent interaction of the band carriers with the localized spins of the magnetic ions. The search for new DMSs with large spin splittings takes both the path of increasing the concentration of magnetic ions and the path of achieving large exchange constants. In the last few years a new gapless DMS containing chromium rather than the traditional Mn, Co, or Fe as the magnetic ion in the diamagnetic matrix has been attracting attention. A number of new physical effects observed[1–3] in $Hg_{1-x}Cr_xSe$ distinguish this system from the other DMSs known previously.

Our more recent experimental studies of electron spin resonance and magnetic susceptibility in samples of the DMS $Hg_{1-x}Cr_xSe$ with different chromium concentrations in the interval $0.00112\leqslant x\leqslant 0.07$ in the temperature range 50–300 K have revealed a transition of this system to a phase similar to a spin-glass phase.[3] The transition is accompanied by an asymmetric lattice distortion due to the deformation of the crystal as a result of the change in temperature. Both the temperature at which the change in lattice symmetry occurs and the phase transition temperature T_g increase with increasing chromium concentration x. In particular, the curves of the temperature dependence of the magnetic susceptibility χ measured by an inductive method[3] exhibit a pronounced maximum at $T=T_g$ (Fig. 1). The character of the change in $\chi(T)$ was the same at the four chromium concentrations $x=0.01$, 0.03, 0.05, and 0.07, although the temperature T_g at which the susceptibility reached its maximum value and the values of χ at $T\leqslant T_g$ were different for the different x. Nevertheless, for the sample with $x=0.07$ an inexplicable (at that time) sharp growth of $\chi(T)$, disproportionate to the change in the chromium concentration, was observed. Here the value of χ at the transition temperature was approximately an order of magnitude higher than those for the samples with $x\leqslant 0.05$, and the susceptibility remained larger all the way down to 50 K. This behavior of the magnetic susceptibility is apparently related to an increase of the chromium concentration in the initial HgSe lattice above $x=0.05$, which leads to a substantial change in the magnetic

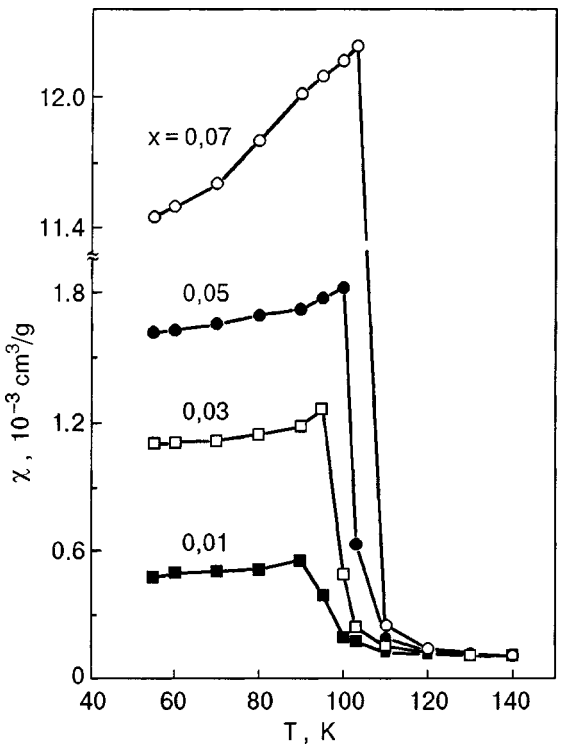

FIG. 1. Temperature dependence of the magnetic susceptibility for $Hg_{1-x}Cr_xSe$ samples with different chromium concentrations x (Ref. 3).

properties of the system. In view of this circumstance and the known fact that chromium is less soluble in HgSe than are manganese and iron, for example, and also the fact that interstitial chromium atoms can create local inhomogeneities in the crystal, it is of great interest to study the solubility of chromium in HgSe and the dependence of the structural and magnetic properties of $Hg_{1-x}Cr_xSe$ on x, particularly since no data on the state diagram of this system have been published before.

EXPERIMENT

Single-crystal samples of $Hg_{1-x}Cr_xSe$ were grown by a modified Bridgman method at a temperature gradient in the region of the crystallization front of around 2.5–3.0 K/mm and a rate of crystallization of 1.2 mm/h. The chromium concentration in the samples was varied over the range $0 \leqslant x \leqslant 0.07$.

Structural studies of the samples were done on a Hitachi 4100-S scanning electron microscope (SEM) in both the secondary and scattered modes and on a Philips 515 SEM equipped with a system for x-ray energy dispersion analysis (EDAX). Additional structural studies were carried out on $Hg_{1-x}Cr_xSe$ powders ($0 \leqslant x \leqslant 0.07$) with a Siefert XRD-3000TT biaxial x-ray diffractometer by a powder diffraction technique.

Measurements of the magnetic susceptibility were made in the temperature region 50–300 K by an inductive method on an apparatus consisting of a modified differential magnetometer with modulation by a low-frequency field.[3] The frequency of the alternating magnetic field inducing the emf in the measuring coils of the device was chosen so as to reduce dynamic effects to a minimum while providing sufficient signal for the measurements. The frequency was 233 Hz at an amplitude of the modulating field of 1 Oe. For the magnetic susceptibility measurements the samples were made in the form of circular cylinders 10 mm in height and 1 mm in diameter. The axis of the cylinder coincided with the fourfold crystalline axis along which the $Hg_{1-x}Cr_xSe$ samples were grown. The system of modulation and measurement coils made it possible to study the susceptibility along this axis. The sensitivity of the apparatus was sufficient for measuring the differential magnetic susceptibility to an accuracy of 2×10^{-5} cm^3/g.

RESULTS AND DISCUSSION

To determine the miscibility coefficient of chromium in the initial HgSe lattice we did electron-microscope and structural studies of $Hg_{1-x}Cr_xSe$ single crystals and powders with $0 \leqslant x \leqslant 0.07$. The structural characteristic obtained as a result of the EDAX showed that for solid solutions with $x < 0.05$ the samples were stoichiometrically single-phase crystals, but when the chromium concentration was increased above 5% the excess (superstoichiometric) Hg, Cr, and Se atoms form macroscopic inclusions. These needle-shaped inclusions appeared as inner (dark) and outer (gray) regions against a bright field. The EDAX analysis of the chromium concentration showed that the inner region of the inclusions consists of CrSe, while the adjacent regions contain compounds of Hg, Cr, and Se. The main part of the sample (the bright field) is an $Hg_{1-x}Cr_xSe$ solid solution.

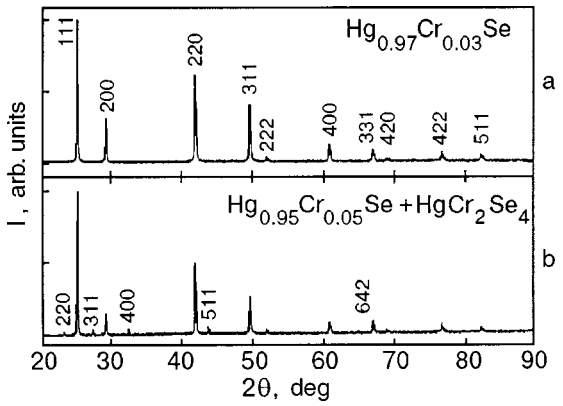

FIG. 2. Powder diffractograms of a homogeneous sample of $Hg_{0.97}Cr_{0.03}Se$ (a) and a sample of $Hg_{0.95}Cr_{0.05}Se$ containing inclusions (b).

In addition, x-ray structural studies by the powder diffraction technique were carried out on the two types of compounds—with and without inclusions. The results of x-ray diffractometric studies for $Hg_{1-x}Cr_xSe$ samples with $x = 0.03$ and 0.05 are presented in Fig. 2. The diffractogram for the $Hg_{0.97}Cr_{0.03}Se$ sample (Fig. 2a) has clearly visible peaks corresponding to the cubic lattice of the original HgSe with a slight deviation of the lattice parameter. These peaks were identified and indexed as shown in the diffractogram. For comparison, in Fig. 2b we show the diffractogram of the $Hg_{0.95}Cr_{0.05}Se$ sample, which exhibits peaks due to the presence of a new phase. The identification of these peaks indicated the presence of the compound $HgCr_2Se_4$. Other phases, such as CrSe, were not observed in this x-ray diffraction study for either sample. As a result, the combined analysis by the electron microscope and x-ray diffraction methods showed that the inclusions present in $Hg_{1-x}Cr_xSe$ samples with $x \geqslant 0.05$ are made up of CrSe surrounded by regions of $HgCr_2Se_4$, while the main part of the sample remains unchanged.

In addition, the powder diffractograms obtained can be used to calculate the crystal lattice parameter a as a function of the chromium concentration x (Fig. 3). As is seen in the figure, a decreases linearly with increasing chromium concentration up to 5%, i.e., Vegard's law for a three-component crystal lattice is obeyed in this concentration region. For $x > 0.05$ the lattice parameter starts to increase.

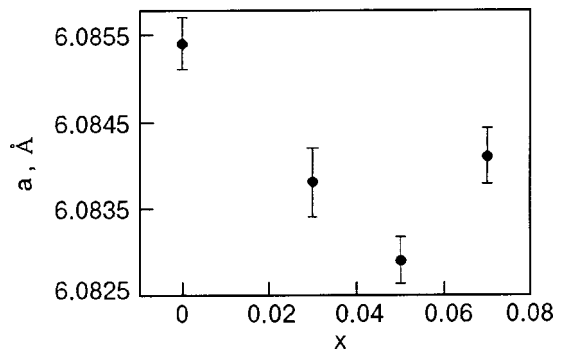

FIG. 3. Dependence of the lattice constant a on the chromium concentration x in $Hg_{1-x}Cr_xSe$.

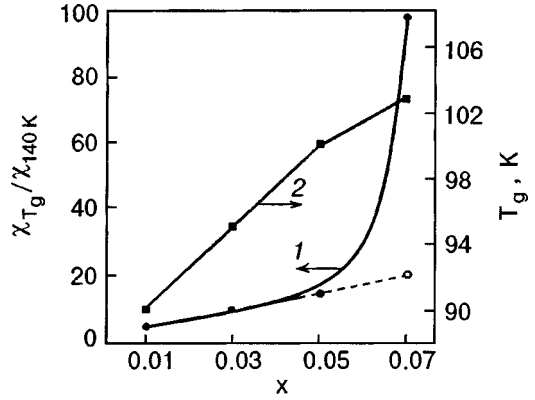

FIG. 4. Relative value of the magnetic susceptibility $\chi_{T_g}/\chi_{140\,\mathrm{K}}$ (*1*) and the phase transition temperature T_g (*2*) as functions of the chromium concentration x.

Thus the present studies have established a region of chromium concentrations in the solid solution (below 5%) in which the chromium dissolves in the initial HgSe lattice without the formation of inclusions. When the percent chromium content increases above that value, other phases appear, mainly forming inclusions of CrSe and $HgCr_2Se_4$, and the homogeneity of the samples is broken. Let us compare the results obtained from the structural analysis with the data on the temperature dependence of the magnetic susceptibility for $Hg_{1-x}Cr_xSe$ samples ($0<x\leqslant 0.07$). The maximum values of χ measured at the temperature T_g of the magnetic phase transition for the samples with different chromium concentrations are divided by the value of χ at 140 K, where their magnetic susceptibilities are the same, within the experimental error, and we construct the dependence of the relative value of the magnetic susceptibility $\chi_{T_g}/\chi_{140\,\mathrm{K}}$ on the chromium concentration in the solid solution (see Fig. 4). We note that extrapolation of the linear dependence observed for the first three samples to the region of higher chromium concentration (the dashed line in Fig. 4) gives a considerably lower value of the magnetic susceptibility for the sample with $x=0.07$ as compared to experiment. Consequently, the jump of the magnetic susceptibility in samples with $x\geqslant 0.05$ is due not only to the transition to a phase similar to a spin-glass phase (this transition is observed in all the samples studied) but also to ferromagnetism arising on account of the presence of CrSe and $HgCr_2Se_4$ inclusions in these samples. Indeed, it is known[4] that the chalcogenide spinel $HgCr_2Se_4$ at temperatures down to 4.2 K is a ferromagnet with a Curie temperature $T_C=106$ K. The proximity of T_C to the temperature of the phase transition to the spin-glass phase, which is $T_g=103$ K for the sample with $x=0.07$, should be noted. Thus it is clear that the observation of high values of the susceptibility in the the sample with $x=0.07$ as the temperature is lowered from T_g to 50 K is explained by the ferromagnetic contribution of $HgCr_2Se_4$ to χ. Furthermore, there is also a contribution to χ from CrSe inclusions, which, by analogy with CrTe ($T_C=333$ K),[5] are apparently also ferromagnetic. Starting from the experimental data shown in Figs. 1 and 4 (curve *1*), we can obtain a numerical estimate of this ferromagnetic contribution of the $HgCr_2Se_4$ and CrSe inclusions at the magnetic phase transition point T_g. The experimental value of χ_{T_g} can be written as a sum of the contribution χ' from the homogeneous solid solution (the quantity obtained as the result of an extrapolation of the linear dependence, illustrated by the dashed line in Fig. 4) and the contribution χ'' of the ferromagnetic inclusions. Then the contribution of the ferromagnetic inclusions is calculated as $\chi''=\chi_{T_g}-\chi'=9.72\times 10^{-3}$ cm^3/g, which is 5 times larger than the contribution χ' due to the magnetic phase transition.

The fact that 5% chromium is a critical concentration for the $Hg_{1-x}Cr_xSe$ solid solutions under study is confirmed by a change in the linear dependence of the transition temperature T_g on x (curve *2* in Fig. 4). The observed increase of the temperature of the transition to the spin-glass phase when an additional fraction of the mercury ions is substituted by chromium ions is disproportionate to the rise of the susceptibility. This is also consistent with attributing the growth of the magnetic susceptibility for samples with $x>0.05$ to the presence of ferromagnetic inclusions of $HgCr_2Se_4$ and CrSe. Moreover, needle-shaped inclusions in $Hg_{1-x}Cr_xSe$ crystals with $x>0.05$ have been linked to anomalies in the temperature dependence of the magnetoresistance which were observed in recent studies on these same samples.[6] The presence of such inclusions in samples with $x>0.05$ caused the largest growth of the magnetoresistance with magnetic field, attesting to an increase of the mobility of the charge carriers in that case.

Thus we have established on the basis of structural and magnetic studies of $Hg_{1-x}Cr_xSe$ that the existence region of the homogeneous solid solutions lies at chromium concentrations $x<0.05$, while for $x\geqslant 0.05$ there are inclusions of $HgCr_2Se_4$ and CrSe, which have a substantial effect on the magnetic and magnetotransport characteristics of the material. However, progress in the growth of these crystals and improvement of their characteristics will involve not only reducing the concentration of inclusions and defects but also taking advantage of them in basic research and applications.

The authors express their deep gratitude to V. Munnoz and C. Reig [Departament de Aplicada and Institut de Ciencia de Materials, Universitate de Valencia, Edifici d'Investigacio, c/Dr. Moliner, 50, E46100 Burjassot (Spain)] for collaboration and invaluable assistance in making the structural measurements on our samples.

*E-mail: prohorov@pr.fti.ac.donetsk.ua

[1] V. D. Prozorovskiĭ, I. Yu. Reshidova, S. Yu. Paranchich, and Yu. S. Paranchich, Fiz. Tverd. Tela (Leningrad) **34**, 882 (1992) [Sov. Phys. Solid State **34**, 472 (1992)].
[2] V. D. Prozorovskiĭ, I. Yu. Reshidova, and S. Yu. Paranchich, Ukr. Fiz. Zh. **40**, 1005 (1995).
[3] V. D. Prozorovskiĭ, I. Yu. Reshidova, A. I. Puzynya, and Yu. S. Paranchich, Fiz. Nizk. Temp. **21**, 1057 (1995) [Low Temp. Phys. **21**, 813 (1995)].
[4] P. K. Baltzer, P. J. Wojtowicz, M. Robbins, and E. Lopatin, Phys. Rev. **151**, 367 (1966).
[5] S. Chikazumi, *Physics of Ferromagntism* [Russian translation], Mir, Moscow (1983) [English translation of 2nd ed.: Oxford University Press (1997)].
[6] A. I. Savchuk, P. I. Nikitin, S. Yu. Paranchych, M. D. Andriychuk, and S. I. Nikitin, Sens. Actuators A **91**, 173 (2001).

Translated by Steve Torstveit

On the theory of magnetic phase transitions in magnets with a large single-ion anisotropy

V. M. Kalita

Institute of Physics of the National Academy of Sciences of Ukraine, pr. Nauki 46, 03028 Kiev-28, Ukraine

V. M. Loktev*

N. N. Bogolyubov Institute of Theoretical Physics, National Academy of Sciences of Ukraine, ul. Metrologicheskaya 14-b, 03143 Kiev, Ukraine

(Submitted May 8, 2002; revised July 30, 2002)
Fiz. Nizk. Temp. **28**, 1244–1250 (December 2002)

For the example of a system with a ferromagnetic exchange interaction between ions with spins $S=1$, it is shown that the methods of the phenomenological theory based on the use of a Landau potential can be used for a description of processes of ordering and magnetization of magnets with a large single-ion anisotropy. © *2002 American Institute of Physics.*
[DOI: 10.1063/1.1531392]

INTRODUCTION

The study of magnets having large single-ion anisotropy has attracted and continues to attract significant interest. This is because the quasi-classical methods developed for slightly anisotropic magnets and based on the phenomenological theory of magnetism are inapplicable in this case.[1] In particular, in highly anisotropic magnetic crystals in which the anisotropy is of a single-ion character, the value of the one-site magnetization is formed not only by the exchange field but also to a considerable degree by the crystalline field, the constants of which also determine the value of the single-ion anisotropy. If the single-ion anisotropy is of the easy-plane (and not of the easy-axis) type or has a more general character (biaxial, cubic, etc.) and is large enough, then a system consisting of paramagnetic ions with integer S can be found in a nonmagnetic (singlet) state. However, the introduction of a magnetic field, which acts on the spin sublevels of an ion in general and of a crystal in particular, can bring about a transition from an initial nonmagnetic state of the crystal to a magnetic state, and the field dependence of the modulus of the mean one-site (and crystal) magnetization gives an appreciable contribution to the susceptibility of the crystal as a whole, which is reflected in its static and resonance (dynamic) properties.[2]

In this paper we attempt to show that anisotropic ''nonclassical'' magnets in the region of the external-magnetic-field-induced transition from a nonmagnetic to a magnetic state can be described by a potential analogous to the Landau potential that is well known in application to the description of temperature-induced phase transitions from the paramagnetic to a magnetic state. Without restricting the generality we consider the extremely simple case of a uniaxial ferromagnet with ion spin $S=1$ and with anisotropy of an easy-plane character.

As we know,[1] in that case the normalized ground-state wave function in the local coordinate system ξ, η, ζ, where ζ is chosen as the quantization axis, has the form

$$\psi_{qr}=\sum_{M_\zeta=\pm 1} C_{M_\zeta}|M_\zeta\rangle; \quad |C_1|^2+|C_{-1}|^2=1, \tag{1}$$

where $|M_\zeta\rangle$ are the eigenfunctions of the operator S^ζ, and C_{M_ζ} is the quantum-mechanical weight of the function $|M_\zeta\rangle$ in Ψ_{qr}. In accordance with (1) the (quantum-mechanical) mean magnetization of the ion is determined by the relation

$$\langle\Psi_{qr}|S^\zeta|\Psi_{qr}\rangle\equiv s=|C_1|^2-|C_{-1}|^2. \tag{2}$$

from which it follows that $s\neq 0$ when $|C_1|^2\neq|C_{-1}|^2$. This case corresponds to a magnetic state in which the mean spin (and, hence, the mean magnetization) in the ground state can differ substantially from the ''nominal'' value $S=1$. If the probabilities of realizing the states $|\pm 1\rangle$ happen to be equal, then $s=0$, and the ground state of the system will be nonmagnetic. As we see, the ground-state wave function (1) admits the possibility of transformation of the nonmagnetic state into a magnetic state.

We note that the probabilistic definition of the mean spin in (2) differs little from the usual definition of the thermodynamic mean value, which is written as a sum of the observable products of microscopic values times the probabilities of their realization (occupation of the states). This similarity is of a provisional character, since, generally speaking, different calculation procedures are intended. In view of the fact that in highly anisotropic systems admitting the existence of a nonmagnetic state and its transformation to a magnetic state under the influence of an external magnetic field, there is a region of parameters in which the magnetization is small, as in the case of thermodynamic transitions, it seems germane to find out whether the method of the general theory of phase transitions is applicable to such systems.

In the aforementioned case of an easy-plane system the difference (2) depends on the ratio of the single-ion anisotropy constant to the exchange constant. The influence of these constants is opposite in character:[1] while the exchange ''restores'' the value of the spin projection, tending to make it equal to the initial value $S=1$, the anisotropy decreases

this projection to zero. From this we infer a certain formal but physically justified assumption that the effect of single-ion anisotropy is similar to the disordering effect of temperature—in both situations there is a limiting value $s=0$, at which the system becomes nonmagnetic. And, although the single-ion anisotropy constant, which is a characteristic of the particular substance, is essentially unchanging, the macroscopic state of the system can be altered by applying an external magnetic field. In this way the corresponding phase transitions can be observed experimentally even at $T=0$ K (actually for $T \ll T_{\rm cr}$, where $T_{\rm cr}$ is the Curie or Néel temperature). A magnetic field, as we shall see, can affect C_{M_ζ} [see Eq. (1)], making s finite, so that for small s one can expand the ground-state energy of the magnet in a series, as is done in the Landau theory of phase transitions.[3] Here, of course, the order parameter is s.

It should be kept in mind that the effect of an external magnetic field will depend on its orientation, and for this reason the two different field directions—parallel and perpendicular to the hard axis, which is the initial axis of symmetry—will be considered separately. The spin configurations of such a ferromagnet were considered in Refs. 4 and 5 (see also Ref. 1) and, with allowance for biquadratic exchange, in Refs. 6–8. In those papers the calculations were done with the use of a self-consistency procedure,[1] which, however, does not permit determination of the stability of the phases. For those purposes, as in the quasi-classical approach, one uses expressions for the ground-state energy which are obtained quantum-mechanically and, as will be shown, have the form of a Landau potential for an exchange ferromagnet in a magnetic field.

MODEL

Let us first restrict consideration to the bilinear exchange interaction, the single-ion anisotropy, and the Zeeman term. In this case the Hamiltonian of the ferromagnet has the standard form (in the crystallographic coordinate system)

$$\mathcal{H}=-\frac{J}{2}\sum_{\mathbf{n},\rho}\mathbf{S}_{\mathbf{n}}\cdot\mathbf{S}_{\mathbf{n}+\rho}+D\sum_{\mathbf{n}}(S_{\mathbf{n}}^{Z})^2-h\sum_{\mathbf{n}}S_{\mathbf{n}}, \tag{3}$$

where $J>0$ is the exchange interaction between nearest-neighbor spins $\mathbf{n}$ and $\mathbf{n}+\boldsymbol{\rho}$, $D>0$ is the easy-plane anisotropy constant, and the magnetic field vector $\mathbf{h}$ is defined in energy units, $\mathbf{h}=\mu_B g\mathbf{H}$ (μ_B is the Bohr magneton, and g is the g factor) and the $\mathbf{Z}$ axis is directed along the hard axis.

Neglecting the spin fluctuations and using the function (1), we write the ground-state energy per spin, E_{qr}, as

$$E_{qr}=-\frac{1}{2}Jzs^2+DQ-hs, \tag{4}$$

where z is the number of nearest neighbors, s is the mean spin vector defined in Eq. (2), and Q is the quantum-mechanical mean of the squares of the Z projections of the spin operators , which is easily related to the components of the quadrupole spin moment.[1]

If we transform to the local axes in such a way that the angle between the spin quantization axis ζ and the Z axis is equal to θ, while the ξ axis lies in the $Z\zeta$ plane, then in accordance with (1) the wave function of each ion will be given by the simple linear combination[9]

$$\Psi_{qr}=\cos\varphi|1\rangle+\sin\varphi|-1\rangle, \tag{5}$$

where the angle φ (see below) is determined from the condition that the ground-state energy be minimum.

It is easily shown by a direct calculation using the explicit form of the function (5) that the spin projections and the spin quadrupole moment have the following nonzero components in the local coordinate frame:

$$s=\cos 2\varphi;\quad Q^{\zeta\zeta}=1;\quad Q^{\xi\xi}=\frac{1}{2}(1+\sin 2\varphi);$$

$$Q^{\eta\eta}=\frac{1}{2}(1-\sin^2 2\varphi). \tag{6}$$

Using them, we can write the energy (4) in the form

$$E_{qr}=-\frac{1}{2}Jz\cos^2 2\varphi+D\left[\cos^2 0+\frac{\sin^2\theta}{2}(1+\sin 2\varphi)\right]$$
$$-(h_\parallel\cos\theta+h_\perp\sin\theta)\cos 2\varphi, \tag{7}$$

where the vector $\mathbf{h}$ is decomposed as $\mathbf{h}=\mathbf{h}_\parallel+\mathbf{h}_\perp$, where $\mathbf{h}_\parallel\|\mathbf{Z}$ and $\mathbf{h}_\perp\perp\mathbf{Z}$.

It was pointed out above that the spin configurations (in contrast to the self-consistency procedures proposed in Ref. 9 (see also Ref. 1) and used, e.g., in Refs. 5–8) are more conveniently found in the usual way by minimizing expression (7) with respect to the unknown ''geometric'' angle and unknown ''mixing'' angle φ of the states;[1] as a result, we arrive at the equations

$$Jz\sin 4\varphi+D\sin^2\theta\cos 2\varphi+2$$
$$\times(h_\parallel\cos\theta+h_\perp\sin\theta)\sin 2\varphi=0,$$
$$-D\sin 2\theta(1-\sin 2\varphi)+2(h_\parallel\sin\theta-h_\perp\cos\theta)$$
$$\times\cos 2\varphi=0. \tag{8}$$

For an arbitrary direction of the field $\mathbf{h}$ or, equivalently, arbitrary $\mathbf{h}_\parallel$ and $\mathbf{h}_\perp$, the system of equations (8) cannot be solved analytically. However, it can be stated unequivocally that the value of the mean spin s at an arbitrary orientation except for strictly longitudinal along the hard axis of the crystal, $\mathbf{h}\|\mathbf{Z}$, is always nonzero (the Van Vleck mechanism of magnetization).

In the absence of external field ($\mathbf{h}=0$), two solutions can be obtained from system (8): a nonmagnetic state with $s=0$, which is realized for $D>2Jz$, and a magnetic state for $D<2Jz$, which corresponds to a value

$$s_0=\sqrt{1-(D/2Jz)^2}. \tag{9}$$

It is seen that $s_0<1$, and a value $s=1$ is reached only when $D=0$. A small value of the single-ion anisotropy leads only to second-order corrections with respect to the quantity $D/2Jz$.[1)]

Let us consider separately the cases $\mathbf{h}\perp\mathbf{Z}$, when the field is oriented in the easy plane, and $\mathbf{h}\|\mathbf{Z}$, when the field is oriented along the hard axis.

TRANSVERSE FIELD

We find from system (8) that $\theta=\pi/2$ or, in other words, the quantum-mechanical mean value of the spin is formed and lies in the easy plane along the $\mathbf{h}_\perp$ direction. Here, according to (6), the quantity which we seek has the value $s=\cos 2\varphi$; assuming that it is small, we write the ground-state energy (7) for this orientation of the field as an expansion in s:

$$E_{qr}=\frac{1}{4}(D-2Jz)s^2+\frac{D}{16}s^4+\frac{D}{32}s^6-h_\perp s. \tag{10}$$

Minimizing (10) with respect to s, we obtain the equation of state

$$\frac{1}{2}(D-2Jz)s+\frac{D}{4}s^3+\frac{3D}{16}s^5-h_\perp=0. \tag{11}$$

If $\mathbf{h}_\perp=0$, we obtain from (11) the solutions described above: $s=0$ for $D\geqslant 2Jz$, and $s_0=\sqrt{2(2Jz/D-1)}$ under the opposite inequality. The second solution is just solution (9) under the condition $2Jz/D-1\to 0$.

It can already be seen from (10) that the type of solution is determined by the sign of the coefficient of the s^2 term in (10), which changes at the point $D=2Jz$ where the phase transition would occur (see the monograph[2] and the literature cited therein) if the value of D could be varied.

For comparison we give the expression for the Landau potential describing an isotropic ferromagnet with $S=1$ in an external magnetic field at a finite temperature $T\neq 0$. The free energy of such a ferromagnet is $F=E-TS_{\text{en}}$, where E is the internal energy and S_{en} is the entropy, which in the mean-field method is of a configurational nature and depends only on the order parameter. The nonequilibrium free energy of this ferromagnet can be written as[10]

$$F(s)=-\frac{1}{2}Jzs^2+T\times\left(s\ln\frac{s+\sqrt{4-3s^2}}{2(1-s)}+\ln\frac{1+\sqrt{4-3s^2}}{1-s^2}\right)-hs, \tag{12}$$

where s is the thermodynamic mean value of the spin, the direction of which in the case of an exchange ferromagnet is always along $\mathbf{h}$. Expanding (12) in a series in s, we write the Landau potential as

$$F(s)=\frac{3}{4}\left(T-\frac{2}{3}Jz\right)s^2+\frac{3^2}{2^6}Ts^4+\frac{3^2\cdot 17}{2^9\cdot 5}Ts^6-hs. \tag{13}$$

The coefficients in (13) due to the entropy are positive and proportional to T. Comparing expressions (13) and (10), we see that for $T=0$ the single-ion anisotropy D formally plays the same role as T. Moreover, the value $D=2Jz$ divides the magnetic states in the same way as does the Curie temperature $T_C=2Jz/3$—a magnetically ordered phase for $T<T_C$ and a paramagnetic phase for $T>T_C$. In view of the similarity found, one can say that for $D>2Jz$ the magnetization of a highly anisotropic ferromagnet in an applied magnetic field is similar to the magnetization of an isotropic ferromagnet for $T>T_C$, and, in the opposite case, the magnetization for $D<2Jz$ is analogous to the case $T<T_C$.

Using (11), one can easily calculate the magnetic susceptibility for $\mathbf{h}_\perp\to 0$:

$$\chi_{\perp,\perp}=\left.\frac{\partial s}{\partial h_\perp}\right|h_{\perp\to 0}=\frac{2}{D-2Jz+\frac{3}{2}Ds^2(0)+\frac{15}{8}Ds^4(0)}. \tag{14}$$

In expression (14) the quantity $s(0)$ in the denominator denotes the mean value of the spin for the case $\mathbf{h}_\perp=0$, which is either equal to zero or to the expression in (9), depending on the ratio of the constants D and Jz. In particular, when $D>2Jz$, the susceptibility

$$\chi_{\perp,\perp}=\frac{2}{D-2Jz} \tag{15}$$

is the Van Vleck susceptibility, and as a result of the singlet nature of the ground state it is independent of the external field.

LONGITUDINAL FIELD

This case is more unusual. In fact, from the second equation of system (8) we obtain an expression for the angle θ:

$$\cos\theta=\frac{h_\parallel\cos 2\varphi}{D(1-\sin 2\varphi)}. \tag{16}$$

Then it follows from (16) and the first equation of system (8) that for field values $h_\parallel\geqslant D$ a state characterized by $\cos\theta=1$ is realized. Here the projection of the mean spin on the external field direction is equal to the limiting value, i.e., $s=\cos 2\varphi=1$.

Substituting (16) into (7), we write an expression for the ground-state energy in fields less than the single-ion anisotropy, i.e., $h_\parallel<D$:

$$E_{qr}=-\frac{1}{2}Jzs^2+\frac{1}{2}\left(D-\frac{h_\parallel^2}{D}\right)(1-\sqrt{1-s^2}). \tag{17}$$

By minimizing (17), we obtain the same two solutions: a singlet state with $s=0$, and a magnetic state in which[5]

$$s=\frac{1}{2JzD}\sqrt{(2JzD)^2-(D^2-h_\parallel^2)^2}. \tag{18}$$

These solutions transform into each other in a field

$$h_{QP}=\sqrt{D(D-2Jz)}. \tag{19}$$

The value of E_{qr} for the solution (18) has the simple form

$$E_{qr}=-\frac{(h_\parallel^2-h_{QP}^2)^2}{8JzD^2}, \tag{20}$$

from which we see that it goes to zero at the point $h_\parallel=h_{QP}$, where the energies of the magnetic and nonmagnetic ground states turn out to be equal. It follows from this that the transition from a singlet (nonpolar) to a magnetic (polar) state occurs continuously. In the region $h_\parallel>h_{QP}$ the energy of the latter is negative and less than the energy of the singlet state.

The projection of the spin on the direction $\mathbf{h}_\parallel\|\mathbf{Z}$ can be found by differentiating expression (20):

$$s_{\|}=\frac{h_{\|}(h_{\|}^2-h_{QP}^2)}{2JzD^2}. \tag{21}$$

The value of this projection increases continuously with increasing $h_{\|}$, and its derivative, i.e., the magnetic susceptibility, does not go to zero anywhere. The latter statement means that no transformations occur in the system at fields up to $h_{\|}=D$, and the canted phase occupies a finite field region $h_{QP}\leqslant h_{\|}\leqslant D$. One can see this from an analysis of the energy (20).

The stability of solution (18) is ensured by a negative sign of the exchange contribution to the energy (17). In the absence of an exchange interaction the canted phase does not arise in a longitudinal field. In that case there will occur a jumplike transition of the system from the nonmagnetic to a magnetic state with the maximum value $M_Z=1$ of the spin projection on the Z axis.

Let us consider an anisotropic ferromagnetic system placed in a longitudinal field in the framework of the phenomenological theory, expanding the energy (17) in a series in s, which is assumed small:

$$E_{qr}=\frac{1}{2}\left(-Jz+\frac{1}{2}\left(D-\frac{h_{\|}^2}{D}\right)\right)s^2+\frac{1}{16}\left(D-\frac{h_{\|}^2}{D}\right)s^4 + \frac{1}{32}\left(D-\frac{h_{\|}^2}{D}\right)s^6. \tag{22}$$

This expression, in contrast to (10), does not contain a term of first degree in s. The absence of such a term means that the action of a magnetic field in this orientation is of a critical character. Here it counteracts the effect of D, so that all of the expansion coefficients in (22) decrease for $h_{\|}\neq 0$.

Let us analyze in more detail the case $D>2Jz$, when the initial state prior to the turning on of the field is the singlet state. Then we find from (22) that in a field $h_{\|}=h_{QP}$ the coefficient of the s^2 term becomes equal to zero, and at higher values of $h_{\|}$ it is negative. The other coefficients do not change sign. In complete correspondence with the Landau theory of phase transitions, a field-induced second-order transition from the singlet to the magnetic state occurs at this point. If we assume that $s\ll 1$, then we have the approximate relation

$$E_{qr}=\frac{h_{QP}}{2D}(h_{QP}-h_{\|})s^2+\frac{D}{16}s^4 \tag{23}$$

which gives the equation of state

$$\frac{h_{QP}}{D}(h_{QP}-h_{\|})s+\frac{D}{4}s^3=0. \tag{24}$$

We see from (24) that the solution $s=0$ is realized for fields $h_{\|}\leqslant h_{QP}$, while in higher fields

$$s=\frac{2\sqrt{h_{QP}}}{D}\sqrt{h_{\|}-h_{QP}}. \tag{25}$$

The same critical dependence was obtained in Ref. 8 on the basis of a solution of the self-consistency equations. However, Ref. 8 made use of an expansion of the wave function (6) in the parameter φ, which is not the order parameter and is not an observable quantity, since it specifies a "rotation" of the eigenfunctions of the spin operator S^{ζ} in Hilbert space.

Using (16) and (25), we can determine the spin projection on the hard axis and on the plane when $h_{\|}>h_{QP}$ (but $h_{\|}<D$):

$$s_{\|}=2\frac{h_{QP}^2}{D^3}(h_{\|}-h_{QP}); \tag{26}$$

$$s_{\perp}=2\frac{\sqrt{h_{QP}}}{D}\left[1-\frac{h_{QP}^3}{2D^4}(h_{\|}-h_{QP})\right]\sqrt{h_{\|}-h_{QP}}. \tag{27}$$

Thus in a field $h_{\|}>h_{QP}$ the initially nonmagnetic system indeed is found in a canted ferromagnetic phase, in which not only the diagonal but also the off-diagonal components of the magnetic susceptibility tensor, $\chi_{\|,\|}=\partial s_{\|}/\partial h_{\|}$ and $\chi_{\perp,\|}=\partial s_{\perp}/\partial h_{\|}$, are nonzero. These components, which are zero in the nonmagnetic state, are written in the canted phase as

$$\chi_{\|,\|}=\frac{2h_{QP}^2}{D^3};\quad \chi_{\perp,\|}=\frac{\sqrt{h_{QP}}}{D}\frac{1}{\sqrt{h_{\|}-h_{QP}}} \tag{28}$$

(because of its small effect on $\chi_{\perp,\|}$, we drop the contribution from the second term on the right-hand side of (27)).

We see that the longitudinal (along the field) component $\chi_{\|,\|}$ of the susceptibility tensor is constant and does not depend on the value of the magnetic field. Its value is inversely proportional to the third power of D and will be appreciable only for a large value of h_{QP}. The transverse component, however, goes to infinity at the point of the magnetic phase transition, as at a phase transition from a paramagnetic to an ordered state. This, in turn, means that the crucial element for this phase transition is the spontaneous onset of a spin projection oriented in the easy plane perpendicular to the field. We also note that these features of the magnetization under the influence of a magnetic field, which were obtained from an analysis of the energy (22), remain present in the exact solution, although their analysis is not as obvious.

For $D<2Jz$ the solution with $s=0$ is unstable, and for all values of the external field belonging to the interval $h_{\|}\in[0,D]$ only the usual canted phase with a spin value

$$s=s_0\left(1+\frac{h_{\|}^2}{D^2s_0^2}\right) \tag{29}$$

is realized. For this solution the components of the magnetic susceptibility tensor have the values

$$\chi_{\|,\|}=\frac{s_0^2}{2D};\quad \chi_{\perp,\|}=\frac{2h_{\|}}{D^2s_0^2}. \tag{30}$$

We see that for $D<2Jz$ the longitudinal component of the susceptibility tensor $\chi_{\|,\|}$ is constant; here its value is considerably greater than that given in (28). The off-diagonal component of the susceptibility tensor (30) is proportional to the value of the field and goes to zero for $h_{\|}\to 0$. This means that when the magnetic field field is first applied the main factor in the magnetization is the rotation rather than the change in magnitude of s, notwithstanding the fact that $s_0\ll 1$ under the proposed conditions ($D\sim 2Jz$). The change of the magnitude of the mean spin under the influence of the field will

become significant when when the components of the susceptibility tensor (30) become comparable. This will occur in fields $h_{\|}\sim(2Jz-D)^2/D$.

INFLUENCE OF NON-HEISENBERG ISOTROPIC INTERACTIONS

We restrict discussion to non-Heisenberg isotropic interactions of fourth degree in the spin, the Hamiltonian of which has the form

$$\mathcal{H}'=\Pi\sum_{\mathbf{n},\rho}(\mathbf{S_n}\cdot\mathbf{S_{n+\rho}})^2+\Lambda\sum_{\mathbf{n},\rho,\nu}(\mathbf{S_n}\cdot\mathbf{S_{n+\nu}})(\mathbf{S_{n+\nu}}\cdot\mathbf{S_{n+\rho}})$$

$$+P\sum_{\mathbf{n},\rho,\nu,\tau}(\mathbf{S_n}\cdot\mathbf{S_{n+\rho}})(\mathbf{S_{n+\nu}}\cdot\mathbf{S_{n+\tau}}), \tag{31}$$

where the parameters Π, Λ, and P refer to the two-spin (biquadratic), three-spin, and four-spin interactions, respectively.

The non-Heisenberg interactions (31) are isotropic and do not depend on the orientation of the coordinate system. Their contribution to the ground-state energy (4) in the local coordinate system may be written as[11]

$$E'_{qr}=-\frac{1}{2}\Pi s^2+\Lambda s^2Q^{\zeta\zeta}+\Pi[(Q^{\zeta\zeta})^2$$

$$+(Q^{\eta\eta})^2+(Q^{\xi\xi})^2]+Ps^4. \tag{32}$$

Generally speaking, the interaction parameters in (32) should be multiplied by the number of scalar products formed by nearest neighbors. The corresponding renormalization is not included in (31), since all of the non-Heisenberg interactions in it are described by phenomenological parameters.

Taking (6) into account, we write expression (32) in the form

$$E'_{qr}=(\Lambda-\Pi)s^2+Ps^4. \tag{33}$$

Taking the energy (33) into account will lead to a change in the expression for the expansion of the ground-state energy. Thus the expansion in s of the ground-state energy in a longitudinal field (22) with the non-Heisenberg interactions included will become

$$E_{qr}=\left[-\frac{1}{2}Jz+\Lambda-\Pi+\frac{1}{4}\left(D-\frac{h_{\|}^2}{D}\right)\right]s^2+\frac{1}{16}$$

$$\times\left(D+P-\frac{h_{\|}^2}{D}\right)s^4+\frac{1}{32}\left(D-\frac{h_{\|}^2}{D}\right)s^6. \tag{34}$$

We see that the parameters of the non-Heisenberg interactions (31) only affect the expansion coefficients. The parameters of the biquadratic and three-particle exchanges enter the coefficient of the second-degree term. Taking them into account will lead to a change in the value of the field of the phase transition from the singlet to the magnetic state but will not affect the type of phase transition. The four-spin exchange parameter appears in the coefficient of the fourth-degree term. If the four-spin interaction is significant and the condition $P<0$ obtains, it can happen that when a magnetic field is applied the coefficient of the fourth-degree term in (34) will go to zero and become negative before the coefficient of the second-degree term does. For such values of the four-spin interaction parameter the phase transition from the nonmagnetic to the canted phase will occur as a first-order transition.

CONCLUSION

The foregoing calculations lead to the rather unexpected conclusion that the description of phase transitions in magnetic fields in highly anisotropic magnets, which at the present time cannot be considered few in number (see, e.g., Refs. 12 and 13), can be carried out in complete correspondence with the Landau phenomenological theory of phase transitions. Here, as we have said (see also Ref. 12), the anisotropy plays the role of a ''disordering'' factor, while the exchange and external magnetic field are ordering factors. In the vicinity of transitions from a singlet state with no magnetization to a state with nonzero magnetization, the expansion of the energy in the order parameter has a form completely analogous to the Landau potential, so that the order of the corresponding transition can easily be established. It is important that in the proposed description with with both the dipolar and quadrupolar spin averages taken into account, this transition is always second-order, while in the absence of self-consistency the transition can be first-order.[12,13] The approach developed here also makes it possible to take into account in a trivial manner the non-Heisenberg isotropic interactions of fourth degree in the spin. A generalization of the proposed treatment to the case of half-integer spins, anisotropic antiferromagnets, and finite temperatures will be done separately.

We thank Prof. S. M. Ryabchenko for a critical discussion of the results and, in particular, for noting that along with the similarity mentioned between temperature- and field-induced (in highly anisotropic magnets) transitions, there is also an important difference: whereas the first are transitions of the order–disorder type, the second are order–order transitions, i.e., analogous to transitions of the displacive type.

This study was performed as part of two projects supported by the Foundation for Basic Research of Ukraine (Grants 02.07/0114 and 04.07/0114).

*E-mail: vloktev@bitp.kiev.ua

[1)]We note that the classical theory contains only the spatial angles, and the number of equations is accordingly smaller.

[1] V. M. Loktev and V. S. Ostrovskii, Fiz. Nizk. Temp. **20**, 983 (1994) [Low Temp. Phys. **20**, 775 (1994)].
[2] V. V. Val'kov, S. G. Ovchinnikov, *Quasiparticles in Strongly Corrlated Systems* [in Russian], Izd. SO RAN, Novosibirsk (2001).
[3] L. D. Landau and E. M. Lifshitz, *Statistical Physics*, Parts 1 and 2, 3rd ed. [Pergamon Press, Oxford (1980), Nauka, Moscow (1976)].
[4] E. V. Rozenfel'd, JETP Lett. **24**, 50 (1976).
[5] F. P. Onufrieva, Zh. Éksp. Teor. Fiz. **89**, 2270 (1985) [Sov. Phys. JETP **62**, 1311 (1985)].
[6] Yu. N. Mitsaĭ, A. N. Maĭorova, and Yu. A. Fridman, Fiz. Tverd. Tela (Leningrad) **34**, 66 (1992) [Sov. Phys. Solid State **34**, 34 (1992)].
[7] Yu. A. Fridman, O. V. Kozhemyako, and B. L. Eingorn, Fiz. Nizk. Temp. **27**, 495 (2001) [Low Temp. Phys. **27**, 362 (2001)].
[8] V. V. Val'kov and G. N. Matsuleva, IF SO AN SSSR Preprint No. 645F [in Russian], Institute of Physics, Siberian Branch of the Academy of Sciences of the USSR, Krasnoyarsk (1987).
[9] V. M. Loktev and V. S. Ostrovskiĭ, Ukr. Fiz. Zh. (Russ. Ed.) **23**, 1708 (1978).

[10] V. M. Kalita and A. F. Lozenko, Fiz. Nizk. Temp. **23**, 399 (1997) [Low Temp. Phys. **23**, 293 (1997)].
[11] V. M. Kalita, Fiz. Tverd. Tela (Leningrad) **33**, 1940 (1991) [Sov. Phys. Solid State **33**, 1092 (1991)].
[12] A. K. Zvezdin, V. M. Matveev, A. A. Mukhin, and A. I. Popov, *Rare-Earth Ions in Magnetically Ordered Crystals* [in Russian], Nauka, Moscow (1985).
[13] E. L. Nagaev, *Magnets with Complex Exchange Interactions* [in Russian], Nauka, Moscow (1988)

Translated by Steve Torstveit

LOW-DIMENSIONAL AND DISORDERED SYSTEMS

Resonance properties of the quasi-one-dimensional Ising magnet $[(CH_3)_3NH]CoCl_3 \cdot 2H_2O$ in the paramagnetic and magnetically ordered phases

M. I. Kobets, E. N. Khatsko,* V. A. Pashchenko, A. S. Chernyi, and K. G. Dergachev

B. Verkin Institute for Low Temperature Physics and Engineering, National Academy of Sciences of Ukraine, pr. Lenina 47, 61103 Kharkov, Ukraine

V. G. Borisenko

Kharkov Air Force Institute, ul. Volodarskogo 46, 61064 Kharkov, Ukraine

(Submitted May 15, 2002)
Fiz. Nizk. Temp. **28**, 1251–1259 (December 2002)

A study is made of the angular, frequency–field, and temperature dependences of the magnetic resonance of the quasi-one-dimensional Ising magnet $[(CH_3)_3NH]CoCl_3 \cdot 2H_2O$ in the paramagnetic phase. The experimental results obtained are explained in a model of spin-cluster resonance in a strongly exchange-coupled spin chain. The frequency–field dependences of the ferromagnetic resonance spectrum measured below the Néel temperature are studied for magnetic-field directions along the crystallographic axes **a**, **b**, and **c**. It is shown that for $H \to 0$ the spin-wave spectrum of this quasiferromagnet has two gaps ($\nu_1 = 70.1$ GHz and $\nu_2 = 52.5$ GHz). © *2002 American Institute of Physics.* [DOI: 10.1063/1.1531393]

INTRODUCTION

Interest in the dynamic and static properties of low-dimensional multisublattice magnetic systems has been growing for several decades. This is partly due to the application of multisublattice materials (e.g., hexaferrites and yttrium iron garnets) in microwave technique and to the search for analogs of exactly solvable one-dimensional magnetic models. In addition, the behavior of one-dimensional Ising magnetic systems exhibits resonance features due to the presence of spin clusters or magnon bound states. Although the presence of spin clusters should be manifested in all Ising systems, they have been detected experimentally only in a limited number of compounds.

In recent years new compounds have been obtained which have properties close to those of one-dimensional and two-dimensional systems. Promising quasi-one-dimensional multisublattice systems include the family of crystals $[(CH_3)_3NH]MCl_3 \cdot 2H_2O$ (M = Mn, Co, Ni, Fe,...), for which a large body of experimental material has been accumulated, mainly in relation to static magnetic studies. The high-frequency and resonance properties of this class of crystals in the paramagnetic and magnetically ordered phases remain less studied.

The present study investigates the resonance behavior of the Co^{2+} ion in the $[(CH_3)_3NH]CoCl_3 \cdot 2H_2O$ lattice at frequencies in the 14–120 GHz range and at temperatures of 1.8–60 K. An earlier study of the magnetic and thermal properties of the magnet $[(CH_3)_3NH]CoCl_3 \cdot 2H_2O$ showed that this crystal has a sufficient degree of one-dimensionality and a three-dimensional magnetic ordering temperature T_N equal to 4.135 K.[1,2] According to the results of Ref. 1, the exchange interaction in the chain, J/k, is equal to 15.4 K, while the interchain exchange is -0.28 K. This system can therefore be a model for cobalt-containing low-dimensional compounds. Information obtained from resonance studies on the value of the g factors and the identification of effects due to the low dimensionality and multisublattice nature of the magnetic structure are useful for developing model concepts of the behavior of complex magnetic systems.

EXPERIMENTAL TECHNIQUE AND THE PROPERTIES OF THE MAGNETIC SUBSYSTEMS OF THE $[(CH_3)_3NH]CoCl_3 \cdot 2H_2O$ CRYSTAL

Single crystals were grown by the method of slow evaporation from an equimolecular solution of $(CH_3)_3NHCl$ and $CoCl_2 \cdot 6H_2O$ at a temperature of 75 °C. Crystals of a dark blue color with linear dimensions around 5 mm and with distinct faceting were obtained. X-ray measurements showed that the symmetry of the crystal lattice of this compound can be described by the space group $Pnma(D_{2h}^{16})$, in agreement with the results of Ref. 1. The values of the unit cell parameters are $a = 16.67$ Å, $b = 7.273$ Å, and $c = 8.113$ Å. The unit cell contains four magnetic ions Co^{2+}. Geometric fragments of the structure are illustrated in Fig. 1, which was taken from Ref. 1. The principal feature of the $[(CH_3)_3NH]CoCl_3 \cdot 2H_2O$ structure is the presence of parallel chains of Co^{2+} ions extending along the **b** axis. The octahedral environment of the Co^{2+} ion consists of four Cl atoms and two water molecules, and the octahedra in a chain are inclined successively from the **c** axis first to one side and then the other. In the bc plane the chains are separated by trimethylammonium groups, and the crystals are easily delaminated.

From measurements of the heat capacity and magnetic susceptibility, Losee and coauthors[1] established that the mag-

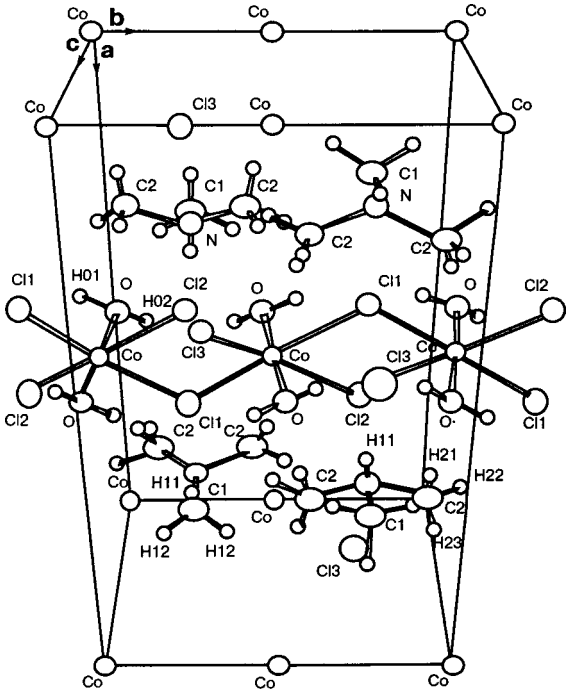

FIG. 1. Fragments of the crystal structure of $[(CH_3)_3NH]CoCl_3 \cdot 2H_2O$ (Ref. 1).

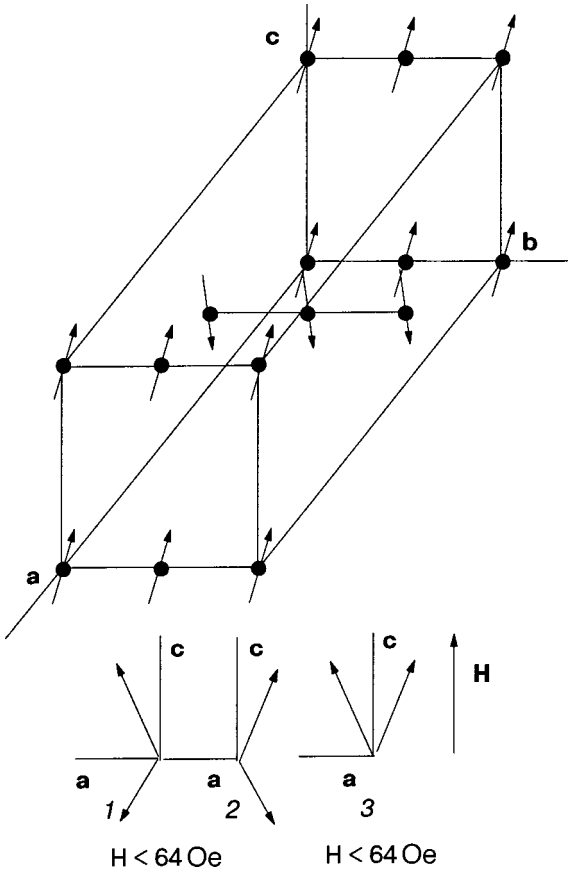

FIG. 2. Noncollinear magnetic structure of the compound $[(CH_3)_3NH]CoCl_3 \cdot 2H_2O$ (Ref. 3). The numbers label possible spin configurations.

netic structure of $[(CH_3)_3NH]CoCl_3 \cdot 2H_2O$ consists of Ising chains along the **c** axis, with a ferromagnetic intrachain exchange $J = 15.4$ K and an antiferromagnetic interchain interaction with $J' = -0.18$ K.

The magnetic structure of the compound $[(CH_3)_3NH]CoCl_3 \cdot 2H_2O$ was determined by Spence and Botterman[3] from the results of magnetization and NMR measurements. The structure in zero magnetic field is presented in Fig. 2. The magnetic moments of the chains lie in the *ac* plane and deviate from the **c** axis by an angle of the order of 10°, which leads to a nonzero magnetic moment along the **a** axis. Since in zero field the directions $\pm\mathbf{a}$ are physically indistinguishable, it is reasonable to assume that for $T < T_N$ the magnetic system of the sample consists of domains having opposite directions of the moment along the **a** axis. These possible configurations are labeled by the numbers *1* and *2* in Fig. 2. When a magnetic field is applied along the **c** axis, a metamagnetic phase transition is observed in a field of 64 Oe. The width of this transition is determined by the demagnetizing fields and can reach 500 Oe (configuration *3*). Above those fields the system is found in a ferromagnetic state. Groenendijk and van Duyneveldt[2] showed on the basis of magnetic susceptibility measurements that there exist three exchange interactions, which differ in sign and magnitude: a strong ferromagnetic interaction in the chain ($J_b = 13.8$ K), a much weaker interaction ($J_c = 0.28$ K) which orders the chains in the *bc* layer, and a still weaker antiferromagnetic interaction ($J_a = -0.032$ K) coupling the ferromagnetic layers, and that the region of short-range magnetic order in this quasi-one-dimensional structure extends to 15–17 K.

We made resonance absorption measurements on a complex of radio spectrometers with replaceable resonator cells. The polarization of the microwave field at the sample was perpendicular to the direction of the external magnetic field. The angular dependences of the absorption spectrum in the *ac* and *bc* planes were recorded at a fixed frequency. The accuracy of adjustment of the sample in the resonator with respect to the crystallographic axes and external magnetic field was $\pm 1°$. The temperature was measured by a gallium arsenide thermometer with an accuracy of 0.01 K or better in the temperature interval 1.8–4.2 K and to 0.2 K or better at the high-temperature end of the range.

EXPERIMENTAL RESULTS

Paramagnetic region

For $\mathbf{H} \| \mathbf{c}$ the absorption spectrum of the Co^{2+} ion in $[(CH_3)_3NH]CoCl_3 \cdot 2H_2O$ at a frequency of 71.59 GHz consists of two intense low-field lines $H_1 = 3.5$ kOe and $H_2 = 7.2$ kOe and three low-intensity lines at resonance fields of $H_3 = 19$ kOe, $H_4 = 22$ kOe, and $H_5 = 24.73$ kOe. Figure 3 shows an example of the recorded trace of the EPR spectrum of the Co^{2+} ion in this compound for $\mathbf{H} \| \mathbf{c}$. Of greatest interest are the two intense low-field components, the behavior of which we shall describe in more detail. Figure 4a shows the angular dependences of the resonance field for these components of the spectrum, taken in the *ac* plane. All of the measurements of the angular dependences were made at a temperature of 9.5 K. The observed doubling of each component of the spectrum attests to the presence of two nonequivalent centers for Co^{2+} ions in the unit cell. This nonequivalence is

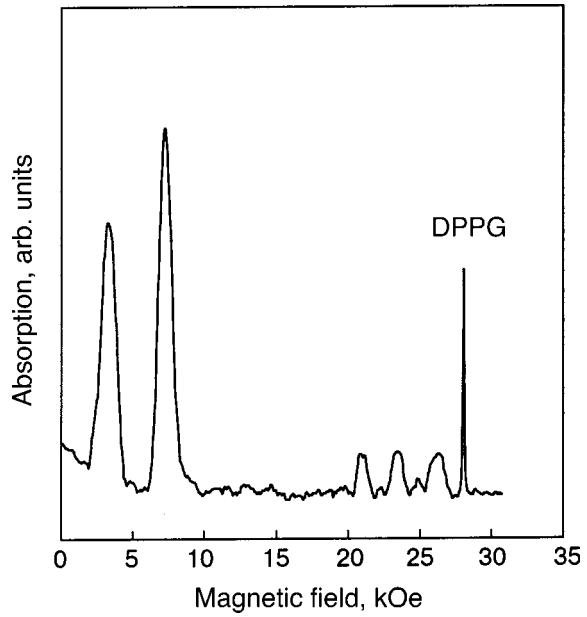

FIG. 3. A sample recording of the absorption spectrum of the Co^{2+} ion in the compound $[(CH_3)_3NH]CoCl_3 \cdot 2H_2O$ for $\mathbf{H} \| \mathbf{c}$. $T = 9.5$ K, $\nu = 71.59$ GHz. The narrow line is the reference signal of diphenyl picryl hydrazyl (DPPH).

expressed in a symmetric rotation of the magnetic axes of the centers in the ac plane relative to the direction of the **c** axis by an angle $\theta = \pm 12°$, while the other parameters of the centers remain identical.

For an Ising system the angular dependences of the resonance fields of the components $H_{\text{res}\,1}$ and $H_{\text{res}\,2}$ for each of the centers can be described by an expression of the form $H_{1(2)} = H_0 / \cos\theta$, since only the component of H along the z projection of the spin plays a role (the other parameters are equal to zero). The solid curves in Fig. 4 were calculated by the formulas

$$H_1 = H_{10}/\cos(\theta \pm \theta');$$

$$H_2 = H_{20}/\cos(\theta \pm \theta'). \quad (1)$$

We see that the angular dependences obtained experimentally are described quite satisfactorily by formulas (1). The deviation from the experimental dependences at large angles is indicative of nonideality of the Ising system (the experimentally determined value of g_x is nonzero).

The angular dependences of the resonance fields of the low-field components of the resonance spectrum in the bc plane are presented in Fig. 4b. It is seen that the structure of the absorption lines remains single at all angles. Furthermore, these curves do not intersect anywhere, as could be the case for two misoriented crystals. The crystallographic axis **b** coincides with the local magnetic axis **y**. The solid curves, as in Fig. 4a, were calculated according to formulas (1) with $\theta' = 0$. The angular dependence of the position of the absorption lines in the ab plane is extremely weak and not very informative.

For the three low-intensity lines presented in Fig. 3 the values of the effective g factors are $g_3 = 2.69 \pm 0.1$, $g_4 = 2.32 \pm 0.1$, and $g_5 = 2.06 \pm 0.1$. These lines have practically no angular dependence.

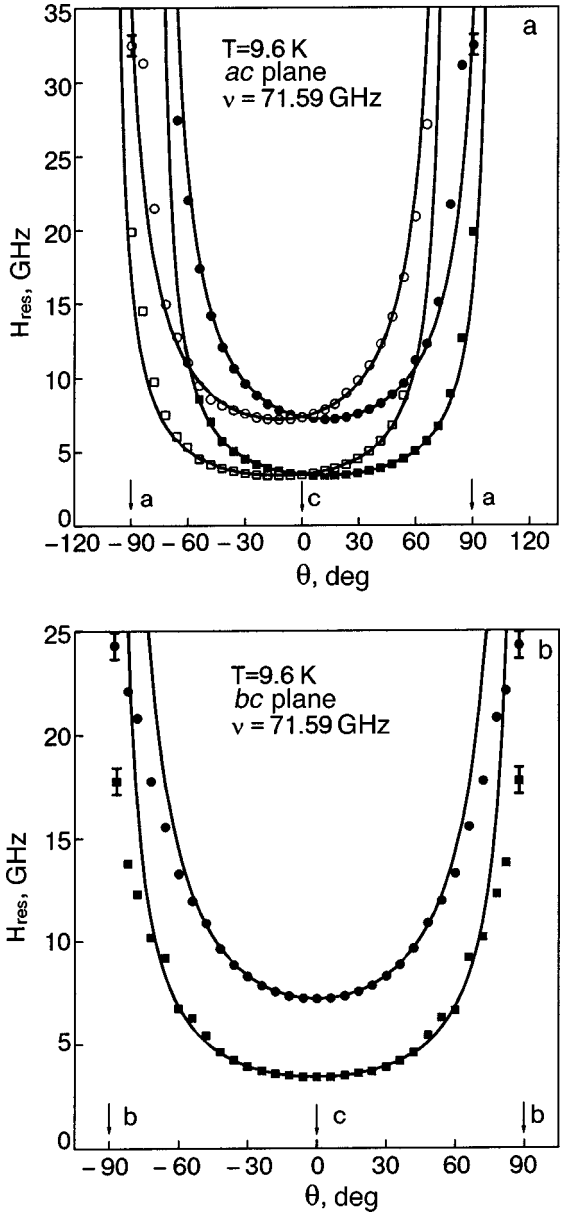

FIG. 4. Angular dependence of the resonance fields of the absorption lines of the Co^{2+} ion in the compound $[(CH_3)_3NH]CoCl_3 \cdot 2H_2O$ in the ac plane (a) and bc plane (b). The square and circular symbols denote the experimental values of the resonance fields for the two low-field lines investigated. The filled and unfilled symbols correspond to different centers. The solid curves were calculated using formulas (1).

To determine the values of the effective g factors in the direction of their maximum values, which is the direction of greatest interest, we studied the frequency–field dependence of the absorption spectrum of $[(CH_3)_3NH]CoCl_3 \cdot 2H_2O$ for an orientation of the external magnetic field along the **z** axis of the crystal (see Fig. 5). As was have said, two low-field absorption lines of the Co^{2+} ions are observed along this direction. The $\nu(H)$ curve obtained shows that in the frequency range 14–105 GHz the absorption lines in this compound are described, within the error limits, by a linear dependence. However, for the two absorption lines an initial splitting of $\Delta E_1 = 1.9$ kOe and $\Delta E_2 = 4.9$ kOe is observed. This linear dependence of the absorption spectrum is described by an expression of the form $\nu = \Delta E_{1(2)} + g_{1(2)}\mu_B H$. From the slopes of the straight lines we deter-

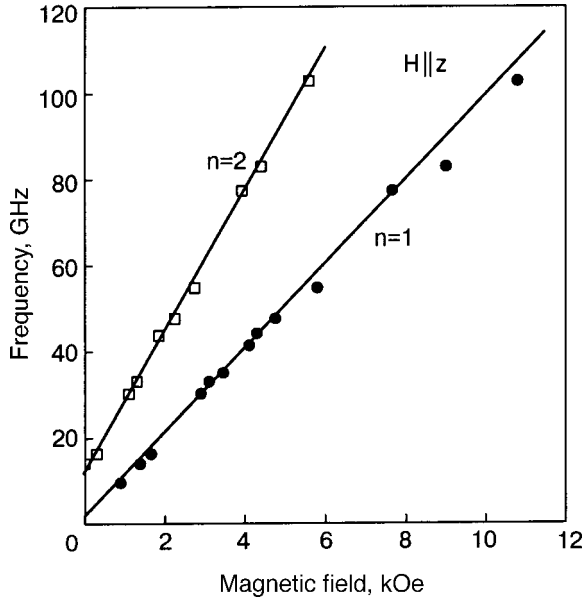

FIG. 5. Frequency–field dependence of the absorption spectrum of the Co^{2+} ion in the compound $[(CH_3)_3NH]CoCl_3 \cdot 2H_2O$ for $\mathbf{H} \| \mathbf{c}$. $T = 9.5$ K.

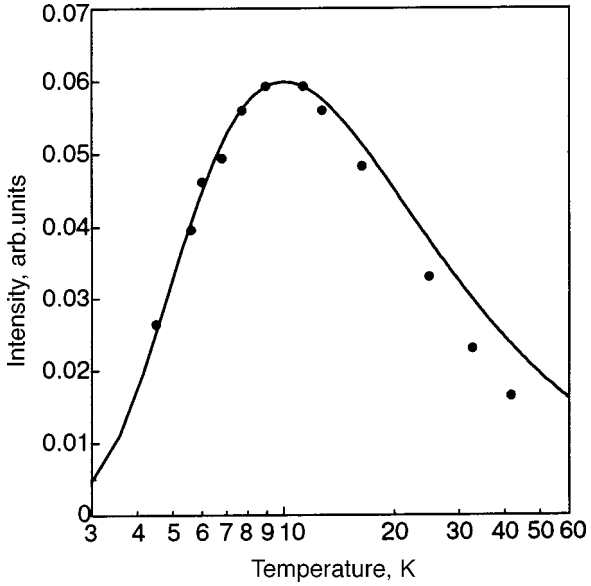

FIG. 6. Temperature dependence of the intensity of the absorption line of the compound $[(CH_3)_3NH]CoCl_3 \cdot 2H_2O$. The points are experimental, and the solid curve was calculated using formula (6), in the spin-cluster resonance model.

mined the values of the effective g factors along this axis of the crystal: $g_{1z} = 6.57 \pm 0.05$ for the first line and $g_{2z} = 11.8 \pm 0.05$ for the second.

The g factors along the other axes were determined in a similar way.

The experimentally measured effective g factors ($g_{1z} = 6.57$, $g_x = 1.91$, $g_y = 2.29$) confirm the conclusions of Ref. 1 that the compound $[(CH_3)_3NH]CoCl_3 \cdot 2H_2O$ can be described to a sufficient degree of accuracy by the Ising model.

The temperature dependence of the intensity of the low-field lines in the absorption spectrum of the Co^{2+} ion was investigated in the temperature interval 4.1–60 K in a static field applied along the local magnetic axis **z**. The main features of the variation of the spectrum are as follows. At a temperature close to $T_N = 4.13$ K the absorption spectrum is not observed. Starting at a temperature of 4.5–4.6 K one observes two narrow resonance lines of low intensity, with g factors $g_{z1} = 6.57 \pm 0.05$ and $g_{z2} = 11.8 \pm 0.05$. The fact that no critical broadening of the absorption line is observed in the investigated temperature interval apparently confirms that the ferromagnetic interaction is dominant in the system. With increasing temperature the peak intensity of the lines increases, reaching a maximum value at 9.5–11 K. The ratio of the intensities of the spectra is about 1:1.5, and the width of the two lines at half maximum in this temperature interval remains constant and equal to 920 Oe. Further increase in temperature leads to a decrease of the intensity of the spectrum without altering the linewidth, and only above 31 K does substantial broadening of the absorption lines occur; after $T = 34$ K the line with the lowest intensity is hardly observed, but the second line is discernable to 60 K and has a width of 3500 Oe. In the whole temperature interval investigated the position of all the lines with respect to magnetic field remains practically unchanged. The described temperature behavior of the absorption intensity of the low-field line is shown in Fig. 6.

The temperature behavior of the high-field lines differs from the that described above for the low-field lines. As we have pointed out, at a temperature of 4.5 K one observes three low-intensity absorption lines. With increasing temperature their intensity decreases, and for $T > 15$ K they are no longer observed.

Magnetically ordered phase

We did a study of the frequency–field dependence of the magnetic resonance $\nu(H)$ of the compound $[(CH_3)_3NH]CoCl_3 \cdot 2H_2O$ in the frequency interval 30–112 GHz and at magnetic fields up to 80 kOe at a temperature $T = 1.8$ K.

The results of these measurements for an orientation of the external magnetic field along the crystallographic directions **a**, **b**, and **c** are presented in Fig. 7. Analysis of the magnetic structure and studies of the magnetization and metamagnetic transition show that the easy axis in this compound is along the **c** direction and the hard axis is along **b**.

If the external magnetic field **H** is directed along the easy axis **c**, then the observed $\nu(H)$ dependence is described within the experimental error by a quadratic function increasing with field. As $H \to 0$ the spin-wave spectrum has a gap equal to 70.1 ± 0.1 GHz. As we have mentioned, a magnetic field applied along the **c** axis will lead to a metamagnetic phase transition, which for $H = 64$ Oe takes the system to a ferromagnet state.[3]

When the external magnetic field **H** is oriented along the **a** axis (the intermediate direction), at a frequency of 47.6 GHz one observes two FMR absorption lines, at fields $H_1 = 5.8$ kOe and $H_2 = 32.5$ kOe. For $\nu > 52.5$ GHz the low-field component is not detected. Unfortunately, because of the strong magnetization of the crystal along this direction, with long relaxation times (several hours), we were unable to measure the frequency–field dependence in this frequency

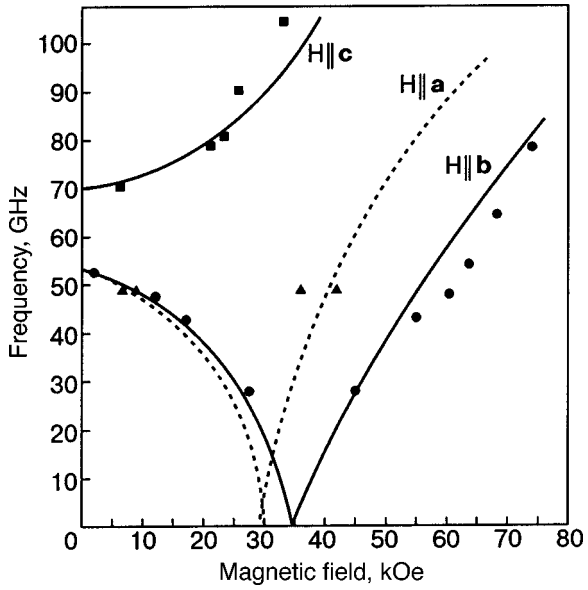

FIG. 7. Frequency–field diagram of the ferromagnetic resonance in the crystal $[(CH_3)_3NH]CoCl_3 \cdot 2H_2O$ for the crystallographic directions **a**, **b**, and **c**. $T = 1.8$ K. The lines are drawn for convenience and represent a qualitative description of the diagram of a two-dimensional biaxial ferromagnet.

interval. However, extrapolation of the experimental dependence to $\nu \to 0$ gives a value of the transition field $H_{cr1} \approx 29$ kOe.

When the external magnetic field is oriented along the hard (**b**) axis, one observes a softening of the resonant mode, and at $H = 35$ kOe its frequency goes to zero. Above a frequency of 52.5 ± 0.1 GHz the soft mode in the FMR spectrum was not detected.

Thus, as can be seen in Fig. 7, for $H \to 0$ there are two gaps in the spectrum of resonance excitations of the spin-wave system, equal to 70.1 ± 0.1 and 52.5 ± 0.1 GHz.

DISCUSSION OF THE RESULTS

Paramagnetic region

It is known that at low temperatures the EPR spectrum of the Co^{2+} ion in a distorted octahedral environment is usually single-component and is described by an effective spin $S = 1/2$ with a sharply anisotropic effective g factor. Here the local magnetic axes of the paramagnetic center corresponding to the extremal values of the g factor are determined by the symmetry and character of the intracrystalline field, and the sum of the principal values of the effective g factor does not exceed 13.[4] As a rule, observations of the EPR spectrum are made at low temperatures. Increasing the temperature leads to a sharp broadening of the resonance line and a decrease in its intensity.

The resonance absorption spectrum of the compound $[(CH_3)_3NH]CoCl_3 \cdot 2H_2O$ differs appreciably from those which are usually observed. The characteristic features of the absorption spectrum of the Co^{2+} ion in the paramagnetic phase of the multisublattice magnet $[(CH_3)_3NH]CoCl_3 \cdot 2H_2O$ cannot provide an explanation for the following experimental facts: the presence of several absorption lines with values of the g factor exceeding the limiting values for a "nearly free" ion, the presence of initial splitting in the excitation spectrum, and anomalous temperature behavior of the intensity of the low-field absorption lines. These effects may result from features of the magnetic structure and exchange interactions in this system. As was pointed out above, in this quasi-one-dimensional system the region of short-range magnetic order extends to 15–17 K, making it possible to treat it above the magnetic ordering point as a set of weakly coupled ferromagnetic ordered chains, the length of which (the correlation length) depends on the temperature.

To explain the experimental results we have used the spin-cluster model first introduced by Date and Motokawa[5] for explaining the magnetic resonance in the quasi-one-dimensional Ising ferromagnet $CoCl_2 \cdot 2H_2O$. The ratio of the effective g factors for $[(CH_3)_3NH]CoCl_3 \cdot 2H_2O$ also permit one to describe its quasi-one-dimensional magnetic structure in a first approximation by an Ising model of exchange interactions.

The concept of spin clusters, according to the model of Date and Motokawa, is based on the assumption that an exchange-coupled ferromagnetic Ising chain contains thermally excited groups of spins whose moments are flipped with respect to those in the rest of the chain. A spin-cluster resonance consists in the excitation (flip) of one ($n = 1$) or several ($n = 2$, 3, etc.) of these spins at the edge of the cluster under the influence of a high-frequency field. The Hamiltonian of this system has the form

$$H = -2J \sum_i S_i S_{i+1} - g_z \mu_B H \sum_i S_i . \tag{2}$$

With the weak interactions taken into account, one obtains the following expression[6] for the energy of excitation of n-fold clusters in an Ising ferromagnetic chain with effective spin $S = 1/2$:

$$E_n = 2|J| + n \sum_i \alpha_i J_i + n \mu \mathbf{H}, \tag{3}$$

where α_i contains information about the features of the local magnetic ordering; $\mu = g \mu_B S$ is the magnetic moment of the site of the chain, and n is the number of sites in the cluster. Since the exchange interaction in the chain along the **b** axis is $J/k = 15.4$ K, at low temperatures the excited level will be found a distance 22 cm^{-1} above the ground state, and there will be no absorption in a microwave field. As the temperature is raised, however, when thermally excited spin clusters appear, it becomes possible to observe transitions within the excited level, which correspond to a change in the number of cluster sites n, i.e., an additional flip of one or several spins at the edge of the cluster. The frequency of such a resonant transition will be determined by the change in the energy of the system upon a change in the cluster length by n sites:

$$h\nu = n(\Delta E + 2\mu H), \tag{4}$$

where

$$\Delta E = 4J_2 + 2J_1, \tag{5}$$

and J_1 and J_2 are the weak ferromagnetic and weak antiferromagnetic exchange parameters. Date and Motokawa called these transitions "spin-cluster resonance."

Starting from this model, one can interpret the results on the frequency–field curves (Fig. 5) of the absorption spec-

trum of the compound $[(CH_3)_3NH]CoCl_3 \cdot 2H_2O$. The solid lines correspond to expression (4) for the cases $n=1$ and $n=2$, according to which the angular coefficients are proportional to the values of the effective g factors for the two components of the spectrum, and the initial splittings $\Delta E_{1(2)}$ should differ by a factor of two. The values obtained, $g_{1z}=6.57\pm0.05$, $g_{2z}=11.8\pm0.05$ and $\Delta E_1=1.9$ kOe, $\Delta E_2=4.9$ kOe have close to this ratio.

Using these values, we can estimate the exchange parameters of the system under study. Recall that the magnetic structure of the compound $[(CH_3)_3NH]CoCl_3 \cdot 2H_2O$ can be regarded as a set of ferromagnetic chains with a weak interchain ferromagnetic interaction, and the ferromagnetic planes are coupled by a very weak antiferromagnetic exchange. Therefore an external field $H_c=64$ Oe applied along the axis of anisotropy breaks the weak antiferromagnetic interactions and brings the system to a ferromagnetic state.

In the effective-field model the interplane exchange can be estimated from the relation $2zJ_2S^2=g\mu_B SH_c$ with $z=4$, $S=1/2$, and $g=6.57$; this gives a value $J_2=-0.007$ K. An estimate of J_1 from expressions (4) and (5) gives values of 0.16 K ($n=1$) and 0.202 K ($n=2$), the average value being $J_1=0.18$ K. Then, using the well-known Onsager formula for a rectangular Ising lattice,[7] $\sinh(J/kT_N)\sinh(J_1/kT_N)=1$, and the averaged value of J_1, we obtain $J=15.6$ K. This estimate is in good agreement with the values obtained by other authors: 15.4 K,[1] 13.3 K,[2] and 14.7 K,[6] and the ratios of the exchange parameters obtained on the basis of these results confirm the high degree of magnetic one-dimensionality of the system under study.

A characteristic feature of the spin-cluster resonance is the anomalous temperature dependence of the absorption intensity I in comparison with the usual magnetic resonance. According to Refs. 8 and 9, for a ferromagnetic Ising chain the absorption intensity is described by the expression

$$I=\exp(-2J/kT)[1-\exp(-\xi g\mu_B H/kT)], \tag{6}$$

where $\xi=[-\ln\{\tanh(|J|/2kT)\}]^{-1}$ is the correlation length for a one-dimensional Ising magnet.[10]

Figure 6 shows the temperature dependence of the absorption intensity (the solid curve) calculated according to formula (6) for an $n=2$ cluster, where $J/k=15.4$ K and $g\mu_B H=3.43$ K. It can be seen from Fig. 6 that the qualitative and quantitative description of the experimental data is quite good. The slight disagreement at high temperatures is apparently due to the broadening of the line and the error in the estimate of the intensity. Furthermore, expression (6) was obtained for an isolated Ising chain without taking the weak interchain interactions into account. The temperature behavior of the intensity of the absorption line for an $n=1$ cluster was calculated in an analogous way. The resonance line for clusters of greater length ($n>2$) are not observed experimentally. This is apparently because the correlation length λ of the chain decreases rapidly with increasing temperature, and $l\approx2$ at typical experimental temperatures.

Thus the spin-cluster resonance model gives a rather good description of the resonance properties of the Co^{2+} ion in the $[(CH_3)_3NH]CoCl_3 \cdot 2H_2O$ lattice in the paramagnetic phase.

The presence of low-intensity high-field lines in the spectrum may be due, we believe, to the presence of paramagnetic impurity ions or defects in the system. This is confirmed by the characteristic features of the those lines: the values of the g factors, the absence of anisotropy in them, and the temperature behavior of the absorption intensity.

Magnetically ordered phase

It should be noted that although the three-dimensional magnetic ordering in $[(CH_3)_3NH]CoCl_3 \cdot 2H_2O$ is of an antiferromagnetic character, in a real resonance experiment one actually studies a ferromagnetic structure, since, as we have said, for $H\to0$ there is a metamagnetic phase transition to a ferromagnetic structure.

Therefore, for describing such a system one can use the Hamiltonian of a one-sublattice ferromagnet with an orthorhombic structure, which has the following general form:

$$\mathcal{H}=-\frac{1}{2}\sum_{l,m} J_{l,m}\mathbf{S}_l\cdot\mathbf{S}_m-D\sum_l (S_l^2)^2-E \times\sum_l [(S_l^x)^2-(S_l^y)^2]+g\mu\mathrm{H}_i\sum_l S_{l_i}, \tag{7}$$

where the first term describes the exchange interaction, the second and third terms describe the contribution of the axial and rhombic anisotropies, and the last term takes the external magnetic field into account.

It should be noted that the influence of orthorhombicity on the FMR spectrum was observed previously in the compound $[(CH_3)_3NH]NiCl_3 \cdot 2H_2O$ by the authors in Ref. 11. In that paper, theoretical expressions were obtained for the frequency–field dependences of the magnetic resonance in a one-sublattice model with $S=1$ and an external field direction perpendicular to the local axis **z**, which satisfactorily describes the experimental curves. However, the authors did not find the absorption spectrum along the easy axis.

The solution of this Hamiltonian for ferromagnets with spin $S=3/2$ and a theoretical description of the frequency–field curves have not been given in the literature. Nevertheless, the dependences obtained experimentally correspond qualitatively to the behavior of the resonance frequencies obtained in Ref. 11 for an orthorhombic ferromagnet in external magnetic fields directed parallel and perpendicular to the easy axis **c**. This made it possible for us to measure the axial D and rhombic E anisotropy constants and also to estimate the critical fields of the phase transitions in a magnetic field, which have the values $H_{cr1}\approx29$ kOe, $H_{cr2}\approx35$ kOe, $D=18.75$ kOe, and $E=6.28$ kOe.

Apparently this is the first experimental observation of the frequency–field dependences in a biaxial quasiferromagnet along all three crystallographic directions.

CONCLUSIONS

Our resonance studies of the compound $[(CH_3)_3NH]CoCl_3 \cdot 2H_2O$ in the paramagnetic and magnetically ordered phases permit the following conclusions.

1. The angular dependences of the absorption lines at a temperature $T>T_N$ provide grounds for stating that two magnetically nonequivalent centers arise, with an angle of rotation relative to the **c** axis of $\theta'=\pm 12°$.

2. Above T_N in the short-range order region one observes a spin-cluster resonance in strongly exchange-coupled Ising ferromagnetic chains.

3. For temperatures $T<T_N$, in the magnetically ordered phase, we have obtained the ferromagnetic resonance curves $\nu(H)$. We have shown that for $H=0$ ($\mathbf{H}\|\mathbf{b}$) and $H\to 0$ ($\mathbf{H}\|\mathbf{c}$), two gaps exist in the spin-wave spectrum of the the quasiferromagnet $[(CH_3)_3NH]CoCl_3\cdot 2H_2O$. We have determined the values of the effective magnetic interaction parameters in this crystal.

We should point out in closing that only the preliminary experimental results have been presented in this report, and our study of $[(CH_3)_3NH]CoCl_3\cdot 2H_2O$ continues.

*E-mail: khatsko@ilt.kharkov.ua

[1] D. B. Losee, J. N. McElearney, G. E. Shankle, R. L. Carlin, P. J. Cresswell, and W. T. Robinson, Phys. Rev. B **8**, 2185 (1973).
[2] H. A. Groenendijk and A. J. van Duyneveldt, Physica B **115**, 41 (1982).
[3] R. D. Spence and A. C. Botterman, Phys. Rev. B **9**, 2993 (1974).
[4] W. Low, in *Solid State Physics*, Suppl. 2, Academic Press, New York (1960), *Paramagnetic Resonance in Solids* [Russian trans.], IL, Moscow (1962).
[5] M. Date and M. Motokawa, Phys. Rev. Lett. **16**, 1111 (1966).
[6] A. C. Phaff, C. H. W. Swüste, and W. J. M. de Jonge, Phys. Rev. B **25**, 6570 (1982).
[7] L. Onsager, Phys. Rev. **65**, 117 (1944).
[8] M. Date and M. Motokawa, J. Phys. Soc. Jpn. **24**, 41 (1968).
[9] Y. Ajiro, K. Adachi, and T. Sharyo, J. Phys. Soc. Jpn. **50**, 1 (1981).
[10] M. Steiner, J. Villain, and C. G. Windsor, Adv. Phys. **25**, 87 (1976).
[11] A. G. Anders, V. G. Borisenko, S. V. Volotskii, and Yu. V. Pereverzev, Fiz. Nizk. Temp., **15**, 39 (1989) [Sov. J. Low Temp. Phys. **15**, 21 (1989)].

Translated by Steve Torstveit

On correlated heterogeneities of glass-forming liquids

A. S. Bakai*

National Science Center "Kharkov Institute of Physics and Technology," 61108 Kharkov, Ukraine
(Submitted June 3, 2002)
Fiz. Nizk. Temp. **28**, 1260–1273 (December 2002)

The thermodynamics and structure of glass-forming liquids are considered within the framework of the heterophase fluctuation (HPF) model. The main goal of the theory developed is to find a description for the long-range correlations (LRC) of the density fluctuations known as the Fischer cluster. The van der Waals approximation of the HPF model shows that the liquid can have an isolated solid–fluid critical point analogous to the critical point of a gas–liquid system. Heterophase fluctuations in the form of solidlike noncrystalline and fluidlike clusters can have LRC in a narrow vicinity of the critical point. An analysis shows that the properties of the conventional critical fluctuations differ from those of the Fisher cluster. This forces one to look for another explanation of the observed LRC in glass-forming liquids. Large configurational entropy of liquids and glasses is a manifestation of multiplicity of the short-range ordering of molecules in the amorphous solidlike and fluidlike clusters. The multiplicity of short-range order results in structural heterogeneities. Random-field Ginzburg–Landau equations for the HPFs are deduced taking into account the structural heterogeneities. The random field is generated by these heterogeneities. It is found that at least three characteristic correlation scales are inherent to the HPFs: the radius of local order, r_0, which is comparable with the radius of the first coordination sphere; the random-field-controlled radius of critical fluctuations, R_c; the average correlation length ξ_{av} of fractal aggregations formed by the correlated domains (the domains have size $\sim R_c$). The length ξ_{av} is the characteristic size of the Fischer cluster. The conditions for the appearance of the listed correlations are deduced by requiring that they provide minimization of the free energy of the system. The annealing kinetics and dynamics (the ultraslow modes) of the Fischer cluster are described. [DOI: 10.1063/1.1531394]

1. INTRODUCTION

Structural and dynamic heterogeneities of the glass-forming liquids have wide spectrum of space and time scales, see, e.g., Ref. 1 and the references cited therein. The most mysterious is the phenomenon of long-range correlations (LRC) of the density fluctuations (Fischer cluster) discovered and investigated during the last decade.[2–9] In a wide temperature range above the glass transition temperature T_g, the correlation length of density fluctuations is much larger than the molecule size. The annealing time of the Fischer cluster is many orders of magnitude larger than the α-relaxation time τ_α. The main peculiarities of the Fischer cluster are following:

1) It exists in a rather large temperature range, ~100 K, above T_g.

2) The correlation length is up to 300 nm, while the short-range order (SRO) radius $r_0 \sim 1$ nm.

3) No critical behavior of the heat capacity, compressibility, and thermal expansion coefficient is observed above T_g.

4) The density fluctuations have a fractal structure of dimension $D<3$. The dimension depends on the temperature T and the substance. It differs from the universal critical exponent of the pair correlation function.

5) Ultraslow modes characterizing the Fischer cluster dynamics are some orders of magnitude faster than the Fischer cluster equilibration (annealing) time.

The α-relaxation is insensitive to the Fischer cluster formation. The ultraslow dynamics is considerably slower than the α-relaxation processes.

A few papers are devoted to theory of the Fischer cluster.[10–12] The approach proposed in[10] to description of the fluctuation patterning is not completed as yet. In Ref. 11 the LRC are treated as long-range critical fluctuations. They are described within the framework of a two-order-parameter model. But the features 3)–5) still have no proper explanation in Ref. 11.

In Ref. 12 it is shown that the LRC appears as result of aggregation of heterophase correlated domains (CDs) having the same short-range order. This paper is devoted to a further development of the theory.

We start from the idea that the glass-forming liquids have heterophase mesoscopic structure consisting of solidlike and fluidlike species. The average lifetime of each species is comparable with the α-relaxation time τ_α. As a result of the rearrangements the species change their SRO and type (solidlike species become fluidlike and vice versa) but the average concentration of the species possessing a specified SRO is constant at a fixed pressure P and temperature T. The fraction of molecules belonging to the solidlike species, $n_s(x,t)$, is chosen as the order parameter. It is a random field due to the randomness of the configurations formed by the species. The correlation properties of these configurations have to be found by minimization of the free energy of the

system. These ideals form the basis of the heterophase fluctuation model of the glass-forming liquids. For brevity a liquid with developed heterophase fluctuations (HPFs) will be called a heterophase liquid.

In one form or another the idea of an important role of HPFs in the liquid-to-glass transition has been used in many treatments of the glass-forming liquids. In Refs. 13–23 the free energy of the heterophase liquid is described in the mean field approximation. Equations proposed in Refs. 12, 14, 15, 17, 22, 23 show that the heterophase liquid can have a critical point. Moreover these equations are isomorphic to the van der Waals theory of the gas–liquid critical point (see below). By adding a gradient term to the van der Waals free energy one can get the Ginzburg–Landau (GL) description of the gas–liquid states.[24] The same procedure allows one to use the GL equation for heterophase liquids.[25] Assuming that the supercooled liquid above T_g is close to the critical point, one can get a description of the correlation phenomena in heterophase liquids. Apparently the formation of a Fischer cluster possessing the properties 3)–5) cannot be treated as conventional critical fluctuations. This way of explaining the LRC fails. To come up with a solution of the problem while staying in the framework of the HPF model, one has to take into account the SRO statistics and correlations. The free energy of a heterophase liquid is a functional of the order parameter and of the space distributions of the species possessing different SRO. In seeking the free energy one is led straightforwardly to the random-field Ginzburg–Landau model (RFGLM).[12] Subsequent minimization of the free energy shows when and why the aforementioned correlations are beneficial.

It should be noted that the mean field approach is valid only outside the fluctuational critical region[24] and that the location and size of fluctuational region depend strongly on the random field properties. Therefore the applicability conditions of the mean field model have to be checked.

The outline of this paper is as follows. Theoretical models of heterophase liquid states are considered in Sec. 2. The free energies of solidlike and fluidlike clusters are formulated in terms of constituent species possessing different free energies. The space distribution of these species in the framework of mean field theory (MFT) are described by fields $\mu_s(P,T,x)$, $\mu_f(P,T,x)$; the subscripts s and f mean solidlike and fluidlike, respectively. With the space-averaged quantities $\overline{\mu}_s(P,T)$ and $\overline{\mu}_f(P,T)$ the free energy takes the form of a two-species model which, as is shown below, is isomorphic to the van der Waals theory of a gas–liquid system. A generalization of the van der Waals theory including the gradient term and random fields $\mu_s(P,T,x)$ and $\mu_f(P,T,x)$ is the Ginzburg–Landau random-field model. Equations of this model are deduced. Short-range and long-range correlations of the random fields are investigated in Sec. 3. A theory of the critical point in the framework of RFGLM is developed in Sec. 4. Section 5 is devoted to the static properties of the long-range density fluctuations, while the dynamics of the heterophase fluctuations including description of the ultraslow modes and annealing kinetics of the Fischer cluster are considered in Sec. 6. The conclusion in Sec. 7 includes a discussion of the theory developed.

2. THEORETICAL MODELS OF THE HETEROPHASE LIQUIDS

The phenomenological description of heterophase liquids (HPLs) usually starts with the introduction of the basic thermodynamic quantities μ_f, μ_s and $\mu_{\rm int}$, which are chemical potentials of the ''pure'' fluid and solid phases and of the interface, respectively. This last one for simplicity is assumed to be independent of the interface geometry. Here we are interested in consideration of the liquid states with comparable fractions of the solidlike and fluidlike clusters,

$$0.15<n_s,n_f<0.85, \tag{1}$$

where $n_f=1-n_s$ is the fraction of fluidlike clusters. The numbers 0.15 and 0.85 are the percolation thresholds of the clusters.[26] The condition (1) means that the solidlike and fluidlike species form interpercolating clusters.

The interpercolating heterophase states form easily when the interfacial free energy is small,

$$0<\Delta\mu_{\rm int}\ll T, \tag{2}$$

where

$$\Delta\mu_{\rm int}=\mu_{\rm int}-\frac{1}{2}(\mu_f+\mu_s). \tag{3}$$

The condition (2) provides for comparatively small (positive) contributions from the interfaces to the free energy of the system. As a result of that, the interface turns out to be rather developed to gain large phase-mixing entropy. Because the phase formation is a cooperative phenomenon, single molecules can not be statistically independent species in the heterophase states. The phase miscibility is characterized by the associativity parameters k_0. It determines the size of statistically independent units in calculations of the mixing entropy. Evidently, $k_0>1$.

2.1. Chemical potentials of the pure phases

Macroscopically homogeneous condensed amorphous phases-liquid and (or) noncrystalline solids-are heterogeneous on microscopic scales due to multiplicity of the SRO. The number of structure states of N molecules ($N\gg1$) in these states can be presented in the following form (see, e.g., Ref. 27)

$$W_i(N)=\exp(\zeta_i N),\quad i=s,f, \tag{4}$$

ζ_i is the configurational entropy of ergodic states, or the complexity of nonergodic states,

$$s_{c,i}=k_B\zeta_i, \tag{5}$$

and k_B is Boltzmann's constant.

The multiplicity of the structure states reflects randomness of the potential relief of molecules. The set of minima of the relief is often called inherent structures.[27,28] The distribution of the potential energy minima, $\psi(\varepsilon,N)$, describing the density of structure states of a solid cluster in liquid, is[21]

$$\psi_s(\varepsilon,N)=\frac{N}{\sqrt{2\pi\delta_s^2}}\exp\{N[\zeta_s-(\varepsilon-\overline{\varepsilon_s})^2/2\delta_s^2]\}, \tag{6}$$

where ε is the potential energy per molecule at a minimum, $\overline{\varepsilon_s}$ is its average value, and δ_s^2 is the variance per molecule.

The chemical potential of a noncrystalline solid cluster can be presented in the following form:

$$\mu_s(P,T,x)=\overline{\mu_s}(P,T)+\tilde{\mu}_s(P,T,x), \tag{7}$$

where $\overline{\mu_s}$ is the average value and $\tilde{\mu}_s$ describes variations of the chemical potential due to randomness of the potential relief. Ignoring dependence of the molecule vibrations and librations on the depth of the potential well, we have $\tilde{\mu}_s(x) \approx \varepsilon(x)-\overline{\varepsilon_s}$.

The first and second moments of this random quantity are

$$\langle\tilde{\mu}_s(x)\rangle=\frac{1}{V}\int \tilde{\mu}_s(x)d^3x=0,$$

$$\langle\tilde{\mu}_s(x)\rangle^2=\frac{1}{V}\int \tilde{\mu}_s^2(x)d^3x=\delta_s^2. \tag{8}$$

Here V is volume of the system, and $\langle ... \rangle$ means the ensemble average, which is equal to space average by virtue of ergodicity.

For $\overline{\mu_s}$ the following expression is obtained:[21]

$$\overline{\mu_s}(P,T)=\overline{\varepsilon_s}-\frac{\delta_s^2}{T}-s_{c,s}T+\mu_{s,\mathrm{vib}}(P,T)+P\upsilon_s. \tag{9}$$

Here $\mu_{s,\mathrm{vib}}$ is the vibrational part of the chemical potential, and υ_s is the specific volume.

In analogy with (6)–(9) the chemical potential of the fluid phase can be written as

$$\mu_f(P,T,x)=\overline{\mu_f}(P,T)+\tilde{\mu}_f(P,T,x), \tag{10}$$

$$\overline{\mu_f}(P,T)=\overline{\varepsilon_f}-\frac{\delta_f^2}{T}-s_{c,f}T+\mu_{f,\mathrm{vib,trans}}(P,T)+P\upsilon_f. \tag{11}$$

In the last term the translational mode of the motion is included.

The moments of $\tilde{\mu}_f(x)$, like (8), are

$$\langle\tilde{\mu}_f(x)\rangle=0,\ \langle\tilde{\mu}_f^2(x)\rangle=\frac{1}{V}\int \tilde{\mu}_f^2(x)d^3x=\delta_f^2. \tag{12}$$

2.2. Mean field model of HPFs (van der Waals approximation)

The average chemical potentials of the phases, $\overline{\mu_s}(P,T)$ and $\overline{\mu_f}(P,T)$, determined by (9) and (11), respectively, are used in this approximation. The chemical potential of the heterophase liquid is[22]

$$\begin{aligned}\mu(P,T)=&\overline{n_s}\,\overline{\mu_s}(P,T)+(1-\overline{n_s})\,\overline{\mu_f}(P,T)\\&+\overline{n_s}(1-\overline{n_s})\Delta\mu_{\mathrm{int}}(P,T)+k_0^{-1}T[\overline{n_s}\ln\overline{n_s}\\&+(1-\overline{n_s})\ln(1-\overline{n_s})],\end{aligned} \tag{13}$$

where $\overline{n_s}$ is the average value of the order parameter.

The solid–fluid coexistence curve on the (P,T) plane is determined by the equation

$$\overline{\mu_s}(P,T)=\overline{\mu_f}(P,T). \tag{14}$$

The equilibrium value of the order parameter $\overline{n_s}$ is determined by the equations

$$\frac{\delta\mu(P,T)}{\partial\overline{n_s}}=0, \tag{15}$$

$$\frac{\partial^2\mu(P,T)}{\partial\overline{n_s^2}}>0. \tag{16}$$

It follows from (13)–(16) that on the coexistence curve

$$\overline{n_s}(P,T)=1/2. \tag{17}$$

The solution of this equation, which is a direct analog of the critical isochore in the van der Waals theory of the gas–liquid critical point, gives the pressure dependence of the coexistence temperature $T_e(P)$, at which both phases are in equilibrium.

Routine analysis[22] shows that (15) has only one stable solution with

$$0<\Delta\mu_{\mathrm{int}}|_{T_e}<\frac{2T_e(P)}{k_0}. \tag{18}$$

If

$$\Delta\mu_{\mathrm{int}}|_{T_e}>\frac{2T_e(P)}{k_0}, \tag{19}$$

then Eq. (15) has three solutions in the vicinity of

$$T_c=T_e(P_c)=k_0\Delta\mu_{\mathrm{int}}/2. \tag{20}$$

Equation (20) determines the location of an isolated critical point on the coexistence curve. At this point a second-order phase transition takes place. On the coexistence curve below the critical point a first-order phase transition takes place. A continuous phase transformation with crossing of the coexistence curve occurs above the critical point. The condition $\Delta\mu_{\mathrm{int}}>0$ in (17) is needed to provide the phase separation in the supercritical region.

It is worth noting once again that the expression (13) is isomorphic to the free energy of a liquid–gas system in van der Waals theory (see Ref. 24), but the order parameter used here is different. This follows immediately from (26) after omitting the gradient term and putting $h=\overline{\mu_s}-\overline{\mu_f}$.

An approximate solution of (13), (15) with the condition (18) is

$$\overline{n_s}\approx\frac{1}{1+\exp(H\beta)}, \tag{21}$$

where

$$H=\frac{k_0[\overline{\mu_s}(T)-\overline{\mu_f}(T)]}{1-k_0\Delta\mu_{\mathrm{int}}/2T_e(P)}. \tag{22}$$

In the vicinity of the coexistence curve

$$\begin{aligned}&\mu_s(T)-\mu_f(T)\approx\Delta s(T_e)(T-T_e),\\&\Delta s(T_e)=s_f(T_e)-s_s(T_e).\end{aligned} \tag{23}$$

Here $s_s(T)$, $s_f(T)$ is the entropy per molecule in the solid and fluid states, respectively.

Equation (21) describes the evolution of the order parameter with a continuous phase transformation.

It should be pointed out that the two-state, two-species, two-phase models considered in Ref. 13–17 formally are particular cases of (or can be presented in the form of) Eqs. (13)–(16).

As is shown in Ref. 23, the mean field approach developed gives a reasonable description of the observed continu-

ous phase transformation in glass-forming liquids. Along with that, the above-mentioned LRC are outside the framework of this model.

2.3. Random-field Ginzburg–Landau model

The GL approach allows one to investigate the structure of HPFs in the vicinity of critical points. Near the coexistence curve the free energy with the fields $\nabla n_s(P,T,x)$ and $\tilde{\mu}_s(P,T,x)$, $\tilde{\mu}_f(P,T,x)$ taken into account can be presented in the GL form:[27]

$$G = G_0 + G_1, \tag{24}$$

$$G_0 = N\overline{\mu}(P,T_e), \tag{25}$$

$$G_1 = \frac{1}{\upsilon}\int\left[\frac{1}{2}A(\nabla\alpha)^2 + \frac{1}{2}B\alpha^2 + \frac{1}{4}C\alpha^4 - h\alpha\right]d^3x, \tag{26}$$

where υ is the specific volume,

$$\alpha \equiv \alpha(P,T,x) = n_s(P,T,x) - \overline{n_s}(P,T_e) = n_s(P,T,x) - \frac{1}{2}, \tag{27}$$

$$B \equiv 4k_0^{-1}T - 2\Delta\overline{\mu}_{\rm int}(P,T) + \tilde{\mu}_s(x) + \tilde{\mu}_f(x)$$
$$\equiv 4k_0^{-1}T - \Delta\overline{\mu}_{\rm int}(P,T) + \tilde{\mu}_{\rm int}(x), \tag{28}$$

$$C = 16k_0^{-1}T/3, \tag{29}$$

$$h = \overline{\mu}_s(P,T) - \overline{\mu}_f(P,T) + \tilde{\mu}_s(P,T,x) - \tilde{\mu}_f(P,T,x)$$
$$= \overline{h} + \tilde{h},$$

$$\overline{h} = \overline{\mu}_s - \overline{\mu}_f; \quad \tilde{h}(x) = \tilde{\mu}_s(x) - \tilde{\mu}_f(x). \tag{30}$$

The coefficient A is connected with the interfacial energy,

$$A = r_0^2 A_0 \sim r_0^2 \Delta\mu_{\rm int}, \tag{31}$$

and r_0 is the correlation radius outside the critical region; it is comparable with the molecular size. Apparently the associativity parameter k_0 is proportional to r_0^3,

$$k_0 \sim (r_0/a)^3, \tag{32}$$

where a is the characteristic size of a molecule.

With $\tilde{h}=0$, $\nabla n_s(P,T,x)=0$, and $\tilde{\mu}_{\rm int}=0$ the equations (24)–(26) are equivalent to (13) with accuracy $O(\alpha^6)$. In this case the free energy (26) is isomorphic to that of the van der Waals theory of the critical point.

The random field $\tilde{h}(x)$ plays an important role in the formation of the order parameter and density fluctuations in the vicinity of T_c.

Equation (26) implies the saddle-point equation:

$$-A\Delta\alpha(x) + B\alpha(x) + C\alpha^3(x) = \overline{h} + \tilde{h}(x). \tag{33}$$

It describes both the conventional critical fluctuations and fluctuations driven by the random field $\tilde{h}(x)$. The equations (24)–(33) form the framework of the RFGLM.

3. CORRELATION PROPERTIES OF THE HPF

3.1. Critical fluctuations with $\tilde{h}(x)=0$

To study out the role of random fields we start from a brief description of correlation phenomena without random fields, putting $\tilde{\mu}_s(x)=\tilde{\mu}_f(x)=0$. With $\tilde{h}(x)=0$ the equation (33) describes the conventional critical fluctuations of the order parameter in the absence of the random fields. The dimensionless parameter

$$\tau_0 = B_e/A_0, \quad B_e = 4k_0^{-1}T_e - 2\overline{\mu}_{\rm int}(T_e) \tag{34}$$

determines how close the system is to the critical point. In the region (18), this parameter is $\sim 2/k_0$.

According to the conventional theory of critical fluctuations, the correlation radius of the order parameter fluctuations is

$$R_c \sim r_0|\tau_0|^{-\nu}, \quad \overline{h} \ll \overline{h_c}(B),$$
$$R_c \sim r_0|\overline{h}|^{-\mu}, \quad \overline{h} \gg \overline{h_c}(B), \tag{35}$$
$$\overline{h_c}(B_e) = B_e(B_e/C)^{1/2},$$

where ν, μ, and γ are the critical exponents. They have the mean field values with

$$\tau_0 \gg (a/r_0)^6 \sim k_0^{-2} \tag{36}$$

when mean field theory is valid ((36) is the Levanyuk-Ginzburg condition). In the fluctuational region, with $\tau_0 < (a/r_0)^6$, the universal values of the critical exponents (known, e.g., from Wilson's theory) have to be used. It is worth noting that for $k_0 \gg 1$ the fluctuational region is quite narrow.

The pair correlation function of the critical density fluctuations in the mean field approximation is known (see, e.g., Ref. 24) to be

$$\overline{\rho}^{-2}\langle\delta\rho_T(x)\,\delta\rho_T(x_1)\rangle = \kappa_T T V^{-1}\delta(x-x_1), \tag{37}$$
$$|x-x_1| \gg R_c.$$

Here κ_T is the compressibility of the HPL,[22]

$$\kappa_T = \frac{n_s\upsilon_s\kappa_{T_s} + (1-n_s)\upsilon_f\kappa_f}{n_s\upsilon_s + (1-n_s)\upsilon_f} + \frac{n_s(1-n_s)(\upsilon_s-\upsilon_f)^2}{[n_s\upsilon_s + (1-n_s)\upsilon_f](B_e + 3C\alpha^2)}, \tag{38}$$

where υ_s and υ_f are the specific volumes of the solid and fluid fractions, respectively.

In the critical region $\kappa_T \sim |\tau_0|^{-\gamma} \sim R_c^{\gamma/\nu}$, $\gamma > 0$ is a critical exponent. Accordingly to experimental data,[4] the compressibility does not show any changes when the correlation length of the Fischer cluster grows. Therefore the observed LRC can not be identified as the conventional correlation of critical fluctuations. If $\tilde{h}(x) \neq 0$, a new set of correlation lengths can appear due to correlations of $\tilde{h}(x)$.

3.2. Correlations driven by the random fields

To consider the order parameter fluctuations generated by the random fields, let us put

$$\alpha(x) = \overline{\alpha} + \tilde{\alpha}(x). \tag{39}$$

Substitution of (39) into (33) and space averaging give the following equation:

$$(B_e + 3C\delta_\alpha^2)\overline{\alpha} + C\overline{\alpha}^3 = \overline{h}, \tag{40}$$

$$\delta_\alpha^2=\frac{1}{V}\int \tilde{\alpha}^2(x)d^3x.$$

Combining (33) and (39) and using averaging of the nonlinearities, it is easy to get

$$-A\Delta\tilde{\alpha}(x)+(B+3C\overline{\alpha}^2+3C\delta_\alpha^2)\tilde{\alpha}(x)=\tilde{h}(x). \tag{41}$$

The resulting equation (41) includes two random fields, $\tilde{h}(x)$ and $\tilde{\mu}_{\rm int}(x)$. It is known[29,30] that the fluctuations $\tilde{\mu}_{\rm int}(x)$ (fluctuations of B) result in strong coupling effects of the fluctuations in a small vicinity of the critical temperature, with $|T-T_c|\sim T_c\exp(-\text{const}/\langle\tilde{\mu}_{\rm int}^2\rangle)$. This effect is small. We neglect it here and put $\tilde{\mu}_{\rm int}=0$.

The equation (40) has solution (21) when $\delta_\alpha^2=0$.

To calculate δ_α^2 the equation (41) has to be solved. The solution is

$$\tilde{\alpha}(x)=\frac{1}{4\pi A}\int K(|x-x_1|)\tilde{h}(x_1)d^3x_1, \tag{42}$$

$$K(r)=r^{-1}\exp(-\kappa r), \tag{43}$$

$$\kappa^2=\frac{\tilde{B}}{A},\quad \tilde{B}=B_e+3C\overline{\alpha}^2+3C\delta_\alpha^2. \tag{44}$$

Let us consider the contribution of the random fields to the free energy. Combining (26) and (42), we have

$$\tilde{G}=\tilde{G}_1+\tilde{G}_\nabla,$$

$$\tilde{G}_1=-\frac{1}{2v}\int \tilde{h}(x)\tilde{\alpha}(x)d^3x$$

$$=-\frac{1}{8\pi Av}\int \tilde{h}(x)K(|x-x_1|)\tilde{h}(x_1)d^3xd^3x_1$$

$$\equiv-\frac{1}{8\pi Av}\int K(|x-x_1|)\langle\tilde{h}(x)\tilde{h}(x_1)\rangle d^3xd^3x_1, \tag{45}$$

and

$$\tilde{G}_\nabla\sim\frac{1}{2v}\int A(\nabla\tilde{\alpha})^2d^3x \tag{46}$$

is the contribution of the gradient term to the free energy. It is a positive quantity, while $\tilde{G}_1$ is negative. A minimum of $\tilde{G}$ can be achieved if $\tilde{G}_\nabla$ is minimal while $\tilde{G}_1$ has a maximum. It is seen that these conditions are independent of each other because $\tilde{G}_\nabla$ depends on the gradient of $\tilde{h}(x)$ on a scale $\sim R_c$, while $\tilde{G}_1$ is proportional to the correlator of the random field $\tilde{h}(x)$. Therefore the short-range and even long-range correlations of $\tilde{h}(x)$ are needed to minimize $\tilde{G}_1$.

It follows from (42) that

$$(\nabla\tilde{\alpha}(x))^2\sim\kappa^{-2}(\tilde{h}(x))^2+\kappa^{-4}\left(\frac{\partial\tilde{h}(x)}{\partial x}\right)^2+\dots. \tag{47}$$

The term proportional to $\partial\tilde{h}/\partial x$ is omitted in (47) because it gives zero after integration. It is seen from (46) and (47) that $\tilde{G}_\nabla$ has a minimal value, $\tilde{G}_\nabla\sim NA\kappa^2\langle\tilde{\alpha}^2\rangle$, if $\tilde{h}$ is nearly constant within the CD and the second term of the right-hand side of (47) is small compared to the first.

Thus each CD is specified by the value of $\tilde{h}$ within it. This value fluctuates around the mean $\langle\tilde{h}(x)\rangle_{cd}$, where $\langle\dots\rangle_{cd}$ means averaging over CDs. The order parameter fluctuation within a CD has the estimate[24]

$$\langle\delta\tilde{\alpha}^2\rangle_{cd}=\frac{3Tv}{4\pi AV_{cd}}\int_0^{V_c}K(|x|)d^3x\approx\frac{T}{4z_{cd}\tilde{B}},$$

$$z_{cd}\equiv\frac{V_{cd}}{v}=\frac{4\pi R_c^3}{3v}=\frac{4\pi r_0^3}{3v}\left(\frac{A_0}{\tilde{B}}\right)^{3/2}. \tag{48}$$

Noting that (42) gives

$$\tilde{\alpha}\approx\tilde{h}/\tilde{B}, \tag{49}$$

we see that therefore

$$\Delta_h^2=\langle\tilde{h}^2(x)-\langle\tilde{h}^2(x)\rangle_{cd}\rangle\approx\frac{T|\tilde{B}|}{4z_{cd}}. \tag{50}$$

Apparently a CD can be specified by a value $\tilde{h}$ only if

$$\tilde{h}^2\gg\Delta_h^2. \tag{51}$$

Because $\tilde{h}$ is a finite quantity, $|\tilde{h}|\leqslant\tilde{h}_{\max}<\infty$, the condition (51) has to be valid with $|\tilde{h}|=\tilde{h}_{\max}$, or otherwise the thermal fluctuations depress the random-field-driven effects.

The distribution of the random field values is

$$P(\tilde{h})=\frac{1}{V}\int\delta[\tilde{h}(x)-\tilde{h}]d^3x, \tag{52}$$

and

$$c_{cd}(\tilde{h})=\frac{1}{V}\int_{\tilde{h}-\Delta_h}^{\tilde{h}+\Delta_h}\int\delta[\tilde{h}(x)-\tilde{h}]d^3x\,d\tilde{h}\approx2P(\tilde{h})\Delta_h \tag{53}$$

is the concentration of CDs with $|\tilde{h}(x)-\tilde{h}|<\Delta_h$.

In CDs with $|\tilde{h}|<\Delta_h$ the average value of field $\tilde{h}(x)$ is smaller than Δ_h and the field correlation effects are depressed by the fluctuations. The concentration of such domains, c_{nc}, is

$$c_{nc}\approx2P(0)\Delta_h. \tag{54}$$

The relations (52), (53) determine the distribution of CDs on $\tilde{h}$.

As it follows from (45) and (46) that the change of the free energy per molecule driven by field $\tilde{h}$ is

$$g(\tilde{h})\approx-\frac{\tilde{h}^2}{2\tilde{B}}. \tag{55}$$

Now it is clear that the LRC of the field $\tilde{h}(x)$ (when it exists) is a correlation of CDs having nearly the same values of the mean $\tilde{h}$. In other words, the CDs of nearly the same $\tilde{h}$ have to form a correlated aggregation to provide the long-range correlations of the field $\tilde{h}(x)$. The pair correlation function of such an aggregation can be presented as

$$\tilde{f}(\tilde{h},r)=\begin{cases}1, & r<R_c,\\ r^{D(\tilde{h})-3}\exp(-r/\xi(\tilde{h})), & r>R_c.\end{cases} \tag{56}$$

Here $D(\tilde{h})$, $\xi(\tilde{h})$ are the dimension and correlation length of the aggregation.

Because the average concentration of CDs within the aggregation is[31]

$$c(D,\xi)\approx\frac{3}{4\pi}\left(\frac{\xi}{R_c}\right)^{D-3} \tag{57}$$

and $c(D,\xi(\tilde{h}))=c_{cd}(\tilde{h})$, the correlation length $\xi(\tilde{h})$ is related to the concentration $c_{cd}(\tilde{h})$:

$$\xi(\tilde{h})=R_c[c_{cd}(\tilde{h})]^{1/D-3}=R_c[2P(\tilde{h})\Delta_h]^{1/D-3}. \tag{58}$$

The (fractal) dimension D depends on the nature of the aggregating species. Usually it is within the range 1.8–2.5.[31] There is no reason to suspect that it depends strongly on $\tilde{h}$. Therefore we consider it here as an $\tilde{h}$-independent constant which is a property of the liquid.

To show that the aggregation of CDs diminishes the free energy, we compare the free energy of a liquid with aggregated and nonaggregated CDs. With nonaggregated CDs, by virtue of (50), (51)

$$\tilde{H}(r)=\langle\tilde{h}(x)\tilde{h}(x_1)\rangle\approx\langle\tilde{h}^2(x)\rangle=\delta_h^2 \tag{59}$$

and

$$\tilde{G}_1=-\frac{N}{2A}\int K(r)\tilde{H}(r)r^2dr\approx-\frac{N\delta_h^2R_c^2}{2A_0r_0^2}. \tag{60}$$

When the CDs are aggregated we have to use (56), and

$$\tilde{H}(r)\approx\begin{cases}\delta_h^2, & r<R_c,\\ \displaystyle\int P(\tilde{h})\tilde{h}^2\tilde{f}(\tilde{h},r)d\tilde{h}, & r>R_c\end{cases} \tag{61}$$

or

$$\tilde{H}(r)\approx\begin{cases}\delta_h^2, & r<R_c,\\ \delta_h^2r^{D-3}\exp(-r/\xi_{\rm av}), & r>R_c.\end{cases} \tag{62}$$

Here $\xi_{\rm av}$ is the average correlation length and D is the average fractal dimension.

Substitution of (62) into (45) gives

$$\tilde{G}_1(\xi)\approx-\frac{N\delta_h^2R_c^2}{8A_0r_0^2}\left[1+4e^{-1}\left(\frac{\xi_{\rm av}}{R_c+\xi_{\rm av}}\right)^{D-1}\right]. \tag{63}$$

It is seen from (60), (63) that the fractal aggregation of CDs really does lower the free energy.

Because $\tilde{G}_1\sim-\delta_h^2$, the random fields $\tilde{\mu}_s(x),\tilde{\mu}_f(x)$ have to provide a maximal value of δ_h^2 for minimization of the free energy $\tilde{G}_1$. Variation of

$$\delta_h^2=\frac{1}{V}\int\tilde{h}^2(x)d^3x=\frac{1}{V}\int[\tilde{\mu}_s(x)-\tilde{\mu}_f(x)]^2d^3x \tag{64}$$

with conditions (41), (45) and the assumption that the distributions of $\tilde{\mu}_s$, $\tilde{\mu}_f$ can be approximated by a Gaussian function with variances gives the result that (63) attains a maximum for

$$\tilde{\mu}_s(x)=-(\delta_s/\delta_f)\tilde{\mu}_f(x). \tag{65}$$

This result is obvious: in this case δ_h^2 has the maximal value, $\delta_h^2=(\delta_s+\delta_f)^2$. If $\tilde{\mu}_s(x)$ and $\tilde{\mu}_f(x)$ are uncorrelated, then $\delta_h^2=\delta_s^2+\delta_f^2\leqslant(\delta_s+\delta_f)^2$.

Is worth noting that the relation (64) describes the correlation of solid and fluid short-range orders within CDs. Thus the inherent structures of the solid and fluid fractions are correlated on this scale.

The entropy of the system is reduced due to the correlations. The main entropy reduction is caused by the inhomogeneous redistribution of species having the same SRO in the granulated liquid. By virtue of relation (65) $\tilde{\mu}_s(x)$ and $\tilde{\mu}_f(x)$, i.e., the SRO of the solidlike and fluidlike species, are determined by $\tilde{h}(x)$. When the species of the same $\tilde{h}$ are collected in CDs of size z_c, the mixing entropy per molecule is

$$s(\tilde{h})=2z_c^{-1}\ln c_{cd}(\tilde{h}). \tag{66}$$

Note that when they are homogeneously distributed, one has $s(\tilde{h})=k_0^{-1}\ln c_{cd}(\tilde{h})$. Thus the entropy reduction due to formation of correlated domains is

$$\Delta s(\tilde{h})=k_0^{-1}\ln c_{cd}(\tilde{h})(1-2k_0/z_c). \tag{67}$$

It follows that the total change of the free energy per molecule due to the field $\tilde{h}$ is

$$\Delta g(\tilde{h})=-\frac{\tilde{h}^2}{2\tilde{B}}+T\Delta s(\tilde{h}). \tag{68}$$

It has to be negative,

$$\frac{\tilde{h}^2}{2\tilde{B}}>T\Delta s(\tilde{h}), \tag{69}$$

to provide the random-field-driven formation of CDs.

4. RANDOM-FIELD-DRIVEN CRITICAL FLUCTUATIONS

The correlation properties of the random fields result in correlations of the order parameter and density fluctuations. Besides the location of the critical point, even the order of the phase transition can change due to the random field, as is shown below.

4.1. Critical fluctuations and location of the critical point

Returning to Eqs. (40)–(42) and taking into account (50), (51), we have

$$\tilde{\alpha}(x)=\frac{\tilde{h}(x)}{\tilde{B}}+O\left(\frac{1}{\kappa\xi}\right) \tag{70}$$

and

$$(B_e+3C\tilde{\delta}_\alpha^2)\overline{\alpha}+C\overline{\alpha^3}=\left[B_e+\frac{3C\delta_h^2}{\tilde{B}^2}\right]\overline{\alpha}+C\overline{\alpha^3}=\overline{h}, \tag{71}$$

where it is considered that

$$\delta_\alpha^2=\delta_h^2/\tilde{B}^2. \tag{72}$$

These relations complete the RFGLM equations.

The impact of the chemical potential fluctuations on the location of the critical point is seen from (71), (72). On the coexistence curve ($T=T_e$) these equations give

$$\tilde{B}_e\overline{\alpha}+C_e\overline{\alpha}^3=0,\ \ \tilde{B}_e=B_e+3C_e\delta_\alpha^2. \tag{73}$$

Equations (72) has only one solution, $\overline{\alpha}=0$, with $\tilde{B}_e>0$, and two additional solutions

$$\overline{\alpha}_{1,2}=\pm(-\tilde{B}_e/C_e)^{1/2} \tag{74}$$

with $\tilde{B}_e<0$.

With $\overline{\alpha}^2=0$, i.e., on the coexistence curve above the critical point, the equation (72) has just one solution,

$$\delta_{\alpha,1}^2\approx\left(\frac{\delta_h^2}{9C_e^2}\right)^{1/3}-\frac{2B_e}{9C_e}, \tag{75}$$

if

$$B_e>B_{e,c}=-9C_e\left(\frac{\delta_h^2}{36C_e^2}\right)^{1/3}. \tag{76}$$

For $B<B_{e,c}$ and $\overline{\alpha}^2=0$ the equation (72) has three real solutions. The additional two roots turn out less than $\delta_{\alpha,1}$. Because the free energy $\tilde{G}_1$ is proportional to $-\delta_\alpha^2$, it has a minimal value for $\delta_\alpha^2=\delta_{\alpha,1}^2$. Therefore the aforementioned additional roots of (72) with $B_e<B_{e,c}$ belong to unstable and metastable states and are not of interest to us.

A similar analysis with $\overline{\alpha}\neq0$ shows that Eq. (72) has three real roots with

$$B_e<B_{e,c1}=-9C_e\left(\frac{\delta_h^2}{144C_e^2}\right)^{1/3}. \tag{77}$$

The smallest of them, $\delta_{\alpha,2}^2$, is

$$\delta_{\alpha,2}^2\approx\frac{\delta_h^2}{4B_e}\left(1-\frac{3C_e\delta_h^2}{2B_e^3}\right),$$

$$|B_e-B_{e,c1}|\gg|B_{e,c1}|;$$

$$\delta_{\alpha,2}^2\cong\left(\frac{\delta_h^2}{24C_e^2}\right)^{1/3}\left[1-2\left(\frac{B_{e,c1}-B_e}{B_{e,c1}}\right)^{1/2}\right],$$

$$B_{e,c1}-B_e\sim|B_{e,c1}|. \tag{78}$$

It provides a minimal value of the free energy (which is less than that with $\overline{\alpha}^2=0$ and $\delta_\alpha^2=\delta_{\alpha,1}^2$) when

$$B_e<B_e^*\approx-2(C_e\delta_h^2)^{1/3}. \tag{79}$$

Thus the average value of the order parameter, $\overline{\alpha}$, for $B_e=B_e^*$ is nonzero:

$$\overline{\alpha}>\overline{\alpha}_c\approx(B_e^*/C_e)^{1/2} \tag{80}$$

for $B_e<B_e^*$, but $\overline{\alpha}=0$ for $B_e>B_e^*$.

This result shows that at $B_e=B_e^*$, i.e., at

$$T_c(\delta_h,P)=\frac{k_0\Delta\mu_{\rm int}(P,T_e)}{2}-\frac{k_0}{2}(C\delta_h^2)^{1/3}$$

$$=T_c(0)-\frac{k_0}{2}(C\delta_h^2)^{1/3}, \tag{81}$$

a first-order phase transition takes place. $T_c(0)$ is the critical temperature of the system for $\tilde{h}=0$. The order parameter jump at $T=T_c(\delta_h,P)$, accordingly to (80), is $\sim(\delta_h)^{1/3}$. Thus the random field changes not only the critical point location but also the order of the phase transition.

A similar result is known for the mean field version of the random field Ising model (RFIM) with a frozen-in random field.[29,30]

The relations obtained show that for

$$|B_e|=A_0\tau_0<2(C_e\delta_h^2)^{1/3}\ \text{ and }\ |\overline{h}|<\tilde{h}_{\max} \tag{82}$$

the random-field-driven fluctuations of the order parameter are dominant. Taking into account the condition (36), the first of relations (82) can be presented as follows:

$$2(C_e\delta_h^2)^{1/3}\gg A_0k_0^{-2}. \tag{83}$$

The relation (82) determines the critical region of the RFGLM, where $\tilde{B}\sim(C_e\delta_h^2)^{1/3}$ and

$$R_c^3\sim r_0(A_0/\tilde{B})^{3/2}\sim r_0^3(A_0^3/C\delta_h^2)^{1/2}. \tag{84}$$

Condition (51) and relation (84) show that the correlation effects considered are relevant if

$$\delta_h^2\gg\left(\frac{a}{r_0}\right)^{18}\frac{T^6C^5}{A_0^9}\sim\frac{T^6C^5}{k_0^6A_0^9}. \tag{85}$$

Noting that the coefficients A_0, C, T all are of the same order of magnitude, we see that condition (85) is compatible with condition (83).

The condition (69) in the critical region (where $\tilde{B}\sim(C_e\delta_h^2)^{1/3}\sim(T\delta_h^2)^{1/3}$) reads

$$\tilde{h}^2>\tilde{h}_c^2=\frac{2(1-2x)}{k_0x^{4/3}}\delta_h^2\ln c_{cd}(\tilde{h}), \tag{86}$$

$$x=\delta_h/T.$$

Thus the RFGLM used here is valid when the variance of the random field obeys the condition (85) and LRC are setting in, if there are some CDs for which the inequality (86) is fulfilled.

5. LONG-RANGE DENSITY FLUCTUATIONS

It follows from (24)–(26) that the specific volume of liquid is

$$v=\frac{1}{2}(v_f+v_s)-(v_f-v_s)\alpha(x). \tag{87}$$

Density fluctuations include the conventional thermal fluctuations $\delta\rho_T(x)$ around $\overline{\rho}$ and the random-field-driven fluctuations $\tilde{\rho}(x)$. It follows from (42) and (87) that the random-field-driven density fluctuations have the following pair correlation function:

$$\frac{1}{\overline{\rho}^2}\langle\tilde{\rho}(x)\tilde{\rho}(x_1)\rangle=\left(\frac{v_s-v_f}{\overline{v}}\right)^2\langle\tilde{\alpha}(x)\tilde{\alpha}(x_1)\rangle$$

$$=\left(\frac{v_s-v_f}{\overline{v}}\right)^2\frac{\tilde{H}(|x-x_1|)}{\tilde{B}^2}. \tag{88}$$

Noting that the correlation function (88) has to be added to (37) to get the complete pair correlation function, we have

$$\frac{1}{\overline{\rho}^2}\langle \delta\rho(x)\,\delta\rho(x_1)\rangle = \frac{1}{\overline{\rho}^2}[\langle \delta\rho_T(x)\,\delta\rho_T(x_1)\rangle + \langle \tilde{\rho}(x)\tilde{\rho}(x_1)\rangle]$$

$$\cong \kappa_T T\frac{1}{V}\,\delta(x-x_1) + \left(\frac{v_s - v_f}{\overline{v}}\right)^2 \times \frac{(\delta_s+\delta_f)^2}{\tilde{B}^2}\,\frac{1}{r^{3-D}}\exp\left(-\frac{r}{\xi}\right). \tag{89}$$

The first term of the right-hand side of (89) is proportional to $\tilde{B}^{-1}$ (see (38)), while the second is $\sim\tilde{B}^{-2}$. Therefore the random-field-driven density fluctuations are dominant when condition (85) is fulfilled.

Fourier transformation of (89) gives the spectral components $\delta\rho_q^2$:

$$\frac{\rho_q^2}{\overline{\rho}^2} = \kappa_T T\frac{1}{V} + \left(\frac{v_s - v_f}{\overline{v}}\right)^2 \frac{(\delta_s+\delta_f)^2}{\tilde{B}^2}\,\frac{\Gamma(D-1)}{(1+q^2\xi^2)^{(D-1)/2}} \times \left(\frac{\xi}{R_c}\right)^D \frac{\sin[(D-1)\arctan(q\xi)]}{q\xi}, \tag{90}$$

where $\Gamma(x)$ is the gamma function.

The second term of the right-hand side of (90) describes the random-field-driven heterophase fluctuations $\tilde{\rho}_q^2$. It has simpler forms in two limiting cases, with small q and with $q\xi>1$:

$$\frac{\tilde{\rho}_q^2}{\overline{\rho}^2} = \begin{cases} \left(\dfrac{v_s - v_f}{\overline{v}}\right)^2 \dfrac{(\delta_s+\delta_f)^2\Gamma(D)}{\tilde{B}^2}\left(\dfrac{\xi}{R_c}\right)^D, & q\to 0, \\ \left(\dfrac{v_s - v_f}{\overline{v}}\right)^2 \dfrac{(\delta_s+\delta_f)^2}{\tilde{B}^2}\,\dfrac{\Gamma(D-1)}{(q\xi)^D}\left(\dfrac{\xi}{R_c}\right)^D \times \sin\left[(D-1)\dfrac{\pi}{2}\right], & q\xi>1. \end{cases} \tag{91}$$

6. TIME-DEPENDENT GL EQUATIONS

The HPFs have short-range correlation on a scale $r\sim R_c$ and long-range correlation with $r\sim\xi$. The parameters δ_n^2 and ξ and the Fourier components $\{\tilde{\alpha}_q\}$ are time-dependent quantities. Conventional dynamic equations for them describe the short-range and long-range relaxation as well as the ultraslow modes. We are using here the time-dependent GL approach[32] to describe these relaxation processes and ultraslow modes.

6.1. Short-range correlation relaxation

It follows from (65) that in equilibrium ($t\to\infty$)

$$\langle \tilde{\mu}_s(x,t)\,\tilde{\mu}_f(x,t)\rangle \approx -\,\delta_s\delta_f \tag{92}$$

and

$$\delta_h^2(\infty) = \delta_s^2 + \delta_f^2 - 2\langle \tilde{\mu}_s(x,\infty)\,\tilde{\mu}_s(x,\infty)\rangle \approx (\delta_s+\delta_f)^2. \tag{93}$$

In (92), (93) the thermal fluctuations of the random fields within a CD are not taken into account, as is justifiable if (see (52))

$$2\,\delta_s\delta_f \gg T\tilde{B}/z_{cd}, \tag{94}$$

i.e., if the fluctuations of the product (92) are much smaller than its average value.

The solid–fluid short-range order correlation (64) relaxes to the equilibrium value (92) if the condition (94) is fulfilled. An elementary short-range structure transformation involves not a single molecule but a group of them. The conventional name of such a group is the cooperatively rearranging domain (CRR). The part of the average free energy of the CRR which varies with $\delta_h^2(t)$ is

$$\langle \tilde{g}_{crr}\rangle \approx \frac{z_{crr}}{\tilde{B}}\,\delta_h^2(t), \tag{95}$$

where z_{crr} is the number of molecules in the CRR.

The average free energy deviation from the equilibrium value of these molecules due to the difference

$$\Delta\,\delta_h^2(t) = \delta_h^2(t) - \delta_h^2(\infty) \tag{96}$$

is evidently $\sim z_{crr}\tilde{B}^{-1}\Delta\,\delta_h^2$, and thus the dynamics of the short-range correlation is described by the following equation:

$$\frac{1}{2}\,\frac{\partial\,\delta_h^2(t)}{\partial t} = \frac{\partial\langle \delta\mu_s(t)\,\delta\mu_f(t)\rangle}{\partial t} = -\,\frac{1}{2\,\tau_\alpha}\,\frac{z_{crr}\tilde{B}}{T}[\,\delta_h^2(t) - \delta_h^2(\infty)], \tag{97}$$

where τ_α is the CRR rearrangement time, which is the α-relaxation time.

The Langevin term is not included in (97). It is not important under the condition (94). It is seen that τ_α is a characteristic relaxation time of the short-range correlations.

6.2. The long-range relaxation

To describe the relaxation kinetics of $\xi(t)$ we assume that a fractal cluster consisting of CDs with the same value of $\tilde{h}$ appears as a result of an aggregation process of CDs in analogy with the aggregation of small species which are forming fractal structures.[31] The kinetic equation of fractal cluster formation in the simplest form is

$$\frac{\partial\xi(\tilde{h},t)}{\partial t} = \frac{R_c}{D}\,\Gamma_\xi\left(\frac{\xi(\tilde{h},t)}{R_c}\right)^{1-D}\frac{\xi(\tilde{h},\infty) - \xi(\tilde{h},t)}{\xi(\tilde{h},\infty)}, \tag{98}$$

where Γ_ξ is the growth rate of the fractal. The last term on the right-hand side describes saturation of the fractal growth when the correlation length approaches its stable equilibrium value $\xi(\tilde{h},\infty)$, determined by (58). To get an estimate of Γ_ξ we note that the free energy of a CD within a fractal cluster of correlation length $\xi(t)$, as is seen from (63), is

$$\tilde{g}_{cd}(\tilde{h}^2,\xi) = \frac{z_{cd}R_c^2}{8A_0r_0^2}\,\tilde{h}^2\left[1 + 4e^{-1}\left(\frac{\xi}{R_c+\xi}\right)^{D-1}\right] \approx \frac{z_{cd}R_c^2}{8A_0r_0^2}\,\tilde{h}^2\left[1 + 4e^{-1}\left(1 - (D-1)\,\frac{R_c}{\xi}\right)\right]. \tag{99}$$

Then

$$\Gamma_\xi \sim \frac{R_c}{\tau_\alpha}\frac{z_c c(\tilde{h})}{T}\frac{\partial g_c}{\partial \xi}R_c = (D-1)\frac{z_{cd}}{2eA}\frac{c_{cd}(\tilde{h})\tilde{h}^2}{\tau_\alpha T}\frac{R_c^4}{\xi^2}$$

$$\equiv (D-1)\gamma_0\frac{\tilde{h}^2}{2eAT}\frac{R_c^4}{\xi^2}. \quad (100)$$

In (100) τ_α is taken as the characteristic time of CD rearrangement: R_c/τ_α is the rate of the one step of the cluster growth; $T^{-1}R_c\partial g_{cd}/\partial\xi$ is the thermodynamic driving force of the fractal growth; the term $c_{cd}(\tilde{h})$ is introduced to take into account that just $c_{cd}(\tilde{h})$ of CD transformations result in the formation of CDs specified by the field strength $\tilde{h}$.

The solution of (98), (100) with the initial condition $\xi(\tilde{h},0)=0$ and $\xi(\infty)-\xi(t)\sim\xi(\infty)$ (not very close to the equilibrium value) is

$$\xi(\tilde{h},t)=R_c\left(\frac{(D-1)(D+2)}{D}\frac{\tilde{h}^2R_c^2}{2eAT}\gamma_0 t\right)^{1/D+2}. \quad (101)$$

To estimate the growth-rate exponent it should be noted that for $D=1.5$–2.5 the exponent $1/(D+2)$ varies from 0.29 to 0.22.

In the vicinity of $\xi(\infty)$, for $|\xi(\infty)-\xi(t)|\ll\xi(\infty)$, the difference $|\xi(\infty)-\xi(t)|$ decreases exponentially, as is easy to see from (98).

The solution (100) describes the kinetics of fractals with the specified field strength $\tilde{h}$. this result has to be averaged with the distribution (52) to get an averaged description.

The relaxation time of the long-range correlation, $\tau_{\rm rel}$, can be estimated by substituting into (101) $\xi_{\rm av}$ and δ_h^2 instead of ξ and $\tilde{h}^2$:

$$\tau_{\rm rel}\approx\frac{D}{(D-1)(D+2)}\frac{2eAT}{R_c^2\delta_h^2\gamma_0}\left(\frac{\xi_{\rm av}}{R_c}\right)^{D+2}. \quad (102)$$

6.3. Ultraslow modes

To get a dynamical equation for the Fourier components $\tilde{\alpha}_q$ of the long-range order parameter fluctuations, the free energy (45) has to be presented in a proper form:

$$\tilde{G}_1=-\frac{1}{2}\int\tilde{h}(x)\tilde{a}(x)d^3x=-\frac{1}{2}\sum_q\tilde{h}_q\tilde{a}_q$$

$$=-\frac{1}{2}\sum_q(Aq^2+\tilde{B})|\tilde{\alpha}_q^2|. \quad (103)$$

Then the time-dependent GL equations for $\tilde{\alpha}_q$ are

$$\frac{\partial\tilde{\alpha}_q}{\partial t}=-\Gamma_q\frac{1}{T}\frac{\partial\tilde{G}_1}{\partial\tilde{\alpha}_q}=-\Gamma_q\left(\frac{Aq^2+\tilde{B}}{T}\right)\tilde{\alpha}_q. \quad (104)$$

Here the Langevin force providing the equilibrium value of $\langle\tilde{\alpha}_q^2\rangle$ is omitted because our main goal is to get the spectrum of ultraslow modes.

In an isotropic medium

$$\Gamma_q=\Gamma_0+\gamma_1q^2+\gamma_2q^4+\dots. \quad (105)$$

As follows from textbooks (e.g., Ref. 32), the parameter Γ_0 in our case is equal to 0 due to conservation of $|\tilde{\alpha}_{q=0}^2|=\langle\tilde{\alpha}(x)\rangle^2=0$. Therefore

$$\Gamma_q=\gamma_1q^2+\gamma_2q^4+\dots. \quad (106)$$

This equation determines the form of the ultraslow mode spectrum.

Because the CD transformations which are controlling the fractal growth are also responsible for the fractal structure rearrangements, we can put

$$\gamma_1\sim\gamma_0R_c^2 \text{ and } \gamma_2\sim\gamma_0R_c^4. \quad (107)$$

The factors R_c^2, R_c^4 are included to preserve the correct dimension of Γ_q. It is seen from (104), (106), and (107) that the ultraslow mode spectrum has the following form:

$$\omega_{us}(q)=(\gamma_1q^2+\gamma_2q^4)\left(\frac{Aq^2+\tilde{B}}{T}\right)=c_1\tilde{B}\gamma_0R_c^2q^2$$

$$+\left(\frac{c_1A+c_2\tilde{B}R_c^2}{T}\right)\gamma_0R_c^4q^4+\dots$$

$$\approx c_1\gamma_0R_c^2q^2\frac{\tilde{B}}{T}\left(1+\frac{c_1+c_2}{c_1}R_c^2q^2\right), \quad (108)$$

where c_1 and c_2 are some q-independent coefficients which can be considered as constants in the critical region. The resulting expression of the ultraslow mode spectrum is obtained taking into account that $A/\tilde{B}\sim Tr_0^2/\tilde{B}\approx R_c^2$.

7. DISCUSSION AND CONCLUDING REMARKS

In the theory developed, based on the concept of heterophase fluctuations, the multiplicity of the SRO, which is a basic property of the glass-forming liquids, is taken into account. In particular this property manifests itself in the developed inherent structure and in the free-energy landscape.[27,28] The free-energy landscape results in the appearance of the random-field term in the GL equations.

The relation of the present theory to the other models of supercooled liquid and to the theory of the critical fluctuations was already elucidated. To emphasize this connection it should be noted that the RFGLM developed can be reduced to the models of supercooled liquid proposed in Refs. 13–23. For example, to get the equations of two-state model[13,17] from (26)–(30) we have to put $\delta_s^2=\delta_f^2=\Delta\mu_{\rm int}=A=0$, and $k_0=1$.

Multiplicity of the short-range order results in polychromatic fractal heterophase structure. Polychromatic cluster structures are described, e.g., in Ref. 33 in connection with the percolation problem. If clusters have a property described by a parameter, this last one can be used as a ''color'' specifying a cluster. In a three-dimensional system the percolation threshold is about 0.15. Thus several interpercolating clusters can form a polychromatic structure. Along with that, any number of differently colored clusters can coexist if they have finite correlation lengths. In the heterophase liquid $\tilde{h}_c$ plays the role of CD color. It parameterizes the chromatic spectrum of CDs. The correlation lengths are finite. Thus Fischer clusters are polychromatic fractal aggregations. A specific feature of these polychromatic structures is the ability of a CD to change its color.

It is worth noting that if the conditions (51), (69) are satisfied, the field $\tilde{h}$ changes the criticality (the mean field approximation is correct), the location of the critical point (81), and the order of the phase transition at the critical point.

The order parameter jump at $T_c(\delta_h, P)$ is $\sim(\delta_h/T_e)^{1/3}$. Relation (81) shows that the random field lowers the critical temperature. This is one of reasons why the majority of the glass-forming liquids do not have a polymorphous liquid–liquid phase transition.

Since the mean field model (13) is isomorphic to the van der Waals theory of the critical point and (26) is a generalization of this theory taking into account the gradient term, one could ask why the random field $\tilde{h}(x)$ does not play a significant role in the critical fluctuations of gas–liquid systems. It is due to predominance of the thermal fluctuations in the gas–liquid critical region. The Ginzburg number is near 1 for the gas–liquid phase transition, i.e., $(a/r_0)^6 \sim 1$, and conditions (36), (82), and (85) are not fulfilled. According to relation (36), the Ginzburg number is proportional to k_0^{-2}. Therefore within the gas–liquid critical region $k_0^{-2} \sim 1$, i.e., the assossiativity of the molecules is small, ~ 1, and the fluctuational region is rather wide. In the solid–fluid system the correlation radius far from the critical point, r_0, is approximately equal to the radius of the first coordination shell. Therefore k_0 is ~ 10 in this case and, according to (36), the mean field theory has a wide region of applicability even if $\tilde{h}(x)$ is neglected.

The random-field-driven LRC qualitatively differs from the conventional critical LRC. The former LRC possess the properties 3)–5) of the Fischer cluster (see Introduction), while the latter LRC cannot have them. In Refs. 18 and 19 it was attempted to identify the Fischer cluster as critical fluctuations, assuming that the critical temperature is below T_g. The analysis performed in Ref. 12 shows that the theory proposed in Refs. 18 and 19 for the LRC observed by Fischer *et al.* in ortho-terphenil does not fit the experimental data even if the features 3)–5) of Fischer's cluster are ignored.

Glass inherits the structural features of supercooled liquid. For this reason short-range and long-range correlations of liquid are also present in the glassy state. Because the annealing time needed for the Fischer cluster formation is rather long compared to τ_α, the structure and properties of the glass are sensitive to the thermal history of the liquid. The correlations and topology of SRO in the glassy state play a rather important role in phase transformations taking place in glasses. For example, ordering and relaxation of the spin system of a magnetic glass are extremely sensitive to the structural and compositional correlations.[34] The structural heterogeneities play the role of a ''frozen'' random field in this case. Another example is the polymorphous phase transitions in the glassy state. This phenomenon is observed in some glasses (see Refs. 35 and 36). It has also been revealed in amorphous carbon using computer simulations.[37] Because glass is a nonergodic system, a phase transformation is possible due to changes of SRO resulting in a long-range ordering. The structural heterogeneities cause an inhomogeneous distribution of internal stresses due to thermoelastic effects. Therefore the transformations of the SRO are necessarily inhomogeneous and depend on the distribution and correlation properties of the internal stresses and compositional ordering.

A topological phase transition connected with the formation of a percolating cluster possessing some SRO stipulates a thermodynamic phase transition due to the singular behavior of the thermodynamic coefficients, e.g., the compressibility or thermal expansion. Therefore polymorphous phase transitions in the glassy state have to be sensitive to structural correlations that depend on the thermal history of the liquid.

Recently anomalous behavior of the thermal expansion coefficient $\lambda(T)$ of pure and inert-gas doped fullerite at $T < 20$ K was observed.[38,39] Fullerite C_{60} is a fcc cubic crystal. Due to the fivefold symmetry of the C_{60} molecules, long-range orientational order is impossible in fullerite. For this reason fullerite is an orientational glass below $T_g \cong 90$ K. Impurities distort the crystalline structure and disturb the intermolecular interactions in the fullerite. The thermal expansion coefficient depends considerably on the concentration and kind of inert gas impurities. It is remarkable that hysteresis of $\lambda(T)$ was observed at $T < 20$ K in krypton-doped fullerite. It is attributed to a phase transition connected with changes of the short-range orientational order of the C_{60} molecules. One can expect that the observed hysteresis phenomenon depends considerably on the concentration of krypton and on the thermal history of samples at $T > T_g$ due to changes of the short-range and medium-range orientational order in the orientational liquid state.

Many fruitful discussions with E. W. Fischer are cordially acknowledged.

This work was supported in part by the Science and Technology Center of Ukraine, project N655.

*E-mail: bakai@kipt.kharkov.ua

[1] H. Silescu, J. Non-Cryst. Solids **243**, 81 (1999).
[2] E. W. Fischer, Ch. Becker, I.-U. Hagenah, and G. Meier, Prog. Colloid Polym. Sci. **80**, 198 (1989).
[3] E. W. Fischer, G. Meier, T. Rabenau, A. Patkowski, W. Steffen, and W. Thonnes, J. Non-Cryst. Solids **131–133**, 134 (1991).
[4] E. W. Fischer, Physica A **201**, 183 (1993).
[5] T. Kanaya, A. Patkowski, E. W. Fischer, J. Seils, H. Glaser, and K. Kaji, Acta Polym. **45**, 137 (1994).
[6] A. Patkowski, Th. Thurn-Albrecht, E. Banachowicz, W. Steffen, T. Narayan, and E. W. Fischer, Phys. Rev. E **61**, 6909 (2000).
[7] A. Patkowski, E. W. Fischer, W. Steffen, H. Glaeser, M. Baumann, T. Ruths, and G. Meier, Phys. Rev. E **63**, 061503 (2001).
[8] A. Patkowski, H. Glaeser, T. Kanaya, and E. W. Fischer, Phys. Rev. E **64**, 031503 (2001).
[9] E. W. Fischer, A. Bakai, A. Patkowski, W. Steffen, and L. Reinhardt, J. Non-Cryst. Solids (2002) (in press).
[10] K. Kawasaki, Physica A **217**, 124 (1995).
[11] H. Tanaka, J. Chem. Phys. **111**, 3163; 3175 (1999); Phys. Rev. B **62**, 6968 (2000).
[12] A. S. Bakai, J. Non-Cryst. Solids **307–310**, 623 (2002).
[13] P. B. Macedo, W. Capps, and T. A. Litovitz, J. Chem. Phys. **44**, 3357 (1966).
[14] I. L. Apteker and E. G. Ponyatovsky, Dokl. Akad. Nauk SSSR **173**, 851 (1967); E. G. Ponyativsky and O. I. Barkalov, Mater. Sci. Rep. **8**, 147 (1992).
[15] E. Rapoport, J. Chem. Phys. **46**, 2891 (1967).
[16] C. A. Angell and K. I. Rao, J. Chem. Phys. **57**, 470 (1972).
[17] M. H. Cohen and G. S. Grest, Phys. Rev. B **20**, 1077 (1979); **26**, 6313 (1982).
[18] I. T. Bendler and M. F. Shlessinger, J. Stat. Phys. **53**, 531 (1988).
[19] I. T. Bendler and M. F. Shlessinger, J. Chem. Phys. **96**, 3970 (1992).
[20] A. S. Bakai, in *Glassy Metals III*, Vol. 72 of Topics in Applied Physics, H. Beck and H.-J. Guentherodt (Eds.), Springer, Heidelberg (1994), p. 209.
[21] A. S. Bakai, Fiz. Nizk. Temp. **20**, 469 (1994) [Low Temp. Phys. **20**, 373 (1994)].

[22] A. S. Bakai, Fiz. Nizk. Temp. **22**, 956 (1996); *ibid.* **24**, 27 (1998) [Low Temp. Phys. **22**, 733 (1996); *ibid.* **24**, 20 (1998)].
[23] E. W. Fischer and A. S. Bakai, Slow Dynamics in Complex Systems, AIP Conf. Proc. **469**, M. Tokuyama and I. Oppenheim (Eds.) (1999), p. 325.
[24] L. D. Landau and E. M. Lifshitz, *Statistical Physics*, Parts 1 and 2, 3rd ed., Pergamon Press, Oxford (1980), Nauka, Moscow (1976).
[25] A. S. Bakai, Condens. Matter Phys. **3**, 675 (2000).
[26] H. Sher and R. Zallen, J. Chem. Phys. **53**, 3759 (1970); R. Zallen and H. Sher, Phys. Rev. B **4**, 4471 (1971).
[27] F. H. Stillinger and T. A. Weber, Phys. Rev. A **28**, 2408 (1983).
[28] S. Sastry, P. G. Debenedetty, and F. H. Stillinger, Nature (London) **394**, 554 (1998).
[29] Vik. S. Dotsenko, Usp. Fiz. Nauk **165**, 481 (1995).
[30] *Spin Glasses and Random Fields*, A. P. Young (Ed.), World Sci. Publ. Co. Ltd., Singapore (1998).
[31] J. Feder, *Fractals*, Plenum Press, New York (1988).
[32] S. Ma, *Modern Theory of Critical Phenomena*, W. A. Benjamin, Inc., (1976).
[33] R. Zallen, *The Physics of Amorphous Solids*, Wiley, New York (1983).
[34] A. S. Bakai, Fiz. Nizk. Temp. **28**, 584 (2002) [Low Temp. Phys. **28**, 415 (2002)].
[35] C. A. Angell, Science **267**, 1924 (1994).
[36] P. H. Pool, T. Grande, F. Sciortino, H. E. Stanley, and C. A. Angell, Comput. Mater. Sci. **4**, 373 (1995).
[37] A. S. Bakai, M. P. Fateev, and Yu. A. Turkin, in *Nanostructured Carbon for Advanced Applications*, NATO ASI series, G. Benedeck *et al.* (Eds.), Kluwer Ac. Publishers (2001), p. 185; *Preprint Cond-Mat/0108518* (2001).
[38] A. N. Alexandrovskii, V. G. Gavrilko, V. B. Essel'son, V. G. Manzhelii, B. G. Udovichenko, and V. P. Maletskiy, Fiz. Nizk. Temp. **27**, 1401 (2001) [Low Temp. Phys. **27**, 1033 (2001)].
[39] A. N. Aleksandrovskii, A. V. Dolbin, V. B. Esel'-son, G. Gadd, V. G. Gavrilko, V. G. Manzhelii, B. Sundqvist, and B. G. Udovidchenko (to be published).

This article was published in English in the original Russian journal. Reproduced here with stylistic changes by AIP.

Non-Fermi-liquid behavior: Exact results for ensembles of magnetic impurities

A. A. Zvyagin*

Max Planck Institut für Chemische Physik fester Stoffe, D-01187 Dresden, Germany and B. Verkin Institute for Low Temperature Physics and Engineering of the National Academy of Sciences of Ukraine, 47 Lenin Ave., Kharkov, 61103, Ukraine

(Submitted June 11, 2002)
Fiz. Nizk. Temp. **28**, 1274–1291 (December 2002)

In this work we consider several exactly solvable models of magnetic impurities in critical quantum antiferromagnetic spin chains and multichannel Kondo impurities. Their ground-state properties are studied, and the finite set of nonlinear integral equations which exactly describe the thermodynamics of the models is constructed. We obtain several analytical low-energy expressions for the temperature, magnetic field, and frequency dependences of important characteristics of exactly solvable disordered quantum spin models and disordered multichannel Kondo impurities with essential many-body interactions. We show that the only low-energy parameter that gets renormalized is the velocity of the low-lying excitations (or the effective crossover scale connected with each impurity); the others appear to be universal. In our study several kinds of strong disorder important for experiments were used. Some of them produce low divergences in certain characteristics of our strongly disordered critical systems (compared with finite values for the homogeneous case or a single impurity). For weak disorder, or for narrow distributions of the local Kondo temperatures, our exact results reveal the presence of Kondo screening of disordered ensembles of magnetic impurities by low-lying excitations of the host. We point out that our results qualitatively coincide with the data of experiments on real disordered quasi-one-dimensional antiferromagnetic systems and with the similar behavior of some heavy metallic alloys.
[DOI: 10.1063/1.1531395]

1. INTRODUCTION

The study of the behavior of magnetic impurities coupled to paramagnetic hosts remains one of the most interesting problems of the many-body physics. The Kondo effect,[1] which describes the exchange interaction between the spin of a magnetic impurity and the spins of itinerant electrons, is, perhaps, the best known example in which modern theoretical methods like renormalization group (RG) theory, Bethe ansatz, bosonization, conformal field theory, etc. have displayed their strength.[2–4] The crossover from the strong coupling to the weak coupling regime is one of the most famous examples of nonperturbative effects in condensed matter theory.

In the last few years, interest in the non-Fermi-liquid (NFL) behavior of magnetic systems and metallic alloys has grown considerably. A large class of conducting nonmagnetic materials does not behave as usual Fermi liquids (FLs) at low temperatures. One of the best-known examples of such behavior is the Kondo effect for multi (n) channel electron systems: For an impurity spin less than $n/2$ a NFL critical behavior results.[5] The critical behavior of a single magnetic impurity can also be connected with a quadrupolar Kondo effect or nonmagnetic two-channel Kondo effect.[6] However, for most dirty metals and alloys in which the NFL behavior has been observed (see, e.g., the recent reviews[7–10] and Refs. 11–20), the magnetic susceptibility χ and low-temperature specific heat c usually manifest logarithmic or weak power-law behavior with temperature T. The resistivity decreases linearly with temperature, showing a large residual resistivity. That is different from the predictions of the theory of the overscreened Kondo effect.[4,5]

The last property together with the alloy nature of compounds suggests that disorder (a random distribution of localized f electrons or a random coupling to the conducting electron host) may play the main role in the low-temperature NFL character of such systems. The idea of (nonscreened) local moments existing in disordered metallic systems has already been formulated recently.[21–23] It was proposed that near metal-insulator transitions (or for sufficiently alloyed systems far from the quantum critical point) disordered correlated metals contain localized moments. The change in the interactions between impurity sites and host spins can be considered as a modification of the characteristic energy scale, the Kondo temperature T_K. At that scale the behavior of the magnetic impurity manifests the crossover from the strong coupling regime (for $T, h \ll T_K$, where h is the external magnetic field) to the weak coupling regime $T_K \ll h, T$. The impurity spin behaves asymptotically free in the weak coupling case, and it is screened by the host spins in the strong coupling case. The random distribution of magnetic characteristics of the impurities (i.e., their Kondo temperatures) may be connected either with the randomness of exchange couplings of itinerant electrons with the local moments[22] or with the randomness of the densities of conduction electron states.[21] In fact, both types of randomness renormalize the single universal parameter—the Kondo temperature—which characterizes the state of the magnetic impurity. In Ref. 16 the results of the measurements of the

magnetic susceptibility, nuclear magnetic resonance (NMR) Knight shift, and low-temperature specific heat have been reported. To explain the observed features it was necessary to assume some disorder, with a Gaussian distribution of the Kondo temperatures. However, the model used for the explanation of the experiment was oversimplified by an inadequate representation of the Kondo magnetization by the simple replacement $T \to T + bT_K$ in the Brillouin function, $B(ah/T + bT_K)$, with which the magnetization of a single magnetic moment was approximated (a and b are some constants). It was noted[16] that the data for the specific heat and Knight shift did not agree with the predictions of that simple theory, especially for nonzero values of the magnetic field. The inhomogeneous magnetic susceptibility was confirmed recently[24] by muon spin rotation experiments. The role of the long-range Ruderman–Kittel–Kasuya–Yosida (RKKY) coupling between the local moments was taken into account recently[25,26] (Griffiths phase theory), and the model was found to exhibit properties qualitatively similar to those of models with noninteracting local moments.[24] In addition, the presence of the spin–orbit interaction in some disordered heavy fermion alloys demands the study of magnetic anisotropy, which can play an essential role in the physics of disordered spin interactions.[25,26]

Another interesting topic of research, which is related to the one mentioned above, is the behavior of disordered magnetic impurities in one-dimensional (1D) antiferromagnetic (AF) spin chains. Here we can mention several experiments on spin chains.[27–30] The theoretical works devoted to the description of disordered magnetic impurities in critical spin chains have mostly involved the approximate RG treatment of the problem.[31–35] Recently, however, we proposed an exact solution to the problem of the behavior of spin-1/2 AF quantum spin chain coupled to disordered magnetic impurities,[36–38] which was later generalized to the description of disordered magnetic impurities in correlated electron chains.[39]

It is known that the physics of a single magnetic impurity in a 1D AF Heisenberg spin $S = 1/2$ chain and that of a single Kondo impurity in a 3D free electron host are described by similar Bethe ansatz theories,[2,3,40,41] e.g., the magnetization and the low-temperature magnetic specific heat of the impurity for the two models coincide. The Heisenberg model is the seminal model for correlated many-body systems. Most of its static properties are exactly known. A single spin-1/2 magnetic impurity in the AF spin chain and the Kondo impurity manifest total screening with the (marginal) FL-like low-temperature behavior of the magnetic susceptibility and specific heat, i.e., the finite values of $\chi(T)$ and $c(T)/T$ in the low-temperature limit.[2,3,41,42] In other words, the moment of the impurity is quenched by the localized host spins or by the spins of the conduction electrons, respectively. The magnetic anisotropy of the Kondo exchange interaction between the impurity spin and the spins of the free electron host has also been taken into account exactly for the single Kondo impurity[3,43] and for a magnetic impurity in a AF spin chain.[44,45] It was pointed out that the magnetic anisotropy does not change drastically the Kondo effect of a single impurity. On the other hand, for the integrable lattice models one can incorporate a finite concentration of magnetic impurities[46,47] without destroying the exact solvability. Hence, for a random distribution of magnetic impurities we can suppose that low dimensionality is not essential for the Kondo screening. The absence of magnetic ordering in the NFL Kondo systems[7,9,10] also confirms this assumption.

The goal of our present study is to find exactly the ground state and thermodynamic characteristics of disordered ensembles of spin-S' magnetic impurities in magnetically uniaxial spin-S chains in the critical region, i.e., in the domain of values of the magnetic anisotropy where excitations of the homogeneous host are gapless. As a byproduct, we find the exact solution to the behavior of random ensembles of multichannel Kondo impurities, coupled locally to the free-electron host with an ''easy-plane'' magnetic anisotropy of that coupling. We allow for various *random* distributions of the impurity–host couplings for arbitrary values of external magnetic field and temperature. The magnetic anisotropy parameter is assumed to be homogeneous for the host spins and for the impurity spins. In this paper we show that for several kinds of strong disorder of the impurity–host couplings the (Kondo) screening is absent, but for a weaker disorder the quenching persists, but with a NFL temperature behavior of the magnetic characteristics. We also show that the magnetic field lifts the degeneracy and effectively enhances the quenching of the impurity spins, hence decreasing the effect of disorder.

This paper is organized as follows. After the introduction in Sec. 1, the Hamiltonians for the spin chains studied are introduced in Sec. 2. Section 3 is devoted to the standard Bethe ansatz equations of the problem, and to the connection with the multichannel Kondo case. In Sec. 4 we present the ground-state properties of the systems considered. The thermodynamic Bethe ansatz is introduced in Sec. 5 for random ensembles of magnetic impurities in the ''easy-plane'' spin chains and the multichannel Kondo situation, by use of the ''quantum transfer matrix'' approach. In Sec. 6 we present our results for the temperature and magnetic field dependence of the magnetic susceptibility and the specific heat obtained analytically and compare them with numerical calculations of the nonlinear integral equations. Section 7 contains concluding remarks.

2. BETHE–ANSATZ SOLVABLE HAMILTONIANS

In our treatment we shall use the Bethe ansatz method (for a review, see, e.g., the monograph[48] and references therein). Let us start with $R^{\mu_i \mu_{i+1}}_{\alpha_i \beta_i}(u)$, the standard R matrix of a spin-S chain with uniaxial easy-plane anisotropy (see, e.g., Refs. 44, 45, 49). The indices α_i and β_i denote states of the spin at site i (acting in the Hilbert space V_i), and μ denotes states in the auxiliary space (Hilbert space V_a). The R matrix has the form

$$R=P\sum_{j=0}^{2S}\prod_{l=0}^{j-1}\frac{\sinh\gamma[i2(2S-l)-u]}{\sinh\gamma[i2(2S-l)]}\times\prod_{i=j}^{2S-1}\frac{\sinh\gamma[i2(2S-l)+u]}{\sinh\gamma[i2(2S-l)]}\times\prod_{\substack{p=0\\p\neq j}}^{2S}\frac{2\sin^2\gamma\hat{X}_{ia}-\sin\gamma p\sin\gamma(p+1)}{\sin\gamma(j-p)\sin\gamma(j+p+1)},\quad(1)$$

where u is the spectral parameter, γ is the parameter of the (easy-plane) magnetic anisotropy, the operator P permutes the spaces V_i and V_a, and

$$\hat{X}_{ia}=e^{i\gamma S_i^z}\left(\frac{1}{2}[S_i^+S_a^-+S_i^-S_a^+]+\frac{\cos\gamma S\cos\gamma(S+1)}{\sin\gamma}S_i^zS_a^z+\frac{\sin\gamma S\sin\gamma(S+1)}{\sin^2\gamma}\cos\gamma S_i^z\cos\gamma S_a^z\right)e^{-i\gamma S_a^z},\quad(2)$$

where $S^{\pm}=S^x\pm iS^y$, and which in the limit of the SU(2)-symmetric system ($\gamma\to 0$) simplifies to $\mathbf{S}_i\mathbf{S}_a+S(S+1)$. The R matrices satisfy the Yang–Baxter (triangle) relations.[3,48] The row-to-row (from the viewpoint of the associated statistical 2D problem), "standard" transfer matrix $\tau_\alpha^\beta(u)$ has the form of the trace over the auxiliary space of the product of R matrices with the same values of the spins (S) in sites i

$$\tau_\alpha^\beta(u,\{\theta\}_{i=1}^L)=\sum_\mu\prod_{i=1}^L R_{\alpha_i\beta_i}^{\mu_i\mu_{i+1}}(u,\theta_i),\quad(3)$$

where L is the length of the quantum chain and θ_i are the inhomogeneity parameters, which are shifts of the spectral parameter. The R matrices satisfy the Yang–Baxter equations, and, hence, the transfer matrices with different spectral parameters commute.[48] The Hamiltonian of the uniaxial spin-S quantum chain with impurities of the same spin S is obtained as the derivative of the logarithm of the transfer matrix with respect to the spectral parameter (taken at $u=0$).[49]

The Hamiltonian of the uniaxial spin-S chain with spin-S' impurities is obtained as the derivative of the logarithm of the transfer matrix, which is the trace over the auxiliary space of the product of R matrices with *different* values of spin (S for host sites and S' for impurity sites) in the spaces V_i, with respect to the spectral parameter (at $u=0$). Notice that R matrices with different values of the spins for the quantum and auxiliary spaces mutually satisfy the Yang–Baxter relations. The Hamiltonian has the form

$$H=\sum_j 2H_{j,j+1}+H_{\rm imp}+H_{\rm imp-imp}$$

(the host exchange constant J is set to 2). In general, the form of the lattice Hamiltonian is very complicated; it depends on S, S', θ_j, and the anisotropy γ. We can directly write down several important limiting cases of the Hamiltonian to clarify the situation. For example, for a spin-S' impurity introduced into the spin-1/2 Heisenberg chain we have $H_{j,j+1}=\mathbf{S}_j\mathbf{S}_{j+1}$. The impurity part of the Hamiltonian has the form, say for the jth impurity situated between sites m and $m+1$ of the host[36,41,50]

$$H_{\rm imp}=\left[\theta_j^2+\left(S'+\frac{1}{2}\right)^2\right]^{-1}\left\{(H_{m,\rm imp}+H_{\rm imp,m+1})+\{H_{m,\rm imp},H_{\rm imp,m+1}\}-\left(\frac{1}{4}+3S'(S'+1)\right)\times H_{m,m+1}-2i\theta_j[H_{m,\rm imp},H_{\rm imp,m+1}]\right\},\quad(4)$$

where [.,.] ({.,.}) denotes the (anti)commutator. One can see that $\theta_j=0$ and $S'=1/2$ corresponds to the simple inclusion of an additional site coupled to the system by the bulk interaction. On the other hand, for $\theta_j\to\infty$ one obtains an impurity spin totally decoupled from the host. For the easy-plane spin-1/2 chain with spin-1/2 impurities we have[38]

$$H_{\rm imp}=\frac{\sin^2\gamma}{\sinh^2\theta_j+\sin^2\gamma}\left\{\hat{B}^j(H_{m,\rm imp},H_{\rm imp,m+1})-H_{m,m+1}-i2\frac{\tanh\theta_j}{\sin\gamma}[H_{m,\rm imp},H_{\rm imp,m+1}]\right\},\quad(5)$$

where the operator $\hat{B}^j$ modifies the Heisenberg-like interaction by multiplying the transverse terms by $\cosh\theta_j$. For the isotropic SU(2)-symmetric spin-S host the structure of the Hamiltonian is more complicated (without the impurity it corresponds to the Takhtajan–Babujian chain[51,52]) with

$$\mathcal{H}_{a,b}=\sum_{j=|S-S'|+1}^{S+S'}\sum_{k=|S-S'|+1}^{j}\frac{k}{k^2+\theta^2}\prod_{l=|S-S'|}^{S+S'}\frac{x-x_l}{x_j-x_l},\quad(6)$$

$x=\mathbf{S}_a\mathbf{S}_b$ ($a,b=m,m+1,$imp), and $2x_j=j(j+1)-S(S+1)-S'(S'+1)$. Note that in this case the overall multiplier is $[\theta^2+(S+S')^2]^{-1}$ and the coefficient in front of $H_{m,m+1}$ becomes $-2S'(S'+1)-(S'+S)^2$. For the anisotropic case one has to replace x by $\hat{X}_{m,m+1}$, cf. Eq. (2), and x_j by the appropriate coefficients from Eq. (1).

If two impurities are situated between two neighboring host sites, they can interact *directly*, e.g., for the isotropic case the impurity–impurity part of the Hamiltonian is $H_{\rm imp\text{-}imp}=\Sigma_j\theta_j^2J_{\rm imp}^j\mathcal{H}_{j,j+1}$; for illustration, see Fig. 1. These impurity–impurity couplings can model, e.g., a RKKY interaction (one of short range though) between the impurities in oncentrated metallic alloys. In the following we shall study the case with a *small* number of such neighboring impurities.

One can independently incorporate any number of impurities, described above, into the host spin chain. Each of them will be characterized by its own coupling to the host, i.e., by its own θ_j. The lattice Hamiltonian has additional terms, which renormalize the coupling between the neighboring sites of the host, and three-spin terms. However, it has been shown[50] that in the long-wavelength limit such a lattice form of the impurity Hamiltonian yields the well-known form of

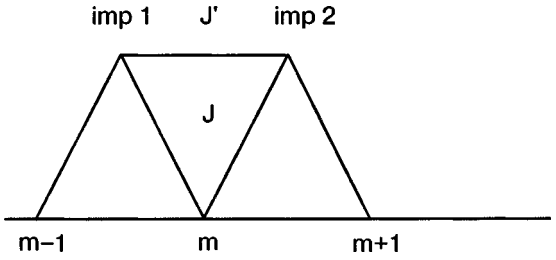

FIG. 1. Illustration of the impurity–host and impurity–impurity interactions. Here in the simplest case of the isotropic Heisenberg interaction the local impurity–host exchange constant $J=2[\theta_j^2+(S+S')^2]^{-1}$ and $J'\sim 2\theta_j^2 J$ in units of the host exchange constant 2.

the contact impurity–host interaction, similar to that of the usual Kondo problem.[2,3] The contact impurity coupling in this (conformal) limit is also determined by the same constant θ_j. We also point out that it was shown that the magnetic behavior of the impurities in the bulk and the magnetic behavior of the impurity situated at the edge of the chain (where the renormalization of the coupling between the neighboring sites of the host and three-spin terms can be eliminated, and the only interaction between the impurity and the host is the standard two-spin exchange interaction) coincide.[41,53] Finally, we would like to note that all the impurities considered in our work are *elastic* scatterers, i.e., each excitation only changes its phase when scattering off each impurity, but is not reflected. It is worthwhile to note the same property holds for the theory of a standard Kondo impurity in a free-electron host.[2,3] Equally important to mention is that we are studying a *lattice* model, and, hence, all two-particle scattering processes, in particular, from one Fermi point to the other (backscattering), are taken into account in our work. However, we emphasize again that our model (as well as the exact solution for the Kondo problem in metals)[2,3] does not describe reflecting impurities.

The Hamiltonian and other integrals of motion, which can be constructed in a similar way as higher-order logarithmic derivatives, commute with the transfer matrix.

3. BETHE ANSATZ AND RELATION TO THE KONDO PROBLEM

The eigenvalues and eigenstates of the above-mentioned problem are parametrized by the quantum numbers (*rapidities*) $\{u_j\}_{j=1}^M$, where M is related to the z projection of the total spin as $S^z=(S+S'c_{\rm imp})L-M$, where L is the total length of the chain (including the impurity sites) and $c_{\rm imp}$ is the concentration of impurities. Notice that the Hamiltonian commutes with the z projection of the total spin; hence, M enumerates all possible states. We shall consider not very large concentrations of impurities. Those rapidites are the solutions of the Bethe equations

$$\prod_{j=1}^{L} e_{2s}(u_j-0_j)=-\prod_{k=1}^{M} e_2(u_j-u_k), \tag{7}$$

where $j=1,...,M$,

$$e_n(x)=\frac{\sinh\gamma(x+in)}{\sinh\gamma(x-in)},$$

$s=S$ for the host sites (with $\theta_f=0$) and $s=S'$ for impurity sites, where θ_f can be nonzero. The energy of the state with the z projection of the total spin, characterized by M, is equal to

$$E_0\equiv Le_0=-i\frac{\sin(2\gamma S)}{4S}\sum_{j=1}^{M}\frac{d}{du_j}\ln e_s(u_j). \tag{8}$$

This formula is valid for the cases in which the lengths of the clusters of neighboring impurities, which interact with each other, are small.

It is easy to show that the behavior of the ensemble of multichannel (with $2S$ channels) Kondo impurities, each of which is coupled to the free-electron gas via its own easy-plane-anisotropic local exchange interaction, with the Hamiltonian

$$\begin{aligned}H_K=&\sum_{k,l,\sigma}\epsilon_k c^\dagger_{k,l,\sigma}c_{k,l,\sigma}+\frac{1}{2}\sum_j\ \delta(x-x_j)\\&\times\sum_{l=1}^{2S}\{\Delta_j[(S')^z_j]^2+J_j^{\rm par}(S')^z_j(c^\dagger_{x,l,\uparrow}c_{x,l,\uparrow}\\&-c^\dagger_{x,l,\downarrow}c_{x,l,\downarrow})+J_j^{\rm perp}[(S')^+_j c^\dagger_{x,l,\downarrow}c_{x,l,\uparrow}\\&+(S')^-_j c^\dagger_{x,l,\uparrow}c_{x,l,\downarrow}]\},\end{aligned} \tag{9}$$

where $c^\dagger_{k,l,\sigma}$ creates an electron of channel l with the spin σ and impurities are situated at sites x_j, can be also described within the Bethe ansatz scheme. In the scaling limit for small magnetic anisotropy one has $J_j^{\rm par}=2\gamma/\theta_j\rho$, $J_j^{\rm perp}=J_j^{\rm par}(1-\delta_j/3)$, and $\Delta_j=-J_j^{\rm par}\delta_j/3$, where $\delta_j=(\theta_j^2/2)+(\gamma^2/8)$ and ρ is the density of states of conduction electrons at the Fermi level. In this case the low-energy spin behavior (which is the most important one for the Kondo impurities) is determined by the solution of Eqs. (7), while the energy is determined via

$$E_K\equiv L_{e_{0K}}=-i\frac{\sin(2\gamma S)}{4S}\sum_{j=1}^{M}\ \ln e_s(u_j). \tag{10}$$

The condition of applicability of the Bethe ansatz scheme for ensembles of disordered impurities is the presence of large enough numbers of magnetic impurities with equal exchange constants, while those constants for other impurities can be randomly distributed. For small enough impurity concentrations the probability of having long clusters of impurities connected by the direct impurity–impurity interactions is small, and in the thermodynamic limit $L\to\infty$ one can neglect the contribution of such clusters. In this case the contribution of each impurity (or of each small cluster of directly coupled impurities) is *additive*, and we can solve the problem for each impurity (cluster), determined by the local exchange coupling constant (related to θ_j) and, then, introducing the distribution of θ_j over the chain (in the volume of the metal for the case of the Kondo impurities), average the answers for the thermodynamic characteristics. Such an additive property is a consequence of the exact integrability of the problem and is strictly connected with the structure of the Hamiltonians considered. It turns out, however, that in the

long-wavelength limit the "triangular" structure of the impurity–host interaction actually produces a local contact impurity–host interaction,[36–38,50] and the "fine-tuning" structure of the couplings between magnetic impurities and the host becomes nonessential.

4. THE GROUND-STATE BEHAVIOR

Let us first study the ground-state behavior of the systems considered. In the absence of magnetic field the ground-state energy of the impurity is

$$e_0(\theta_j)=-\frac{\pi\sin(2\gamma S)}{4\gamma S}\int d\omega e^{i(\pi\omega\theta_j)/\gamma}\frac{\sinh\left[\frac{\pi\omega}{\gamma}\min(S,S')\right]\sinh\left[\left(\frac{\pi^2}{2\gamma}-\pi\max(S,S')\right)\omega\right]}{\sinh(\pi\omega)\sinh\left(\frac{\pi\omega}{2}\right)}, \tag{11}$$

and the total ground-state energy is equal to

$$E_0=\sum_j e_0\left(\frac{\pi}{\gamma}\theta_j\right), \tag{12}$$

where the sum is taken over all the sites (for sites without impurities we get $e_0(0)$). Notice that for $\theta_j=0$ and for $S'=S$ the impurity is just an additional site of the host, the ground-state energy per site of which is

$$e_0(0)=-\frac{\pi\sin(2\gamma S)}{4\gamma S}\times\int d\omega\frac{\sinh\left(\frac{\pi\omega}{\gamma}S\right)\sinh\left[\left(\frac{\pi^2}{2\gamma}-\pi S\right)\omega\right]}{\sinh(\pi\omega)\sinh\left(\frac{\pi\omega}{2}\right)}. \tag{13}$$

For the Kondo impurities Eq. (11) can be used with the overall multiplier 1/2.

The coupling of the impurity to the host ($J^j_{\rm imp}$) is determined by the constant θ_j. We can show (see also Refs. 41 and 50) that precisely this constant determines the effective Kondo temperature of the impurity in a spin chain via $T_{jK}\propto\exp(-\pi|\theta_j|)$. For energies higher than this crossover Kondo scale one has the asymptotically free impurity spin S, while for lower energies the impurity spin is underscreened for $S'>S$ (with the Curie-like behavior of the remnant effective spin $S'-S$), totally screened for $S'=S$ (with the usual marginal FL-like behavior persisting with the finite susceptibility and linear temperature dependence of the specific heat at low temperature, and, hence, finite Wilson ratio in the ground state) and overscreened for $S'<S$ (with the critical non-FL behavior of a single spin[5]). It is similar to the findings in the theory of a Kondo impurity in a free-electron matrix.[2,3] In other words, θ measures the shift off the Kondo resonance (higher values of $|\theta_j|$ correspond to lower values on the Kondo scale) of the impurity level with the host spin excitations, similar to the standard picture of the Kondo effect in the electron host. The difference between the two models is that in the free-electron host the spins of free electrons screen the magnetic impurity, while in the spin chain the low-lying spin excitations (spinons for the AF chain) quench the spin of the impurity.

Let us illustrate this with the help of the ground-state behavior of impurities in small magnetic field h. The ground-state energy per site is equal to (we shall consider sufficiently small $\gamma<\pi/2S$)

$$e_0(\theta_j,h)=e_0(\theta_j)-\int d\omega e^{i\omega\pi\theta_j/\gamma}\frac{y^+\left(\frac{\pi\omega}{\gamma}\right)\sinh(\omega\pi S')}{2\cosh\left(\frac{\pi\omega}{2}\right)\sinh(\omega\pi S)} \tag{14}$$

for $S'\leqslant S$ and

$$e_0(\theta_j,h)=e_0(\theta_j)-\frac{\pi(S'-S)h}{\pi-2S\gamma}-\int\frac{d\omega}{2\gamma}e^{i\omega\pi\theta_j/\gamma}\frac{y^+\left(\frac{\pi\omega}{\gamma}\right)\sinh\left[\omega\left(\frac{\pi^2}{2\gamma}-\pi S'\right)\right]}{2\cosh\left(\frac{\pi\omega}{2}\right)\sinh\left[\omega\left(\frac{\pi^2}{2\gamma}-\pi S\right)\right]} \tag{15}$$

for $S'\geqslant S$. Here $y^+(\omega)$ is the positive part of the solution of the equation

$$y(u)+\int_0^\infty du'y(u')J(u-u')-\frac{h}{2}+\frac{\pi\sin(2\gamma S)}{4\gamma S\cosh\left[\frac{\pi(u+B)}{\gamma}\right]}=-\int_0^\infty du'y(u')J(u+u'+2B), \tag{16}$$

where the Fourier transform of $J(x)$ is

$$J(\omega)=\frac{\sinh\left(\frac{\gamma\omega}{2}\right)\sinh\left(\frac{\pi\omega}{2}\right)}{2\cosh\left(\frac{\gamma\omega}{2}\right)\sinh(\gamma\omega S)\sinh\left[\omega\left(\frac{\pi}{2}-\gamma S\right)\right]} \tag{17}$$

and B is connected with the value of the external magnetic field. Notice that for the Kondo problem the right-hand side of Eq. (16) is small and is usually dropped (see, however, Ref. 54). Equation (16) for small fields can be solved as the sequence of Wiener–Hopf equations. It also gives the connection between h and B:

$$h=\frac{\pi^2\sin(2\gamma S)}{2\gamma S}\mathrm{e}^{-(B+a)\pi/\gamma}\times\frac{\Gamma\left(1+\frac{\pi}{2\gamma}\right)}{\Gamma(1+S)\Gamma\left(1-S+\frac{\pi}{2\gamma}\right)}+\ldots, \tag{18}$$

where a is some nonuniversal constant.

For $S'=S$ we close the contour of integration in Eq. (15) through the upper half plane (the main pole is that of $\cosh(\pi\omega/2)$) and have

$$e_0(\theta_j,h)=e_0(\theta_j)-\frac{2S^2\gamma(\pi-2\gamma S)h^2}{2\pi^3\sin(2\gamma S)T_{jK}}-\frac{Ah^{2+2\gamma(\pi-2\gamma S)}}{T_{jK}}-\ldots, \tag{19}$$

for $h\ll T_{jK}$, where for small γ, $T_{jK}=v\,\mathrm{e}^{-\pi|\theta_j|/\gamma}$ ($v=\pi\sin(2\gamma S)/2\gamma S$ is the Fermi velocity of low-lying excitations) plays the role of the ''local'' Kondo temperature, and A is some nonuniversal constant. Each single magnetic impurity is *totally compensated* for $h\ll T_{jK}$. The susceptibility of a single impurity is *finite* as $h\to 0$ and is renormalized by a factor of T_{jK} with respect to the host susceptibility. Again, the total ground state energy is the sum of energies of all impurities and host spins (the latter with $\theta_j=0$, i.e., $T_{jK}=v$). We shall show below (see Sec. 4) that the strong disorder in the distribution of the local Kondo temperatures can lead to the divergent magnetic susceptibility for $h\to 0$, i.e., to the NFL behavior.

It turns out that some studies connect the multiplier $(1-2\gamma S/\pi)$ with the renormalization of the effective g factor of the spins,[3] while other works relate such a change to the NFL behavior caused by the magnetic anisotropy.[43,44]

For $S'>S$ the main contribution to the integral arises from the poles at $\omega=i\pi/\gamma$ (and then $\omega=2\pi/(\pi-2\gamma S)$) which produces for $h\ll T_{jK}$

$$e_0(\theta_j,h)=e_0(\theta_j)-\frac{(S'-S)\pi h}{(\pi-2\gamma S)}-Ch\left(\frac{h}{T_{jK}}\right)^{2\gamma/(\pi-2\gamma S)}+\ldots, \tag{20}$$

where C is a nonuniversal constant. We can see that for $h\to 0$ the magnetization is *finite* for a single impurity, and spins of single impurities are *underscreened* to the value $S'-S$ by host low-lying excitations.

Finally, for $S'<S$ and $h\ll T_{jK}$ we have

$$e_0(\theta_j,h)=e_0(\theta_j)-C'h\left(\frac{h}{T_{jK}}\right)^{1/S}+\ldots, \tag{21}$$

for $S>1$, where C' is a nonuniversal constant, and for $S=1$, $S'=1/2$ we have

$$e_0(\theta_j,h)=e_0(\theta_j)-\frac{2\gamma(\pi-2\gamma)h^2}{4\pi^3\sin(2\gamma)T_{jK}}\ln(T_{jK}/h)+\ldots\ . \tag{22}$$

Hence, for $S'<S$ the spins of single impurities are *overscreened*, and that produces the NFL behavior.

5. THERMODYNAMICS AND THE "QUANTUM TRANSFER MATRIX" APPROACH

For our 1D inhomogeneous quantum spin system at finite temperature we choose a suitable lattice path integral representation by a mapping which preserves integrability. For a general formulation of the Trotter–Suzuki decompositions used in our approach we refer to Refs. 55–58. As usual, we study the associated 2D classical vertex model instead of the direct treatment of the 1D quantum system.

One can introduce R matrices of different types, related to the initial one by a counterlockwise rotation, $\overline{R}^{\mu\nu}_{\alpha\beta}(u)=R^{\alpha\beta}_{\nu\mu}(u)$, and by a clockwise rotation, $\tilde{R}^{\mu\nu}_{\alpha\beta}(u)=R^{\beta\alpha}_{\mu\nu}(u)$. The transfer matrix $\overline{\tau}(u,\{\theta\}_{i=1}^{L})$ can be constructed in a way similar to the case of τ. Then we substitute $u=-J\sin\gamma/NT$, where N is the Trotter number. We find

$$[\tau(u)\overline{\tau}(u)]^{N/2}=\mathrm{e}^{-H/T}+O(1/N). \tag{23}$$

Hence, the partition function of the quantum 1D system is identical to the partition function of an inhomogeneous classical vertex model with alternating rows on a square lattice of size $L\times N$:

$$Z=\lim_{N\to\infty}\mathrm{Tr}[\tau(u)\overline{\tau}(u)]^{N/2}. \tag{24}$$

The interactions on the 2D lattice are four-spin interactions with coupling parameters depending on $(NT)^{-1}$ and interaction parameters θ_i, where i is the number of the column to which that particular vertex of the lattice belongs. Note that the interactions are homogeneous in each column, but vary from column to column. This is similar to the McCoy–Wu model,[59] which is the Ising model with disorder. (However in its 1D realization the Hamiltonian of the McCoy–Wu model can be mapped on the quadratic fermion form by means of the Jordan–Wigner transformation, i.e., there are no interactions in that model. Our models definitely reveal an essential coupling between particles.) We study this system in the thermodynamic limit N, $L\to\infty$ using an approach which is based on a transfer matrix describing transfers in the horizontal direction. The corresponding column-to-column transfer matrices are referred to as ''quantum transfer matrices'' (QTMs) (where an external magnetic field h is included by means of twisted boundary conditions):

$$\tau_{QTM}(\theta_j,u)=\sum_{\mu}\mathrm{e}^{\mu_1 h/T}\prod_{i=1}^{N/2}R^{\mu_{2i-1}\mu_{2i}}_{\alpha_{2i-1}\beta_{2i-1}}\times(u+i\theta_j)\tilde{R}^{\mu_{2i}\mu_{2i+1}}_{\alpha_{2i}\beta_{2i}}(u-i\theta_j). \tag{25}$$

See Fig. 2 for an illustration of the transfer matrices of the associated 2D statistical model.

In general all QTMs corresponding to the L columns are different. However, all these operators commute pairwise. Therefore, the free energy per lattice site of our 1D quantum system can be calculated from the largest eigenvalues of the quantum transfer matrices (corresponding to only one eigenstate). The free energy per site f of the 1D inhomogeneous quantum spin chain is given by only the largest eigenvalue of the quantum transfer matrix Λ_{QTM} as

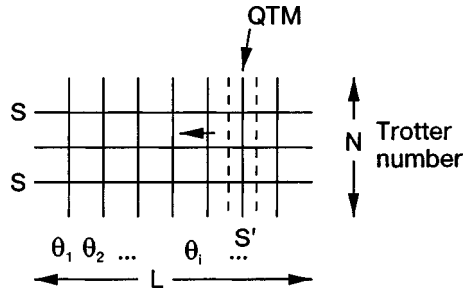

FIG. 2. The classical 2D model with four-spin interaction around vertices and alternating coupling parameters from column to column, related to the quantum 1D chain.

$$f=-\lim_{L\to\infty}\frac{T}{L}\sum_{i=1}^{L}\lim_{N\to\infty}\ln\Lambda_{QTM}(\theta_i,u), \tag{26}$$

where $u=-J\sin\gamma/TN$ and the dependence on N is understood implicitly.

Let us consider the hierarchy of QTMs acting on the subspace $\otimes^N V_{2S}$ (the index specifies the spins of the scatterers) with T_n being a member of such hierarchy with the auxiliary subspace V_n (here the index n specifies the spin of the auxiliary particle, i.e., the auxiliary particle with spin $n/2=S'$ scatters off N spins S). By means of a Bethe ansatz procedure we find the eigenvalue of the quantum transfer matrix to be given by

$$\Lambda_{QTM}(\theta_i)=\frac{\Lambda_{2S'}\left(\dfrac{2\theta_i}{\gamma}\right)}{\Pi_{p=1}^{2S'}[\sinh(ip\gamma)]^{N/2}} \tag{27}$$

and

$$\Lambda_p(x)=\sum_{l=1}^{p+1}\lambda_l^{(p)}(x),$$

$$\lambda_l^p(x)=\psi_l^{(p)}(x)e^{h(p+2-2l)/T}\times\frac{Q[x+i(p+1)]Q[x-i(p+1)]}{Q[x+i(2l-p-1)]Q[x+i(2l-p-3)]},$$

$$\psi_l^{(p)}(x)=\prod_{z=1}^{p-l+1}\phi_-[x-i(p-2S-2z)]\phi_+[x+i(p-2S+2-2z)]\prod_{z=1}^{l-1}\phi_-[x-i(p-2S+2-2z)]\phi_+[x+i(p-2S-2z)] \tag{28}$$

with $p\geqslant 2$, $\Lambda_0=1$ and

$$\Lambda_1(x)=\phi_+[x-i(2S-1)]\phi_-[x-i(2S+1)]e^{h/T}\times\frac{Q(x+2i)}{Q(x)}+\phi_-[x+i(2S-1)]\times\phi_+[x+i(2S+1)]e^{-h/T}\frac{Q(x-2i)}{Q(x)}. \tag{29}$$

Here we have dropped the dependence on u and θ_i, which are fixed, and consider the dependence on the spectral parameter x explicitly. We have used

$$\phi_\pm(x)=\sinh^{N/2}\left(\gamma\frac{x\pm iu'}{2}\right),$$

$$Q(x)=\prod_{j=1}^{m}\sinh\left(\gamma\frac{x-x_j}{2}\right) \tag{30}$$

with "renormalized" $u'=2u/\gamma$. Here $\{x_j\}_{j=1}^m$ is the set of Bethe ansatz rapidities, which are subject to the "local" Bethe ansatz equations

$$\frac{\phi_-[x_j+i(2S-1)]\phi_+[x_j+i(2S+1)]}{\phi_+[x_j-i(2S-1)]\phi_-[x_j-i(2S+1)]}=e^{-2h/T}\frac{Q(x_j+2i)}{Q(x_j-2i)}, \tag{31}$$

where m is the number of the roots of the "local" Bethe ansatz equations, being different for different eigenstates of the QTM. For the largest eigenvalue we have to take $m=NS$. However, we shall not solve Eqs. (31) directly but rather shall be interested in the functional properties of the eigenvalue of the transfer matrix. Note that $\Lambda_0=1$ and

$$\Lambda_p(x+i)\Lambda_p(x-i)=f_p(x)+\Lambda_{p-1}(x)\Lambda_{p+1}(x), \tag{32}$$

where $p\geqslant 1$ and

$$f_n(x)=\prod_{j=1}^{n}\prod_{\pm}\phi_\pm[x\pm i(n-2S-2j+1)]\times\phi_\pm[x\pm i(2S-n+2j+1)]. \tag{33}$$

For this purpose we introduce auxiliary functions $y_n(x)$, $Y_n(x)=1+y_n(x)$, $b(x)$, $\overline{b}(x)$, $B(x)=1+b(x)$, and $\overline{B}(x)=1+\overline{b}(x)$ by

$$y_n(x)=\Lambda_{n-1}(x)\Lambda_{n+1}(x)/f_n(x),\quad n\geqslant 1,$$

$$b(x)=\frac{\lambda_1^{(2S')}(x+i)+\ldots+\lambda_{2S'}^{(2S')}(x+i)}{\lambda_{2S'+1}^{(2S')}(x+i)},$$

$$\overline{b}(x)=\frac{\lambda_2^{(2S')}(x-i)+\ldots+\lambda_{2S'+1}^{(2S')}(x-i)}{\lambda_1^{(2S')}(x-i)}, \tag{34}$$

where $n\geqslant 1$. Then one can straightforwardly check that ($y_0=0$)

$$y_n(x+i)y_n(x-i)=Y_{n-1}(x)Y_{n+1}(x),$$

$$\Lambda_{2S'}(x+i)=B(x)\lambda_{2S'+1}^{(2S')}(x+i)=e^{-2S'/T}\prod_{\pm}\prod_{j=1}^{2S'}\phi_\pm[x+i(2j+2S-2S'-\pm 1)]\frac{Q(x-2iS')}{Q(x+2iS')},$$

$$\Lambda_{2S'}(x-i)=\overline{B}(x)\lambda_1^{(2S')}(x-i)=e^{-2S'h/T}\prod_{\pm}\prod_{j=1}^{2S'}\phi_\pm[x-i(2j+2S-2S'\pm 1)]\times\frac{Q(x+2iS')}{Q(x-2iS')}. \tag{35}$$

Notice that the first set of equations is nothing but the fusion hierarchy (so-called Y system). Let us use the first $2S'-2$ equations of the Y system as they are. In the equation for $y_{2S'-1}$ we replace $Y_{2S'}(x)$ by $B(x)\overline{B}(x)$, due to

$$Y_p(x)=B(x)\overline{B}(x), \tag{36}$$

i.e., we have

$$y_{2S'-1}(x-i)y_{2S'-1}(x+i)=Y_{2S'-2}B(x)\overline{B}(x). \tag{37}$$

Then we obviously have

$$\begin{aligned} b(x)&=\mathrm{e}^{(2S'+1)h/T}\\ &\times\prod_{\pm}\frac{\phi_{\pm}[x+i(2S-2S'\pm1)]\Lambda_{2S'-1}(x)}{\Pi_{j=1}^{2S'}\phi_{\pm}[x+i(2j+2S-2S'\pm1)]}\\ &\times\frac{Q[x+i(2S'+2)]}{Q(x-2iS')},\\ \overline{b}(x)&=\mathrm{e}^{-(2S'+1)h/T}\\ &\times\prod_{\pm}\frac{\phi_{\pm}[x+i(2S-2S'\pm1)]\Lambda_{2S'-1}(x)}{\Pi_{j=1}^{2S'}\phi_{\pm}[x-i(2j+2S-2S'\pm1)]}\\ &\times\frac{Q[x-i(2S'+2)]}{Q(x+2iS')} \end{aligned} \tag{38}$$

and

$$\Lambda_{k-1}(x-i)\Lambda_{k-1}(x+i)=Y_{k-1}(x)f_{k-1}(x), \tag{39}$$

which are consequences of the definitions.

What do these additional functions describe? We can understand this by taking into consideration only the SU(2)-symmetric case, i.e., $\gamma=0$. Here according to Ref. 60 the scattering matrix of excitations of the quantum spin-1/2 system factorizes into the matrix of the spin-1/2 SU(2)-symmetric model and the matrix of the level-$2S$ sl_2-symmetric RSOS (restricted solid-on-solid) model[61,62] (consistent with the quantum field theory prediction that the conformal field theory (CFT) is the level-$2S$ Wess–Zumino–Novikov–Witten (WZNW) model, which can be approximately written as the sum of a Gaussian sector with the central charge $c=1$ and the Z_{2S} parafermionic sector with $c=(2S-1)/(S+1)$.[63] In the scaling limit Z_k parafermionic theory is approximately equivalent to the sl_2 RSOS model. Hence the functions b, $\overline{b}$, B, and $\overline{B}$ describe the spinon sector (spinons of the spin $S=1/2$ model), which pertains to the Gaussian for the SU(2)-symmetric case, while the y_j functions (with the additional condition $y_k=0$) describe the RSOS sector.

One can see that these auxiliary functions are analytic, nonzero, and have constant asymptotic behavior for the strip $-1<\mathrm{Im}\,x\leqslant 0$ for $b(x)$ and $B(x)$, for the strip $0\leqslant\mathrm{Im}\,x<1$ for $\overline{b}(x)$ and $\overline{B}(x)$, and for the strip $-1\geqslant\mathrm{Im}\,x\geqslant 1$ for y_n and Y_n. Introducing $a(x)=b(2(x+i\epsilon)/\pi)$ and $\overline{a}(x)=\overline{b}(2(x-i\epsilon)/\pi)$ (infinitesimal $\epsilon>0$), taking the logarithmic derivative of these functions, then Fourier transforming the equations, eliminating the functions $Q(x)$, and finally inverse-Fourier transforming, we obtain the final set of nonlinear integral equations. Eventually, we take the limit $N\to\infty$. Proceeding in this way we find for our system the following set of nonlinear integral equations for the "energy density" functions of spinons a, $\overline{a}$, $A=1+a$, $\overline{A}=1+\overline{a}$, y_n and Y_n in dependence on the spectral parameter x:

$$\begin{aligned} &\ln y_1(x)=\int k'(x-y)\ln Y_2(y)dy,\\ &\ln y_j(x)=\int k'(x-y)\ln[Y_{j-1}(y)Y_{j+1}(y)]dy,\\ &2\leqslant j\leqslant 2S'-1,\\ &\int [k'(x-y)\ln Y_{2S'-2}(y)+k'(x-y+i\epsilon)\ln A(y)\\ &\quad+k(x-y-i\epsilon)\ln\overline{A}(y)]dy=\ln y_{2S'-1}(x),\\ &\int [k(x-y)\ln\overline{A}(y)-k(x-y-i\pi+i\epsilon)\ln A(y)\\ &\quad+k'(x-y+i\epsilon)\ln Y_{2S'-1}(y)]dy\\ &\quad=\ln a(x)+\frac{v}{T\cosh x}+\frac{\pi h}{2(\pi-\gamma)T},\\ &\int [k(x-y)\ln A(y)-k(x-y+i\pi-i\epsilon)\ln\overline{A}(y)\\ &\quad+k'(x-y-i\epsilon)\ln Y_{2S'-1}(y)]dy\\ &\quad=\ln\overline{a}(x)+\frac{v}{T\cosh x}+\frac{\pi h}{2(\pi-\gamma)T} \end{aligned} \tag{40}$$

with kernel functions

$$k(x)=\frac{1}{2\pi}\int d\omega\,\frac{\sinh[(\pi^2S/\gamma-(2S+1)\pi)\omega]\cos(x\omega)}{2\cosh(\pi\omega/2)\sinh(S\pi\omega(\pi-\gamma)/\gamma)} \tag{41}$$

and

$$k'(x)=\frac{1}{2\pi}\int d\omega\,\frac{\cos(x\omega)}{2\cosh(\pi\omega/2)}. \tag{42}$$

The free energy per site f is given by

$$\begin{aligned} f(x)=e_0(x)&-\frac{T}{2\pi}\int\frac{\ln A(y)dy}{\cosh(x-y+i\epsilon)}\\ &-\frac{T}{2\pi}\int\frac{\ln\overline{A}(y)dy}{\cosh(x-y-i\epsilon)}, \end{aligned} \tag{43}$$

where e_0 is the ground-state energy. The free energy of the total chain with impurities is

$$F=\sum_j f\left[\frac{\pi}{\gamma}\theta_j+i\pi(S'-S)\right], \tag{44}$$

where the sum is taken over all the sites (for sites without impurities we get $f(0)$).

The free energy per impurity of the multichannel Kondo problem of the ensemble of disordered impurities f_K is given by

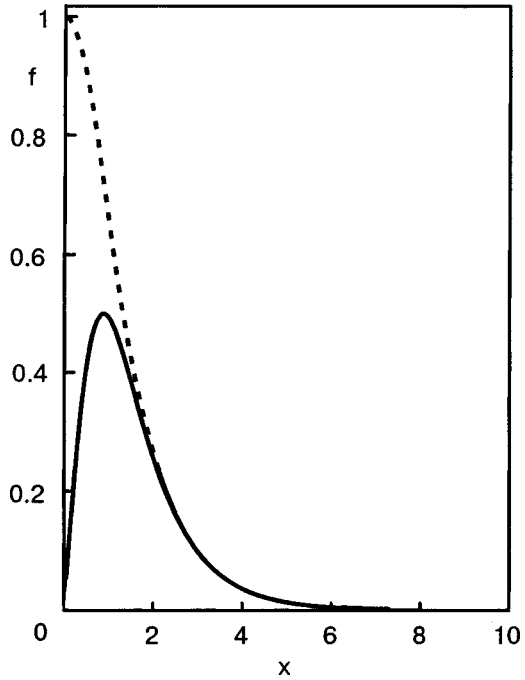

FIG. 3. The behavior of the kernels of Eq. (43) (dashed line) and Eq. (45) (solid line).

$$f_K(x)=e_{0K}(x)-\frac{T}{2\pi}\int\frac{\sinh(x-y+i\epsilon)\ln A(y)dy}{\cosh^2(x-y+i\epsilon)}$$
$$-\frac{T}{2\pi}\int\frac{\sinh(x-y-i\epsilon)\ln\overline{a}(y)dy}{\cosh^2(x-y-i\epsilon)}, \qquad (45)$$

where e_{0K} is the ground-state energy. Notice that for $S'<S$ one has to put $\ln Y_{2S'}$ into Eqs. (43)–(45) instead of $\ln A\overline{A}$, see Eq. (36). The free energy of the total ensemble of Kondo impurities is equal to

$$F_K=\sum_j f_K\left[\frac{\pi}{\gamma}\theta_j+i\pi(S'-S)\right], \qquad (46)$$

where the sum is taken over all the impurities. It turns our that for large arguments, which are important for the low-temperature characteristics, the behaviors of the kernels of Eqs. (43) and (45) are similar. The difference appears to be important for the energies of order of the values of local exchange constants and higher, cf. Fig. 3.

These equations can be easily solved numerically for arbitrary magnetic field values and temperatures. The random distribution of the values θ_j can be described by a distribution function $P(\theta_j)$. It is worthwhile to emphasize here the simplicity of the equations derived. For each impurity there are only two parameters, the real and imaginary shifts of the spectral parameter in the formula for the free energy per site, Eqs. (43), (45). Then the exact solvability of the problem for any number of impurities permits one to introduce the distribution of these shifts (the strengths of the impurity–host couplings pertinent to the local Kondo temperatures and the spins of the impurities). We have only $2S'+1$ nonlinear integral equations, Eqs. (40), to solve, and the answer can in principle be obtained for arbitrary temperature and magnetic field ranges.

6. DISORDERED ENSEMBLES OF MAGNETIC IMPURITIES

One can see from Eqs. (40)–(46) that for low T the temperature behavior of the magnetic susceptibility and specific heat of single impurities depends strongly on the relative values of the host spins S and impurity spin S'.

For $S>S'$ the impurity is *underscreened* by low-lying excitations of the chain (in the case of the Kondo impurity—by spins of conduction electrons). The magnetic susceptibility χ_j of such an impurity is divergent at $h=0$ for $T\to 0$. The specific heat c_j exhibits the Schottky anomaly, related to the undercompensated spin of the impurity. The entropy of a single impurity at $T=h=0$ becomes nonzero, $S_j=\ln[1+2\pi(S'-S)/(\pi-2\gamma S)]$. A finite magnetic field lifts the degeneracy and the remnant entropy becomes zero. Naturally, the total low-temperature magnetic susceptibility of any disordered ensemble of such impurities is also divergent at low temperatures.

On the other hand, for $S'<S$ the spins of low-lying excitations of the antiferromagnetic critical chain (spins of itinerant electrons for the multichannel Kondo case) *overscreen* the spin of a single magnetic impurity. This yields the critical behavior, which reveals itself in the divergences of the $T\to 0$ magnetic susceptibility of a single magnetic impurity and of the low-T Sommerfeld coefficient of the specific heat c_j/T for $h=0$. In this case one has a remnant $T=h=0$ entropy of each impurity

$$\mathcal{S}_j=\ln\frac{\sin[\pi(2S'+1)/(2S'+2)]}{\sin[\pi/(2S+2)]},$$

which is removed by a finite magnetic field that lifts the spin degeneracy of the system. It is not difficult to show by solving Eqs. (40)–(43) that at low T one has $c_j\propto T\chi_j \sim (T/T_{jK})^{2/(S+1)}$ for $S>1$ and $T_{jK}c_j/T\propto T_{jK}\chi_j\sim\ln(T_{jK}/T)$ for $S=1/2$ at zero magnetic field $h=0$. The total low-temperature χ_j and the Sommerfeld coefficient of any disordered ensemble of such impurities are also divergent at low temperatures.

Here the disorder of the distributions of the impurity–host couplings (local exchanges between Kondo impurities and conduction electrons) does not yield any qualitative changes but introduces only specific additional features of the NFL behavior of the system, which is already present for a single magnetic impurity.

A more interesting situation arises in the case $S'=S$. Here the solution of Eqs. (40)–(43) can be obtained[62] analytically. We know that at sufficiently low temperatures the functions a and $\ln A$ manifest a sharp crossover behavior, reminiscent of a step function: $|a|\ll 1$ and $|\ln A|\ll 1$ for $x<\ln \alpha T_{jK}/T$, and $|a|$, $|\ln A|\sim O(1)$ for $x>\ln \alpha T_{jK}/T$, where α is some constant and T_{jK} was introduced in Sec. 4. We can introduce[37] the scaling functions

$$\ln a^{\pm}=\ln a\{\pm[x+\ln(\alpha T_{jK}/T)]\},$$
$$\ln \overline{a}^{\pm}=\ln \overline{a}\{\pm[x+\ln(\alpha T_{jK}/T)]\},$$
$$\ln A^{\pm}=\ln A\{\pm[x+\ln(\alpha T_{jK}/T)]\},$$
$$\ln \overline{A}^{\pm}=\ln \overline{A}\{\pm[x+\ln(\alpha T_{jK}/T)]\},$$
$$\ln y_p^{\pm}=\ln y_p\{\pm[x+\ln(\alpha T_{jK}/T)]\},$$

$$\ln Y_p^{\pm} = \ln Y_p\{\pm[x + \ln(\alpha T_{jK}/T)]\},$$

where $p = 1,...,2S' - 1$. In terms of those scaling functions Eqs. (40) are renormalized in such a way that the driving terms (those which do not depend on functions $a, \bar{a}, \ldots, y_p$ and Y_p) in the last two equations for $h = 0$ become proportional to $v \exp(-x \pm i\epsilon)$ (where small corrections of order $O(T)$ have been neglected). Hence only the asymptotic behavior of A and $\bar{A}$ at large spectral parameter is essential.[62] Following the procedure described in Ref. 62, we obtain the low-temperature behavior of the free energy per site (for $h = 0$)

$$f(\theta_j) = e_0(\theta_j) - \frac{\pi S \gamma T^2}{2(S+1)\sin(2\gamma S) T_{jK}} \times \left[1 + \frac{3S^3}{[\ln(\alpha T_{jK}/T)]^3}\right] + \ldots . \quad (47)$$

In the presence of a weak magnetic field $h \ll T$ we can calculate the temperature corrections to the free energy per site:

$$f(\theta_j) = e_0^j(\theta_j, h) - \frac{\pi S \gamma T^2}{2(S+1)\sin(2\gamma S) T_{jK}} - \frac{h^2}{4\pi T_{jK}}\left[1 + \frac{1}{(2S+1)\ln(aT_{jK}/T)} + \frac{\ln|\ln(\alpha T_{jK}/T)|}{(2S+1)^2 \ln^2(\alpha T_{jK}/T)}\right] + O(T^2). \quad (48)$$

For a single impurity $P(T_{jK}) = \delta(T_{jK} - T_K)$ we immediately recover the famous Kondo behavior of the asymptotically free spin (characteristic for a Kondo impurity in a free-electron host[2,3] and for a single impurity in a Heisenberg AF chain).[41] For the homogeneous case we put $\theta_j = 0$ (which means that $T_{jK} \to v$, where v is the Fermi velocity of spinons). Naturally our result in this case coincides with the Bethe ansatz solution[58] and with the field theoretical prediction.[64] It turns out that the central charge of the CFT is $c = 3S/(S+1)$ and does not depend on the parameter of the impurity θ_j. One can see that only one parameter gets renormalized in the disordered case—the Fermi velocity of the U(1)-symmetric low-lying excitations: spinons (the Kondo scale plays the role of a "local Fermi velocity" for an impurity).[37]

Our models permit averaging over a distribution of θ_j (or "local" Fermi velocities) because of the factorization of the free energy of the system. This is a consequence of the integrability of our models (i.e., of the presence of only *elastic* scattering off impurities). Note that the θ_j dependence present in the low-energy characteristics results only in the universal scales T_{jK} (that is not so for higher energies, but the latter are irrelevant for the low-temperature disorder-driven divergences). Hence for low energies we can use distributions of T_{jK}, which are also more appropriate in connection to the experiments.[11–20,27–29] That is why the main features of the low-energy characteristics of our disordered spin chain are determined by the distributions of the effective Fermi velocities for the impurities. Let us consider the strong disorder distribution, which starts with the term $P(T_{jK}) \propto G^{-\lambda}(T_{jK})^{\lambda-1}$ ($\lambda < 1$) valid till some energy scale G for the lowest values of T_{jK} (that distribution has been shown to pertain to real disordered quantum spin chains[27–29] and some heavy fermion alloys;[11–20,25] see Figs. 4, 5, curves 3, for which we took $\lambda = 0.7$ and $G = 2$. Now we can calculate the low-temperature behavior of the average magnetic susceptibility χ, the Sommerfeld coefficient of the specific heat, and the correlation length of the form (the lower limit of the integral over the distribution of T_{jK} gives a regular contribution)

$$\langle \chi \rangle \propto \frac{\langle c \rangle}{T} \sim G^{-\lambda} T^{\lambda - 1}. \quad (49)$$

These formulas definitely manifest the low-T divergences of $\langle \chi \rangle$ and $\langle c \rangle / T$ and strong renormalization in the disordered spin chain as compared to the homogeneous situation. The ground-state average magnetization displays $M^z \sim (h/G)^{\lambda}$ behavior, also different from the homogeneous case.

Other important characteristics of our disordered spin chain, e.g., the dynamic magnetic susceptibility $\langle \chi'' \rangle(\omega, T)$, can be calculated. We can use the standard ansatz for the relaxational form of the susceptibility of a single magnetic impurity,[22,23]

$$\chi''(\omega, T) = \chi(T) \frac{\Gamma(T)\omega}{\omega^2 + \Gamma^2(T)}, \quad (50)$$

in which one supposes that the relaxation rate (proportional to the half-linewidth of the resonance line) Γ does not depend on the frequency ω. That ansatz automatically satisfies the Kramers—Kronig relation. At low temperatures the use of the Shiba approximation[22,23] determines the first ($T = 0$) term in the expansion of $\Gamma(T)$ via

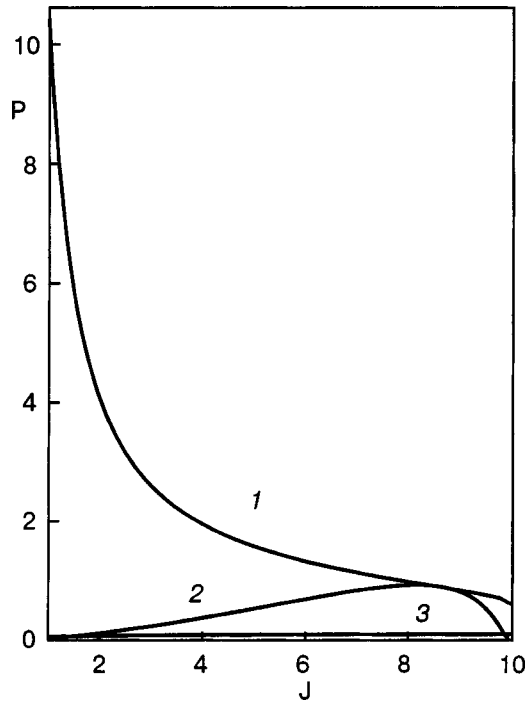

FIG. 4. Distributions, as functions of the local exchange constant (with $\gamma = 2$), used in this study, which produce the NFL behavior of the ensembles of spin-S impurities in the spin-S host: *1*—the Lorentzian distribution of θ_j; *2*—the log-normal distribution of θ_j; *3*—the power-law distribution. Very small values of the exchange constant are excluded.

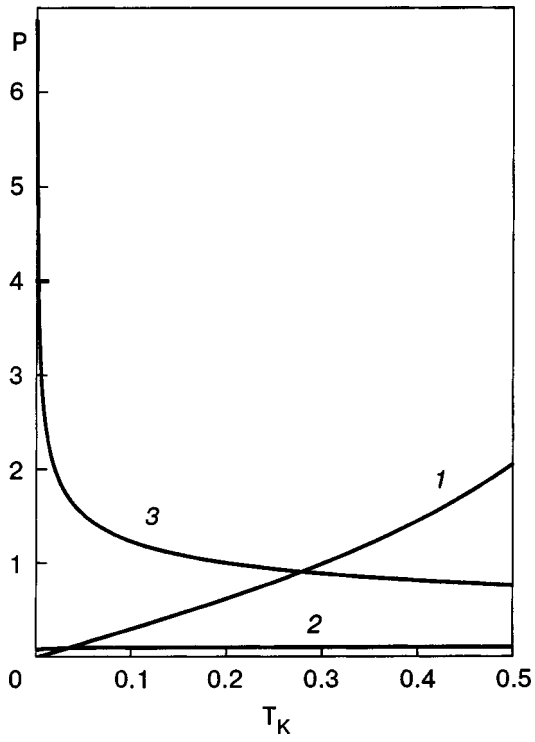

FIG. 5. Distributions, as function of T_K, used in this study, which produce the NFL behavior of the ensembles of spin-S impurities in the spin-S host: *1*—the Lorentzian distribution of θ_j; *2*—the log-normal distribution of θ_j; *3*—the power-law distribution. Notice that we have used only small values of T_K.

$$\lim_{\omega\to\infty}\frac{\chi''(\omega,0)}{\pi\omega}=2\chi^2(0). \tag{51}$$

That gives the low-temperature dependence of the relaxation rate per site for the disordered spin chain $\Gamma(T)\sim T_{jK}$. Hence we get

$$\langle\chi''\rangle(\omega,T)\sim G^{-1}(G/T)^{\lambda-1}g(\omega/T), \tag{52}$$

with g being the universal scaling function determined by $g(x)=x\int_1^\infty dy/y^{\lambda-1}(x^2+y^2)$, which differs drastically from the homogeneous case. Similar calculations, e.g., for the variation of the Knight shift and for the NMR relaxation rate yield $\delta K/K\propto\delta\chi/\chi\sim T^{-\lambda/2}$ where δA denotes the mean square deviation of A due to the distribution of T_{jK} and $T_1^{-1}\sim G^{-1}(G/T)^{\lambda-1}g(\omega/T)$.

For the important *marginal* case $\lambda=1$, logarithmic T divergences appear. Here one has the distribution $P(T_{jK}=0)=P_0\neq 0$ valid till G. Then averaging the low-temperature part of the susceptibility and Sommerfeld coefficient, we obtain

$$\langle\chi\rangle\propto\frac{\langle c\rangle}{T}\sim-\frac{P_0}{2\pi}\left[\ln\frac{G}{T}+\frac{1}{2}\ln\ln\alpha\frac{G}{T}+\ldots\right]. \tag{53}$$

Here we again see the zero-temperature divergences of $\langle\chi\rangle$ and $\langle c\rangle/T$ (weaker, though, than in the previous case). We can also calculate the low-field ground-state magnetization:

$$\langle M^z\rangle\sim hP_0[-\ln(h/G)-\ln(\ln(h/C'G))+\ldots].$$

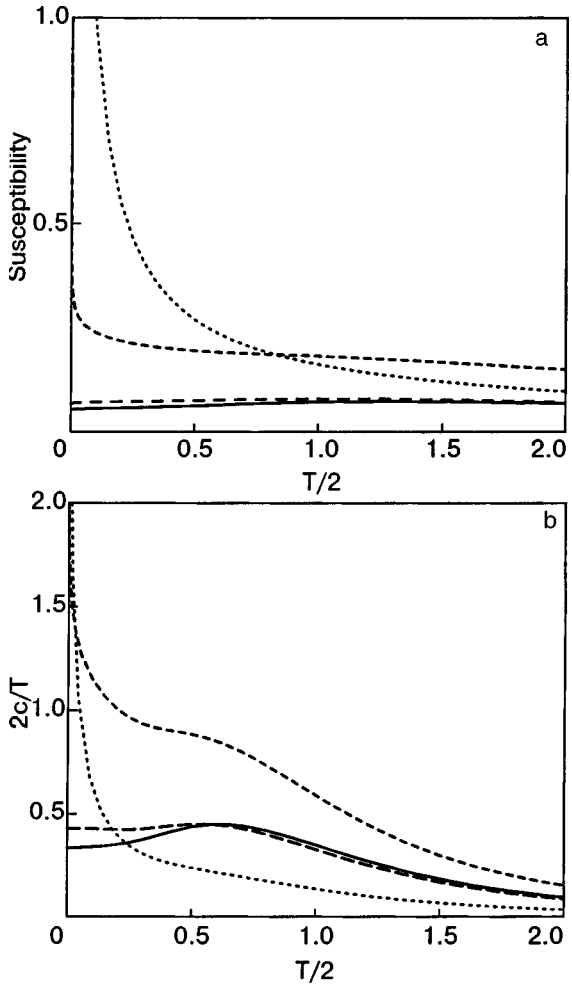

FIG. 6. Magnetic susceptibility (a) and the Sommerfeld coefficient c/T (b) at $h=0$ for the isotropic spin-1/2 antiferromagnetic chain with spin-1/2 magnetic impurities. The exchange constant of the host is 2. The solid line shows the homogeneous chain; the long-dashed line—the Gaussian distribution; the dashed line—the log-normal distribution; the dotted line—the Lorentzian distribution of θ_j.

We obtain for the dynamic magnetic susceptibility the scaling behavior

$$\langle\chi''\rangle(\omega,T)\sim P_0[(\pi/2)-\tan^{-1}(2GT/0.41\pi\omega)]$$

(which is again in drastic contrast to the homogeneous case).

The weak power-law or logarithmic dependence pertains to the Griffiths singularities in the proximity of the critical point $T=0$ (cf. Refs. 25 and 26). For these distributions of T_{jK} the Wilson ratio at $T=0$ is equal to $2\pi^2/3$, characteristic for a FL-like situation. It turns out that our above-mentioned results for low temperatures are also valid for random ensembles of $S'=n/2$ (where n is the number of channels) multichannel Kondo impurities with a local anisotropic, generally speaking, interaction of the latter with conduction electrons, because at low temperatures the difference between the energy of the spin chain and the spin subsystem of the Kondo system is small (cf. Fig. 3).

We can illustrate our analytical results by numerical calculations for the solutions of Eqs. (40)–(44) (for accurate numerical calculations see Ref. 38). In Fig. 6 the temperature dependences of the magnetic susceptibility and the Sommerfeld coefficient for the most usual AF spin magnetically iso-

tropic spin $S=1/2$ chain are depicted. The solid lines show the finite values of the low-T χ and c/T in this case. However, the dashed and dotted lines present the answers for the distributions of θ_j (which, in turn, corresponds to the distributions of either the impurity–host exchange constants, see curves 1 and 2 of Fig. 4, or local effective Kondo temperatures, see Fig. 5, which presents results for $\gamma=2$) with strong disorder. The latter means that the wings of the distributions are large enough compared to the maxima of the distributions. The dotted line corresponds to the Lorentzian distribution $P(\theta_j)=[(2\theta_j/\gamma)^2+\pi^2]^{-1}$. The dashed line pertains to the so-called logarithmically normal distribution[65]

$$P(\theta_j)=\frac{\exp(-[\ln(|2\theta_j/\gamma|+10^{-6})+1/4]^2)}{\sqrt{\pi}(|2\theta_j/\gamma|+10^{-6})},$$

which is also characteristic for strong disorder. One can see the qualitative difference between the behavior of $S'=S$ magnetic impurities with the strong disorder of the distribution of their couplings to the host as compared to the isotropic spin chain. The magnetic susceptibility and the Sommerfeld coefficient diverge strongly at $T\to 0$ for the highly randomly distributed parameters of the impurity–host couplings (note that in Ref. 37 we have shown that at low temperatures only the T_{jK} determine the scaling behavior of local impurities). This is in stark contrast with the homogeneous case. It turns out that the low-temperature asymptotics of the log-normal case of the disorder are[38]

$$c\sim\{\ln(1/T)\exp([\ln\ln(1/T)]^2\}^{-1},$$
$$\chi\sim\{T\ln\ln(1/T)\exp([\ln\ln(1/T)]^2\}^{-1}, \quad (54)$$

while for the Lorentzian distribution one has

$$c\sim[\ln(1/T)]^{-2},\ \ \chi\sim[T\ln(1/T)]^{-1}. \quad (55)$$

The latter case is similar to the situation present for the so-called Griffiths phase[26] at very low temperatures.

In Fig. 7 similar behaviors are seen for the magnetic susceptibilities and Sommerfeld coefficients of the homogeneous case and the cases with the log-normal and Lorentzian distributions (strong disorder) and the Gaussian distribution (weak disorder, see below) for the mostly anisotropic easy-plane case $\gamma=\pi/2$ (for $S=1/2$ this corresponds to the XX model, which for the homogeneous case pertains to the free spinless fermion gas). One can see that the changes due to the nonzero magnetic anisotropy of the easy-plane type are only qualitative. This is clear, because such an easy-plane magnetic anisotropy does not produce gaps for the low-energy excitations (i.e., it is a marginally irrelevant perturbation from the RG viewpoint), and, hence, the system remains in the critical regime.

On the other hand, the weak disorder does not produce such qualitative changes in the behavior of random ensembles of disordered magnetic impurities. By weak disorder we mean a narrow distribution of θ_j. The long-dashed lines of Figs. 6 and 7 depict the temperature behavior of the ensemble of magnetic impurities with the weak Gaussian distribution of θ_j (which is close to a single impurity distribution $P(\theta_j)=\delta(\theta_j)$). One can obviously see that such a narrow distribution (weak disorder) does not yield the divergences of the low-temperature magnetic susceptibility and the Sommerfeld coefficient of the specific heat.

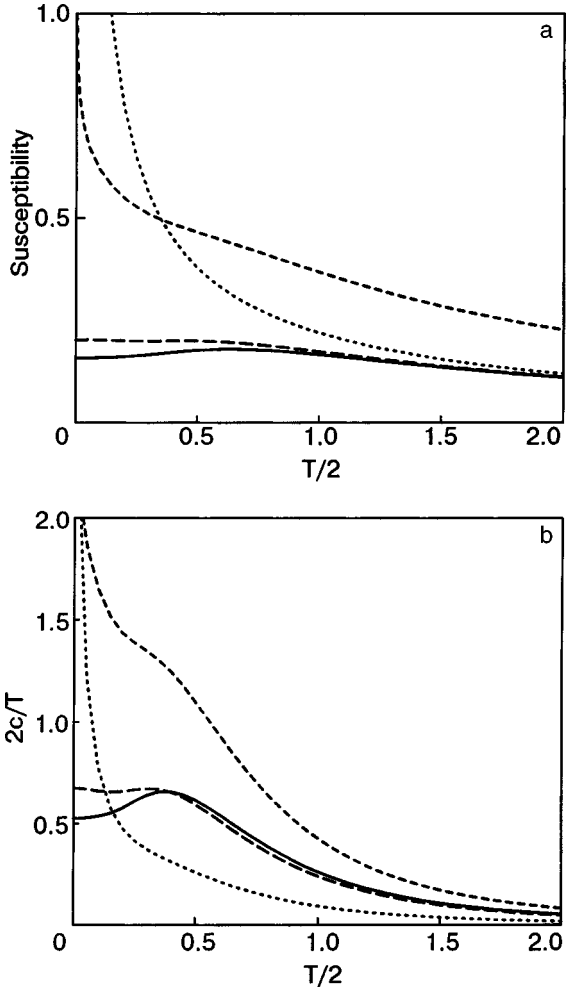

FIG. 7. Magnetic susceptibility (a) and the Sommerfeld coefficient c/T (b) at $h=0$ for the anisotropic $\gamma=\pi/2$ spin-1/2 antiferromagnetic chain with spin-1/2 magnetic impurities. The solid line shows the homogeneous chain; the long-dashed line—the Gaussian distribution; the dashed line—the log-normal distribution; the dotted line—the Lorentzian distribution of θ_j.

The reason for such a different behavior of wide and narrow distributions of the parameters that determine the impurity–host couplings (or strong–weak disorder, respectively) is clear. At low energies the local Kondo temperature determines the crossover scale for the behavior of the magnetic impurity. For the case $S'=S$ a single magnetic impurity is screened by low-lying excitations of the host for $T<T_{jK}$, and is not screened for $T>T_{jK}$ (with the Curie-like behavior of the unscreened remnant spin). For ensembles of magnetic impurities with weak disorder the temperature is larger than the average Kondo temperature of the ensemble of impurities, and, hence, the total magnetic susceptibility and the Sommerfeld coefficient are finite for $T\to 0$. For the strong disorder, on the contrary, many local Kondo temperatures are less than the temperature. Those impurities remain unscreened by the low-lying excitations of the host, and, hence, the total magnetic susceptibility and the Sommerfeld coefficient become divergent for $T\to 0$.

Finally we would like to show how the magnetic field

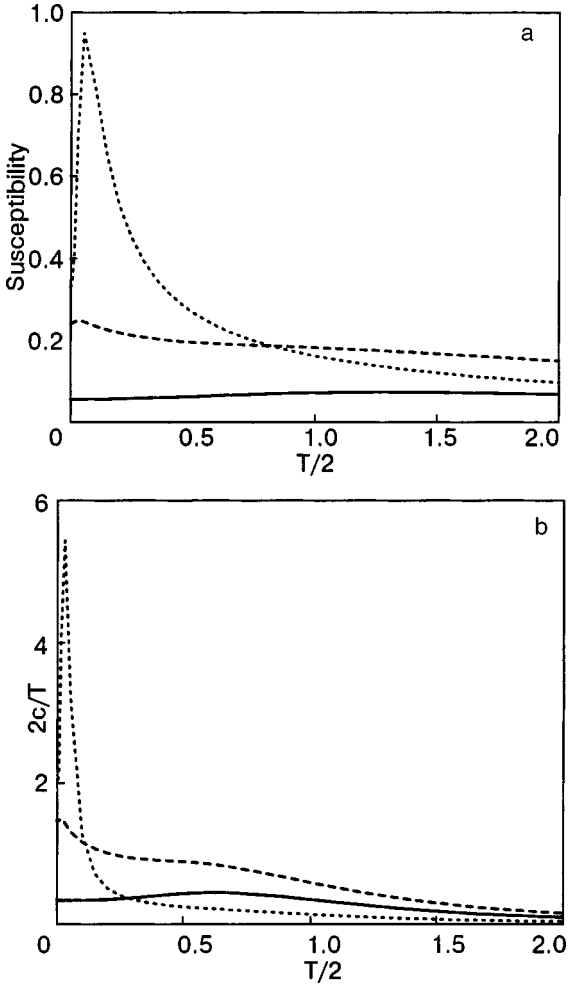

FIG. 8. Magnetic susceptibility (a) and the Sommerfeld coefficient c/T (b) at $h=0.2$ for the isotropic spin-1/2 antiferromagnetic chain with spin-1/2 magnetic impurities. The solid line shows the homogeneous chain; the dashed line—the log-normal distribution; the dotted line—the Lorentzian distribution.

lifts the degeneracy. In Fig. 8 the temperature behavior of the magnetic susceptibilities and the Sommerfeld coefficients in the isotropic cases is shown for the log-normal and Lorentzian distributions (cf. Fig. 6), but for the nonzero magnetic field $h=0.2$. One can clearly see that such a field removes the divergences in the low-T susceptibilities and Sommerfeld coefficients for the models with strong disorder. As an example, the temperature dependences of the same values for $h=0.2$ are shown for the homogeneous chain. It turns out that the weak magnetic field does not yield any qualitative changes in the temperature behaviors, as expected.

For higher values of the spins the changes, compared to the case $S'=S=1/2$, are only quantitative. For example, the values of χ and c become larger for larger spin values. However, there are no drastic changes in the behavior of disordered ensembles of impurities, in comparison with the case discussed above. This seems to be natural, because only low-lying excitations (which have Dirac seas in the ground state) are responsible for the Kondo-like screening of spins of impurities, while other excitations (the quasienergies of which are described by y_p and Y_p), are higher-energy. In other words, spinons, which describe the SU(2) (or U(1)) symmetries of the system (or the Gaussian of the WZNW model) are essential for the process of screening of magnetic impurities, while excitations that describe the sl_2 symmetry of the RSOS sector (or parafermions of the WZNW model) do not play a qualitative role in that process.

We point out again that for low temperatures ($T<2$) the numerical data are applicable to the behavior of the ensembles of Kondo impurities with easy-plane magnetic anisotropy (and, naturally, without it) of the local exchange interaction between magnetic impurities and conduction electrons.

7. CONCLUSIONS

Summarizing, in this work we have considered a number of exactly solvable models of magnetic impurities in critical quantum antiferromagnetic spin chains and multichannel Kondo impurities. We have studied their ground-state properties and constructed the finite set of nonlinear integral equations which exactly describe the thermodynamics of the models. We have obtained several analytical low-energy expressions for the temperature, magnetic field, and frequency dependences of important characteristics of the exactly solvable disordered quantum spin models and disordered multichannel Kondo impurities with essential many-body interactions. We also have analyzed the data of numerical calculations of those nonlinear integral equations. We have shown that the only low-energy parameter that gets renormalized is the velocity of the low-lying excitations (or the effective crossover scale connected with each impurity); the others appear to be universal. [Note that the finite-size corrections to the ground-state behavior of our disordered spin chains can be obtained just by replacing $(G/T)\to L$]. We used several kinds of strong disorder important for experiments. Some of them produce low divergences in certain characteristics of our strongly disordered critical systems (compared with the finite values for the homogeneous case or a single impurity). They pertain to wide distributions of the local Kondo temperatures, i.e., to strong disorder in the system. On the other hand, for weak disorder, or, in other words, for narrow distributions of the local Kondo temperatures, our exact results reveal the presence of the Kondo screening of the disordered ensembles of magnetic impurities by low-lying excitations of the host. We point out that our results qualitatively coincide with the data of experiments on real disordered quasi-1D quantum AF system[27–29] with $\lambda \sim 0.26-0.42$. Also, qualitatively similar behavior has been observed in 3D heavy metallic alloys[11–20] with $\lambda \sim 0.60-0.85$. It is interesting to note that similar results were recently obtained in which the distributions of Kondo temperatures used in this work were derived either from the proximity to a phase transition point in the Griffiths phase approximation (cluster percolation)[26] or from the Anderson localization effects in the infinite-dimensional statistical dynamical mean field theory approximation.[66] Also our results can be useful for the description of the Kondo necklace model.[67,68] All these similarities can be considered as the manifestation of generic features of the behavior of concentrated disordered magnetic systems for temperatures higher than a critical temperature in our effectively one-dimensional exactly integrable quantum models.

*E-mail: zvyagin@ilt.kharkov.ua

[1] J. Kondo, in *Solid State Physics: Advances in Research and Applications*, F. Seitz, D. Turnbull, and H. Ehrenreich (Eds.), Academic, New York (1969), Vol. 23, p. 184.
[2] N. Andrei, K. Furuya, and J. H. Lowenstein, Rev. Mod. Phys. **55**, 331 (1983).
[3] A. M. Tsvelick and P. B. Wiegmann, Adv. Phys. **32**, 453 (1983).
[4] I. Affleck, Acta Phys. Polonica B **26**, 1869 (1995).
[5] P. Schlottmann and P. D. Sacramento, Adv. Phys. **42**, 641 (1993).
[6] D. L. Cox and A. Zawadowski, Adv. Phys. **47**, 599 (1998).
[7] H. v. Löhneysen, F. Huster, S. Mock, A. Neubert, T. Pietrus, M. Sieck, O. Stockert, and M. M. Waffenschmidt, Physica B **230–232**, 550 (1997).
[8] M. B. Maple, M. C. de Andrade, J. Herrmann, Y. Dalichaouch, D. A. Gajewski, C. L. Seaman, R. Chau, R. Movshovich, M. C. Aronson, and R. Osborn, J. Low Temp. Phys. **99**, 223 (1995).
[9] F. Steglich, J. Magn. Magn. Mater. **226**, 1 (2001).
[10] G. R. Stewart, Rev. Mod. Phys. **73**, 797 (2001).
[11] C. Seaman, M. B. Maple, B. W. Lee, S. Ghamaty, M. S. Torikachvili, J.-S. Kang, L. Z. Liu, J. W. Allen, and D. L. Cox, Phys. Rev. Lett. **67**, 2882 (1991).
[12] G. R. Stewart, Phys. Rev. B **47**, 3208 (1993).
[13] M. C. Aronson, R. Osborn, R. A. Robinson, J. W. Lynn, R. Chau, S. L. Seaman, and M. B. Maple, Phys. Rev. Lett. **75**, 725 (1995).
[14] B. Andraka, Phys. Rev. B **49**, 348 (1994).
[15] B. Andraka, Phys. Rev. B **49**, 3589 (1994).
[16] O. O. Bernal, D. E. MacLaughlin, H. G. Lukefahr, and B. Andraka, Phys. Rev. Lett. **75**, 2023 (1995).
[17] M. C. de Andrade, R. Chau, R. P. Dickey, N. R. Dilley, E. J. Freeman, D. A. Gajewski, M. B. Maple, R. Movshovich, A. H. Castro Neto, G. E. Castilla, and B. A. Jones, Phys. Rev. Lett. **81**, 5620 (1998).
[18] C. H. Booth, D. E. MacLaughlin, R. H. Heffner, R. Chau, M. B. Maple, and G. H. Kwei, Phys. Rev. Lett. **81**, 3960 (1998).
[19] J. Matsuhira, T. Sakakibara, and H. Amitsuka, Physica B **206–207**, 326 (1995).
[20] L. Shlyk, J. C. Waerenborgh, P. Estrela, L. E. DeLong, A. de Visser, and M. Almeida, J. Phys.: Condens. Matter **11**, 3525 (1999).
[21] R. N. Bhatt and D. S. Fisher, Phys. Rev. Lett. **68**, 3072 (1992).
[22] V. Dobrosavljević, T. R. Kirkpatrick, and G. Kotliar, Phys. Rev. Lett. **69**, 1113 (1992).
[23] E. Miranda, V. Dobrosavljević, and G. Kotliar, Phys. Rev. Lett. **78**, 290 (1997); J. Phys.: Condens. Matter **8**, 9871 (1996).
[24] D. E. MacLaughlin, R. H. Heffener, G. J. Nieuwenhuys, G. M. Luke, Y. Fudamoto, Y. J. Uemura, R. Chau, M. B. Maple, and B. Andraka, Phys. Rev. B **58**, R11849 (1998).
[25] A. H. Castro Neto, G. Castilla, and B. A. Jones, Phys. Rev. Lett. **81**, 3531 (1998).
[26] A. H. Castro Neto and B. A. Jones, Phys. Rev. B **62**, 14975 (2000).
[27] L. N. Bulaevsky, A. V. Zvarykina, Yu. S. Karimov, R. B. Lyubosky, and I. F. Shchegolev, Zh. Éksp. Teor. Fiz. **62**, 725 (1972) [JETP **35**, 384 (1972)].
[28] K. Ikegami, S. Kuroda, M. Saito, K. Saito, M. Sugi, T. Nakamura, M. Matsumoto, and Y. Kawabata, Phys. Rev. B **35**, 3667 (1987).
[29] K. Mukai, K. Suzuki, K. Ohara, J. B. Jamali, and N. Achiwa, J. Phys. Soc. Jpn. **68**, 3078 (1999).
[30] S. V. Demishev, R. V. Bunting, L. I. Leonyuk, E. D. Obraztsova, A. A. Pronin, N. E. Sluchanko, N. A. Samarin, and S. V. Terekhov, JETP Lett. **73**, 31 (2001).
[31] S.-K. Ma, C. Dasgupta, and C.-K. Hu, Phys. Rev. Lett. **43**, 1434 (1979).
[32] B. Dasgupta and S.-K. Ma, Phys. Rev. B **22**, 1305 (1980).
[33] J. E. Hirsch and J. V. José, J. Phys. C **13**, L53 (1980).
[34] J. E. Hirsch, Phys. Rev. B **22**, 5355 (1980).
[35] D. S. Fisher, Phys. Rev. B **50**, 3799 (1994).
[36] A. Klümper and A. A. Zvyagin, Phys. Rev. Lett. **81**, 4975 (1998).
[37] A. A. Zvyagin, Phys. Rev. B **62**, R6069 (2000).
[38] A. Klümper and A. A. Zvyagin, J. Phys.: Condens. Matter **12**, 8705 (2000).
[39] A. A. Zvyagin, Phys. Rev. B **63**, 033101 (2001).
[40] M. Andrei and H. Johannesson, Phys. Lett. A **100**, 108 (1984).
[41] H. Frahm and A. A. Zvyagin, J. Phys.: Condens. Matter **9**, 9939 (1997).
[42] A. A. Zvyagin, Phys. Rev. Lett. **87**, 059701 (2001).
[43] P. Schlottmann, Phys. Rev. Lett. **84**, 1559 (2000).
[44] P. Schlottmann, Nucl. Phys. B **552** [FS], 727 (1999).
[45] P. Schlottmann, Nucl. Phys. B **565** [FS], 535 (2000).
[46] P. Schlottmann, Phys. Rev. B **49**, 9202 (1994).
[47] A. A. Zvyagin and P. Schlottmann, Phys. Rev. B **52**, 6569 (1995).
[48] V. E. Korepin, N. M. Bogoliubov, and A. G. Izergin, *Quantum Inverse Scattering Method and Correlation Functions*, Cambridge University Press, Cambridge (1993).
[49] H. M. Babujian and A. M. Tsvelick, Nucl. Phys. B **265** [FS15], 24 (1986).
[50] A. A. Zvyagin and P. Schlottmann, J. Phys.: Condens. Matter **9**, 3543 (1997); **9**, 6479(E) (1997).
[51] L. A. Takhtajan, Phys. Lett. A **87**, 479 (1982).
[52] H. M. Babujian, Nucl. Phys. B **215**, 317 (1983).
[53] A. A. Zvyagin, Phys. Rev. Lett. **79**, 4641 (1997).
[54] A. A. Zvyagin, Phys. Rev. B **64**, 060405(R) (2001); *ibid.* **65**, 109902(E) (2002); preprint condmat/0201027 (unpublished).
[55] N. Suzuki and M. Inoue, Prog. Theor. Phys. **78**, 787 (1987).
[56] A. Klümper, Ann. Phys. **1**, 540 (1992).
[57] A. Klümper, Z. Phys. B **91**, 507 (1993).
[58] A. Klümper, Eur. Phys. J. B **5**, 677 (1998).
[59] B. M. McCoy and T. T. Wu, Phys. Rev. **176**, 631 (1968).
[60] N. Yu. Reshetikhin, J. Phys. A **24**, 3299 (1991).
[61] V. V. Bazhanov and N. Yu. Reshetikhin, Int. J. Mod. Phys. **A 4**, 115 (1989).
[62] A. Klümper and P. A. Pearce, Physica A **183**, 304 (1992).
[63] A. B. Zamolodchikov and V. A. Fateev, Zh. Éksp. Teor. Fiz. **89**, 380 (1985) [Sov. Phys. JETP **62**, 215 (1985)].
[64] I. Affleck, D. Gepner, H. J. Schulz, and T. Ziman, J. Phys. A **22**, 511 (1989).
[65] B. L. Al'tshuler and V. N. Prigodin, JETP Lett. **45**, 687 (1987).
[66] D. Miranda and V. Dobrosavljević, Phys. Rev. Lett. **86**, 264 (2001).
[67] S. Doniach, Physica B **91**, 231 (1977).
[68] T. G. Rappoport and M. A. Continentino, J. Phys. A **34**, 10829 (2001).

This article was published in English in the original Russian journal. Reproduced here with stylistic changes by AIP.

Mechanism of vortex switching in magnetic nanodots under a circular magnetic field. I. Resonance action of the field on the nanodot eigenmodes

A. S. Kovalev* and J. E. Prilepsky

B. Verkin Institute for Low Temperature Physics and Engineering National Academy of Sciences of Ukraine, pr. Lenina 47, 61103 Kharkov, Ukraine

(Submitted June 20, 2002)
Fiz. Nizk. Temp. **28**, 1292–1303 (December 2002)

The resonance activation of the eigenmodes of a two-dimensional easy-plane ferromagnet of finite size by a circular magnetic field is considered as a basis for theoretical explanation of the mechanism of vortex switching in magnetic nanodots under the influence of such a field. It is shown analytically that in the case of weak easy-plane anisotropy, when the vortex has a nonzero polarization (a total magnetization along the hard axis), the influence of the field on the eigenmodes of the system is of a complicated nature. A circular field acts in a resonance manner on the azimuthal modes of the system, in which the magnetization depends on the azimuthal coordinate (in the form of a direct resonance at the eigenfrequencies of the azimuthal modes). The coupling of the azimuthal and symmetric (independent of the azimuthal coordinate) modes via the external field gives rise to complex parametric resonances at sum frequencies. The results obtained are compared with the data of previous numerical studies. [DOI: 10.1063/1.1531396]

INTRODUCTION

Theoretical and experimental research on the nonlinear dynamics of magnetically ordered media is now one of the most important fields of study in modern nonlinear solid-state physics.[1,2] By the end of the 1980s the construction of the theory of nonlinear waves and solitons in magnets of different physical natures was basically complete, and the existence of such waves had been confirmed in a number of experiments. However, the main body of results, both experimental and theoretical, had been obtained for one-dimensional models or quasi-one-dimensional magnets.[1–3] In recent years there has been a growing interest in the dynamics of magnets in connection with the synthesis of many new magnetic materials with unusual physical properties. We mention first the quasi-two-dimensional metalorganic compounds consisting of magnetic layers with an organic intercalant,[4–11] magnetically ordered isostructural analogs of high-T_c superconducting compounds and those same compounds with the stoichiometric composition, and also two-dimensional magnets based on Langmuir–Blodgett films.[12,13] An important difference in the nonlinear dynamics of one-dimensional and two-dimensional magnets is the possibility of existence in the latter of specific two-dimensional topological excitations: magnetic skyrmions (in easy-axis ferromagnets)[1,14,15] and magnetic vortices (in easy-plane ferromagnets and antiferromagnets).[1,16–18] The role of the latter is especially important because in 2D magnets a phase transition to a magnetically ordered state occurs by the Berezinskii–Kosterlitz–Thouless mechanism,[19,20] and near the point of the transition the number of vortices and vortex pairs should be anomalously large. The existence of these topological excitations has now been confirmed experimentally in a number of studies.[7,8,21] In their structure and dynamic properties, magnetic vortices are very close to point vortices in the two-dimensional hydrodynamics of an incompressible liquid,[22] to Pitaevskii vortices in a gas of weakly interacting bosons,[23] and to optical vortices in nonlinear optics.[24] The main difference of the magnetic vortices from vortices in these other media is that besides the usual topological charge (which distinguishes a vortex from an antivortex) they have an additional characteristic associated with the polarization of the vortex—the direction of the magnetization (or of the antiferromagnetic vector) at its center.[18] In the long-wavelength approximation in the description of the structure of the vortex in the framework of differential equations, its polarization is a topological invariant and is conserved. However, in real magnets the magnetization field is defined on a discrete crystal lattice, and the polarization of the vortices (like certain other topological characteristics of multidimensional solitons)[25] is no longer a topological invariant. The experimental study of the out-of-plane structure of a magnetic vortex is a rather complicated problem, since in real systems the core of a magnetic vortex, where substantial deviation of the spins from the plane occurs, is very small in size. At the same time, there is now some weighty experimental evidence both for the existence of vortices in nanosize magnetic particles (magnetic dots)[26,27] and for the presence of an out-of-plane maximum of the magnetization at the center of the vortex (see Fig. 1). Studies by numerical methods[28] have shown that the inclusion of a noise signal modeling the finite temperature of the magnet can cause the vortices to change their polarization. A more important question is whether one can deliberately act on the vortices to change their polarization, e.g., by applying a circular magnetic field. It was shown in Ref. 29 by a numerical simulation that a vortex can change its polarization when acted on by a circular magnetic field, and the situation is not symmetric with respect to the sign of the vortex polarization: only vortices of one polarity are switched. This indicates that it is possible in principle to use such a field to bring the over-

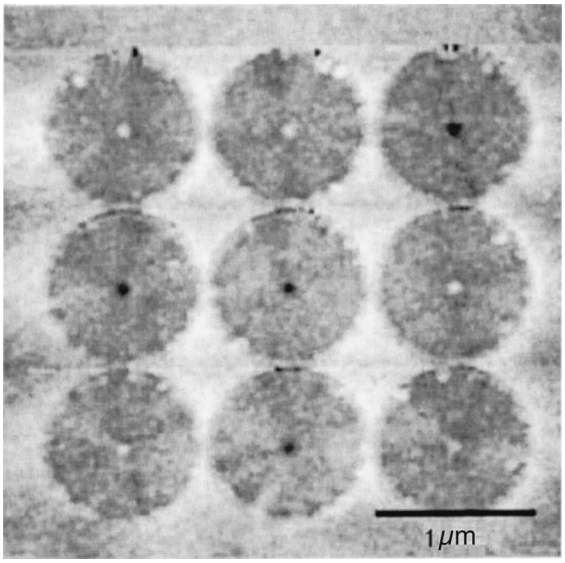

FIG. 1. Magnetic-force microscope image (taken from Ref. 27) of an array of magnetic dots made of Permalloy ($Ni_{80}Fe_{20}$), each with a diameter of 1 μm. The point at the center of each dot corresponds to the maximum of the out-of-plane component of the magnetization in the vortex core, and the dark and bright spots correspond to different signs of the polarization of the vortex.

whelming majority of vortices in a magnetic sample to a unipolar orientation. This should give rise to a macroscopic magnetization proportional to the density of vortices in an easy-plane ferromagnet; such a magnetization should in principle be detectable experimentally. This would provide additional direct proof of the existence of magnetic vortices and serve as a tool for their experimental investigation. Such a process of changing the polarity of a vortex by means of an external magnetic field applied perpendicular to the plane of an arrangement of nanoparticles was implemented experimentally in Ref. 27, where confirmation of the possibility of directed change of the vortex polarity was obtained. A theoretical model for estimating the switching of the polarization of vortices was proposed in Refs. 28 and 29. The authors assumed that, at least in the initial stage of the switching, the external field leads to a rise in the amplitude of the linear eigenmodes of the system in the presence of the vortex, and they took into account the dynamics of only a few spins in the core of the vortex. It was assumed for simplicity that the precession of these magnetic moments is in-phase, i.e., only one low-frequency ''symmetric'' magnon mode was taken into account. However, because of the symmetry of that mode with respect to the sign of the frequency, the matter of the asymmetries of the vortex switching dynamics observed in the number simulation[29] has remained unclear.

In the present paper we consider the spin dynamics of a two-dimensional magnetic nanodot of finite size L in a vortex configuration under the influence of a spatially uniform external rotational field, but here we take into account several magnon eigenmodes of the system in the presence of the vortex. As will be shown below, to explain the results of the numerical simulations it is not enough to take into account a single symmetric mode, but it is necessary to take into account additional modes with azimuthal dependence of the phase of the spin precession (''azimuthal modes'').

1. MODEL AND STRUCTURE OF THE VORTICAL SOLUTIONS

It is customary to treat the structure and dynamics of magnetically ordered media theoretically in the framework of the classical Heisenberg model with an exchange interaction of near-neighbor magnetic moments. In our case it is necessary to take into account the weak anisotropy, assumed uniaxial, of this interaction. Here the Hamiltonian has the form

$$H_0 = -J\sum_{n,\delta}\,(S_n^x S_{n+\delta}^x + S_n^y S_{n+\delta}^y + \lambda S_n^z S_{n+\delta}^2), \tag{1}$$

where $\mathbf{S}_n$ is the classical site spin (we shall henceforth assume that the modulus of the spin vector is the same for all sites and, with a suitable renormalization, $|\mathbf{S}_n| = 1$), the index n is the number of the site of the spin lattice (in our case two-dimensional), δ enumerates its nearest neighbors, the exchange interaction constant $J > 0$ in the case of a ferromagnet, and the exchange anisotropy parameter λ for easy-plane symmetry varies in the range $0 \leqslant \lambda \leqslant 1$. In actuality the exchange anisotropy, which is of a relativistic origin, is weak, and $(1-\lambda) \sim 10^{-2}$. In this case its effect on the structure and dynamics of the magnetic interactions is qualitatively similar to that of a weak single-ion anisotropy, which leads to the appearance of an additional term of the form $\beta\Sigma_n (S_n^z)^2$ in the Hamiltonian (1).

The classical dynamics of the magnetization vector are described by the Landau–Lifshitz equations (LLEs),[1,2] in the framework of which the length of the magnetization vector (site spin) is conserved, and the vector can be characterized by two variables. It is convenient to use the z projection of the spin on the hard axis, $m_n = S_n^z$, and the azimuthal angle of the spin, $\varphi_n = \arctan(S_n^y/S_n^x)$, since in terms of these variables the LLEs take on a Hamiltonian form, and φ_n and m_n play the role of canonically conjugate coordinates and momentum for the Hamiltonian $\mathcal{H}_0(m_n, \varphi_n)$. The Hamiltonian (1) in terms of these variables is written as

$$\mathcal{H}_0 = -J\sum_{n,\delta}\,[\lambda m_n m_{n+\delta} + \sqrt{1-m_n^2}\,\times\sqrt{1-m_{n+\delta}^2}\cos(\varphi_n - \varphi_{n+\delta})], \tag{2}$$

and the LLEs have the form

$$\frac{d\varphi_n}{dt} = \frac{\partial \mathcal{H}_0}{\partial m_n}, \quad \frac{dm_n}{dt} = -\frac{\partial \mathcal{H}_0}{\partial \varphi_n}. \tag{3}$$

In the long-wavelength limit the solution of the LLEs with the Hamiltonian (1) for a static magnetic vortex in an infinite system was obtained in Refs. 16 and 17 (see also Refs. 30–32). In polar coordinates (r, χ) tied to the center of the vortex this solution has the form

$$\varphi^0(\chi) = q\chi + C, \tag{4}$$

$$m^0(r) = p\left[1 - a\left(\frac{r}{r_v}\right)^2\right], \quad \text{for } r \to 0,$$

$$m^0(r) = pb\sqrt{\frac{r_0}{r}}\exp\left(-\frac{r}{r_v}\right), \quad \text{for } r \to \infty, \tag{5}$$

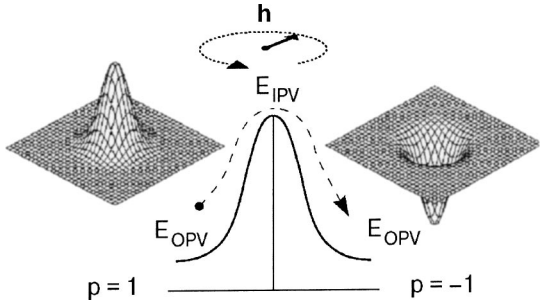

FIG. 2. Illustration of vortex switching in a circular field as a process of overcoming an energy barrier Δ.

where a and b are numerical constants of order unity and C is an arbitrary constant, the presence of which reflects the continuous degeneracy of the ground state with respect to the direction of the spins in the easy plane; the parameter $r_v = [\lambda/4(1-\lambda)]^{1/2}$ characterizes the radius of the vortex. We note that even for a weak anisotropy $(1-\lambda)=0.1$, the value for which the numerical simulations were mainly done, one has $r_v = 1.5$, i.e., the size of the vortex core is of the order of the interatomic distance $(a_0 = 1)$, and it is necessary to take into account the discreteness of the system in the vortex core. The parameters q and p characterize the topological structure of the vortex: $q = \pm 1, \pm 2, \ldots$ is its topological charge ($q>0$ for a vortex, and $q<0$ for an antivortex), and $p = \pm 1$ is the polarization (the value of m at the center of the vortex). The product of these two characteristics specifies the so-called gyrovector $\mathbf{G} = 2\pi p q \mathbf{i}_z$, which is directed perpendicular to the plane of the two-dimensional magnet and governs the vortex dynamics. In the long-wavelength limit (in the description of the spatial distribution of the magnetization in the framework of differential equations) the two parameters q and p are topological invariants. In a discrete system only the topological charge q is an invariant quantity, while the polarization p is no longer an invariant. In Ref. 33 the dependence of the discrete analog of the gyrovector (and, hence, of the polarization of the vortex) on the anisotropy parameter λ was calculated, and it was shown that the polarization of the vortex vanishes at a critical value of the anisotropy $\lambda = \lambda_c \approx 0.72$. At a larger value of the anisotropy the static vortex undergoes a transition to an in-plane configuration with a nonzero z component of the magnetization which is independent of the parameter λ.[32] In the long-wavelength description an in-plane vortex (IPV) does not exist, since the energy of its core diverges, while the energy (4), (5) of an out-of-plane vortex (OPV) remains finite. In the discrete model the core energy of the in-plane configuration is finite, and it is stable for $\lambda < \lambda_c$. Here the energy difference of the in-plane and out-of-plane vortices is equal in order of magnitude to $E_{OPV} - E_{IPV} = \Delta \sim \pi J \ln(a_0/r_v)$, where a_0 is the interatomic distance. It is seen from the above estimates that a transition of the vortex from one configuration to the other occurs at $a_0 \sim r_v$. It follows that for a small anisotropy, when the OPV is stable, it is in principle possible in the discrete model for a switching of its polarization to occur: for this it is necessary to overcome a finite energy barrier Δ (see Fig. 2), as may occur under the influence of temperature[28] or an external magnetic field.[27,29]

In this paper we consider the dynamics of an OPV under the influence of a circular external magnetic field applied in the easy plane, $\mathbf{h} = h(\cos\omega t, \sin\omega t, 0)$, which leads to the appearance of an additional term in the Hamiltonian:

$$\mathcal{H}_{\text{int}}(t) = -h\sum_n \sqrt{1-m_n^2}\cos(\varphi_n - \omega t). \tag{6}$$

Then the LLEs (3), with the damping taken into account in Gilbert form,[34] become

$$\frac{d\varphi_n}{dt} = \frac{\partial}{\partial m_n}(\mathcal{H}_0 + \mathcal{H}_{\text{int}}(t)) - \frac{\gamma}{1-m_n^2}\frac{\partial \mathcal{H}_0}{\partial \varphi_n},$$

$$\frac{dm_n}{dt} = -\frac{\partial}{\partial \varphi_n}(\mathcal{H}_0 - \mathcal{H}_{\text{int}}(t)) - \gamma(1-m_n^2)\frac{\partial \mathcal{H}_0}{\partial m_n}, \tag{7}$$

where γ is the damping coefficient (assuming that the external field and the damping are small, in the last terms we take only $\mathcal{H}_0$ into account). Smallness of the damping γ must be defined in comparison to the characteristic time scales of the processes under consideration.

Substituting the expressions for $\mathcal{H}_0$ and $\mathcal{H}_{\text{int}}$ into Eq. (7), we obtain the dynamical equations in final form:

$$\frac{d\varphi_n}{dt} = \sum_\delta \left(\frac{m_{\perp\delta}}{m_{\perp n}}[m_n \cos(\varphi_n - \varphi_{n+\delta}) - \gamma \sin(\varphi_n - \varphi_{n+\delta})] - \lambda m_{n+\delta} \right) + h\frac{m_n}{m_{-n}}\cos(\varphi_n - \omega t), \tag{8}$$

$$\frac{dm_n}{dt} = \sum_\delta \left(-m_{\perp n} m_{\perp n-\delta}[\gamma m_n \cos(\varphi_n - \varphi_{n+\delta}) + \sin(\varphi_n - \varphi_{n+\delta})] + \gamma\lambda m_{\perp n}^2 m_{n+\delta} \right) - h m_{\perp n} \times \sin(\varphi_n - \omega t), \tag{9}$$

where we have introduced the notation $m_{\perp n} \equiv \sqrt{1-m_n^2}$ and have set $J = 1$.

2. NUMERICAL SIMULATION AND ANALYSIS OF THE SWITCHING OF THE VORTEX IN A CIRCULAR FIELD

In Ref. 29, Eqs. (8) and (9) were solved numerically for a two-dimensional easy-plane ferromagnet with a square lattice (for which the critical value of the anisotropy for the IPV–OPV transition is $\lambda_c \approx 0.72$). Computations were done for a region of radius $L = 24$ (the lattice constant is set equal to unity), containing ~ 1800 spins, at values of the anisotropy parameter $\lambda = 0.9$ and damping parameter $\gamma = 2 \times 10^{-3}$. The amplitude of the external field was chosen in the regions $h \leqslant 0.02$, and its frequency in the interval $|\omega| < 0.5$. As the initial condition we took a configuration with an OPV and various polarizations. The main results obtained in the numerical calculations of Ref. 29 reduce to the following: 1. The switching dynamics of vortices and antivortices is identical, i.e., the character of the switching does not depend on the topological charge of the vortex. 2. Switching occurs in a threshold manner when the field amplitude exceeds a certain critical value h_{cr}, which depends on the sign of the external pump frequency ω (at a fixed value of the damping γ). 3. The $h_{\text{cr}} = h_{\text{cr}}(\omega)$ dependence is substantially nonmonotonic and is of a resonance character. Figure 3 shows this dependence, taken from Ref. 29. We have added the point

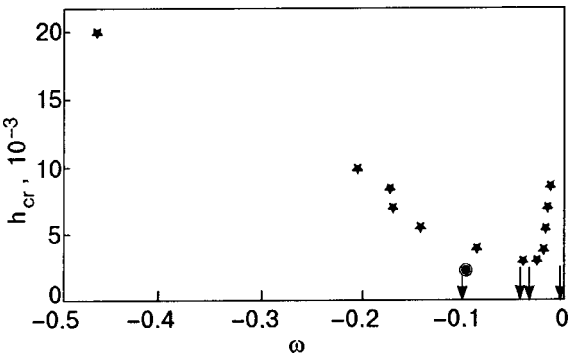

FIG. 3. Dependence of the critical amplitude of the external field on its frequency. The figure was taken from Ref. 29. We have added the point denoted by a circle at the frequency $\omega=-0.1$; this point was discussed in the text of Ref. 29.

(denoted by a circular dot) corresponding to the value $\omega=-0.1$, which was discussed in the text of Ref. 29. 4. The vortex switching process is asymmetric with respect to the sign of the polarization and the direction of rotation of the magnetic field and depends essentially on the sign of the product $p\omega$. For $p\omega<0$ (e.g., in the case of a vortex with a positive polarization in a field rotating clockwise) the switching occurs easily, and for $\omega=-0.1$ the critical value of the field amplitude is $h_{cr}\approx 0.0025$. When the field is rotating in the counterclockwise direction ($\omega=0.1$) the critical value of the amplitude of the circular field is an order of magnitude higher: $h_{cr}\approx 0.02$. 5. For $p\omega<0$, the switching results in a stable vortex configuration with a switched vortex, while for $p\omega>0$ the structure of the vortex core after the switching is completely destroyed by large-amplitude spin waves. This last circumstance follows in a natural way from the previous result: for $p\omega<0$ and a field slightly above the threshold value, the system after the switching will be in the subthreshold region with $p\omega>0$, while for $p\omega>0$ in the initial state and a field exceeding the high threshold value, the field after the switching of the system will be found in a far above-threshold region with $p\omega<0$.

3. SCENARIOS FOR VORTEX SWITCHING

It is natural to propose the following scenario for the observed vortex switching process in an external circular magnetic field. In the initial stage the field excites one or several linear eigenmodes of the system in a resonance manner. Then a nonlinear growth of the amplitude of these modes occurs, leading to switching of the vortex. However, to explain the data of the numerical simulation this mechanism must satisfy a number of conditions. First, the frequencies of the eignmodes should be close to the resonance frequencies observed in the simulation. (In Fig. 3 one can clearly see the minima of the absorption threshold at frequencies $\omega=-0.05$, $\omega=-0.06$, and $\omega=-0.1$.) Second, the profile of these normal modes must have an appreciable maximum amplitude in the region in which the vortex is localized in order to lead basically to its excitation and not to the activation of the entire system. Finally, the modes mentioned must have a pronounced asymmetry with respect to the sign of the frequency in order to explain the difference of the threshold values for vortex switching for different signs of the frequency of the external pump in the simulation.

In Ref. 29 the authors assumed that the switching of the polarity of a vortex in a field is due to excitation of a "soft" (the lowest-frequency) symmetric eigenmode of the system. This mode corresponds to small corrections to the static vortex solution (φ,m) (4), (5) of the form $\varphi(\mathbf{r},t)-\varphi^0(\chi)=\nu(\mathbf{r},t)$, $m(\mathbf{r},t)-m^0(r)=\mu(\mathbf{r},t)$, where r is the distance from the center of the vortex (when the vortex is located at the center of the circular region). Here it was shown that the dynamics of the amplitude of this mode is described by an effective equation for an anharmonic oscillator under the influence of direct and parametric activation.

In our view, the scenario proposed by the authors of Ref. 29 has a number of shortcomings. 1. The analytical treatment was done for small-amplitude vortices, which exist at values of the anisotropy parameter λ close to the critical value $\lambda=\lambda_c\approx 0.72$, while the numerical simulations were done at a value $\lambda=0.9$, and the frequencies of the eigenmodes at these values of λ are substantially different. 2. The proposed approach is applicable only for fixed boundary spins of the system (Dirichlet conditions: $m|_{r=L}=0$ and $\varphi|_{r=L}=\chi$), while the numerical simulations revealed the presence of vortex switching in the case of a free boundary also $(\partial\varphi/\partial r|_{r=L}=\partial m/\partial r|_{r=L}=0)$. 3. In the analytical approach of those authors the vortex switching could be realized only when the vortex was displaced from the center of the system: the effect of the external field was small in the parameter R/L, where R is the distance between the center of the vortex and the center of the system. 4. As was shown in Ref. 35, the distribution of the magnetization field of the fundamental symmetric mode is not localized near the vortex. It is practically the same as in the absence of the vortex and, moreover, vanishes in the vortex core. Thus this mode "shakes" the entire magnetic system rather than the vortex itself. 5. Finally, the field variables in this mode are independent of the azimuthal coordinate, and its properties are therefore symmetric with respect to the sign of the frequency, and their slight asymmetry arises in the process of pumping only on account of a shift of the center of the vortex from the center of the system and a slight deviation of the total magnetization of the vortex from the hard axis. However, it is easily shown using the results of Ref. 29 that the ratio of the threshold fields for vortex switching at pump frequencies of equal absolute value and opposite sign in the resonance region has the form $h_{cr}(\omega)/h_{cr}(-\omega)\approx(1+\xi\omega)/(1-\xi\omega)$, where $\xi\sim 1$. Since for $\lambda>\lambda_c$ in the investigated system of radius $L=24$ the frequencies of the soft symmetric mode lie in the interval $0\leqslant\Omega\leqslant 0.063$, we have, to good accuracy, $h_{cr}(\omega)/h_{cr}(-\omega)\approx 1$, whereas in the numerical simulation this ratio was of the order of 10.

The disagreements mentioned made it necessary to formulate a different scenario for the changing of the vortex polarity. Since a central role in it is played by several eigenmodes of the system, let us briefly discuss their classification.

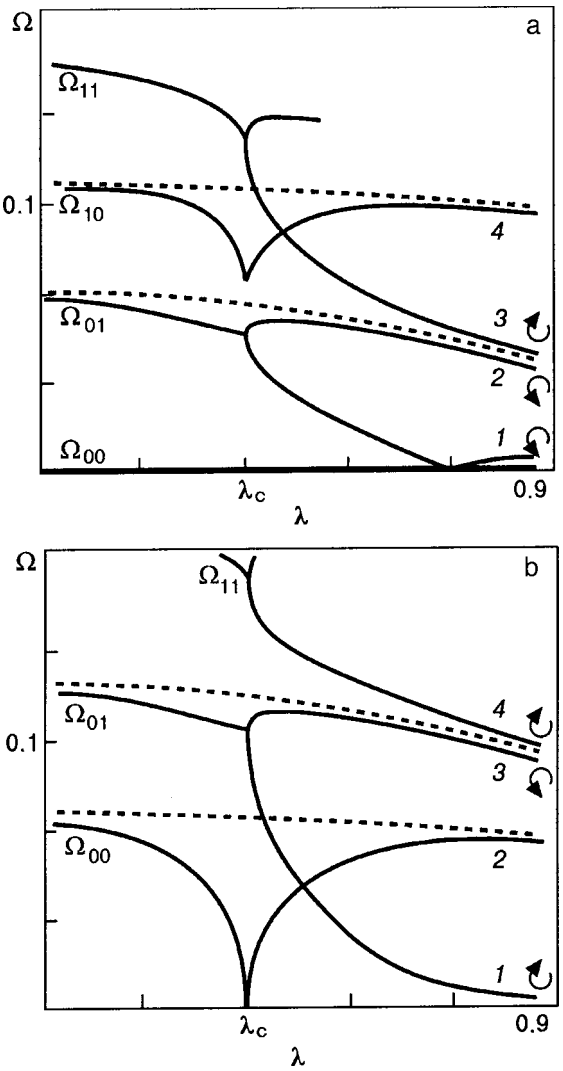

FIG. 4. Frequencies of the lowest-lying magnon modes of a system of size $L=24$ with a vortex at the center:[37] for free boundary conditions (a) and for a fixed boundary (b). The dashed curves show the corresponding eigenmode frequencies for the system in the absence of the vortex.

3.1. Classification of the eigenmodes of a system with a vortex

We start by considering a vortex located at the center of a circular system of radius L $(R=0)$. The eigenmodes of the LLEs linearized in the small additions $\nu(\mathbf{r},t)$ and $\mu(\mathbf{r},t)$ will have the form

$$\nu(\mathbf{r},t)=\nu_{lk}(r)\sin(k\chi-\Omega t),$$
$$\mu(\mathbf{r},\mathbf{t})=\mu_{lk}(r)\cos(k\chi-\Omega t). \qquad (10)$$

where the index l classifies the radial functions with respect to the number of nodes. The functions $\nu_{lk}(r)$ and $\mu_{lk}(r)$ and the corresponding frequency dependences $\Omega=\Omega_{lk}(\lambda)$ have been investigated in detail in Refs. 35–38 for both fixed and free boundaries. Figure 4 shows (qualitatively) the functions $\Omega=\Omega_{lk}(\lambda)$ of the four low-lying modes of a system of radius $L=24$ for the case of free (Fig. 4a) and fixed (Fig. 4b) boundary conditions. It is seen that at the critical value of the anisotropy $\lambda=\lambda_c$ a bifurcation of modes with $k\neq 0$ occurs. (Curves are plotted only for the modes with $k=1$, which we shall call the ''first azimuthal modes.'' The splitting of the modes with large values of k is substantially smaller.) The symmetric modes with $k=0$ are not split. What will be important for us below is the classification of modes at small values of the anisotropy $(1-\lambda\ll 1)$. Importantly, in this region the functions $\Omega=\Omega(\lambda)$ for the modes in the presence of a vortex are practically the same as the corresponding functions for the eigenmodes of the system in the absence of a vortex. Moreover, the profiles of the field distributions $\nu_{lk}(r;\lambda)$ and $\mu_{ik}(r;\lambda)$ are close to those in the system without the vortex in the region outside of the vortex core and is expressed to high accuracy in terms of Bessel functions. An exception is the case of the lowest-frequency quasilocal modes (*1* in Fig. 4), which do not have analogs in the ideal system and which describe a gyroscopic precession of the vortex. The frequencies of these modes are anomalously low $(\Omega_{(1)}\sim(L^2-R^2)^{-1}\approx 0.0015)$ and depend on the rotation radius R of the vortex. The frequencies of the remaining modes lie significantly higher $(\Omega_{s>1}\sim L^{-1}\gg\Omega_{(1)})$, and, importantly, are practically independent of the value of the displacement of the vortex from the center of the system.[37] Therefore, the results obtained in Ref. 35 for a vortex at the center of the system may be used for these modes.

As we see from Fig. 4, the symmetric modes (e.g., Ω_{00} in Fig. 4b and Ω_{10} in Fig. 4a) are degenerate with respect to the sign of the frequency, while for the azimuthal modes the frequencies split. Here it must be kept in mind that the different branches of the doublets that appear correspond to different directions of rotation of the spin waves (i.e., to different signs of the frequency). In the case of a free boundary the vortex rotates counterclockwise, as does the wave in mode *2* (mode *3* rotates clockwise). In the case of a fixed boundary the vortex rotates clockwise, as does mode *4*, while in mode *3* the wave rotates counterclockwise. As was pointed out above, the radial profile of the symmetric modes practically coincides with the profile of these modes in the system without a vortex and vanish in the vortex core, i.e., in the region $r\leqslant r_{\nu}$. The shape of the azimuthal modes changes substantially in the presence of a vortex: it is almost the same as the profile of the wave function in the absence of a vortex at $r\sim L$, but it deforms and has appreciable maxima (exceeding the average mode amplitude) near its core. According to the results of Refs. 35, 37, and 38, which are in rough agreement with the estimates for modes in the absence of a vortex, the absolute values of the frequencies of the modes in Fig. 4 have the following values for $L=24$ and $\lambda=0.9$. For a free boundary: $\Omega_{(1)}\approx 0.0015$, $\Omega_{(2)}\approx 0.044$, $\Omega_{(3)}\approx 0.051$, and $\Omega_{(4)}\approx 0.1$, and for a fixed boundary: $\Omega_{(1)}\approx 0.0015$, $\Omega_{(2)}\approx 0.063$, and $\Omega_{(3)}\approx\Omega_{(4)}\approx 0.1$. Comparing these data with Fig. 3, we see that the frequencies of modes *2*, *3*, and *4* for the two types of boundary conditions are close to the minima of the numerical dependence of the critical field amplitude on the pump frequency.

The arguments given above indicate that the scenarios for the switching of vortices under an external influence must be much more complex than that proposed in Ref. 29, and the excitation of azimuthal modes must be included in it. At first glance this seems strange, since we are interested in the change of polarity of the vortex, i.e., the change of the total projection of the magnetization of the system. In the symmetric modes this change is nonzero and varies with time,

while in the azimuthal modes it is equal to zero. However, in the presence of an external influence the situation is altered.

3.2. Analysis of the action of a circular field on the symmetric and azimuthal modes

For a qualitative description of the phenomenon, let us first restrict discussion to a long-wavelength treatment and neglect damping in the system. Then the dynamical equations (8), (9) take the form

$$\frac{\partial\varphi}{\partial t}=m(4(1-\lambda)-(\nabla\varphi)^2)-\left(\frac{1}{m_\perp^2}-1+\lambda\right)\Delta\varphi - \frac{m(\nabla m)^2}{m_-^4}+h\frac{m}{m_\perp}\cos(\varphi-\omega t), \tag{11}$$

$$\frac{\partial m}{\partial t}=\nabla(m_\perp^2\nabla\varphi)-hm_-\sin(\varphi-\omega t). \tag{12}$$

We consider a vortex found at a short distance $R\ll L$ from the center of a circular system of radius L. Since the velocity of the gyrotropic motion of the vortex in this case is small: $V\approx R/L^2\ll c=2(1-\lambda)^{1/2}$ (where c is the spin-wave velocity), we can limit consideration to the static vortex approximation. Here the gyrotropic rotation of the vortex with frequency $\Omega\sim L^{-2}$ and the change of its shape (in particular, the appearance of power-law additions $\delta m\sim V/R$ to solution (5)) is taken into account for $R\to 0$ by the presence of the lower azimuthal mode (*1* in Figs. 4a and 4b). In a static vortex the mth component of the magnetization is nonzero only in its core of radius r_ν. Outside that region we can set $m(\mathbf{r},t)\approx\mu(\mathbf{r},t)$ in Eqs. (11) and (12). To satisfy the boundary conditions for a vortex displaced from the center, solution (4), which is written in polar coordinates tied to the center of the vortex, must be modified as follows:

$$\varphi_0\approx\chi+\frac{Rt}{L^2}\sin\chi. \tag{13}$$

For a qualitative treatment of the case $r\ll L$ we can limit consideration to the region $r\gg R$ and treat r and χ as polar coordinates tied to the center of the system. For the previously introduced small additions μ and ν to the static vortex solution, Eqs. (11) and (12) reduce approximately to the following:

$$\frac{\partial\nu}{\partial t}=\frac{1}{r_\nu^2}\mu+hm\cos(\varphi_0-\nu-\omega t), \tag{14}$$

$$\frac{\partial\mu}{\partial t}=\Delta\nu-h\sin(\varphi_0-\nu-\omega t), \tag{15}$$

with φ_0 given by formula (13). (In the derivation of Eqs. (14) and (15) we have dropped terms $\sim\Delta\mu$ and $\sim\mu(\nabla\varphi_0)^2$, which are small compared to the main terms μ/r_ν^2 in (14).) Equations (14) and (15) are supplemented by the boundary conditions $\nu|_L=\mu|_L=0$ at the (fixed) boundary of the magnet.

For a qualitative understanding of the difference between the different scenarios for the action of a circular field on the system, let us analyze the dynamics of only two spin modes—one symmetric and one azimuthal. As the symmetric mode we choose the lowest-frequency symmetric mode (*2* in Fig. 4b). In the absence of the vortex and external field, the solution corresponding to this mode has the form

$$\nu_{(2)}^{(0)}=AJ_0\left(\rho\frac{r}{L}\right)\sin\Omega_{(2)}t,$$

$$\mu_{(2)}^{(0)}=A\Omega_{(2)}r_\nu^2J_0\left(\rho\frac{r}{L}\right)\cos\Omega_{(2)}t, \tag{16}$$

where $J_0(z)$ is the Bessel function, $\Omega_{(2)}=\rho/r_\nu L$, and $\rho\approx 2.4$ is the smallest root of the equation $J_0(z)=0$.

As the azimuthal mode we choose the mode which in the absence of the vortex and pump goes over to the low-frequency azimuthal mode with the solution

$$\nu_{(3)}^{(0)}=BJ_1\left(\tilde{\rho}\frac{r}{L}\right)\sin\chi\sin\Omega_{(3)}t,$$

$$\mu_{(3)}^{(0)}=B\Omega_{(3)}r_\nu^2J_1\left(\tilde{\rho}\frac{r}{L}\right)\sin\chi\cos\Omega_{(3)}t, \tag{17}$$

where $\Omega_{(3)}=\tilde{\rho}/r_\nu L$ and $\tilde{\rho}\approx 3.8$ is the smallest nontrivial root of the equation $J_1(z)=0$. Generally speaking, the given solution corresponds to a standing wave. The mode in question is twofold degenerate, and the two different solutions correspond to spin waves rotating in opposite directions and depending on time and the angular coordinates as $\sin(\pm\chi+\Omega t)$. In the absence of the vortex these two solutions have slightly different frequencies and shapes. These differences may be the cause of the asymmetry of the process of vortex switching in a circular field. Nevertheless, being interested in the qualitative influence of the azimuthal modes on the change in polarity of a vortex, we shall ignore this circumstance and use the following ansatz for the solution of equations (14) and (15):

$$\nu=\nu_{(2)}(r,t)+\nu_{(3)}(r,t)\sin\chi,$$

$$\mu=\mu_{(2)}(r,t)+\mu_{(3)}(r,t)\sin\chi, \tag{18}$$

where the radial dependences of the functions $\nu_{(n)}$ and $\mu_{(n)}$ are close to those in solutions (16) and (17). Indeed, as was shown in Ref. 35, the profiles of all the modes except mode *1* differ only slightly from the profiles for the corresponding solution in the absence of the vortex in all regions except the vortex core.

Here we must make an important remark. In this Section we are actually ignoring the z component of the vortex solution, and, although we are considering small values of the anisotropy, we are nevertheless dealing with a vortex in a plane. In this case there should be no asymmetry of the vortex switching. Asymmetry can appear only when the difference between azimuthal modes *3* and *4* is taken into account along with the lowest-frequency mode *1*, which alone, unlike all the higher-lying azimuthal modes, does not belong to a doublet pair of close-lying modes. Then the problem is complicated substantially, since we cannot use ansatz (18) for ''standing waves'' and are forced to consider spin waves rotating in different directions. But the consideration of two modes, *2* and (*3*,*4*), allows one to demonstrate clearly the process of interaction of modes of different symmetry on a qualitative level.

After substituting ansatz (18) into Eqs. (14) and (15), performing a linearization of the trigonometric functions in them with respect to small $\nu_{(n)}$, and integrating the awkward equations obtained over the angular variable χ, we obtain the following pair of equations:

$$\frac{\partial \nu_{(2)}}{\partial t}=\frac{1}{r_\nu^2}\mu_{(2)}-\frac{h}{2}\frac{Rr}{L^2}\mu_{(2)}\cos\omega t+\frac{h}{2}\mu_{(3)}\sin\omega t, \quad (19)$$

$$\frac{\partial \mu_{(2)}}{\partial t}=\Delta_r\nu_{(2)}+\frac{h}{2}\frac{Rt}{L^2}\sin\omega t+\frac{h}{2}\nu_{(2)}\frac{Rr}{L^2}\cos\omega t - \frac{h}{2}\nu_{(3)}\sin\omega t, \quad (20)$$

where $\Delta_r=\partial^2/\partial r^2=-(1/r)\partial/\partial r$. We see that these equations do not form a complete system, since they contain all 4 functions $\nu_{(n)}$ and $\mu_{(n)}$. The other two equations needed are easily obtained if before integrating Eqs. (14) and (15) over the coordinate one first multiplies them by $\sin\chi$. Then one obtains the following additional pair of equations:

$$\frac{\partial \nu_{(3)}}{\partial t}=\frac{1}{r_\nu^2}\mu_{(3)}-h\mu_{(2)}\sin\omega t-\frac{3h}{2}\frac{Rr}{L^2}\cos\omega t, \quad (21)$$

$$\frac{\partial \mu_{(3)}}{\partial t}=\left(\Delta_r-\frac{1}{r_\nu^2}\right)\nu_{(3)}-h\cos\omega t-h\nu_{(2)}\sin\omega t + \frac{3h}{2}\nu_{(3)}\frac{Rt}{L^2}\cos\omega t. \quad (22)$$

We shall assume approximately that the radial dependence of the functions $\nu_{(n)}$ and $\mu_{(n)}$ remain the same as in the functions $\nu_{(n)}^{(0)}$ and $\mu_{(n)}^{(0)}$. (Here $\Delta_r\nu_{(2)}=-r_\nu^2\Omega_{(2)}^2\nu_{(2)}$ and $(\Delta_r-1/r^2)\nu_{(3)}=-r_\nu^2\Omega_{(3)}^2\nu_{(3)}$.) Setting

$$\nu_{(2)}=\Phi_{(2)}(t)J_0(\rho r/L)/r_\nu^2\Omega_{(2)},$$

$$\mu_{(2)}=\mathcal{M}_{(2)}(t)J_0(\rho r/L),$$

$$\nu_{(3)}=\Phi_{(3)}(t)J_1(\tilde{\rho} r/L)/r_\nu^2\Omega_{(3)},$$

$$\mu_{(3)}=\mathcal{M}_{(3)}(t)J_1(\tilde{\rho} r/L)$$

and integrating Eqs. (19)–(22) over r from 0 to L, we obtain the final system of equations:

$$\frac{d\Phi_{(2)}}{dt}-\Omega_{(2)}\mathcal{M}_{(2)}=-h\frac{R}{L}a\Omega_{(2)}r_\nu^2\mathcal{M}_{(2)}\cos\omega t - hb\Omega_{(2)}r_\nu^2\mathcal{M}_{(3)}\sin\omega t, \quad (23)$$

$$\frac{d\mathcal{M}_{(2)}}{dt}+\Omega_{(2)}\Phi_{(2)}=h\frac{R}{L}a\frac{\Phi_{(2)}}{\Omega_{(2)}r_\nu^2}\cos\omega t - hb\frac{\Phi_{(3)}}{\Omega_{(3)}r_\nu^2}\sin\omega t+h\frac{R}{L}c\sin\omega t, \quad (24)$$

$$\frac{d\Phi_{(3)}}{dt}-\Omega_{(3)}\mathcal{M}_{(3)}=-h\frac{R}{L}f\Omega_{(3)}r_\nu^2\mathcal{M}_{(3)}\cos\omega t + hg\Omega_{(3)}r_\nu^2\mathcal{M}_{(2)}\sin\omega t, \quad (25)$$

$$\frac{d\mathcal{M}_{(3)}}{dt}+\Omega_{(3)}\Phi_{(3)}=h\frac{R}{L}f\frac{\Phi_{(3)}}{\Omega_{(3)}r_\nu^2}\cos\omega t - hg\frac{\Phi_{(2)}}{\Omega_{(2)}r_\nu^2}\sin\omega t-hs\cos\omega t, \quad (26)$$

where

$$a\approx 0.25,\quad b\approx 0.42,\quad c\approx 0.77,$$

$$f\approx 0.88,\quad g\approx 1.2,\quad \text{and}\quad s\approx 2.79.$$

One notices the complicated character of the excitation of the system under study. There is a direct excitation of the system, described by the last terms on the right-hand sides of (24) and (26), a parametric pumping—the first terms on the right-hand sides of all the equations, and a complicated mutual influence of the different modes—the second terms on the right-hand sides. In addition, an asymmetry of the direct action of a circular field on different modes is seen: it is large for the azimuthal mode and small (in the parameter $R/L\ll 1$) for the symmetric mode.

3.3. Effect of the field on the symmetric modes

As we have said above, in Ref. 29 a simple scenario was proposed for the action of a circular field on a vortex wherein only a symmetric mode is taken into account. If we set $\mathcal{M}_{(3)}=\Phi_{(3)}=0$ in (23) and (24) and introduce the new variables $\Phi=\Phi_{(2)}/\Omega_{(2)}$ and $\mathcal{M}=\mathcal{M}_{(2)}/\Omega_{(2)}^2$, then Eqs. (23) and (24) take the form

$$\frac{d\Phi}{dt}=\Omega_{(2)}^2\mathcal{M}-hB\mathcal{M}\cos\omega t, \quad (27)$$

$$\frac{d\mathcal{M}}{dt}=-\Phi-hA_2\Phi\cos\omega t+hA_1\sin\omega t, \quad (28)$$

where $A_1=(R/L)c/\Omega_{(2)}^2$, $A_2=(R/L)a/(\Omega_{(2)}r_\nu^2)$, and $B=(R/L)a\Omega_{(2)}^2r_\nu^2$. In the linear limit and in the absence of damping, these equations are the same as those derived by the authors of Ref. 29. Unfortunately, the values of the parameters A_i and B were not calculated or even estimated in Ref. 29. The nonlinear analog of Eqs. (27) and (28) with damping taken into account was used by the authors of Ref. 29 to explain the asymmetry of the vortex switching process with respect to the sign of the frequency of the external field. They showed that the asymmetry of the function $h_{\rm cr}=h_{\rm cr}(\omega)$ comes entirely from values $h_{\rm cr}\sim|\omega/\Omega_{(2)}-B/A_1|^{-1}$. For estimation they took the values $B=A_1$ and reached the unjustified conclusion that there is a strong difference in the value of $h_{\rm cr}$ at frequencies of opposite sign which are close to the resonance frequencies $\omega\approx\pm\Omega_{(2)}$ (we are talking about a vortex with a fixed sign of the polarization). However, as is seen from our approximate calculations, $B/A\approx 4L^{-4}\sim 10^{-3}$. Thus in actuality there is no asymmetry of the vortex switching with respect to the sign of the frequency in the scenario proposed in Ref. 29. It is also seen from Eqs. (27) and (28) that since A_1, $B\sim R/L$, all of the effects due to the external field are small and vanish in the limit $R\to 0$. Meanwhile, in experimental studies of vortices and the switching of their polarity in magnetic nanodots, as a

rule, the vortex is located at the center of a circular system.[26,27] It is easy to show that as a consequence of this smallness, the second term on the right-hand side of Eq. (24) can be dropped, and system (27), (28) reduces to the equation of an oscillator under the simultaneous influence of a direct and a parametric pump:

$$\frac{d^2\Phi}{dt^2}+\Omega_{(2)}^2\left(1-h\frac{R}{L}\frac{a}{r_\nu^2\Omega_{(2)}^2}\cos\omega t\right)\Phi=h\frac{R}{L}c\sin\omega t. \tag{29}$$

In this equation the amplitudes of the two types of excitation are small and approximately equal: $hRa/La^2 \approx hRc/L=\varepsilon\ll 1$. It is seen that at frequencies $\omega=\pm\Omega_{(2)}$ there are direct resonances, the solutions for which are easily found in the form an expansion in powers of the parameter ε:

$$\Phi\approx\frac{\varepsilon\sin\omega t}{(\Omega_{(2)}^2-\omega^2)}+O(\varepsilon^2).$$

Here additional weaker resonances arise at frequencies $\Omega_{(2)}/2(\sim\varepsilon^2)$, $\Omega_{(2)}/3(\sim\varepsilon^3)$, etc. Parametric resonances arise at frequencies $\omega=\pm 2\Omega_{(2)}$, and the corresponding solutions are also constructed in the form of expansions in power of ε. The regions of exponential growth of the amplitude, as usual, are bounded by the straight lines $\omega\approx 2\Omega_{(2)} \pm 0.03hR$. Here we see that the picture of the resonance excitation of the system (both direct and parametric) is absolutely symmetric with respect to a change in the sign of the frequency.

3.4. Taking azimuthal modes into account

We propose a different scenario for the effect of field on the system—one incorporating the excitation of the azimuthal modes. It is seen from Eqs. (23)–(26) that in this case a circular field influences the vortex even when it is located at the center of the system. Here the terms proportional to the small parameter $R/L\sim\varepsilon$ can be dropped in the leading approximation, and we arrive at the simplified system of equations

$$\frac{d\Phi_{(2)}}{dt}-\Omega_{(2)}\mathcal{M}_{(2)}=hb\Omega_{(2)}r_\nu^2\mathcal{M}_{(3)}\sin\omega t, \tag{30}$$

$$\frac{d\mathcal{M}_{(2)}}{dt}+\Omega_{(2)}\Phi_{(2)}=-hb\frac{\Phi_{(3)}}{\Omega_{(3)}r_\nu^2}\sin\omega t, \tag{31}$$

$$\frac{d\Phi_{(3)}}{dt}-\Omega_{(3)}\mathcal{M}_{(3)}=hg\Omega_{(3)}r_\nu^2\mathcal{M}_{(2)}\sin\omega t, \tag{32}$$

$$\frac{d\mathcal{M}_{(3)}}{dt}+\Omega_{(3)}\Phi_{(3)}=-hg\frac{\Phi_{(2)}}{\Omega_{(2)}r_\nu^2}\sin\omega t-hs\cos\omega t. \tag{33}$$

We see that in this case the direct pumping acts only on the azimuthal mode, while the symmetric mode is acted on indirectly by the field—also via the azimuthal mode. As in the previous case, by making use of the smallness of the parameter L^{-2} the system of equations (30)–(36) can be substantially simplified, reducing it to two second-order equations:

$$\frac{d\Phi_{(2)}}{dt^2}+\Omega_{(2)}^2\Phi_{(2)}=-h\frac{b}{r_\nu^2}\frac{\Omega_{(2)}}{\Omega_{(3)}}\Phi_{(3)}\sin\omega t, \tag{34}$$

$$\frac{d^2\Phi_{(3)}}{dt^2}+\Omega_{(3)}^2\Phi_{(3)}=-h\frac{g}{r_\nu^2}\frac{\Omega_{(3)}}{\Omega_{(2)}}\Phi_{(2)}\sin\omega t - hs\Omega_{(3)}\cos\omega t. \tag{35}$$

We have arrived at an unusual system describing two oscillators coupled via the external field. Here the essential difference of the symmetric mode *2* and the azimuthal mode *3* lies in the fact that a direct resonance action occurs only on the azimuthal mode. At the frequency of this azimuthal mode there is an ordinary resonance with $\Phi_{(3)}=-hs\Omega_{(3)}\cos\omega t/(\Omega_{(3)}^2-\omega^2)\sim hL$, which is symmetric with respect to a change in the sign of the frequency. It is accompanied by a resonance at one-half the frequency of the symmetric mode:

$$\Phi_{(2)}=\frac{2h^2sb\Omega_{(2)}\sin 2\omega t}{r_\nu^2(\Omega_{(2)}^2-4\omega)(4\Omega_{(3)}^2-\Omega_{(2)}^2)}\sim h^2L^3$$

and by a sequence of resonances at lower frequencies.

The parametric resonances in this system are rather unusual. The main resonances ($\sim h$) are observed at the sum frequencies $\omega=\pm(\Omega_{(3)}+\Omega_{(2)})$, and the region of exponential growth of the amplitude of the solutions is bounded by the lines

$$\omega\approx\Omega_{(3)}+\Omega_{(2)}\pm\frac{h}{2r_\nu^2}\frac{\sqrt{gb}}{\sqrt{\Omega_{(2)}\Omega_{(3)}}}. \tag{36}$$

Here each of the two generalized oscillators oscillates at approximately its own eigenfrequency:

$$\Omega_{(2,3)}(h)=\Omega_{(2,3)}\pm\frac{h}{4r_\nu^2}\frac{\sqrt{gb}}{\sqrt{\Omega_{(2)}\Omega_{(3)}}}. \tag{37}$$

Besides these resonances there also exist weaker ($\sim h^2$) parametric resonances of the usual type at the doubled eigenfrequencies of the system, $2\Omega_{(2)}$ and $2\Omega_{(3)}$. In those resonances both generalized oscillators oscillate at a common frequency ($\Omega_{(2)}$ or $\Omega_{(3)}$). The region of exponential growth of the amplitude is bounded by the parabolas

$$\omega\approx 2\Omega_{(i)}+h^2\frac{gb}{4r_\nu^2}\frac{1}{\Omega_{(i)}}\frac{1}{(\Omega_{(3)}^2-\Omega_{(2)}^2))}, \tag{38}$$

where $i=2,3$, i.e., unlike the previous case (when only the symmetric mode was taken into account), where $\omega-2\Omega_{(2)} \sim hR$, now the regions of this resonance have a width of the order of $\omega-2\Omega_{(i)}\sim h^2L^3$. It becomes quadratic in the amplitude of the external field, but it increases with increasing size of the system.

We see that inclusion of the influence of azimuthal modes on the system radically alters the picture of the effect of an external field on a spin system in the presence of a vortex and is absolutely necessary for solving the problem of vortex switching in a circular field. However, for explaining the asymmetry of this process upon a change in the direction of rotation of the field (or of the polarization of the vortex) it is necessary to take into account the presence of a nonzero projection of the magnetization and the asymmetry of the properties of the azimuthal modes with respect to the direc-

tion of rotation of the spin waves. This problem is much more complicated. Therefore, we shall treat it in full measure in a subsequent based on consideration of a small spin plaquette, which models a magnetic dot in a vortex configuration.

The authors thank Yu. Gaididei and A. M. Kosevich for some stimulating discussions and helpful comments. One of the authors (A.S.K.) is also grateful to the INTAS program for support of this study under the grant INTAS No. 99-0167.

Some of the materials of this paper were presented at the Workshop on Nonlinear Lattice Structure and Dynamics, Dresden, 2001.

*E-mail: kovalev@ilt.kharkov.ua

[1] A. M. Kosevich, B. A. Ivanov, and A. S. Kovalev, *Nonlinear Magnetization Waves. Dynamical and Topological Solitons* [in Russian], Naukova Dumka, Kiev (1983).
[2] A. M. Kosevich, B. A. Ivanov, and A. S. Kovalev, Phys. Rep. **194**, 117 (1990).
[3] A. J. Mikeska and M. Steiner, Adv. Phys. **90**, 191 (1991).
[4] L. J. de Jong and A. R. Miedema, Adv. Phys. **23**, 2 (1974).
[5] H. R. Boesch, U. Schmocker, F. Waldner, K. Emerson, and J. E. Drumheller, Phys. Lett. **36**, 461 (1971).
[6] H. Hagen, H. Reimann, U. Schmocker, and F. Waldner, Physica B **36–38**, 461 (1971).
[7] F. Waldner, J. Magn. Magn. Mater. **31–34**, 1203 (1983).
[8] F. Waldner, J. Magn. Magn. Mater. **54–57**, 837 (1986).
[9] A. A. Stepanov, M. I. Kobets, and V. A. Pashchenko, Fiz. Nizk. Temp. **20**, 267 (1994) [Low Temp. Phys. **20**, 426 (1994)].
[10] H. Yamazaki and M. Mino, Suppl. Prog. Theor. Phys. **94**, 400 (1989).
[11] A. I. Zvyagin, V. N. Krivoruchko, V. A. Pashchenko, A. A. Stepanov, and D. A. Yablonskiĭ, Zh. Éksp. Teor Fiz. **92**, 311 (1887) [Sov. Phys. JETP **65**, 177 (1987)].
[12] M. Pomerantz, Surf. Sci. **142**, 556 (1984).
[13] D. I. Head, B. H. Blott, and D. Melvill, J. Phys. C **8**, 1649 (1988).
[14] A. S. Kovalev, A. M. Kosevich, and K. V. Maslov, JETP Lett. **30**, 296 (1979).
[15] N. R. Cooper, Phys. Rev. Lett. **80**, 4554 (1998); **82**, 1554 (1999).
[16] A. M. Kosevich, V. P. Voronov, and I. V. Manzhos, Zh. Éksp. Teor Fiz. **84**, 148, (1983) [Sov. Phys. JETP **57**, 86 (1983)].
[17] A. V. Nikiforov and E. B. Sonin, Zh. Éksp. Teor Fiz. **85**, 642, (1983) [Sov. Phys. JETP **58**, 373 (1983)].
[18] F. G. Mertens and A. R. Bishop, ''Nonlinear sciences at the dawn of the 21st century,'' *Lecture Notes in Physics*, P. L. Christiansen, M. P. Soerensen, and A. C. Scott (eds.), Springer, Berlin (2000), p. 137.
[19] V. L. Berezinskiĭ, Zh. Éksp. Teor Fiz. **61**, 1144 (1971) [Sov. Phys. JETP **34**, 2147 (1972)].
[20] J. M. Kosterlitz and D. J. Thouless, J. Phys. C **6**, 1181 (1973).
[21] D. G. Wiesker, H. Zabel, and S. M. Shapiro, Z. Phys. B: Condens. Matter **93**, 277 (1994).
[22] G. K. Batchelor, *An Introduction to Fluid Dynamics*, University Press, Cambridge (1967).
[23] E. M. Lifshitz and L. P. Pitaevskiĭ, *Statistical Physics*, Part 2, Pergamon Press, Oxford (1980), Nauka, Moscow (1978).
[24] M. Soskin and M. Vasnetsov, Photonics Sci. News **4**, 21 (2000).
[25] I. L. Bogolubsky, Phys. Lett. A **126**, 511 (1988).
[26] R. P. Cowburn, D. K. Koltsov, A. O. Adeyeye, M. E. Welland, and D. M. Tricker, Phys. Rev. Lett. **83**, 1042 (1999); R. P. Cowburn, J. Phys. D **33**, R1 (2000).
[27] T. Shinjo, T. Okuno, R. Hassdorf, K. Shigeto, and T. Ono, Science **289**, 930 (2000); ICR Ann. Rep. **7**, 16 (2000).
[28] Yu. Gaididei, T. Kamppeter, F. G. Mertens, and A. R. Bishop, Phys. Rev. B **59**, 7010 (1999).
[29] Yu. Gaididei, T. Kampetter, F. G. Mertens, and A. R. Bishop, Phys. Rev. B **61**, 9449 (2000).
[30] S. Nikami and T. Tsunedo, Prog. Theor. Phys. **63**, 387 (1980).
[31] S. Takeno and S. Homma, Prog. Theor. Phys. **65**, 172 (1980).
[32] M. E. Gouvea, G. M. Wysin, A. R. Bishop, and F. G. Mertens, Phys. Rev. B **39**, 11840 (1989).
[33] G. M. Wysin, Phys. Rev. B **54**, 15156 (1996).
[34] S. Iida, J. Phys. Chem. Solids **24**, 625 (1963).
[35] B. A. Ivanov, H. J. Schnitzer, F. G. Mertens, and G. M. Wysin, Phys. Rev. B **58**, 8464 (1998).
[36] G. M. Wysin and A. R. Volkel, Phys. Rev. B **52**, 7412 (1995).
[37] H. J. Schnitzer, *Zur Dynamik Kollektiver Anregungen in Hamiltonschen Systemen*, Ph.D. Thesis, Bayreuth, University of Bayreuth (1996).
[38] F. G. Mertens, H. J. Schnitzer, and A. R. Bishop, Phys. Rev. B **56**, 2510 (1997).

Translated by Steve Torstveit

Wigner-like crystallization of Anderson-localized electron systems with low electron densities

A. A. Slutskin* and H. A. Kovtun

B. Verkin Institute for Low Temperature Physics and Engineering of the National Academy of Sciences of Ukraine, 47 Lenin Ave., Kharkov 61103, Ukraine

M. Pepper

Cavendish Laboratory, University of Cambridge, Madingley Road, Cambridge CB3 0HE, United Kingdom
(Submitted July 2, 2002)
Fiz. Nizk. Temp. **28**, 1304–1309 (December 2002)

We consider an electron system under conditions of strong Anderson localization, taking into account interelectron long-range Coulomb repulsion. We establish that at sufficiently low electron densities and sufficiently low temperatures the Coulomb electron interaction brings about ordering of the Anderson-localized electrons into a structure that is close to an ideal (Wigner) crystal lattice, provided the dimension of the system is >1. This Anderson–Wigner glass (AWG) is a new macroscopic electron state that, on the one hand, is beyond the conventional Fermi glass concept, and on the other hand, qualitatively differs from the known ''plain'' Wigner glass (inherent in self-localized electron systems) in that the random slight electron displacements from the ideal crystal sites depend essentially on the electron density. With increasing electron density the AWG is found to turn into the plain Wigner glass or Fermi glass, depending on the width of the random spread of the electron levels. It is shown that the residual disorder of the AWG is characterized by a multivalley ground-state degeneracy akin to that in a spin glass. Some general features of the AWG are discussed, and a new conduction mechanism of a creep type is predicted.
[DOI: 10.1063/1.1531397]

1. INTRODUCTION

As was shown by Wigner long ago,[1] the slow decrease in the Coulomb electron-electron interaction potential $e^2/\kappa r$ (e is the free electron charge, r is the distance between the interacting electrons, and κ is the permittivity) with increasing interelectron distance inevitably causes the Coulomb energy of a free-electron gas to exceed its kinetic energy at sufficiently low electron densities, with the resulting transition of the gas into an electron crystal (Wigner crystal). In the wake of Wigner's prediction a natural question was raised whether long-range (weakly screened) Coulomb forces can lead to ordering of charge carrier ensembles in conductors. The experimental evidence that has been collected to date shows that it is very difficult (if possible at all) to observe the Wigner crystallization in conventional conductors. Therefore, charge carrier Coulomb ordering should be expected to exist first of all under conditions such that the kinetic energies of the charge carrier movement over a conductor are sufficiently small.

At present much attention is being given to electron/hole lattice systems with so small an overlap integral that tunneling of the charge carriers between the host-lattice sites is suppressed by their mutual Coulomb repulsion. Under these conditions a *Coulomb self-localization* of the electrons/holes inevitably takes place, bringing about their ordering in the following two cases: 1) If the host lattice is regular, an incommensurate electron/hole structure is generally formed for any charge carrier density.[2,3] 2) If the host lattice is disordered, but the mean separation of its sites, a_0, is much less than that of the electrons/holes $\overline{r}$, the ground-state space structure of the lattice gas of the charge carriers, though disordered, is obviously close to the corresponding Wigner crystal lattice (WCL), since the WCL spacing $a_W \sim \overline{r}$, while the random charge carriers' displacements from the WCL sites are $\sim a_0$. Such a randomly but slightly disordered WCL is often called Wigner glass.[1)]

The present paper aims to draw attention to a new type of Coulomb ordering that can occur in Anderson-localized electron systems. (For definiteness, we consider the localized charge carriers to be electrons.) The Anderson localization is considered to be ''strong'' in the sense that the external random potential localizing the electrons exceeds the mean energy of the Coulomb repulsion per electron $\varepsilon_C \sim e^2/\kappa\overline{r}$. Without essential loss of generality the external potential can be conceived as a random set of potential wells (centers of electron localization), the spread of their electron levels Δ (the disorder energy) being $\gg \varepsilon_C$. The smallness of ε_C as compared with Δ is believed to be a good reason to describe the influence of the Coulomb electron–electron interaction on an Anderson-localized system in terms of a Fermi glass,[5] a random system of the electrons occupying all wells with energies less than or equal to the Fermi energy ε_F. Up to now, the Fermi-glass approximation, modified to allow for the existence of the so-called Coulomb gap (Efros–Shklovskii gap)[6] at the Fermi energy, has been the basic approach to the problem. We show further that at sufficiently low electron densities, n_e, and sufficiently low temperatures, T, the mutual Coulomb repulsion of the electrons inevitably

forces the Anderson-localized electron ensemble to be arranged close to the WCL, provided the dimension of the system $d>1$. *This Coulomb-ordered Anderson-localized electron system, which can be called an Anderson-Wigner glass (AWG), is beyond the scope of the Fermi-glass concept.*

There are strong reasons to suggest that the random spread of the energy levels of the Anderson-localized electrons results in a qualitative difference of the AWG from the above ''plain'' Wigner glass inherent to the Coulomb self-localized electron systems. As will be seen from the following, in an AWG, unlike the plain Wigner glass, the electron displacements from the WCL sites depend essentially on n_e. This imparts to the AWG a number of new interesting features. In particular, it will be shown below that an increase in n_e turns an AWG into a Fermi glass or a plain Wigner glass, depending on the value of the parameter $\gamma=\Delta/\varepsilon_0$ ($\varepsilon_0=e^2/\kappa r_0$, r_0 is the mean separation of the wells) governing the interplay between the random spread of the electron levels and the Coulomb interelectron repulsion.

The residual disorder in an AWG is further described in terms of a *dipole glass*, a random system of interacting dipoles that issue from the WCL sites. The dipole representation of the disorder offered here turns out to be helpful for revealing a multivalley degeneracy of the AWG ground state, reminiscent of that in spin glasses.

2. THE BASIC ASSUMPTIONS

The quantum numbers of the Anderson-localized electron states are the radius vectors $\mathbf{R}$ of the wells' centers. These states will be denoted by $|\mathbf{R}\rangle$. The electron energies $\varepsilon(\mathbf{R})$ in the states $|\mathbf{R}\rangle$ (we will call them excitation energies) are random values, while the structure of the $\mathbf{R}$ set is assumed to be arbitrary; in particular, it can be regular. The lowest of the excitation energies is taken to be zero. As we are dealing with $\varepsilon(\mathbf{R})\ll\Delta$, the density ν of the number of excitation energies on the interval $[\varepsilon,\varepsilon+d\varepsilon]$ can be written in the form

$$\nu=gn_0/\Delta, \tag{1}$$

where $n_0\sim r_0^{-d}$ is the density of the wells, and the constant $g\sim 1$. For simplicity, in what follows we put $g=1$.

In the considered limiting case of low electron densities we can neglect perturbations produced in the eigenstates of the system by the electron-electron interaction with accuracy to additions of the order of

$$\lambda=\gamma^{-1}\left(\frac{r_0}{\bar{r}}\right)^2\exp\left(-\frac{r_0}{r_l}\right)\ll 1, \tag{2}$$

where $r_l\lesssim r_0$ is the localization radius. In this approximation, the eigenstates can be identified with

$$|\mathcal{R}\rangle=|\mathbf{R}_1\rangle|\mathbf{R}_2\rangle\ldots|\mathbf{R}_N\rangle, \tag{3}$$

where $\mathcal{R}=\mathbf{R}_1,\ldots,\mathbf{R}_N$ denotes the set of wells occupied by the electrons, and N is the number of electrons. The complete set of eigenstates comprises all possible $\mathcal{R}$ with different $\mathbf{R}_1\ldots\mathbf{R}_N$. With the same accuracy, the eigenvalues $E(\mathcal{R})$ corresponding to the states $|\mathcal{R}\rangle$ take the form

$$E(\mathcal{R})=E_C(\mathcal{R})+E_{\rm exc}(\mathcal{R}), \tag{4}$$

where

$$E_C=\frac{e^2}{2\kappa}\sum_{\substack{i,k=1\\ i\neq k}}^{N}|\mathbf{R}_i-\mathbf{R}_k|^{-1} \tag{5}$$

is the energy of the mutual electron repulsion and

$$E_{\rm exc}(\mathcal{R})=\sum_{i=1}^{N}\varepsilon(\mathbf{R}_i) \tag{6}$$

is the total excitation energy, i.e., the energy of the noninteracting electrons localized at the wells.

We aim to find the structure of the electron configuration $\mathcal{R}_g$ that minimizes $E(\mathcal{R})$.

3. ELECTRON ORDERING AND FERMI-GLASS INSTABILITY

Let us first discuss how mutual electron repulsion affects the ground state of the Fermi glass in the limit $n_e\to 0$. As $\varepsilon_F\ll\Delta$, from Eq. (1) we obtain

$$n_e=n_0\varepsilon_F/\Delta,$$

i.e., ε_F decreases *linearly* with n_e. Since ε_C is proportional to $n_e^{1/d}$, we find that for $d>1$ the ratio $\varepsilon_F/\varepsilon_C\propto n_e^{(d-1)/d}$ tends to *zero* with a decrease in n_e. Hence, as n_e goes to zero, the Fermi glass becomes *unstable* with respect to mutual Coulomb repulsion of the electrons, the energy E_C [Eq. (5)] dominating the excitation energies $\varepsilon(\mathbf{R})$.

As is known, the absolute minimum of E_C is realized by a WCL. Since the electrons of Fermi glass are *randomly* arranged, the Coulomb energy per electron of the Fermi glass exceeds that of the WCL, ε_W, significantly, i.e., by an amount $\sim\varepsilon_C$. This suggests that for sufficiently low n_e the configuration $\mathcal{R}_g$ falls into a class of $\mathcal{R}$ that meet the following conditions: i) for each WCL site there is an electron located in a small vicinity of the site; ii) the upper bound ε_b of the excitation energies $\varepsilon(\mathbf{R}_1),\ldots,\varepsilon(\mathbf{R}_N)$ satisfies the inequalities

$$\varepsilon_F\ll\varepsilon_b\ll\varepsilon_C. \tag{7}$$

The energy per electron $\varepsilon_{\mathcal{R}}=E(\mathcal{R})/N$ of such $\mathcal{R}$ is near ε_W. It cannot be less than ε_W, as $\varepsilon_{\rm exc}=E_{\rm exc}/N$ is positive (more precisely, it is $\geqslant\varepsilon_F$).

Any configuration of the above class is bound to belong to the set of points $\mathbf{R}$ at which $\varepsilon(\mathbf{R})\leqslant\varepsilon_b$. The density of these points equals $n_0(\varepsilon_b/\Delta)$. Correspondingly, their mean separation is

$$\rho(\varepsilon_b)\sim r_0(\Delta/\varepsilon_b)^{1/d}. \tag{8}$$

It is much less than the WCL spacing $a_W\sim\bar{r}$ owing to the first of the inequalities (7). Therefore, for each WCL site $\mathbf{m}$ there are inevitably several $\mathbf{R}$ of the set such that $|\mathbf{R}-\mathbf{m}|\sim\rho$. Populating these ''proximate'' states $|\mathbf{R}\rangle$ (one electron per site) yields just the configurations of the class mentioned above. For such a configuration the energy $\varepsilon_{\mathcal{R}}$ is the sum

$$\varepsilon_{\mathcal{R}}=\varepsilon_W+\delta\varepsilon, \tag{9}$$

where $\delta\varepsilon$ is expected to be a small correction to ε_W. It consists of two terms:

$$\delta\varepsilon=a\left(\frac{\rho}{\bar{r}}\right)^2\varepsilon_W+b\left(\frac{r_0}{\rho}\right)^d\Delta. \tag{10}$$

The first term is the deformation energy produced by electron displacements over distances $\sim\rho$ from the WCL sites. The second term is $\varepsilon_{\rm exc}$ expressed in terms of ρ in view of Eq. (8) and the fact that $\varepsilon_{\rm exc}\sim\varepsilon_b$. The factors $a=a(\mathcal{R})$, $b=b(\mathcal{R})$ depend on the details of $\mathcal{R}$, but they are both ~ 1 for any of the configurations considered.

The ground-state correction, $\delta\varepsilon_g$, to ε_W is the least of the $\delta\varepsilon$ values. Putting a, $b=1$ in expression (10) and finding its minimum with respect to ρ, we obtain the estimate

$$\delta\varepsilon_g\sim\gamma^{\frac{2}{d+2}}\left(\frac{r_0}{\overline{r}}\right)^{\frac{2(d-1)}{d+2}}\varepsilon_W, \tag{11}$$

the minimum being reached at

$$\rho=\overline{\rho}\sim\gamma^{\frac{1}{d+2}}\left(\frac{r_0}{\overline{r}}\right)^{\frac{d-1}{d+2}}a_W\sim\left(\frac{\Delta}{\delta E_C}\right)^{\frac{1}{d+2}}r_0, \tag{12}$$

where γ is the parameter defined in Sec. 1; $\delta E_C=(r_0/\overline{r})^2\varepsilon_C$; the physical sense of this energy parameter will be explained below (Sec. 5). The quantity $\overline{\rho}$ characterizes the deviation of $\mathcal{R}_g$ from the WCL.

Expressions (11) and (12) show that $\delta\varepsilon_g/\varepsilon_W$ and $\overline{\rho}/a_W$ both go to zero when $\overline{r}/r_0\to\infty$. Hence, for sufficiently low n_e the ground-state electron configuration is the WCL slightly perturbed by random electron displacements from the WCL sites. This is just the AWG mentioned in Sec. 1. The space structure of the AWG differs from that of the plain Wigner glass in Coulomb self-localized electron systems (Sec. 1) in an important aspect: the typical displacement of the electrons/holes from the WCL sites in the plain Wigner glass is of the order of the geometrical constant a_0, while that in the AWG, $\overline{\rho}$ [Eq. (12)], depends not only on the geometrical parameter r_0 but also on both the disorder energy Δ and the electron density.

It should be noted that estimates (11) and (12) can be rewritten in the form

$$\frac{\overline{\rho}}{a_W}\sim\left(\frac{\varepsilon_F}{\varepsilon_C}\right)^{\frac{1}{d+2}},\quad \frac{\delta\varepsilon_g}{\varepsilon_W}\sim\left(\frac{\varepsilon_F}{\varepsilon_C}\right)^{\frac{2}{d+2}}, \tag{13}$$

It follows herefrom that smallness of ε_F as compared with ε_C is sufficient for the AWG to come into existence.

4. DIPOLE GLASS

To gain better insight into the "residual" disorder of the AWG ground state it is necessary to consider all electron configurations $\mathcal{R}$ that are close to $\mathcal{R}_g$. To this end, it is appropriate to map these electron configurations on the sets of dipoles issuing from the WCL sites. The mapping is based on the fact that each pair consisting of *a neutral (empty) site of the WCL+the electron of a given configuration nearest to the site* is the same as the pair described as *the site with the electron+dipole* $e\mathbf{d_m}$, where the dipole vector $\mathbf{d_m}=\mathbf{R}-\mathbf{m}$, $\mathbf{R}$ and $\mathbf{m}$ are the radius vectors of the electron and the site, respectively. In dipole terms the Hamiltonian (4) takes the form

$$E(\mathcal{R})=N\varepsilon_W+H_{\rm eff},$$

where the effective Hamiltonian $H_{\rm eff}$ is a functional of the dipoles $\mathbf{d_m}$ as the independent variables. Taking into account that $|\mathbf{d_m}|\ll a_W$ for the configurations considered and expanding E_C in powers of $d_{\mathbf{m}}^{\alpha}$ (the index α enumerates the components of vectors), in the quadratic approximation we obtain

$$H_{\rm eff}=\sum_{\mathbf{m}}\widetilde{\varepsilon}(\mathbf{d_m})+\frac{e^2}{2\kappa}\sum_{\mathbf{m},\mathbf{m}'}\Lambda_{\alpha\alpha'}(\mathbf{m}-\mathbf{m}')d_{\mathbf{m}}^{\alpha}d_{\mathbf{m}}^{\alpha'}. \tag{14}$$

Here the matrix

$$\Lambda_{\alpha\alpha'}(\mathbf{m})=|\mathbf{m}|^{-3}(\delta_{\alpha\alpha'}-3m_\alpha m_{\alpha'}/|\mathbf{m}|^2)$$

determines the interaction of two dipoles issuing from sites 0, $\mathbf{m}$; the function

$$\widetilde{\varepsilon}(\mathbf{d_m})=\varepsilon(\mathbf{m}+\mathbf{d_m})+\frac{e^2}{2\kappa}\overline{\Lambda}_{\alpha\alpha'}d_{\mathbf{m}}^{\alpha}d_{\mathbf{m}}^{\alpha'},$$

where

$$\overline{\Lambda}_{\alpha\alpha'}=-\sum_{\mathbf{m}}\Lambda_{\alpha\alpha'}(\mathbf{m}).$$

Here and below, summation over repetitive indexes α, α' is implied, and the sums of $\mathbf{m}$, $\mathbf{m}'$ are taken over all WCL sites. The second term in $\widetilde{\varepsilon}(\mathbf{d_m})$ is the energy of interaction of a given dipole with the WCL; the second term in Eq. (14) is the energy of the dipole—dipole interaction.

The Hamiltonian (14) has sense provided that $H_{\rm eff}\ll N\varepsilon_W$. This is true if not only $|\mathbf{d_m}|\ll a_W$ but also $\varepsilon(\mathbf{m}+\mathbf{d_m})\ll\varepsilon_C$. As follows from the previous Section, the dipoles $\mathbf{d_m}$ meeting these requirements are bound to form some *random* set, i.e., the dipole system considered is in fact a *dipole glass*. There are good reasons to suggest that the dipole glass has much in common with the spin glass.[7] The similarity becomes clear if one considers a fairly simplified model in which $\mathbf{d_m}=d_0\mathbf{e_m}s_{\mathbf{m}}$, the independent variables $s_{\mathbf{m}}=\pm 1$, d_0 is a constant, and the unit vectors $\mathbf{e_m}$ constitute some given random set. In such a case $H_{\rm eff}$ takes the form

$$H_{\rm eff}=\sum_{\mathbf{m}\neq\mathbf{m}'}J_{\mathbf{m}\mathbf{m}'}s_{\mathbf{m}}s_{\mathbf{m}'}+\sum_{\mathbf{m}}h(s_{\mathbf{m}}), \tag{15}$$

where $s_{\mathbf{m}}$ play the role of "spins," $J_{\mathbf{m}\mathbf{m}'}=d_0^2\Lambda_{\alpha\alpha'}(\mathbf{m}-\mathbf{m}')e_{\mathbf{m}}^{\alpha}e_{\mathbf{m}'}^{\alpha'}$, a *random* function of $\mathbf{m}$, $\mathbf{m}'$, is correspondingly an "exchange integral;" the function $h(s_{\mathbf{m}})=\widetilde{\varepsilon}(d_0\mathbf{e_m}s_{\mathbf{m}})$ can be considered as an external random field. The system with the Hamiltonian (15) falls into the class of spin glasses possessing their known general property: a multivalley ground-state degeneracy [7]. The real dipole Hamiltonian (14) differs from the model one (15) only in that each dipole $\mathbf{d_m}$ meeting the above conditions runs through a given finite random set that comprises more than two vectors. Therefore, the multivalley degeneracy of the dipole-glass ground state holds in the general case.

An adequate description of the above-mentioned degeneracy can be given in terms of "$\mathcal{N}$ excitations," which are dipole configurations that contain $\mathcal{N}\gg 1$ dipoles other than those in the ground state. The total number Z of the $\mathcal{N}$ excitations is exponentially large in $\mathcal{N}$, while an increase in the dipole glass energy produced by an $\mathcal{N}$ excitation cannot exceed $\mathcal{N}\varepsilon_C$. Therefore, the typical separation between the neighboring energies of the $\mathcal{N}$-excitation energy spectrum, $\delta E(\mathcal{N})\propto\mathcal{N}/Z$, is exponentially small in $\mathcal{N}$. Due to the dipole-glass randomness the gap between the lower bound of

the $\mathcal{N}$-excitation spectrum and the ground-state energy, $\delta E_g(\mathcal{N})$, is comparable with $\delta E(\mathcal{N})$. This just results in the multivalley degeneracy of the dipole glass ground state, since in the limit $N\to\infty$ there are an infinite set of $\mathcal{N}$ excitations (''valleys'') whose energies differ from that of the ground state only by exponentially small (in N) values, their dipole arrangements having nothing in common with one another.

5. THE AWG EXISTENCE REGION

Estimates (12) show that the ratio $\overline{\rho}/a_W$ is a monotonically increasing function of n_e, though $\overline{\rho}$ itself is a monotonically decreasing one. This brings about, depending on the value of the parameter γ, two different scenarios of what happens with the AWG as n_e increases. If $\gamma\gg 1$, the typical electron deviation from the WCL sites $\overline{\rho}$ inevitably reaches values $\sim a_W$ with an increase in n_e, the ratio $\varepsilon_F/\varepsilon_C$, as is seen from Eq. (13), becoming ~ 1. This allows the conclusion that there exists some critical $n_e=n_{c1}$ at which the AWG turns into a Fermi glass (supposedly, by a second-order phase transition). Denoting by β the critical ratio $\overline{\rho}/a_W$ corresponding to n_{c1} (it is bound to be $<1/2$), we find from Eq. (12)

$$n_{c1}\sim \beta^{\frac{d(d+2)}{d-1}}\gamma^{\frac{-d}{d-1}}n_0.$$

For $\gamma\ll 1$, an increase in n_e reduces $\overline{\rho}$ down to its least possible value, r_0, the ratio $\overline{\rho}/a_W$ remaining $\ll 1$. This occurs for $\Delta\sim\delta E_C$. The parameter δE_C is the typical change in the Coulomb energy of the system as an electron is shifted over a distance $\sim r_0$. Therefore, if $\delta E_C\gg\Delta$, the random spread of the electron levels can be neglected to good accuracy, and the arrangement of the Anderson-localized electrons is entirely determined by the mutual electron repulsion.[2)] In such a case the space structure of the Anderson-localized electron system is in fact the same as that of the self-localized systems discussed in Sec. 1, i.e., it is an incommensurate electron structure[3] (the potential wells are regularly arranged) or plain Wigner crystal[4] (a disordered arrangement of the wells). Hence, for sufficiently small γ the AWG is bound to turn into a structure of the self-localized type at some critical $n_e=n_{c2}$ meeting the condition $\Delta\sim\delta E_C$. From the second of the estimates (12) we have

$$n_{c2}\sim\gamma^{d/3}n_0.$$

It follows from the aforesaid that the AWG existence region on the n_e, γ plane is bounded by the γ axis and the two curves $n_e=n_{c1}(\gamma)$ and $n_e=n_{c2}(\gamma)$ ($n_{c1}(\gamma)\to 0$ as $\gamma\to\infty$; $n_{c2}(0)=0$). They intersect at the point $n_e=\overline{n}_e\sim\beta^d n_0$, $\gamma=\overline{\gamma}\sim\beta^3$, the value $\overline{n}_e$ being the maximal n_e at which the AWG exists.

Heating affects the AWG if T exceeds $\delta\varepsilon_g$, both terms in Eq. (10) ($\rho=\overline{\rho}$) being $\sim T$. Under these conditions the dipole thermal-fluctuations amplitude $d_T\sim\overline{r}(\varepsilon_C/T)^{1/2}$, the fluctuating dipole vector taking values $\sim(T/\delta\varepsilon_g)^{1+d/2}$. As T increases, d_T becomes $\sim a_W$, and at some critical $T\sim\varepsilon_C$ the AWG turns into a glassy state.

6. SOME GENERAL FEATURES OF THE AWG

Macroscopically, the AWG manifests both electron-crystal and glassy-state features.

Due to the proximity of the AWG space structure to a WCL the only possible one-electron excitations that can transfer charge in the AWG are point defects, positively charged WCL vacancies, and interstitial electrons. In other words, the one-electron variable-range hopping that is inherent to the Fermi glass[5] is impossible in the AWG. In this respect the AWG is similar to an ideal Wigner crystal.

Conduction in the AWG is by two mechanisms: i) transfer of charged point defects, ii) multi-electron processes of a creep type that reside in the dipole glass. Here we only outline them.

The above point defects form an ideal gas whose conductivity $\sigma_{\rm def}$, being proportional to the concentration of defects, depends on the inverse temperature exponentially to within a pre-exponential factor:

$$\sigma_{\rm def}\propto\exp\left(\frac{\varepsilon_v-\varepsilon_i}{T}\right).$$

Here $\varepsilon_v\sim\varepsilon_C$ and $\varepsilon_i\sim\varepsilon_C$ are the energies of vacancy and interstitial-electron formation, respectively ($\varepsilon_i>\varepsilon_v$). It is interesting that at sufficiently low temperatures the pre-exponential factor obeys Mott's law for the Fermi glass.[5] Namely, T is bound to be less than the quantity $\delta\varepsilon_g\ll\varepsilon_C$ (Eq. (11)), which is the typical value of the random spread of the electron energies in an AWG. With respect to the hopping of a point defect between WCL sites, $\delta\varepsilon_g$ plays the same role as the disorder energy of the familiar Mott's picture.

The conduction of the second type is by a creep in the dipole glass (Sec. 4) produced by the creation and annihilation of $\mathcal{N}$ excitations as phonons are adsorbed and emitted by AWG electrons. It is essential that only those $\mathcal{N}$ excitations take part in the charge transfer whose energies $E_{\mathcal{N}}$ *are exponentially close in* $\mathcal{N}$ to the AWG ground-state energy E_g. (According to Sec. 4, it is just these excitations that cause the infinite degeneracy of the AWG ground state). It is just the exponential smallness of $E_{\mathcal{N}}-E_g$ that makes possible the creation and annihilation of $\mathcal{N}$ excitations by one-phonon absorption and emission at temperatures as low as desired. The corresponding $\mathcal{N}$ are determined by the relation $E_{\mathcal{N}}-E_g\sim T$. This gives $\mathcal{N}\sim\ln(\varepsilon_C/T)$. Taking into account that the quantum amplitude of transition (produced by the electron-phonon interaction) between the ground state and an $\mathcal{N}$ excitation is proportional to $\lambda^{\mathcal{N}}$ [the parameter $\lambda\ll 1$ has been defined in Sec. 2, Eq. (2)], we find the contribution $\sigma_{\rm creep}$ made by the creep mechanism to the AWG conductivity to be given by the following estimate:

$$\sigma_{\rm creep}\propto(T/\varepsilon_C)^{-2|\ln\lambda|}.$$

As $\sigma_{\rm creep}$ depends on T by a power law, it exceeds $\sigma_{\rm def}$ at sufficiently low temperatures.

The multivalley degeneracy of the dipole glass, like that in a spin glass,[7] is bound to cause an infinite spectrum of relaxation times, and, in consequence of this, nonergodic behavior of the AWG. This can be revealed by the observation of various relaxation processes in the AWG that go on for anomalously long times. An example is the relaxation of a

nonequilibrium AWG polarization created in one way or another. This has much in common with relaxation of a nonequilibrium magnetic moment in spin glass.

As follows from the evaluations made in Sec. 5, under moderate-disorder conditions ($\gamma \lesssim 1$) the AWG can exist up to values of n_e that are only several times less than n_0. The proper materials to observe the AWG are various amorphous narrow-band conductors, superlattices, and inversion layers wherein n_e can be varied over wide limits without affecting the disorder. Favorable conditions for semiconductor AWGs are expected to exist in super-lattices with the so-called δ layers. Of special interest is a conductive sheet in a metal-*n*-type GaAs-*p*-type GaAs system with charge transfer in an impurity band.[8] It is distinguished by pronounced regular-type oscillations in n_e, which cannot be explained in conventional one-electron terms and most likely are a manifestation of a two-dimensional AWG. We intend to provide new evidence to confirm this suggestion and to specify the electron structure in the very near future.

The main outlines of the AWG mentioned here are to be the subjects of our further detailed publications.

We gratefully acknowledge interesting and useful discussions with I. Lerner and I. Yurkevich. We are sincerely thankful to B. Shklovskii for helpful remarks.

The visit of A. Slutskin to the Cavendish Laboratory was supported by the Royal Society. A. S. would like to express his gratitude.

*E-mail: slutskin@theor.kharkov.ua

[1)] As far as we know, such a system was first considered in the paper [4]. The term ''Wigner glass'' appeared later.

[2)] To avoid misunderstanding, it should be noted that the criterion of Anderson localization $t < \Delta$ (t is the overlap integral for wells separated by a distance r_0) is implicitly assumed to be fulfilled irrespective of the relationship between δE_C and Δ.

[1] E. Wigner, Trans. Faraday Soc. **34**, 678 (1938).
[2] J. Hubbard, Phys. Rev. B **17**, 494 (1978).
[3] A. A. Slutskin, V. V. Slavin, and H. E. Kovtun, Phys. Rev. B **61**, 14184 (2000).
[4] M. S. Bello, E. I. Levin, B. I. Shklovskii, and A. L. Efros, Sov. Phys. JETP, **80**, 1596 (1981) [JETP **53**, 822 (1981)].
[5] N. F. Mott and E. A. Davis, *Electron Processes in Non-crystalline Materials*, Clarendon Press, Oxford (1979).
[6] A. L. Efros and B. I. Shklovskii, J. Phys. C **8**, L49 (1975).
[7] K. Binder and A. P. Young, Rev. Mod. Phys. **58**, 801 (1986).
[8] M. Pepper, J. Phys. C **12**, L617 (1979).

This article was published in English in the original Russian journal. Reproduced here with stylistic changes by AIP.

LOW-TEMPERATURE PHYSICS OF PLASTICITY AND STRENGTH

Staged work hardening of polycrystalline titanium at low temperatures and its relation to substructure evolution

V. A. Moskalenko,* A. R. Smirnov, V. N. Kovaleva, and V. D. Natsik

B. Verkin Institute for Low Temperature Physics and Engineering National Academy of Sciences of Ukraine, pr. Lenina 47, 61103 Kharkov, Ukraine

(Submitted April 26, 2002)
Fiz. Nizk. Temp. **28**, 1310–1319 (December 2002)

Tensile test diagrams of commercial-grade polycrystalline titanium foil are obtained in the temperature range 10–373 K, and the corresponding work hardening curves are plotted as stress versus plastic deformation, $\sigma(\varepsilon_p)$. It is shown that the hardening curves consist of two (at low temperatures) or three (at high temperatures) fragments or stages, which are approximated by the equation $\sigma = \text{const} + h\varepsilon_p^n$ with constant rheological parameters n and h within each stage, and the empirical values of these parameters are determined over the investigated temperature range. The behavior of the hardening curves is compared with the features of the substructure evolution of the polycrystalline titanium at different stages of the plastic deformation, which are revealed by methods of electron and optical microscopy. The presence of correlations between the individual stages of the hardening and the structural states formed in the samples in the process of deformation is established. The effectiveness of the different types of substructures—ensembles of randomly distributed dislocations, reorientation bands, and twins—in the hardening of polycrystalline titanium is discussed. © *2002 American Institute of Physics.* [DOI: 10.1063/1.1531398]

INTRODUCTION

The behavior of the hardening curve in the plastic deformation of crystals reflects the evolution of the system of dislocations which arise and interact. Two factors—the increase of the total density of dislocations and the character of their distribution—underlie the phenomenon of work hardening, determining its rate and level, and, hence, the mechanical properties of crystalline materials beyond the yield point. The changes of the structural state of a sample in the process of plastic flow correspond to specific mechanisms of work hardening and cause the stress–strain curve $\sigma(\varepsilon)$ to have a staged character, i.e., several extended segments with different values of the hardening rate $d\sigma/d\varepsilon$. Usually the staged character is clearly expressed for single crystals with singlet slip.

In polycrystalline metals a distinct staged character of the stress–strain curve is generally not discerned. Granted, in a number of metals with the fcc lattice in the absence of easy slip the linear parts of the second stage of the hardening curves of single crystals and polycrystals turn out to be parallel, while the third stage, varying by a parabolic law, has a complicated character.[1] Polycrystalline samples of bcc iron also exhibit hardening curves similar to those of single crystals with the (001) orientation. In addition, in both cases a cellular substructure arises after a tensile strain greater than 0.03, when the dislocation density is 3×10^9 cm^{-2} (Ref. 2). It should be emphasized here that the dislocation substructures formed and the sequence of structural changes that occur in an individual grain of the polycrystalline aggregate are analogous to those observed in single crystals. Using special methods of analysis of the parabolic deformation curves of single crystals,[3–7] one can reveal the staged character resulting from the succession of structural states: from randomly distributed dislocations to ordered dislocation formations, both disoriented and not.[4–10]

Establishing the interrelation between the behavior of the parameters appearing in the equations used to approximate the stress–strain curves and the regularities in the evolution of the substructure of a deformable sample is key to a deeper understanding of the nature of work hardening. The absence of studies of the evolution of the microstructure along the deformation curve has prevented the majority of authors from obtaining convincing evidence of the staged nature of the work hardening of polycrystals. Information about the dislocation structure is taken from published sources and invoked to explain the features of work hardening, often without the necessary rigor in the interpretation of that information, especially in cases where the studies have been done over a wide temperature range. The results obtained for a number of polycrystalline bcc metals and alloys in Ref. 7 are an exception to this. There a stage-by-stage electron microscope study of the dislocation structure of a sample at values of the strains corresponding to definite stages on the tensile test diagram permitted the authors to establish the correspondence between its structural state and the staged hardening curve.

In the analysis of the stress–strain curves of hcp metals of group IVA (α-Ti and α-Zr) it has been observed[5,8–10] that the presence (or absence) of staged work hardening depends on the straining temperature and on the impurity content of

the given metals. In the absence of systematic investigations, solely on the basis of general information about the dislocation structures formed in these metals, it was conjectured that the regularities observed in the variation of the work hardening are due to the circumstance that the transverse slip of dislocations, with the formation of a cellular substructure, can occur rather easily. However, the direct interrelationship between staged work hardening and the structural state of the sample was not established.

Recently we made a detailed electron microscope study of the evolution of the dislocation structure of polycrystalline titanium under tensile straining in the temperature range 4.2–373 K.[11,12] Knowledge of the substructure that forms along the the strain curve makes it possible to compare the characteristics of the substructure with the behavior of the hardening rate. In the present paper we obtain tensile test diagrams of a polycrystalline titanium foil in the temperature range 10–373 K and construct the hardening curves corresponding to them in coordinates of true stress versus true plastic deformation. A special analytical processing of the hardening curves has revealed their staged nature and made it possible to determine the rheological parameters characterizing the work hardening within the individual stages. A comparison of the hardening curves with the electron microscope data of Refs. 11 and 12 revealed a correlation between the individual stages of hardening and the structural states formed in the sample during the deformation, making it possible to establish the effectiveness of different types of substructures in the hardening process.

EXPERIMENTAL METHODS AND SAMPLES

We investigated commercial-grade titanium containing a concentration of interstitial impurities, mainly oxygen, of around 0.2 at. %. Experiments on tensile testing at a strain rate $\dot{\varepsilon}=2\times10^{-4}$ s^{-1} in the temperature range 10–373 K were carried out on foil samples 30 mm long, 6 mm wide, and 0.1 mm thick, cut in the direction of rolling. After the samples were annealed for 1 h at a temperature of 1025 K in a vacuum of 10^{-4} Pa, the average grain size was ~35 μm. The presence of recrystallization texture in the annealed samples led to the circumstance that the direction of strain in the majority of the grains was in the $\langle 10\bar{1}0\rangle$ direction, while the basal plane (0001) lies at an angle of $\approx25°$ to the plane of the foil.

Intermediate temperatures in the intervals 130–240 K and 10–77 K were obtained by blowing liquid nitrogen or helium through a Shapiro shower which cooled the sample, and they were maintained to within 0.3 K.

The tensile strain diagrams recorded in coordinates of load versus time, $P(t)$, were converted by a computer to coordinates of true stress versus true deformation, taking into account the change in the total length and cross section during the straining. In the region of uniform strain the true strain ε and stress σ can be calculated by the formulas $\varepsilon=\ln l/l_0=\ln(1+\delta)$ and $\sigma=(P/s_0)(1+\delta)$, where l_0 and l are the initial and instantaneous lengths and s_0 is the initial cross-sectional area of the sample. The strain ε and stress σ determined in this way more adequately reflect the physics of the work hardening process as compared to the nominal values often used for them, viz., $\delta=(l-l_0)/l_0$ and $S=P/s_0$.

We note that for interpreting the work hardening rate in the framework of dislocation theory one ordinarily uses the relation $\sigma(\varepsilon_p)$, where ε_p is the true plastic deformation, which can be found from the condition

$$\varepsilon_p=\varepsilon-\sigma/M; \tag{1}$$

here M is the combined modulus of the machine–sample system (in our case $M\approx25$ GPa at load levels up to 750 N). The differences between the $\sigma(\varepsilon_p)$ and $\sigma(\varepsilon)$ curves can be seen by comparing the data in Figs. 1 and 3. To determine the values of the work hardening rate $\theta=d\sigma/d\varepsilon_p$, after constructing the hardening curves $\sigma(\varepsilon_p)$ at different experimental temperatures we differentiated them along each curve. At 10 K the deformation curve for $\varepsilon_p>0.04$ became sawtoothed, reflecting the jumpy character of the plastic flow of titanium (see Fig. 1), and therefore the derivative $\theta=d\sigma/d\varepsilon_p$ for this case was determined from the envelope of the jumps of the curve.

In the dislocation theory of plastic flow the deforming stress σ can be written as a sum of effective and internal stresses: $\sigma=\sigma^*+\sigma_i$. Empirical estimates of the effective stress σ^* and the internal stress σ_i have been obtained by several methods separately in measurements of the rate sensitivity of the deforming stress $\Delta\sigma/\Delta\ln\dot{\varepsilon}$ and the stress relaxation depth.[13–15]

The dislocation substructure of deformable samples was studied on an EM-200 electron microscope at an accelerating voltageof 175 kV using ''self-supporting'' thin foils for transmission electron microscopy. The foils were prepared by the method of double jet electropolishing. For studying the twinned microstructure an optical microscopic was used.

RESULTS AND DISCUSSION

Figure 1 shows the deformation diagrams in the coordinates true stress versus true plastic deformation, $\sigma(\varepsilon_p)$, obtained in the tensile straining of the titanium samples in the temperature range 10–373 K. Studies of the microstructure[11,12] (see below) attest to the formation of different substructures in different stages of plastic deformation. Moreover, the $\sigma(\varepsilon_p)$ curves given in Fig. 1 do not reveal clearly discernable regions corresponding to different struc-

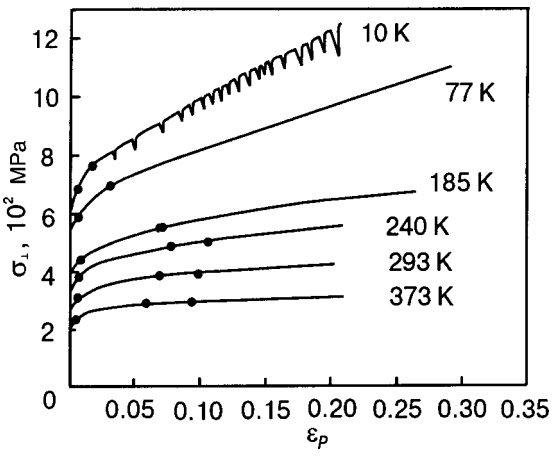

FIG. 1. Work hardening curves of polycrystalline titanium (foil) at different temperatures: ε_p is the true plastic deformation and σ is the true deforming stress; the boundaries of the stages are indicated by the symbol ●.

tural states. The boundaries between the regions (stages) are revealed only by plotting in special coordinates the hardening rate $\theta(\varepsilon_p)=d\sigma(\varepsilon_p)/d\varepsilon_p$ or the second derivative $d^2\sigma/d\varepsilon_p^2$ versus the deformation σ_p.

Various relations are used[6] for analytical approximation of the hardening curves $\sigma(\varepsilon_p)$ of polycrystals. Most often one uses simple parabolic approximations for individual fragments (stages) of the hardening curve. For example, for some stages one can use the Ludwig equation:

$$\sigma=\text{const}+h\varepsilon_p^n, \tag{2}$$

where h and n are rheological parameters of the material, which within a given stage remain constant in many cases: h characterizes the hardening rate, and n is called the hardening index.

Equation (2) is empirical, and the parameters h and n in it do not always have a simple physical meaning. However, in those cases when the staged nature of the hardening is quite pronounced, the transitions from one stage to another are accompanied by sharp jumps in the values and even the signs of these parameters; the hardening index n plays a special role as an indicator of staged hardening.

To reveal the stages recorded in our experiments (Fig. 1), the hardening curves were differentiated numerically and the results were plotted in double logarithmic coordinates, $\log(d\sigma/d\varepsilon_p)$–$\log\varepsilon_p$ (so-called Crussard–Jaoul graphs). As a result of these operations, the hardening curves $\sigma(\varepsilon_p)$ are transformed into broken lines (Fig. 2) consisting of several rectilinear segments with different values of the slope. Figure 2 clearly illustrates the staged nature of the work hardening of polycrystalline titanium: the hardening curves $\sigma(\varepsilon_p)$ consist of two or three (depending on the straining temperature) stages, each of which is described by Eq. (2) or by the corresponding equation

$$\log(d\sigma/d\varepsilon_p)_\nu=\log(h_\nu n_\nu)+(n_\nu-1)\log\varepsilon_p, \tag{3}$$

where the index $\nu=1,\ 2,\ 3$ denotes the number of the individual stage. By comparing Figs. 1 and 2 with Eq. (3), it is easy to find the rheological parameters h_ν and n_ν for each individual stage ($\nu=1,\ 2,\ 3$) and also the values of the critical strains ε_ν and stresses σ_ν, above which the substructure arising in stage $\nu-1$ becomes unstable and undergoes rearrangement. The values of the strain ε_ν correspond to the kinks in the curves in Fig. 2 and allow one to find the values of σ_ν using the data in Fig. 1. The values of the parameters $n_\nu-1$ and $\log(n_\nu h_\nu)$ are determined by the coefficients of the equations of the rectilinear segments in Fig. 2. The complete set of values found for the rheological parameters of polycrystalline titanium for all of the work hardening stages revealed here are presented in Table I.

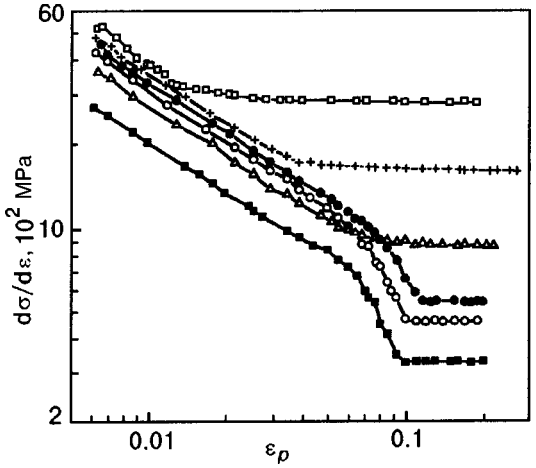

FIG. 2. Work hardening rate versus the true plastic deformation for polycrystalline titanium at different straining temperatures T [K]: 10 (□), 77 (+), 185 (△), 240 (●), 293 (○), and 373 (■).

We note once again that the work hardening rate $\theta=d\sigma/d\varepsilon_p$ in the case of a parabolic $\sigma(\varepsilon_p)$ curve changes continuously with increasing plastic deformation, but the parameters h_ν and n_ν remain constant over rather extended segments of the hardening curves, which can be interpreted in a certain sense as regions of uniform hardening.

Special note should be made of the fact that all of the hardening curves $\sigma(\varepsilon_p)$ shown in Fig. 1 also contain initial stages:

$$\sigma=\sigma_0+\sigma^{(0)}(\varepsilon_p),\quad \varepsilon_p<\varepsilon_1, \tag{4}$$

where σ_0 is the limit of elasticity (proportionality), and $\sigma^{(0)}(\varepsilon_p)$ is a certain function describing the stage of the transition from microplastic to macroplastic deformation. In

TABLE I. Empirical values of the parameters in the Ludwig equation (2) for the three stages of work hardening of polycrystalline titanium.

T, K	Stage I				Stage II				Stage III			
	σ_1, MPa	ε_1	n_1	h_1, MPa	σ_2, MPa	ε_2	n_2	h_2, MPa	σ_3, MPa	ε_3	n_3	h_3, MPa
373	240	0.005	0.45	340	300	0.06	− 0.8	− 6.5	330	0.095	1.0	370
293	325	0.005	0.44	450	430	0.07	− 0.8	− 7.5	460	0.10	1.0	480
240	380	0.006	0.46	480	510	0.08	− 0.6	− 37	530	0.115	1.0	560
185	440	0.006	0.47	460	–	–	–	–	550	0.07	0.95	910
77	600	0.006	0.45	560	–	–	–	–	700	0.035	0.96	1560
10	700	0.006	0.43	520	–	–	–	–	760	0.013	0.95	2790

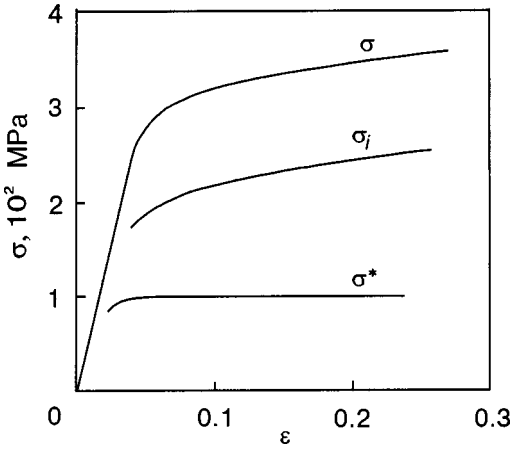

FIG. 3. Variation of the thermal σ^* and athermal σ_i components of the deforming stress σ with increasing deformation; the curves were recorded in the tensile straining of polycrystalline titanium at room temperature.

this stage the plastic deformation rate $\dot{\varepsilon}_p$ increases from zero at the limit of elasticity to the value of the strain rate set by the testing machine. In the region of well-developed plastic deformation, $\varepsilon_p > \varepsilon_1$, the hardening curves, according to Eq. (3), can be approximated by a piecewise continuous function consisting of a sequence of fragments $\nu = 1,\ 2,\ 3$ of the type described by the Ludwig equation (2). An individual fragment with number ν is described by the equation

$$\sigma^{(\nu)}(\varepsilon_p) = \sigma_\nu + h_\nu(\varepsilon_p^{n_\nu} - \varepsilon_\nu^{n_\nu}),$$

$$\varepsilon_\nu < \varepsilon_p < \varepsilon_{\nu+1}. \tag{5}$$

As we have already mentioned, the deforming stress σ can be written as a sum of two components: $\sigma = \sigma^* + \sigma_i$, where σ^* is the effective stress, which depends on the temperature, rate of strain, and chemical composition (the interstitial impurity content in the case of titanium[13]), while σ_i is a characteristic value of the long-range internal stresses and is determined mainly by the substructural state of the sample. As an example, in Fig. 3 we show data obtained in measurements of σ^* and σ_i along the strain curve $\sigma(\varepsilon)$ of a titanium sample at a straining temperature of 293 K. It is found that the thermal component of σ^* is independent of the degree of deformation at $\varepsilon_p \geqslant 0.005$. An analogous result for polycrystalline titanium was obtained previously in Ref. 16. This finding means that the work hardening due to the evolution of the structural state of the sample in the process of plastic deformation turns out to affect only the value of the internal stress σ_i. Thus the increments of deforming stress $\Delta\sigma = h\varepsilon_p^n$ on the right-hand side of Eq. (2) or (5) in our case have the meaning of substructural hardening on the individual stages along the tensile test diagram. In view of what we have said above, analysis of the staged character of the change in work hardening and its comparison with the dislocation substructure that forms is correctly done for deformations $\varepsilon_p > \varepsilon_1 \cong 0.005$.

To elucidate the physical meaning of the rheological parameters given in Table I we compare them with the results of a stage-by-stage study of the substructures formed along the deformation curve. According to the data of transmission electron microscope (TEM) studies,[11,12] in the initial stage of deformation in polycrystalline titanium at all the temperatures studied a disordered substructure is formed which consists of randomly distributed, so-called compensated dislocations (Fig. 4a). These are dislocations of different sign with a mutually compensated (equal to zero) total Burgers vector, which, as they are stopped by various kinds of obstacles, accumulate randomly in the volume. The scalar density ρ of these dislocations increases in proportion to the degree of plastic deformation ε_p:

$$\rho - \rho_0 = A\varepsilon_p, \tag{6}$$

where ρ_0 is the initial density of dislocations, and the coefficient of proportionality A at a straining temperature of 293 K has a value $\approx 1.7 \times 10^{11}$ cm^{-2} (Ref. 17). This substructural state of our samples corresponds to the parts of the deformation curves which are approximated by straight line segments with $n_1 \approx 0.5$ (stage I) on the plots of $\log(d\sigma/d\varepsilon_p)$–$\log \varepsilon_p$ (Fig. 2). In this case Eq. (2) derives from Taylor's dislocation theory of work hardening,[18] according to which the incre-

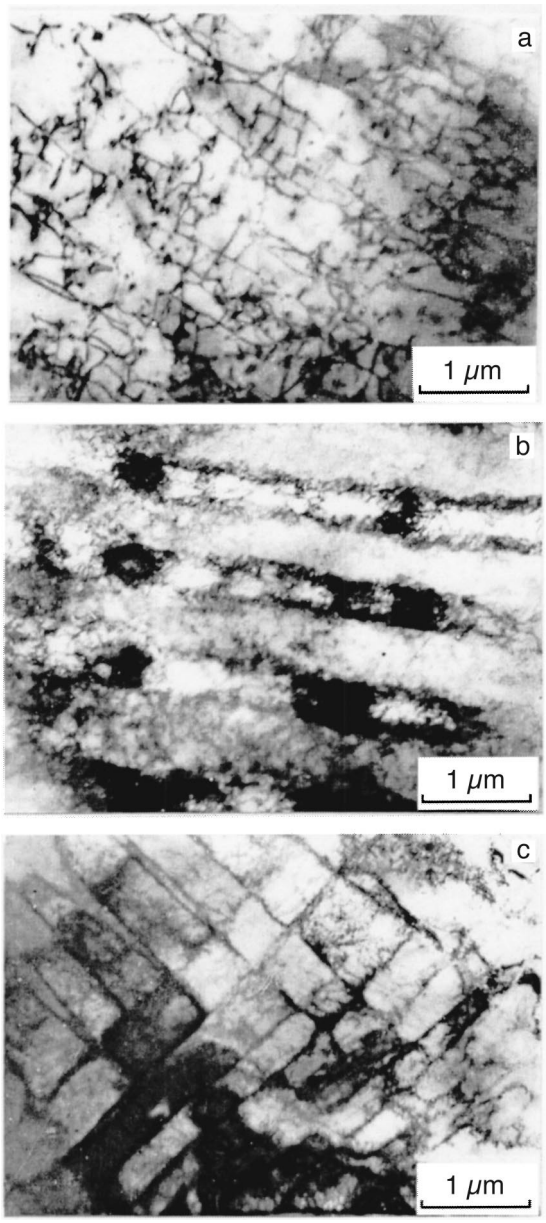

FIG. 4. Dislocation substructure of titanium after deformations $\varepsilon_p = 0.025$ (a), 0.15 (b), and 0.17 (c) at $T = 293$ K.

ment of deforming stress on the initial stage of well-developed plastic flow is described by the relation

$$\Delta\sigma = \alpha G b(\rho - \rho_0)^{1/2}, \tag{7}$$

where b is the Burgers vector, G is the shear modulus, and α is a coefficient which is usually taken close to unity. We note that the value $\alpha \approx 1$ follows from a theoretical analysis of the amplitude of the internal stresses both for coplanar and randomly distributed ''forest'' dislocations.[19,20] Equations (6) and (7) imply a parabolic relation between the true stress and true plastic deformation in the first stage ($n_1 \approx 0.5$):

$$\sigma(\varepsilon_p) = \sigma_1 + h_1 \varepsilon_p^{1/2}. \tag{8}$$

From relations (6)–(8) we obtain an equation relating the rheological parameter h_1 with the coefficient A:

$$h_1 = \alpha G b A^{1/2}. \tag{9}$$

Using the values of the coefficient A and parameter h_1 (see Table I), we find from (9) at $T = 293$ K that in our case $\alpha \approx 0.9$. This value of the coefficient α indicates that our interpretation of the hardening in stage I as being the result of interactions between dislocations is correct. Thus the parameter h_i acquires a concrete physical meaning: it characterizes the intensity of the accumulation of dislocations in the process of plastic deformation.

According to the regularities revealed in the behavior of the hardening index n, which reflect the supposed succession of hardening mechanisms along the $\sigma(\varepsilon_p)$ curve, the investigated temperature interval should be divided into two parts, separated by a temperature $T_h \approx 190$ K. For $T < T_h$ stage I ($n_1 \approx 0.5$) gives way practically immediately to stage III ($n_3 \approx 1$). For $T > T_h$ the parabolic ($n_1 \approx 0.5$) and linear ($n_3 = 1$) hardening stages, each of which is predicted by the dislocation theories of hardening, are separated by a transitional stage II with negative values of the parameter $h_2 < 0$ and $n_2 < 0$ (the deformation interval $\varepsilon_p \approx 0.06$–$0.08$). Of course, these values of the rheological parameters reflect a different physics of work hardening in the transitional stage. In connection with the presence of a characteristic temperature T_h, it is advisable in further analysis of the interrelationship between the structural state of the sample and the hardening parameters to treat the cases of high ($T > T_h$) and low ($T < T_h$) values of the straining temperature separately.

In the temperature region 240–373 K the densities of disordered edge and screw dislocations in titanium are approximately equal, which is an indirect indication that the probabilities of nucleating dislocations in the interior of a grain (internal sources) and on its boundary (surface sources) are relatively equal. As we showed in Ref. 21, this circumstance is a consequence of the approximately equal mobility of the edge and screw components of a dislocation loop at these temperatures. Near grain boundaries the density of dislocations is somewhat higher. When the deformation reaches $\varepsilon_p \geqslant 0.04$, low-angle (with a misorientation of less than 10°) band elements of substructure having a mesoscopic scale (of the order of several microns) appear against the background of the random network of dislocations as a result of processes of their self-organization. These are the so-called dislocation reorientation bands (RBs). Figures 4b and 4c show RBs with the preferred substructural elements for realization

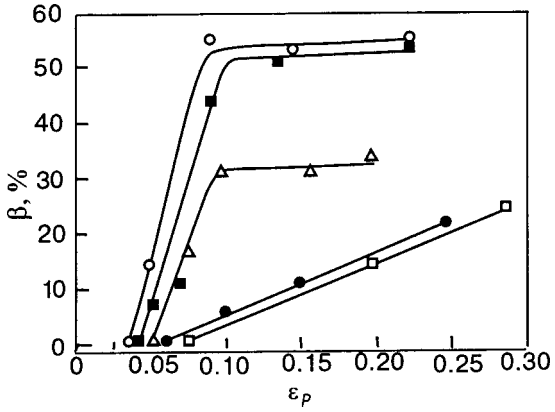

FIG. 5. Specific volume β occupied by reorientation bands versus the deformation ε_p at various temperatures T [K]: 160 (□), 185 (●), 240 (△), 293 (■), and 373 (○).

of one slip system (Fig. 4b) and for the case of activation of two equivalent slip systems (Fig. 4c). Their nucleation and development becomes possible only when a number of conditions are met.[22] One of these conditions is the creation of sufficiently high rotational stresses and their gradients, which usually occurs more rapidly near junctions of grain boundaries. Another condition is that it is necessary to reach a critical density of mobile dislocations ($\rho_{cr} \cong 10^9$–10^{10} cm^{-2}) of the type that make up the walls of the RBs: in our case, these are type-a edge dislocations. The appearance of RBs signifies a transition of the deformation process from the stage of translational (laminar) plastic flow to a stage in which, together with the ongoing translational slip of individual dislocations, a rotational (turbulent) motion of large dislocation ensembles occurs (Fig. 4b,c).

Figure 5 shows the dependence of the specific volume β occupied by the RBs as a function of the deformation for different temperatures. Below $T = 135$ K the RBs are not observed. A comparison of the data in Figs. 2 and 5 and the data given in Table I shows that for temperatures of 240–373 K the transitional stage on the $\log(d\sigma/d\varepsilon_p)$–$\log \varepsilon_p$ plots, with negative values of the hardening parameters n_2 and h_2, corresponds to the onset and rapid growth of the volume fraction of RBs (the interval of deformations $\varepsilon_p \cong 0.04$–0.1), i.e., to a rearrangement of the previous dislocation structure (owing to its instability) to an energetically more favorable state. As a result of this rearrangement, ordered dislocation configurations, RBs, appear, the volume fraction of which reaches 30–60%. Upon further increase in the deformation the value of β remains practically unchanged. The fraction of grains in which RBs is observed grows from 50% to 90% as the temperature is raised from 240 to 373 K. There is a simultaneous growth of the intragrain specific volume occupied by the RBs. Thus at high degrees of deformation the RBs become the main substructural element that determines the parameters of the hardening curve. At any straining temperatures the values of the deformations ε_2 (see Table I) at which the influence of the RBs on the staged character of the $\sigma(\varepsilon_p)$ curves begins to be manifested correspond to the moment when their specific volume β in the samples reaches approximately 20% (Fig. 5). The end of the transitional stage II (or the start of stage III) corresponds to a deformation ε_3

at which the growth of the specific volume of the RBs goes to saturation.

Negative values of the parameters n and h have been observed previously for Fe (Ref. 4) and Zr (Ref. 9) in an analysis of the stress–strain curves with the use of the Crussard–Jaoul method. This feature was explained by a dynamic rotation due to the transverse slip of dislocations during the formation of the cellular structure. The low straining temperatures in our case precludes the appearance of this effect (see Ref. 9). The results of TEM studies attest to the fact that in the region of deformations corresponding to the transitional stage, as a result of the rapid rearrangement of the dislocation structure, edge dislocations are ''expended'' on the creation of the walls of the RBs. As a consequence, the intensity of the accumulation of dislocations falls off, and there is a marked decrease in their density in the space between the walls of the RBs, i.e., in the random disordered substructure which previously had governed the rate of work hardening in the first stage [see Eq. (8)]. This change in the character of the dislocation substructure causes a change of the mechanism of work hardening. Thus the negative values of the parameters h_2 and n_2 obtained are a reflection of the dynamic process due to the transformation of the character of the plastic deformation from purely translation to predominantly rotational.

At deformations $\varepsilon_p \geqslant 0.1$, the volume fraction β of the RBs stops increasing. After that the increase in the dislocation density occurs mainly in the walls of the RBs, which leads to an increase in the rotation of adjacent microregions. These values of the deformation correspond to the start of stage III (Table I), i.e., the linear hardening stage, in which the parameter n_3 in relations (3) and (5) is close to unity. The character of the substructure formed in titanium in this stage is in principle comparable to those of its types (somewhat disoriented ordered dislocation formations) which are considered in the theoretical models of linear hardening mechanisms.[23]

When the temperature is lowered ($T<200$ K) the mobility of edge dislocations becomes much higher than that of screw dislocations. The increase in the density of dislocations with deformation occurs mainly through the accumulation of their screw components. Such a change in the dislocation dynamics leads to an increase of the critical deformation for the onset of RBs as the temperature is lowered (see Fig. 5), which is due to the slower accumulation of the critical density of edge dislocations, from which the walls of the RBs are made up. The $\beta(\varepsilon_p)$ curves for temperatures of 160 and 185 K are qualitatively different than at higher temperatures.[12] In the entire interval of ε the volume fraction of RBs increases in proportion to the deformation, but much more slowly. Even at the highest deformations it does not exceed 20%, and then the process of deformation by twinning begins.

For $T<190$ K stage II is absent, and on the $\log(d\sigma/d\varepsilon_p)$–$\log \varepsilon_p$ plots stage I gives way almost immediately to stage III, and the lower the temperature, the lower the critical deformation ε_3 for the start of stage III and the sharper the transition between stages. Since the two-stage nature of the hardening curves means a change in the mechanism of structural evolution, let us compare the parameters characterizing these stages with the results of the microstructure study.

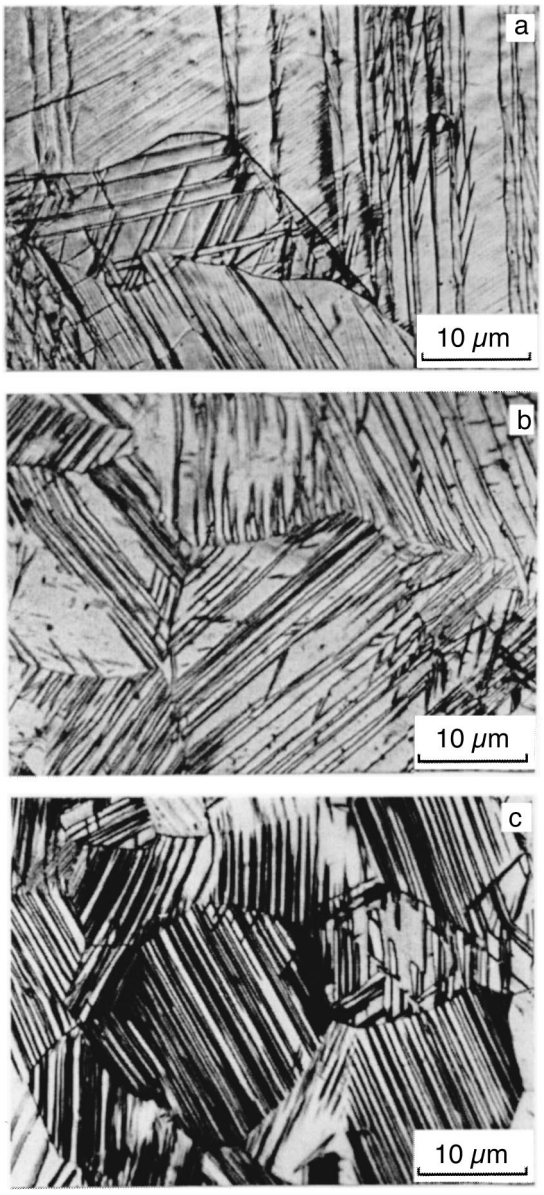

FIG. 6. Twinned microstructure of titanium deformed at $T=77$ K, $\varepsilon_p=0.025$ (a) and 0.15 (b), and at $T=10$ K, $\varepsilon_p=0.11$ (c).

At deformations corresponding to stage I ($\varepsilon_p \leqslant 0.03-0.06$ in the interval 77–185 K), reorientation bands are absent (see Fig. 5) and the main element of substructure consists of rectilinear screw-dislocation segments which are components of slip bands, the development of which is often restricted to the space between twins (Fig. 6a). The volume fraction of twins at these deformations does not exceed 0.05. The value of the parameter $n_1 \approx 0.5$ in this stage also indicates that in the type of substructure that is forming, the ordering is due to an increase of the density of dislocations which are not localized in ordered substructural formations. One notices the lower value of the work hardening rate in stage I at 185 K in comparison with temperatures of 240 and 293 K; this is at odds with the general tendency for the hardening rate $\theta=d\sigma/d\varepsilon_p$ to increase as the temperature is lowered. This fact indicates that the work hardening effect due to uniformly distributed rectilinear segments of screw

dislocations (the planar dislocation substructure) is less than the hardening due to the substructure consisting of screw and edge dislocations distributed randomly in approximately equal numbers. As the temperature is reduced further from 77 to 10 K, the density of twins increases markedly. Therefore the decrease of the critical deformation ε_3 for the start of stage III can be regarded as a consequence of activated twinning.

As we mentioned earlier, at 10 K in the region of deformations corresponding to stage III, the plastic flow becomes discontinuous (or jumplike). The ''instantaneous'' increase of the deformation in this case is manifested as a narrow localized shear band on the wide face of the sample (ribbon), lying at an angle $\approx 50°$ to the axis of tension. The relative deformation in the zone of the localized band was ≈ 0.005 for the first two load overshoots and approximately 0.013 for the last ones. The relative value of the stress jump $\Delta\sigma_{\text{ser}}/\sigma$ in this case increased from 5% to 11%. The presence of a substantial nonuniformity of the plastic deformation does not affect the hardening parameters n and h analyzed in this paper, which in the given stage are practically independent of the degree of deformation.

The microstructure of the sample in stage III is characterized by a high density of twins (Fig. 6b, c) and rectilinear segments of screw dislocations between them. The secondary twinning is very well developed. The deformation in the accomodation zone at the twin–matrix boundary is due exclusively to secondary twinning. The relaxation of the local internal stresses arising at places where the twins intersect and in the twin interlayer itself when the twin interacts with a grain boundary, etc. also occurs on account of secondary twinning. At these temperatures the twinning accounts for up to 30–40% of the elongation of the sample under tension. It is seen from the $\log(d\sigma/d\varepsilon_p)$–$\log\varepsilon_p$ plots (Fig. 2) that such an evolution of the microstructure of the sample corresponds to a practically linear character of the hardening ($n_3 \approx 1$). This result agrees with the data obtained earlier[5,24] for polycrystalline titanium deformed at 77 K.

CONCLUSION

The curves of the stress versus plastic deformation, $\sigma(\varepsilon_p)$, of polycrystalline titanium (a foil of thickness 0.1 mm) recorded in the temperature range 10–373 K have been analyzed on the basis of the analytical approximation $\sigma = \text{const} + h\varepsilon_p^n$ using $\log(d\sigma/d\varepsilon_p)$–$\log\varepsilon_p$ plots. It is shown that the low-temperature work hardening of polycrystalline titanium is a multistage process. The relationship between the hardening parameters n and h and the substructure formed in the sample in the deformation process has been found for each stage.

The analysis showed that the temperature interval investigated can be divided into two parts, separated by a temperature $T_h \approx 190$ K. For $T > T_h$ one has $n_1 \approx 0.5$ in stage I—this is a consequence of ordering due to an increase in the density of randomly distributed edge and screw dislocations ($\Delta\sigma \sim (\Delta\rho)^{1/2}$). As the deformation increases and the critical density of edge dislocations is reached, the random substructure loses stability, and ordered dislocation configurations—reorientation bands (RBs)–are formed. This stage (II) is characterized by negative values of the parameter n_2 and h_2. The sharp decrease of the work hardening rate in this stage is a consequence of the sharp drop in the density of dislocations in the space between walls of the RBs. Eventually the volume fraction of RBs, which have become the main substructure element, goes to saturation, and stage III begins. In stage III the ordering has a linear character: $n_3 = 1$ and $h_3 > 0$. This stage is characterized by the appearance of an appreciable number of mechanical twins, but their volume fraction and their influence on the ordering are insignificant.

At low temperatures $T < T_h$ the ordering in stage I is governed by the increase in the density of rectilinear segments of screw dislocations, stage II is absent, and stage III is dominated by strongly activated mechanical twinning.

The authors are grateful to V. Z. Bengus for a discussion of the features of the deformation diagrams of polycrystalline titanium and to S. N. Smirnov for a helpful discussion of the problem of work hardening. This study was supported in part by INTAS (Grants Nos. 99-01741 and 01-0320).

*E-mail: Moskalenko@ilt.kharkov.ua

[1] R. W. K. Honeycomb, *The Plastic Deformation of Metals*, Arnold, London (1968), Mir, Moscow (1972).
[2] A. S. Keh, Philos. Mag. **12**, 9 (1967).
[3] C. Crussard and B. Jaoul, Rev. Met. Paris **8**, 589 (1950).
[4] S. N. Monteiro and R. E. Reed-Hill, Metallurg. Trans. **2**, 2947 (1971).
[5] S. N. Monteiro and R. E. Reed-Hill, Metallurg. Trans. **4**, 1011 (1973).
[6] H. J. Kleemola and M. A. Nieminen, Metallurg. Trans. **5**, 1863 (1974).
[7] V. I. Trefilov, V. F. Moiseev, E. P. Pechkovskiĭ, I. D. Gornaya, and A. D. Valil'ev, *Work Hardening and Destruction of Polycrystalline Metals* [in Russian], Naukova Dumka, Kiev (1989), p. 256.
[8] V. S. Arunachalam, S. Pattanaik, S. N. Monteiro, and R. E. Reed-Hill, Metallurg. Trans. **3**, 1009 (1972).
[9] S. L. Mannan and P. Rodriguez, Trans. Indian Inst. Met. , No. 6, 49 (1973).
[10] V. A. Moskalenko, V. N. Kovaleva, A. R. Smirnov, and V. I. Startsev, Adv. Cryogenics Eng. Mater. **26**, 102 (1980).
[11] A. R. Smirnov and V. A. Moskalenko, Phys. Met. Metallogr. **66**, 162 (1988).
[12] V. A. Moskalenko and A. R. Smirnov, Mater. Sci. Eng. A **246**, 282 (1998).
[13] V. N. Kovaleva, V. A. Moskalenko, and V. D. Natsik, Philos. Mag. **70**, 423 (1994).
[14] J. C. V. Li, Can. J. Phys. **45**, 493 (1967).
[15] S. R. McEwen, O. A. Kupcis, and B. Ramaswami, Scr. Mater. **3**, 441 (1969).
[16] G. Baur and P. J. Lehr, Less-Common. Met. **69**, 203 (1980).
[17] C. Biswas, M. Cohen, and J. F. Breedis, *The Microstructure and Design of Alloys, Proceedings of the Third International Conference on the Strength of Metals and Alloys*, August 20–25, 1973, Cambridge, England (1973), Vol. 1, p. 16.
[18] G. I. Taylor, Proc. R. Soc. London, Ser. A **145**, 362 (1934).
[19] B. M. Strunin, Fiz. Tverd. Tela (Leningrad) **9**, 805 (1967) [Sov. Phys. Solid State **9**, 630 (1967)].
[20] A. A. Alekseev, Problemy Prochnosti **4**, 62 (1972).
[21] V. N. Kovaleva, V. A. Moskalenko, and V. I. Startsev, Fiz. Met. Metalloved. **52**, 391 (1981).
[22] A. E. Romanov and V. A. Vladimirov, *Dislocations in Solids*, North Holland, Amsterdam (1992).
[23] F. R. N. Nabarro, Z. S. Bazinskii, D. V. Holt, ''The plasticity of pure single crystals,'' Adv. Phys. **50**, 193 (1964), Metallurgiya, Moscow (1967).
[24] M. K. Keshavan, G. Sargent, and H. Conrad, Metall. Trans. A **6**, 1291 (1975).

Translated by Steve Torstveit

LETTERS TO THE EDITOR

Structure and photoluminescence of helium-intercalated fullerite C_{60}

I. V. Legchenkova, A. I. Prokhvatilov, Yu. E. Stetsenko, M. A. Strzhemechny, K. A. Yagotintsev, A. A. Avdeenko,* V. V. Eremenko, P. V. Zinoviev, V. N. Zoryansky, and N. B. Silaeva

B. Verkin Institute for Low Temperature Physics and Engineering of the National Academy of Sciences of Ukraine, 47 Lenin Ave., Kharkov 61103, Ukraine

R. S. Ruoff

Northwestern University, Department of Mechanical Engineering, 2145 Sheridan Road, Evanston, Illinois 60208, USA

(Submitted September 25, 2002)
Fiz. Nizk. Temp. **28**, 1320–1323 (December 2002)

The intercalation of C_{60} single crystals with helium is studied by powder x-ray diffractometry. It is established that the intercalation is a two-stage process: octahedral cavities are filled first and then tetrahedral ones, the chemical pressure being negative during both stages. The low-temperature (5 K) photoluminescence spectra of helium-intercalated fullerite C_{60} are studied for the first time. The presence of helium in lattice voids is shown to reduce that part of the luminescent intensity which is due to the emission of covalently bound pairs of C_{60} molecules, the so-called ''deep traps'' with the 0–0 transition energy close to 1.69 eV. The mechanism of the effect of intercalation with helium on the pair formation in fullerite C_{60} is discussed. [DOI: 10.1063/1.1531399]

The C_{60} fullerite has attracted attention during the last years owing to its unusual properties, such as unique optical and photoelectrical phenomena[1] and magnetism.[2] The high symmetry of the C_{60} molecule determines the geometric and electronic structure of its electronic excited states. Although C_{60} is a typical representative of π-electron systems and exhibits electronic properties inherent in these systems, the (quasi) degeneracy of the lowest excited states and symmetry forbidden transitions between these states and the ground state, and the peculiarities of the low-temperature crystal structure are factors that contribute to the unusual low-temperature luminescence of fullerite.[3,4]

Despite the large number of publications about the low-temperature luminescence spectra of C_{60}, the mechanisms that form these spectra are still far from clear. As it was recently shown, the low-temperature photoluminescence spectrum of C_{60} fullerite is determined by a set of emission centers of different origin, such as Frenkel–Davydov excitons,[3,4] charge transfer excitons,[5] structural defects,[3,4,6,7] as well as pairs or chains of molecules that play the role of deep exciton traps, typical of the C_{60} and C_{70} fullerites.[3,8–10]

In order to further investigate photoluminescence centers in the low-temperature phase of C_{60} we measured photoluminescence spectra of C_{60} fullerite saturated with helium (which has an effective atomic radius of 0.93 Å), which can presumably[11,12] bind to separate molecules in the crystal lattice of C_{60}. In crystalline C_{60} there are two tetrahedral cavities and one octahedral cavity per fullerene molecule, the mean diameters of which are respectively 2.2 and 4.2 Å.[13,14] This allows the straightforward preparation of fullerite-based substitutional solutions over a wide range of dopant concentrations. Surprisingly, given the ever growing number of publications in this field, no general review is yet available. For some types of impurities (for instance, alkali metals), there is a more or less generally accepted physical viewpoint concerning the effects brought about by the impurities, while for the others (for instance, rare gases or simple linear molecules) such a unified concept is still to be worked out. Among the rare gas intercalants the effects of saturation of C_{60} with helium have been the least studied.[11,12] It is perhaps surprising that elevated pressures are not required to reach high helium concentrations in C_{60}, though it is quite reasonable to expect that saturation kinetics as well as the consequences of intercalation will bear much similarity with results for other small-size intercalant species.

In the first stage of this work we studied the kinetics of saturation of fullerite C_{60} with He at room temperature and at pressures close to 10^5 Pa. For structure and luminescence investigations we used C_{60} single crystals from the same batch; the preparation procedure was reported earlier.[15] Evolution of the intercalation process was monitored by means of powder x-ray diffraction (DRON-3 diffractometer); the lattice parameters and other structure characteristics (reflection intensities and half-widths) were measured at particular time intervals during a long-lasting experiment at room temperature, with excursions to low (down to 20 K) temperatures. A detailed description of these structure experiments will be reported in a separate publication. The conclusions about the distribution and saturation level drawn from the structure experiments were used for the interpretation of subsequent optical measurements.

The room-temperature cubic lattice parameter a as a

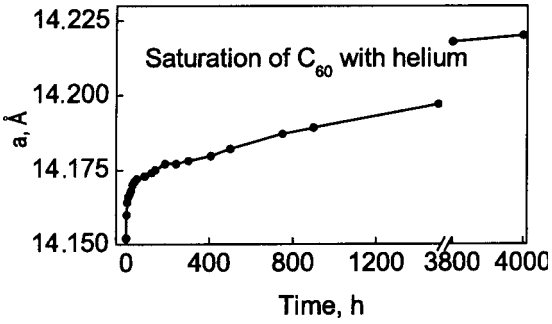

FIG. 1. Variations of the cubic lattice parameter a of C_{60} fullerite versus the time of exposure to a helium atmosphere at a pressure of around 10^5 Pa and a temperature of 295 K.

function of the exposure time of the uninterrupted intercalation process is plotted in Fig. 1. Noteworthy is the rather fast increase of a during the initial 25–30 h of intercalation, which then converted to a much slower gradual increase with distinct indications of a tendency to saturate only after 4000 h of exposure to the helium atmosphere. The half-width of all reflections has a maximum approximately in the same region where the saturation regime changeover was documented for the $a(t)$ dependence.

This temporal behavior of the structure characteristics allows us to tentatively reconstruct the scenario of helium penetration into the sample. During the first stage, octahedral cavities are filled, which are larger in size and have much wider passes in between, as compared to tetrahedral cavities. A characteristic feature of the beginning of stage 1 is an inhomogeneous distribution of helium over the sample (helium diffuses from the sample surface inward), which manifests itself through a substantial broadening of the reflections. As the He concentration gets more homogeneous, the half-width is restored to a value that differs little from that in the pure starting fullerite. After that, a much slower filling of tetrahedral vacancies begins. Estimates of the typical energies of helium in the respective environments of both vacancy types as well as the relevant diffusion problem will be published separately. It should be noted here that, unlike octahedral vacancies, the system of tetrahedral vacancies is filled virtually uniformly over the whole sample. The He content can be roughly (to within 5–10%) evaluated by comparing the Bragg reflection intensities calculated for known He fractions with measured intensities.

In the next stage of this work we studied effects of intercalation on low-temperature photoluminescence spectra of C_{60} fullerite. The luminescence measurement technique, as well as the experimental setup have been reported elsewhere.[7] A minor modification consisted in using a FÉU-62(S_1) photomultiplier, which enabled us to record photoluminescence spectra down to energies around 1.2 eV. Figure 2 shows photoluminescence spectra, normalized to integrated intensity, taken at 5 K for pure fullerite and fullerite with helium impurities, as well as the difference between the two. This difference spectrum is consistent with the luminescence spectrum of "type *A*,"[4] which originates at the so-called deep traps (the 0–0 transition energy being equal to 1.69 eV), formed by a pair or a chain of C_{60} molecules.[4,8,9] Thus, we can infer that the helium impurity, which can form

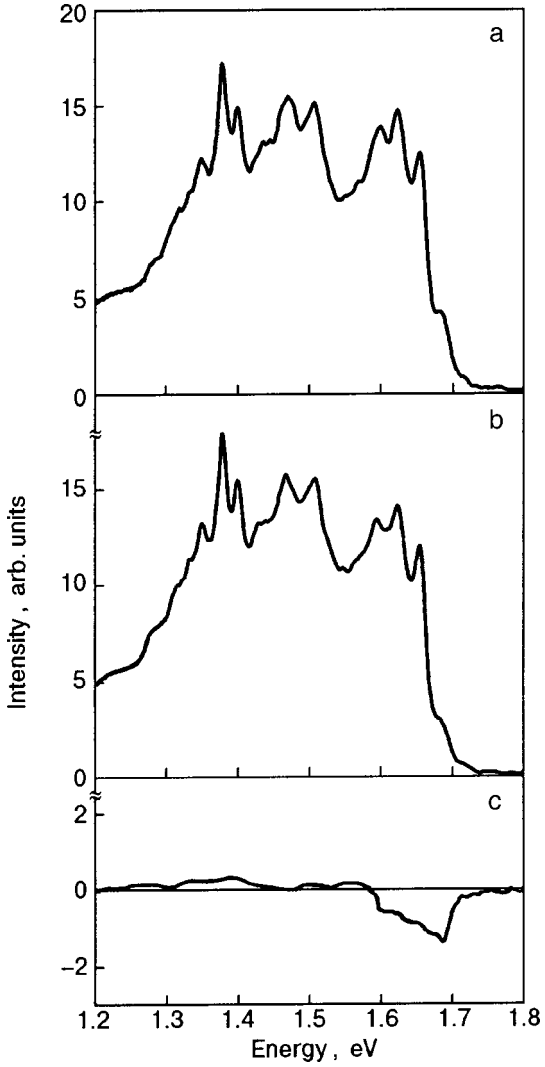

FIG. 2. Photoluminescence spectra of fullerite C_{60} at 5 K under excitation by light with energy 2.84 eV: photoluminescence spectrum of pure C_{60}, normalized to integrated intensity (a); photoluminescence spectrum (normalized to integrated intensity) of C_{60} with helium impurities (the time of exposure to helium at atmospheric pressure and room temperature is 440 h) (b); difference spectrum obtained by subtracting the upper spectrum from the lower one (c).

a weak chemical bond with C_{60} and increase the crystal lattice parameter, hinders the formation of radiation centers that could be responsible for type-*A* luminescence. A possible mechanism of this phenomenon might be as follows. As was shown by Davydov *et al.*,[16] polymerization of C_{60} in its low-temperature phase is affected by the number ratio of hexagon and pentagon pair-wise configurations, the hexagon configuration being the one that favors polymerization. The helium impurity should promote a depletion of hexagon configurations due to larger lattice parameters in doped crystals and thereby inhibit polymerization, which is often initiated by stresses around dislocations.[9] The only known mechanism of producing covalent bonding in the low-temperature phase of C_{60} is polymerization in distorted areas around dislocations.[9,16] Generally speaking, since dimerization is hardly possible even in a purely hexagonal state of C_{60}, orientational disorder, irrespective of its origin, is the necessary condition for the formation of covalent dimers. The presence of orientation disorder in the C_{60} low-temperature

phase is confirmed by the inhomogeneous broadening of the photoluminescence bands, which is removed using site-selective excitation.[4] Thus, the hypothesis that the type-*A* luminescence spectrum in the low-temperature phase of fullerite C_{60} is due to covalently bonded molecules is confirmed by our measurements on C_{60} intercalated with helium.

In conclusion, based on x-ray measurements we conclude that ambient-pressure room-temperature intercalation of C_{60} with helium is accomplished in two stages. First, the octahedral voids are comparatively quickly filled, while during the second stage a much slower filling of tetrahedral vacancies occurs. In this paper we show for the first time that intercalation of C_{60} fullerite with helium gas leads to an intercalated material that displays an appreciably reduced type-*A* luminescence in the low-temperature phase. This effect is tentatively ascribed to the hindering of polymerization owing to a decrease in hexagonal configuration content in helium-intercalated fullerite C_{60}.

*E-mail: avdeenko@ilt.kharkov.ua

[1] *Optical and Electronic Properties of Fullerenes and Fullerene Based Materials*, edited by J. Shinar, Z. V. Vardeny, and Z. H. Kafafi, edited by Marcel Dekker, New York–Basel (2000).
[2] T. L. Makarova, B. Sundqvist, R. Höhne, P. Esquinazi, Y. Kopelevich, P. Sharff, V. A. Davydov, L. S. Kashevarova, and A. V. Rakhmanina, Nature (London) **413**, 716 (2001).
[3] V. Capozzi, M. Santoro, G. Perna, G. Celentano, A. Minafra, and G. Casamassima, Eur. Phys. J. Appl. Phys. **14**, 3 (2001).
[4] I. Akimoto and K. Kan'no, J. Phys. Soc. Jpn. **71**, 630 (2002).
[5] S. Kazaoui, N. Minami, Y. Tanabe, H. J. Byrne, A. Eilmes, and P. Petelenz, Phys. Rev. B **58**, 7689 (1998).
[6] W. Guss, J. Feldmann, E. O. Göbel, C. Taliani, H. Mohn, W. Müller, P. Häussler, and H.-U. ter Meer, Phys. Rev. Lett. **72**, 2644 (1994).
[7] A. A. Avdeenko, N. I. Gorbenko, V. V. Eremenko, P. V. Zinoviev, A. T. Pugachev, N. B. Silaeva, Yu. A. Tiunov, and N. P. Churakova, Fiz. Nizk. Temp. **25**, 49 (1999) [Low Temp. Phys. **25**, 37 (1999)].
[8] D. J. van den Heuvel, G. J. B. van den Berg, E. J. J. Groenen, J. Schmidt, I. Holleman, and G. Meijer, J. Phys. Chem. **99**, 11644 (1995).
[9] D. V. Dyachenko-Dekov, Yu. V. Iunin, A. N. Izotov, V. V. Kveder, R. K. Nikolaev, V. I. Orlov, Yu. A. Ossipyan, N. S. Sidorov, and E. A. Steinman, Phys. Status Solidi B **222**, 111 (2000).
[10] M. Ichida, S. Tanaka, and A. Nakamura, J. Lumin. **87–89**, 785 (2000).
[11] K. Ichimura, K. Imaeda, and H. Inokuchi, Chem. Lett., 196 (2000).
[12] K. Ichimura, K. Imaeda, and H. Inokuchi, Mol. Cryst. Liq. Cryst. **340**, 649 (2000).
[13] P. A. Heiney, J. Phys. Chem. Solids **53**, 1333 (1992).
[14] C. H. Pennington and V. A. Stenger, Rev. Mod. Phys. **68**, 855 (1996).
[15] L. S. Fomenko, V. D. Natsik, S. V. Lubenets, V. G. Lirtsman, N. A. Aksenova, A. P. Isakina, A. I. Prokhvatilov, M. A. Strzhemechny, and R. S. Ruoff, in *Recent Advances in Chemistry and Physics of Fullerenes*, K. Kadish and R. Ruoff (Eds.), Vol. 2, Electrochemical Soc., Pennington (1995), p. 926.
[16] V. A. Davydov, L. S. Kashevarova, A. V. Rakhmanina, V. M. Senyavin, O. P. Pronina, N. N. Oleynikov, V. Agafonov, R. Ceolin, H. Allouchi, and H. Szwarc, Chem. Phys. Lett. **333**, 224 (2001).

This article was published in English in the original Russian journal. Reproduced here with stylistic changes by AIP.

SUBJECT INDEX TO VOLUME 28

Within each subject category papers are arranged in ascending page number order. This index is not a translation. It was produced by computer-aided photocomposition directly from the database of AIP's Current Physics Information system. It is based on the 1999 edition of AIP's Physics and Astronomy Classification Scheme (PACS). Suggestions for improvements as well as other comments are welcome and should be addressed to the Translations and Special Publications Division Office.

01. Communication, education, history, and philosophy

01.10 Announcements, news, and organizational activities

01.10.C Announcements, news, and awards

XIV international seminar on high-temperature superconductivity and school of applied superconductivity (Kurchatovets vacation base, Protvino, Russia, May 28–31, 2001). — M. A. Belogolovskiĭ, S. I. Bondarenko, and L. S. Shirshov; **28** (2), 143-5.

01.10.F Conferences, lectures, and institutes

XIV international seminar on high-temperature superconductivity and school of applied superconductivity (Kurchatovets vacation base, Protvino, Russia, May 28–31, 2001). — M. A. Belogolovskiĭ, S. I. Bondarenko, and L. S. Shirshov; **28** (2), 143-5.

01.30 Physics literature and publications

01.30.R Surveys and tutorial papers; resource letters

Elementary excitations in solid oxygen (Review). — Yu. A. Freiman and H. J. Jodl; **28** (7), 491-504.

Investigation of interlayer coupling in $[Fe/Cr]_n$ magnetic multilayer structures by the ferromagnetic resonance method (Review). — N. M. Kreines; **28** (8), 581-91.

Instability zones and short-lived defects in the physics of crystals. — V. M. Koshkin; **28** (8), 695-705.

Static properties and nonlinear dynamics of domain walls with a vortexlike internal structure in magnetic films (Review). — B. N. Filippov; **28** (10), 707-38.

01.60 Biographies, tributes, personal notes, and obituaries

Victor Valentinovich Eremenko (On His 70th Birthday). — **28** (7), 479.

02. Mathematical methods in physics

02.10 Logic, set theory, and algebra

Magnetoelastic waves in multisublattice systems. — I. R. Kyzyrgulov and M. Kh. Kharrasov; **28** (11), 875-6.

02.30 Function theory, analysis

02.30.H Ordinary differential equations

Solitons in elastic plates. — A. S. Kovalev, E. S. Sokolova, A. P. Mayer, and C. Eckl'; **28** (10), 780-8.

02.60 Numerical approximation and analysis

02.60.C Numerical simulation; solution of equations

Temperature-dependent resistance of a finite one-dimensional Josephson junction array. — K. Engström and J. M. Kinaret; **28** (1), 1-5.

02.70 Computational techniques

02.70.U Applications of Monte Carlo methods

Temperature-dependent resistance of a finite one-dimensional Josephson junction array. — K. Engström and J. M. Kinaret; **28** (1), 1-5.

03. Quantum mechanics, field theories, and special relativity

03.50 Classical field theories

Features of the x-ray bremsstrahlung in the scattering of intermediate-energy electrons on atoms of inert elements. — E. T. Verkhovtseva and E. V. Gnatchenko; **28** (4), 270-8.

03.65 Quantum mechanics

03.65.G Solutions of wave equations: bound states

Exact solution of the problem of an electron in a magnetic field consisting of a uniform field and arbitrarily arranged magnetic strings parallel to the uniform field. — I. M. Dubrovskiĭ; **28** (11), 845-52.

05. Statistical physics, thermodynamics, and nonlinear dynamical systems

05.30 Quantum statistical mechanics

05.30.F Fermion systems and electron gas

On the classification of equilibrium superfluid states with scalar and tensor order parameters. — M. Yu. Kovalevsky, S. V. Peletminsky, and N. N. Chekanova; **28** (4), 227-34.

05.30.J Boson systems

Self-consistent calculation of the spectrum of quasiparticles in a superfluid Bose liquid with a quenched Bose–Einstein condensate. — É. A. Pashitskiĭ, S. I. Vilchinsky, and S. V. Mashkevich; **28** (2), 79-84.

Self-consistent field model for spatially inhomogeneous Bose systems. — Yu. M. Poluéktov; **28** (6), 429-41.

05.45 Nonlinear dynamics and nonlinear dynamical systems

05.45.G Control of chaos, applications of chaos

Static properties and nonlinear dynamics of domain walls with a vortexlike internal structure in magnetic films (Review). — B. N. Filippov; **28** (10), 707-38.

Effects of chaotic local crystal fields in pseudobinary rare-earth intermetallides. — A. S. Ermolenko; **28** (10), 749-54.

05.45.Y Solitons

On the conditions for the existence of 1D magnetic solitons with frequency characteristics falling in the continuous spectrum. — A. M. Kosevich and V. I. Grishaev; **28** (8), 601-5.

Solitons in elastic plates. — A. S. Kovalev, E. S. Sokolova, A. P. Mayer, and C. Eckl'; **28** (10), 780-8.

06. Metrology, measurements, and laboratory procedures

06.30 Measurements common to several branches of physics and astronomy

06.30.D Mass and density

Measurement of the densities of liquids and gases under pressure using magnetic levitation of a standard sample. — A. S. Panfilov and Yu. Ya. Pushkar'; **28** (10), 789-93.

07. Instruments, apparatus, and components common to several branches of physics and astronomy

07.35 High-pressure apparatus; shock tubes; diamond anvil cells

Measurement of the densities of liquids and gases under pressure using magnetic levitation of a standard sample. — A. S. Panfilov and Yu. Ya. Pushkar'; **28** (10), 789-93.

34. Atomic and molecular collision processes and interactions

34.80 Electron scattering

Features of the x-ray bremsstrahlung in the scattering of intermediate-energy electrons on atoms of inert elements. — É. T. Verkhovtseva and E. V. Gnatchenko; **28** (4), 270-8.

41. Electromagnetism; electron and ion optics

41.20 Applied classical electromagnetism

41.20.G Magnetostatics; magnetic shielding, magnetic induction, boundary-value problems

Exact solution of the problem of an electron in a magnetic field consisting of a uniform field and arbitrarily arranged magnetic strings parallel to the uniform field. — I. M. Dubrovskiĭ; **28** (11), 845-52.

41.60 Radiation by moving charges

Features of the x-ray bremsstrahlung in the scattering of intermediate-energy electrons on atoms of inert elements. — É. T. Verkhovtseva and E. V. Gnatchenko; **28** (4), 270-8.

42. Optics

42.65 Nonlinear optics

42.65.K Harmonic generation, frequency conversion

Nonlinear optical spectroscopy of epitaxial magnetic garnet films. — V. V. Pavlov, R. V. Pisarev, M. Fiebig, and D. Fröhlich; **28** (7), 523-7.

43. Acoustics

43.35 Ultrasonics, quantum acoustics, and physical effects of sound

43.35.P Surface waves in solids and liquids

Characteristics of the electric field accompanying a longitudinal acoustic wave in a metal. Anomaly in the superconducting phase. — Yu. A. Avramenko, E. V. Bezuglyi, N. G. Burma, I. G. Kolobov, V. D. Fil', O. A. Shevchenko, and V. M. Gokhfeld; **28** (5), 328-36.

43.35.R Magnetoacoustic effect; oscillations and resonance

Drift of domain walls of the ab type in weak ferromagnets. — V. S. Gerasimchuk and A. A. Shitov; **28** (12), 877-9.

46. Continuum mechanics of solids

46.40 Vibrations and mechanical waves

46.40.C Mechanical wave propagation (including diffraction, scattering, and dispersion)

Solitons in elastic plates. — A. S. Kovalev, E. S. Sokolova, A. P. Mayer, and C. Eckl'; **28** (10), 780-8.

61. Structure of solids and liquids; crystallography

61.20 Structure of liquids

61.20.G Theory and models of liquid structure

On correlated heterogeneities of glass-forming liquids. — A. S. Bakai; **28** (12), 896-906.

61.25 Studies of specific liquid structures

61.25.E Molecular liquids

IR spectra of cryocondensates of an isotopic water mixture on thermocycling. — A. Aldijarov, A. S. Drobyshev, and S. S. Sarsembinov; **28** (4), 290-4.

61.43 Disordered solids

61.43.F Glasses

Field emission microscopy of the cluster and subcluster structure of a Zr–Ti–Cu–Ni–Be bulk metallic glass. — A. S. Bakaĭ, I. M. Mikhailovskij, T. I. Mazilova, and N. Wanderka; **28** (4), 279-83.

On the correlation of nonperturbative fluctuations of glass-forming liquids and magnetic glasses. — A. S. Bakaĭ; **28** (6), 415-22.

61.46 Nanoscale materials: clusters, nanoparticles, nanotubes, and nanocrystals

Field emission microscopy of the cluster and subcluster structure of a Zr–Ti–Cu–Ni–Be bulk metallic glass. — A. S. Bakaĭ, I. M. Mikhailovskij, T. I. Mazilova, and N. Wanderka; **28** (4), 279-83.

Influence of structural inhomogeneity on the luminescence properties of silicon nanocrystallites. — I. V. Blonskiĭ, M. S. Brodyn, A. Yu. Vakhnin, A. Ya. Zhugayevych, V. M. Kadan, and A. K. Kadashchuk; **28** (8), 706-12.

Giant resistance switching effect in nano-scale twinned $La_{0.65}Ca_{0.35}MnO_3$ film. — V. G. Prokhorov, G. G. Kaminsky, V. A. Komashko, Y. P. Lee, A. I. Tovstolytkin, and A. N. Pogorily; **28** (11), 856-8.

61.48 Fullerenes and fullerene-related materials

Structure and photoluminescence of helium-intercalated fullerite C_{60}. — I. V. Legchenkova, A. I. Prokhvatilov, Yu. E. Stetsenko, M. A. Strzhemechny, K. A. Yagotintsev, A. A. Avdeenko, V. V. Eremenko, P. V. Zinoviev, V. N. Zoryansky, N. B. Silaeva, and R. S. Ruoff; **28** (12), 942-4.

61.66 Structure of specific crystalline solids

61.66.B Elemental solids

Orientational order parameter in α-N_2 from x-ray data. — N. N. Galtsov, O. A. Klenova, and M. A. Strzhemechny; **28** (5), 365-8.

61.66.F Inorganic compounds

Magnetic properties of copper metaborate CuB_2O_4. — G. A. Petrakovskiĭ, A. I. Pankrats, M. A. Popov, A. D. Balaev, D. A. Velikanov, A. M.

Vorotynov, K. A. Sablina, B. Roessli, J. Schefer, A. Amato, U. Staub, M. Boehm, and B. Ouladdiaf; **28** (8), 606-12.
Influence of Cr concentration on the structural and magnetic properties of the diluted magnetic semiconductor $Hg_{1-x}Cr_xSe$. — V. D. Prozorovskiĭ, I. Yu. Reshidova, A. I. Puzynya, S. Yu. Paranchych, and V. R. Romanyuk; **28** (12), 880-2.

61.72 Defects and impurities in crystals; microstructure

61.72.H Indirect evidence of dislocations and other defects (resistivity, slip, creep, strains, internal friction, EPR, NMR, etc.)

Low-temperature unsteady creep of parahydrogen single crystals. — L. A. Alekseeva, A. V. Pustovalova, V. I. Khatuntsev, and Yu. V. Butenko; **28** (1), 58-60.

61.72.J Point defects (vacancies, interstitials, color centers, etc.) and defect clusters

Instability zones and short-lived defects in the physics of crystals. — V. M. Koshkin; **28** (8), 695-705.
On the deviations from Matthiessen's rule in quasi-one-dimensional conductors. — A. I. Kopeliovich, A. A. Mamalui, L. G. Petrenko, and T. N. Shelest; **28** (10), 771-3.

61.72.M Grain and twin boundaries

Giant resistance switching effect in nano-scale twinned $La_{0.65}Ca_{0.35}MnO_3$ film. — V. G. Prokhorov, G. G. Kaminsky, V. A. Komashko, Y. P. Lee, A. I. Tovstolytkin, and A. N. Pogorily; **28** (11), 856-8.
Staged work hardening of polycrystalline titanium at low temperatures and its relation to substructure evolution. — V. A. Moskalenko, A. R. Smirnov, V. N. Kovaleva, and V. D. Natsik; **28** (12), 935-41.

61.72.Y Interaction between different crystal defects; gettering effect

Instability zones and short-lived defects in the physics of crystals. — V. M. Koshkin; **28** (8), 695-705.

61.80 Physical radiation effects, radiation damage (for photochemical reactions, see 82.50.-m)

61.80.F Electrons and positron radiation effects

Low-dose radiation effects in thin films of high-temperature superconducting $YBa_2Cu_3O_{7-x}$ irradiated by 1-MeV electrons. — Yu. V. Fedotov, B. A. Danilchenko, and I. S. Rogutskiĭ; **28** (10), 739-43.

62. Mechanical and acoustical properties of condensed matter

62.20 Mechanical properties of solids

62.20.D Elasticity, elastic constants

Kinetics of the low-temperature structural transformation in the In–4.3 at. % Cd solid solution. — S. V. Lubenets, V. D. Natsik, L. N. Pal-Val, P. P. Pal-Val, and L. S. Fomenko; **28** (6), 465-74.

62.20.F Deformation and plasticity (including yield, ductility, and superplasticity)

Low-temperature unsteady creep of parahydrogen single crystals. — L. A. Alekseeva, A. V. Pustovalova, V. I. Khatuntsev, and Yu. V. Butenko; **28** (1), 58-60.
Features of the low-temperature plasticity of Pb–In single crystals. — N. V. Isaev, V. S. Fomenko, V. V. Pustovalov, and I. S. Braude; **28** (5), 369-75.
Low-temperature deformation and fracture of bulk nanostructural titanium obtained by intense plastic deformation using equal channel angular pressing. — V. Z. Bengus, E. D. Tabachnikova, V. D. Natsik, I. Mishkuf, K. Chakh, V. V. Stolyarov, and R. Z. Valiev; **28** (11), 864-74.
Staged work hardening of polycrystalline titanium at low temperatures and its relation to substructure evolution. — V. A. Moskalenko, A. R. Smirnov, V. N. Kovaleva, and V. D. Natsik; **28** (12), 935-41.

62.20.H Creep

Low-temperature unsteady creep of parahydrogen single crystals. — L. A. Alekseeva, A. V. Pustovalova, V. I. Khatuntsev, and Yu. V. Butenko; **28** (1), 58-60.

62.20.M Fatigue, brittleness, fracture, and cracks

Low-temperature deformation and fracture of bulk nanostructural titanium obtained by intense plastic deformation using equal channel angular pressing. — V. Z. Bengus, E. D. Tabachnikova, V. D. Natsik, I. Mishkuf, K. Chakh, V. V. Stolyarov, and R. Z. Valiev; **28** (11), 864-74.

62.30 Mechanical and elastic waves; vibrations

Multidimensional and surface solitons in a nonlinear elastic medium. — A. S. Kovalev, E. S. Syrkin, and J. A. Maugin; **28** (6), 452-61.

62.65 Acoustical properties of solids

MgB_2: Synthesis, sound velocity, and dynamics of the vortex phase. — T. V. Ignatova, G. A. Zvyagina, I. G. Kolobov, E. A. Masalitin, V. D. Fil', Yu. V. Paderno, A. N. Bykov, V. N. Paderno, and V. I. Lyashenko; **28** (3), 190-3.

63. Lattice dynamics

63.20 Phonons in crystal lattices

Molar volume dependence of the thermal conductivity in mixed cryocrystals. — V. A. Konstantinov, E. S. Orel, and V. P. Revyakin; **28** (2), 136-9.
Mechanism for the changes with temperature of the EPR spectrum of the Fe^{3+} ion in polycrystalline materials containing complexes with a multiwell potential. — V. N. Vasyukov; **28** (3), 199-202.
Elementary excitations in solid oxygen (Review). — Yu. A. Freiman and H. J. Jodl; **28** (7), 491-504.
Spin–phonon interaction and mode softening in NiF_2. — D. J. Lockwood; **28** (7), 505-9.
Light scattering on phonons in quasi-one-dimensional antiferromagnet $CsFeCl_3 \cdot 2H_2O$ induced by magnetic ordering. — V. S. Kurnosov, A. V. Peschanskii, V. I. Fomin, A. V. Yeremenko, and Yu. G. Pashkevich; **28** (7), 516-22.
Magnetic field induced phase transition in $KEr(MoO_4)_2$. Vibronic model. — A. A. Loginov; **28** (10), 755-61.

63.20.D Phonon states and bands, normal modes, and phonon dispersion

Lattice dynamics and heat capacity of a two-dimensional monoatomic crystal on a substrate. — T. N. Antsygina, I. I. Poltavsky, M. I. Poltavskaya, and K. A. Chishko; **28** (6), 442-51.

63.20.K Phonon–electron and phonon–phonon interactions

Dependence of semiconductor energy bands on the isotopic composition. A universal relation for monoatomic crystals. — A. P. Zhenov; **28** (2), 128-35.
Raman scattering in a $LiNiPO_4$ single crystal. — V. I. Fomin, V. P. Gnezdilov, V. S. Kurnosov, A. V. Peschanskii, A. V. Yeremenko, H. Schmid, J.-P. Rivera, and S. Gentil; **28** (3), 203-9.

63.20.L Phonon interactions with other quasiparticles

Excitons in the layered insulators ZnI_2 and CdI_2:Zn. — O. N. Yunakova, V. K. Miloslavsky, and E. N. Kovalenko; **28** (4), 284-9.

63.50 Vibrational states in disordered systems

Two-quantum electron spin–lattice relaxation in amorphous solids. — L. G. Zakharov, L. L. Chotorlishvili, and T. L. Buishvili; **28** (6), 412-4.

63.70 Statistical mechanics of lattice vibrations and displacive phase transitions

Spin–phonon interaction and mode softening in NiF_2. — D. J. Lockwood; **28** (7), 505-9.

64. Equations of state, phase equilibria, and phase transitions

64.30 Equations of state of specific substances

Equation of state of an equimolar ^{3}He–^{4}He mixture. — L. V. Karnatsevich, R. M. Sibileva, M. A. Khazhmuradov, I. N. Shapoval, and A. V. Meriuz; **28** (4), 235-8.

64.70 Specific phase transitions

64.70.J Liquid–liquid transitions

IR spectra of cryocondensates of an isotopic water mixture on thermocycling. — A. Aldijarov, A. S. Drobyshev, and S. S. Sarsembinov; **28** (4), 290-4.

64.70.K Solid–solid transitions

Kinetics of the low-temperature structural transformation in the In–4.3 at. % Cd solid solution. — S. V. Lubenets, V. D. Natsik, L. N. Pal-Val, P. P. Pal-Val, and L. S. Fomenko; **28** (6), 465-74.

Elementary excitations in solid oxygen (Review). — Yu. A. Freiman and H. J. Jodl; **28** (7), 491-504.

Phase transformations of the decomposition type in systems with orbital degeneracy. — M. A. Ivanov, N. K. Tkachev, and A. Ya. Fishman; **28** (8), 613-20.

Magnetic field induced phase transition in $KEr(MoO_4)_2$. Vibronic model. — A. A. Loginov; **28** (10), 755-61.

Low-temperature inversion of the magnetoresistance in charge-ordered layered superstructures. — P. V. Gorskyi; **28** (10), 767-70.

64.70.P Glass transitions

On correlated heterogeneities of glass-forming liquids. — A. S. Bakai; **28** (12), 896-906.

64.75 Solubility, segregation, and mixing; phase separation

Phase transformations of the decomposition type in systems with orbital degeneracy. — M. A. Ivanov, N. K. Tkachev, and A. Ya. Fishman; **28** (8), 613-20.

65. Thermal properties of condensed matter

65.20 Thermal properties of liquids: heat capacity, thermal expansion, etc.

On the correlation of nonperturbative fluctuations of glass-forming liquids and magnetic glasses. — A. S. Bakaĭ; **28** (6), 415-22.

On correlated heterogeneities of glass-forming liquids. — A. S. Bakai; **28** (12), 896-906.

65.40 Thermal properties of crystalline solids

65.40.B Heat capacity

Lattice dynamics and heat capacity of a two-dimensional monoatomic crystal on a substrate. — T. N. Antsygina, I. I. Poltavsky, M. I. Poltavskaya, and K. A. Chishko; **28** (6), 442-51.

65.40.G Entropy and other thermodynamical quantities

On correlated heterogeneities of glass-forming liquids. — A. S. Bakai; **28** (12), 896-906.

65.60 Thermal properties of amorphous solids and glasses: heat capacity, thermal expansion, etc.

On the correlation of nonperturbative fluctuations of glass-forming liquids and magnetic glasses. — A. S. Bakaĭ; **28** (6), 415-22.

66. Transport properties of condensed matter (nonelectronic)

66.30 Diffusion in solids

66.30.D Theory of diffusion and ionic conduction in solids

Dynamical chaos and low-temperature surface diffusion of small adatom clusters. — A. S. Kovalev and A. I. Landau; **28** (6), 423-8.

66.30.L Diffusion of other defects

Instability zones and short-lived defects in the physics of crystals. — V. M. Koshkin; **28** (8), 695-705.

66.70 Nonelectronic thermal conduction and heat-pulse propagation in solids; thermal waves

Molar volume dependence of the thermal conductivity in mixed cryocrystals. — V. A. Konstantinov, E. S. Orel, and V. P. Revyakin; **28** (2), 136-9.

Thermal conductivity of a GaAs single crystal grown in microgravity. — A. I. Ivanov, A. N. Luk'yanov, B. A. Merisov, A. V. Sologubenko, and G. Ya. Khadjai; **28** (6), 462-4.

67. Quantum fluids and solids; liquid and solid helium

67.40 Boson degeneracy and superfluidity of ^{4}He

67.40.D Quantum statistical theory; ground state, elementary excitations

Self-consistent calculation of the spectrum of quasiparticles in a superfluid Bose liquid with a quenched Bose–Einstein condensate. — E. A. Pashitskiĭ, S. I. Vilchinsky, and S. V. Mashkevich; **28** (2), 79-84.

Magnetotransport in a quasi-one-dimensional electron system on superfluid helium. — B. A. Nikolaenko, Yu. Z. Kovdrya, and S. P. Gladchenko; **28** (11), 859-63.

67.40.F Dynamics of relaxation phenomena

Asymmetry of relaxation processes and the creation of high-energy phonons in the anisotropic phonon systems of He II. — I. N. Adamenko, K. É. Nemchenko, and A. F. G. Wyatt; **28** (2), 85-94.

67.40.K Thermodynamic properties

Asymmetry of relaxation processes and the creation of high-energy phonons in the anisotropic phonon systems of He II. — I. N. Adamenko, K. É. Nemchenko, and A. F. G. Wyatt; **28** (2), 85-94.

67.40.M First sound

Concentration dependence of the attenuation of first sound in supersaturated superfluid ^{3}He–^{4}He solutions under pressure. — A. A. Zadorozhko, T. V. Kalko, É. Ya. Rudavskiĭ, I. A. Usherov-Marshak, V. K. Chagovets, and G. A. Sheshin; **28** (2), 73-8.

Sound propagation in a porous medium filled with superfluid helium. — Sh. E. Kekutiya and N. D. Chkhaidze; **28** (11), 795-802.

67.55 Normal phase of liquid ^{3}He

Magnetic coupling between liquid ^{3}He and solid insulators (Review). — V. V. Naletov, M. S. Tagirov, and D. A. Tayurskiĭ; **28** (5), 299-311.

67.57 Superfluid phase of liquid ^{3}He

On the classification of equilibrium superfluid states with scalar and tensor order parameters. — M. Yu. Kovalevsky, S. V. Peletminsky, and N. N. Chekanova; **28** (4), 227-34.

67.60 Mixed systems; liquid ^{3}He, ^{4}He mixtures

67.60.D He I–^{3}He

Equation of state of an equimolar ^{3}He–^{4}He mixture. — L. V. Karnatsevich, R. M. Sibileva, M. A. Khazhmuradov, I. N. Shapoval, and A. V. Meriuz; **28** (4), 235-8.

67.60.F He II–^{3}He

Concentration dependence of the attenuation of first sound in supersaturated superfluid ^{3}He–^{4}He solutions under pressure. — A. A. Zadorozhko, T. V. Kalko, É. Ya. Rudavskiĭ, I. A. Usherov-Marshak, V. K. Chagovets, and G. A. Sheshin; **28** (2), 73-8.

67.80 Solid helium and related quantum crystals

67.80.C Structure, lattice dynamics, and sound propagation

Effect of impurity oxygen on the low-temperature plasticity of solid normal hydrogen. — L. A. Alekseeva and Yu. V. Butenko; **28** (2), 140-2.

Spin–lattice relaxation in the bcc phase of phase-separated ^{3}He–^{4}He solid mixtures. — N. P. Mikhin, V. A. Maidanov, and A. V. Polev; **28** (4), 239-41.

67.80.J Magnetic properties and nuclear magnetic resonance

Spin–lattice relaxation in the bcc phase of phase-separated ^{3}He–^{4}He solid mixtures. — N. P. Mikhin, V. A. Maidanov, and A. V. Polev; **28** (4), 239-41.

67.80.M Defects, impurities, and diffusion

Low-temperature unsteady creep of parahydrogen single crystals. — L. A. Alekseeva, A. V. Pustovalova, V. I. Khatuntsev, and Yu. V. Butenko; **28** (1), 58-60.

Effect of impurity oxygen on the low-temperature plasticity of solid normal hydrogen. — L. A. Alekseeva and Yu. V. Butenko; **28** (2), 140-2.

67.90 Other topics in quantum fluids and solids; liquid and solid helium (restricted to new topics in section 67)

Watergel—a new form of water condensed in liquid ^{4}He. — A. M. Kokotin and L. P. Mezhov-Deglin; **28** (3), 165-71.

68. Surfaces and interfaces; thin films and low-dimensional systems (structure and nonelectronic properties)

68.08 Liquid-solid interfaces

Magnetic coupling between liquid ^{3}He and solid insulators (Review). — V. V. Naletov, M. S. Tagirov, and D. A. Tayurskiĭ; **28** (5), 299-311.

68.15 Liquid thin films

IR spectra of cryocondensates of an isotopic water mixture on thermocycling. — A. Aldijarov, A. S. Drobyshev, and S. S. Sarsembinov; **28** (4), 290-4.

68.35 Solid surfaces and solid-solid interfaces: Structure and energetics

68.35.F Diffusion; interface formation

Inelastic electron tunneling across magnetically active interfaces in cuprate and manganite heterostructures modified by electromigration processes. — M. A. Belogolovskiĭ, Yu. F. Revenko, A. Yu. Gerasimenko, V. M. Svistunov, E. Hatta, G. Plitnik, V. E. Shaternik, and E. M. Rudenko; **28** (6), 391-4.

Dynamical chaos and low-temperature surface diffusion of small adatom clusters. — A. S. Kovalev and A. I. Landau; **28** (6), 423-8.

68.35.J Surface and interface dynamics and vibrations

Dynamical chaos and low-temperature surface diffusion of small adatom clusters. — A. S. Kovalev and A. I. Landau; **28** (6), 423-8.

Multidimensional and surface solitons in a nonlinear elastic medium. — A. S. Kovalev, E. S. Syrkin, and J. A. Maugin; **28** (6), 452-61.

68.37 Microscopy of surfaces, interfaces, and thin films

68.37.V Field emission and field-ion microscopy

Field emission microscopy of the cluster and subcluster structure of a Zr–Ti–Cu–Ni–Be bulk metallic glass. — A. S. Bakaĭ, I. M. Mikhailovskij, T. I. Mazilova, and N. Wanderka; **28** (4), 279-83.

68.43 Chemisorption/physisorption: adsorbates on surfaces

68.43.J Diffusion of adsorbates, kinetics of coarsening and aggregation

Dynamical chaos and low-temperature surface diffusion of small adatom clusters. — A. S. Kovalev and A. I. Landau; **28** (6), 423-8.

68.55 Thin film structure and morphology

68.55.J Structure and morphology; thickness; crystalline orientation and texture

Giant resistance switching effect in nano-scale twinned $La_{0.65}Ca_{0.35}MnO_3$ film. — V. G. Prokhorov, G. G. Kaminsky, V. A. Komashko, Y. P. Lee, A. I. Tovstolytkin, and A. N. Pogorily; **28** (11), 856-8.

68.55.L Defects and impurities: doping, implantation, distribution, concentration, etc.

Aging effect on the magnetic and transport properties of laser-deposited $La_{0.5}Sr_{0.5}CoO_{3-\delta}$ films. — V. G. Prokhorov, G. G. Kaminskiĭ, V. M. Ishchuk, I. N. Chukanova, Y. P. Lee, and K. W. Kim; **28** (5), 354-8.

68.65 Low-dimensional, mesoscopic, and nanoscale systems: structure and nonelectronic properties

Structure and photoluminescence of helium-intercalated fullerite C_{60}. — I. V. Legchenkova, A. I. Prokhvatilov, Yu. E. Stetsenko, M. A. Strzhemechny, K. A. Yagotintsev, A. A. Avdeenko, V. V. Eremenko, P. V. Zinoviev, V. N. Zoryansky, N. B. Silaeva, and R. S. Ruoff; **28** (12), 942-4.

71. Electronic structure of bulk materials

71.10 Theories and models of many-electron systems

Self-consistent field model for spatially inhomogeneous Bose systems. — Yu. M. Poluéktov; **28** (6), 429-41.

71.10.H Non-Fermi-liquid ground states, electron phase diagrams and phase transitions in model systems

Exact solution of the problem of an electron in a magnetic field consisting of a uniform field and arbitrarily arranged magnetic strings parallel to the uniform field. — I. M. Dubrovskiĭ; **28** (11), 845-52.

71.10.L Excited states and pairing interactions in model systems

Exact solution of the problem of an electron in a magnetic field consisting of a uniform field and arbitrarily arranged magnetic strings parallel to the uniform field. — I. M. Dubrovskiĭ; **28** (11), 845-52.

71.15 Methods of electronic structure calculations

71.15.D Computational methodology (Brillouin zone sampling, iterative diagonalization, pseudopotential construction)

Dependence of semiconductor energy bands on the isotopic composition. A universal relation for monoatomic crystals. — A. P. Zhenov; **28** (2), 128-35.

71.15.M Density functional theory, local density approximation, gradient and other corrections

Self-consistent field model for spatially inhomogeneous Bose systems. — Yu. M. Poluéktov; **28** (6), 429-41.

71.15.R Relativistic effects

Electronic structure and magneto-optical Kerr effect in the compound $UCuP_2$. — O. Horpynyuk, V. V. Nemoshkalenko, V. N. Antonov, B. N. Harmon, and A. N. Yaresko; **28** (7), 533-8.

Metallic properties of lead dioxide. Band structure and NMR of ^{207}Pb at low temperatures. — L. A. Boyarskiĭ, S. P. Gabuda, S. G. Kozlova, and R. N. Pletnev; **28** (8), 691-4.

71.18 Fermi surface: calculations and measurements; effective mass, g factor

Features of the thermopower of Mo–Re and Mo–Re–Nb alloys and the electronic–topological transition in these systems. — T. A. Ignatyeva and A. N. Velikodny; **28** (6), 403-11.

On the deviations from Matthiessen's rule in quasi-one-dimensional conductors. — A. I. Kopeliovich, A. A. Mamalui, L. G. Petrenko, and T. N. Shelest; **28** (10), 771-3.

71.20 Electron density of states and band structure of crystalline solids

71.20.B Transition metals and alloys

Features of the thermopower of Mo–Re and Mo–Re–Nb alloys and the electronic–topological transition in these systems. — T. A. Ignatyeva and A. N. Velikodny; **28** (6), 403-11.

71.20.N Semiconductor compounds

Dependence of semiconductor energy bands on the isotopic composition. A universal relation for monoatomic crystals. — A. P. Zhenov; **28** (2), 128-35.

71.20.T Fullerenes and related materials; intercalation compounds

On the role of Jahn–Teller vibrations in the mechanism of high-T_c superconductivity of intercalated C_{60} fullerite films with *p*-type conductivity. — V. M. Loktev and E. A. Pashitskiĭ; **28** (4), 295-7.

71.27 Strongly correlated electron systems; heavy fermions

Superconductivity in impurity systems with a lower density of charge carriers and with strong electron correlations. — M. E. Palistrant; **28** (2), 109-16.

Electronic excitations and correlations in quantum bars. — I. Kuzmenko, S. Gredeskul, K. Kikoin, and Y. Avishai; **28** (7), 539-46.

Metallic properties of lead dioxide. Band structure and NMR of ^{207}Pb at low temperatures. — L. A. Boyarskiĭ, S. P. Gabuda, S. G. Kozlova, and R. N. Pletnev; **28** (8), 691-4.

Wigner-like crystallization of Anderson-localized electron systems with low electron densities. — A. A. Slutskin, H. A. Kovtun, and M. Pepper; **28** (12), 930-4.

71.35 Excitons and related phenomena

71.35.C Intrinsic properties of excitons; optical absorption spectra

Excitons in the layered insulators ZnI_2 and CdI_2:Zn. — O. N. Yunakova, V. K. Miloslavsky, and E. N. Kovalenko; **28** (4), 284-9.

71.38 Polarons and electron-phonon interactions

Dependence of semiconductor energy bands on the isotopic composition. A universal relation for monoatomic crystals. — A. P. Zhenov; **28** (2), 128-35.

On the deviations from Matthiessen's rule in quasi-one-dimensional conductors. — A. I. Kopeliovich, A. A. Mamalui, L. G. Petrenko, and T. N. Shelest; **28** (10), 771-3.

71.45 Collective effects

Wigner-like crystallization of Anderson-localized electron systems with low electron densities. — A. A. Slutskin, H. A. Kovtun, and M. Pepper; **28** (12), 930-4.

71.45.G Exchange, correlation, dielectric and magnetic response functions, plasmons

Electronic excitations and correlations in quantum bars. — I. Kuzmenko, S. Gredeskul, K. Kikoin, and Y. Avishai; **28** (7), 539-46.

Exchange interaction and magnetoresistance in $La_{2/3}Ca_{1/3}MnO_3$: experiment and models. — A. B. Beznosov, B. I. Belevtsev, E. L. Fertman, V. A. Desnenko, D. G. Naugle, K. D. D. Rathnayaka, and A. Parasiris; **28** (7), 556-61.

Low-temperature inversion of the magnetoresistance in charge-ordered layered superstructures. — P. V. Gorskyi; **28** (10), 767-70.

71.55 Impurity and defect levels

Magnetization dynamics of electron–impurity systems at paramagnetic resonance. — E. A. Ivanchenko; **28** (2), 117-22.

71.55.H Other nonmetals

Microscopic nature of Pr^{3+} optical centers in Y_2SiO_5, Lu_2SiO_5, and Gd_2SiO_5 crystals. — Yu. V. Malyukin, P. N. Zhmurin, B. V. Grinev, V. P. Seminozhenko, N. V. Znamenskiĭ, E. A. Manykin, E. A. Petrenko, and T. G. Yukina; **28** (10), 774-9.

71.55.J Disordered structures; amorphous and glassy solids

Wigner-like crystallization of Anderson-localized electron systems with low electron densities. — A. A. Slutskin, H. A. Kovtun, and M. Pepper; **28** (12), 930-4.

71.70 Level splitting and interactions

71.70.C Crystal and ligand fields

Microscopic nature of Pr^{3+} optical centers in Y_2SiO_5, Lu_2SiO_5, and Gd_2SiO_5 crystals. — Yu. V. Malyukin, P. N. Zhmurin, B. V. Grinev, V. P. Seminozhenko, N. V. Znamenskiĭ, E. A. Manykin, E. A. Petrenko, and T. G. Yukina; **28** (10), 774-9.

71.70.E Spin–orbit coupling, Zeeman and Stark splitting, Jahn-Teller effect

Phase transformations of the decomposition type in systems with orbital degeneracy. — M. A. Ivanov, N. K. Tkachev, and A. Ya. Fishman; **28** (8), 613-20.

Manifestation of the Jahn–Teller effect in the EPR spectrum of the metalorganic complex $[Cu(en)2H_2O]SO_4$. — A. G. Anders,

A. I. Kaplienko, O. V. Kravchina, V. S. Bondarenko, A. Feher, M. Orendáč, A. Orendáčová, M. Kajňaková, and J. Černák; **28** (8), 642-5.

72. Electronic transport in condensed matter

72.15 Electronic conduction in metals and alloys

72.15.E Electrical and thermal conduction in crystalline metals and alloys

Metallic properties of lead dioxide. Band structure and NMR of ^{207}Pb at low temperatures. — L. A. Boyarskiĭ, S. P. Gabuda, S. G. Kozlova, and R. N. Pletnev; **28** (8), 691-4.

72.15.J Thermoelectric and thermomagnetic effects

Features of the thermopower of Mo–Re and Mo–Re–Nb alloys and the electronic–topological transition in these systems. — T. A. Ignatyeva and A. N. Velikodny; **28** (6), 403-11.

72.15.N Collective modes (e.g., in one-dimensional conductors)

On the deviations from Matthiessen's rule in quasi-one-dimensional conductors. — A. I. Kopeliovich, A. A. Mamalui, L. G. Petrenko, and T. N. Shelest; **28** (10), 771-3.

Magnetotransport in a quasi-one-dimensional electron system on superfluid helium. — B. A. Nikolaenko, Yu. Z. Kovdrya, and S. P. Gladchenko; **28** (11), 859-63.

72.15.Q Scattering mechanisms and Kondo effect

Point-contact studies of the Kondo size effect in the alloys CuMn, CuCr, and AuFe in a magnetic field. — V. V. Fisun, I. K. Yanson, J. M. van Ruitenbeek, and J. A. Mydosh; **28** (2), 123-7.

72.20 Conductivity phenomena in semiconductors and insulators

72.20.E Mobility edges; hopping transport

Role of paramagnetic ions in the formation of the low-temperature current through a molecular wire. — É. G. Petrov; **28** (8), 630-8.

72.20.F Low-field transport and mobility; piezoresistance

Elastic-strain mechanisms for the influence of temperature, magnetic field, and pressure on the resistive and magnetic properties of magnetic semiconductors. — P. I. Polyakov and S. S. Kucherenko; **28** (10), 744-8.

72.20.J Charge carriers: generation, recombination, lifetime, and trapping

Low-temperature inversion of the magnetoresistance in charge-ordered layered superstructures. — P. V. Gorskyi; **28** (10), 767-70.

72.20.M Galvanomagnetic and other magnetotransport effects

Galvanomagnetic effects in the normal state of high-T_c metal oxides in a model two-band superconductor with a narrow band (level) near the Fermi boundary. — V. P. Galaĭko and E. N. Bratus'; **28** (5), 321-7.

Role of paramagnetic ions in the formation of the low-temperature current through a molecular wire. — É. G. Petrov; **28** (8), 630-8.

Low-temperature inversion of the magnetoresistance in charge-ordered layered superstructures. — P. V. Gorskyi; **28** (10), 767-70.

72.30 High-frequency effects; plasma effects

Point-contact studies of the Kondo size effect in the alloys CuMn, CuCr, and AuFe in a magnetic field. — V. V. Fisun, I. K. Yanson, J. M. van Ruitenbeek, and J. A. Mydosh; **28** (2), 123-7.

72.50 Acoustoelectric effects

Characteristics of the electric field accompanying a longitudinal acoustic wave in a metal. Anomaly in the superconducting phase. — Yu. A. Avramenko, E. V. Bezuglyi, N. G. Burma, I. G. Kolobov, V. D. Fil', O. A. Shevchenko, and V. M. Gokhfeld; **28** (5), 328-36.

73. Electronic structure and electrical properties of surfaces, interfaces, thin films, and low-dimensional structures

73.20 Electron states at surfaces and interfaces

73.20.F Weak or Anderson localization

Magnetotransport in a quasi-one-dimensional electron system on superfluid helium. — B. A. Nikolaenko, Yu. Z. Kovdrya, and S. P. Gladchenko; **28** (11), 859-63.

73.20.M Collective excitations (including excitons, polarons, plasmons and other charge-density excitations)

Electromagnetic surface waves in layered conductors. — V. M. Gokhfeld; **28** (3), 215-9.

73.21 Electron states and collective excitations in multilayers, quantum wells, mesoscopic, and nanoscale systems (for electron states in nanoscale materials, see 73.22.-f)

73.21.H Quantum wires

Electronic excitations and correlations in quantum bars. — I. Kuzmenko, S. Gredeskul, K. Kikoin, and Y. Avishai; **28** (7), 539-46.

73.23 Electronic transport in mesoscopic systems

73.23.A Ballistic transport

Influence of dissipation on a low-voltage dc current in a long SNS junction. — S. I. Kulinich and R. I. Shekhter; **28** (7), 547-50.

73.23.H Coulomb blockade; single-electron tunneling

Manifestation of Coulomb blockade effects at an arbitrary degeneracy of the levels of a molecular contact. — Yu. O. Klymenko; **28** (6), 395-402.

Role of paramagnetic ions in the formation of the low-temperature current through a molecular wire. — É. G. Petrov; **28** (8), 630-8.

73.40 Electronic transport in interface structures

73.40.G Tunneling

Role of paramagnetic ions in the formation of the low-temperature current through a molecular wire. — É. G. Petrov; **28** (8), 630-8.

73.40.N Metal–nonmetal contacts

Inelastic electron tunneling across magnetically active interfaces in cuprate and manganite heterostructures modified by electromigration processes. — M. A. Belogolovskiĭ, Yu. F. Revenko, A. Yu. Gerasimenko, V. M. Svistunov, E. Hatta, G. Plitnik, V. E. Shaternik, and E. M. Rudenko; **28** (6), 391-4.

Manifestation of Coulomb blockade effects at an arbitrary degeneracy of the levels of a molecular contact. — Yu. O. Klymenko; **28** (6), 395-402.

73.50 Electronic transport phenomena in thin films

73.50.J Galvanomagnetic and other magnetotransport effects (including thermomagnetic effects)

Low-frequency quantum oscillations of the impedance of layered conductors at high magnetic field. — O. V. Kirichenko and I. V. Kozlov; **28** (5), 359-64.

73.50.M High-frequency effects; plasma effects

Electromagnetic surface waves in layered conductors. — V. M. Gokhfeld; **28** (3), 215-9.

73.61 Electrical properties of specific thin films

73.61.A Metal and metallic alloys

Aging effect on the magnetic and transport properties of laser-deposited $La_{0.5}Sr_{0.5}CoO_{3-\delta}$ films. — V. G. Prokhorov, G. G. Kaminskiĭ, V. M. Ishchuk, I. N. Chukanova, Y. P. Lee, and K. W. Kim; **28** (5), 354-8.

73.61.P Polymers; organic compounds

Low-frequency quantum oscillations of the impedance of layered conductors at high magnetic field. — O. V. Kirichenko and I. V. Kozlov; **28** (5), 359-64.

73.63 Electronic transport in mesoscopic or nanoscale materials and structures

Magnetotransport in a quasi-one-dimensional electron system on superfluid helium. — B. A. Nikolaenko, Yu. Z. Kovdrya, and S. P. Gladchenko; **28** (11), 859-63.

74. Superconductivity

74.10 Occurrence, potential candidates

On the criteria for superconductivity in $PrBa_2Cu_3O_{6.6}$. — F. A. Boyko, G. V. Bukin, V. A. Voloshin, and A. A. Gusev; **28** (2), 95-8.

Key role of intramolecular Jahn–Teller vibrations and multivalley nature of the band spectrum in the mechanism of superconductivity in doped C_{60} fullerites. — V. M. Loktev, É. A. Pashitskiĭ, R. Shekhter, and M. Jonson; **28** (11), 821-9.

74.20 Theories and models of superconducting state

74.20.D Phenomenological theories (two-fluid, Ginzburg-Landau, etc.)

Flux-line pinning by columnar magnetic defects in a type-II superconductor. — S. A. Krivenko and N. M. Suleĭmanov; **28** (4), 247-9.

74.20.F BCS theory and its development

Direct evidence for the occurrence of superconductivity in the magnetic compound YFe_4Al_8. — V. M. Dmitriev, L. F. Rybaltchenko, P. Wyder, A. G. M. Jansen, N. N. Prentslau, and W. Suski; **28** (4), 260-2.

Heat capacity of mesoscopically disordered superconductors: implications for MgB_2. — A. M. Gabovich, A. I. Voitenko, Mai Suan Li, and H. Szymczak; **28** (11), 803-11.

74.20.M Nonconventional mechanisms (spin fluctuations, polarons and bipolarons, resonating valence bond model, anyon mechanism, marginal Fermi liquid, Luttinger liquid, etc.)

Superconductivity in impurity systems with a lower density of charge carriers and with strong electron correlations. — M. E. Palistrant; **28** (2), 109-16.

74.20.R Pairing symmetries (other than s-wave)

Fluctuation conductivity in Y–Ba–Cu–O films with artificially produced defects. — A. L. Solovjov; **28** (11), 812-20.

74.25 General properties; correlations between physical properties in normal and superconducting states

74.25.B Thermodynamic properties

Josephson effect in point contacts between ''*f*-wave'' superconductors. — R. Mahmoodi, S. N. Shevchenko, and Yu. A. Kolesnichenko; **28** (3), 184-9.

Steady state diagram of current-carrying layered superconductors. — A. N. Artemov and Yu. V. Medvedev; **28** (4), 242-6.

Anomalies of the electronic heat capacity of thulium cuprates in the pseudogap phase region. — E. B. Amitin, K. R. Zhdanov, M. Yu. Kameneva, Yu. A. Kovalevskaya, L. P. Kozeeva, I. E. Paukov, and A. G. Blinov; **28** (8), 669-73.

Heat capacity of mesoscopically disordered superconductors: implications for MgB_2. — A. M. Gabovich, A. I. Voitenko, Mai Suan Li, and H. Szymczak; **28** (11), 803-11.

74.25.D Superconductivity phase diagrams

Steady state diagram of current-carrying layered superconductors. — A. N. Artemov and Yu. V. Medvedev; **28** (4), 242-6.

74.25.F Transport properties (electric and thermal conductivity, thermoelectric effects, etc.)

Fluctuation conductivity in $YBa_2Cu_3O_{7-y}$ films with different oxygen content. I. Optimally and lightly doped YBCO films. — A. L. Solovjov, H.-U. Habermeier, and T. Haage; **28** (1), 17-24.

Galvanomagnetic effects in the normal state of high-T_c metal oxides in a model two-band superconductor with a narrow band (level) near the Fermi boundary. — V. P. Galaĭko and E. N. Bratus'; **28** (5), 321-7.

Excitation of oscillations of the magnetic induction in a Nb–Ti slab as a result of a thermomagnetic flux avalanche. — V. V. Chabanenko, V. F. Rusakov, V. A. Yampol'skiĭ, H. Szymczak, S. Piechota, S. Vasiliev, and A. Nabialek; **28** (6), 387-90.

Low-temperature electric conductivity of $Yba_2Cu_3O_{7-\delta}$ ceramic high-T_c superconductors with different oxygen concentrations. — V. A. Finkel; **28** (8), 687-90.

Guided vortex motion in faceted niobium films. — A. K. Soroka and M. Huth; **28** (11), 842-4.

74.25.G Optical properties

Optical study of $4f$ excitations in rare earth cuprates. — V. Nekvasil; **28** (7), 528-32.

74.25.H Magnetic properties

Irreversible magnetostriction and magnetization of superconducting 2*H*-$NbSe_2$ single crystals in a peak-effect regime. — V. V. Eremenko, V. A. Sirenko, Yu. A. Shabakayeva, R. Schleser, and P. L. Gammel; **28** (1), 6-10.

Flux-line pinning by columnar magnetic defects in a type-II superconductor. — S. A. Krivenko and N. M. Suleĭmanov; **28** (4), 247-9.

Reinforcement of pinning by surface magnetic microparticles in high-T_c superconductors. — P. N. Togulev, V. V. Bazarov, I. B. Khaĭbullin, and N. M. Suleĭmanov; **28** (4), 250-3.

Manifestation of two-dimensional behavior of YBCO films in a study of their complex susceptibility. — A. V. Khokhlov, A. Yu. Prokhorov, V. F. Drobotko, G. G. Levchenko, and A. V. Klimov; **28** (6), 377-82.

On the transverse magnetization of the anisotropic superconductor 2*H*–$NbSe_2$. — V. A. Sirenko, N. I. Makedonska, Yu. A. Shabakayeva, and R. Schleser; **28** (7), 574-8.

Magnetic polarons in Y–Ba–Cu–O chains. — V. V. Eremenko, D. V. Lukashev, and B. L. Ponomarchuk; **28** (11), 830-41.

74.25.J Electronic structure

Superconductivity in impurity systems with a lower density of charge carriers and with strong electron correlations. — M. E. Palistrant; **28** (2), 109-16.

Galvanomagnetic effects in the normal state of high-T_c metal oxides in a model two-band superconductor with a narrow band (level) near the Fermi boundary. — V. P. Galaĭko and E. N. Bratus'; **28** (5), 321-7.

Optical study of $4f$ excitations in rare earth cuprates. — V. Nekvasil; **28** (7), 528-32.
Anomalies of the electronic heat capacity of thulium cuprates in the pseudogap phase region. — E. B. Amitin, K. R. Zhdanov, M. Yu. Kameneva, Yu. A. Kovalevskaya, L. P. Kozeeva, I. E. Paukov, and A. G. Blinov; **28** (8), 669-73.
Heat capacity of mesoscopically disordered superconductors: implications for MgB_2. — A. M. Gabovich, A. I. Voitenko, Mai Suan Li, and H. Szymczak; **28** (11), 803-11.
Fluctuation conductivity in Y–Ba–Cu–O films with artificially produced defects. — A. L. Solovjov; **28** (11), 812-20.
Key role of intramolecular Jahn–Teller vibrations and multivalley nature of the band spectrum in the mechanism of superconductivity in doped C_{60} fullerites. — V. M. Loktev, É. A. Pashitskiĭ, R. Shekhter, and M. Jonson; **28** (11), 821-9.
Magnetic polarons in Y–Ba–Cu–O chains. — V. V. Eremenko, D. V. Lukashev, and B. L. Ponomarchuk; **28** (11), 830-41.

74.25.K Phonons

Key role of intramolecular Jahn–Teller vibrations and multivalley nature of the band spectrum in the mechanism of superconductivity in doped C_{60} fullerites. — V. M. Loktev, É. A. Pashitskiĭ, R. Shekhter, and M. Jonson; **28** (11), 821-9.

74.25.L Mechanical and acoustical properties, elasticity, and ultrasonic attenuation

MgB_2: Synthesis, sound velocity, and dynamics of the vortex phase. — T. V. Ignatova, G. A. Zvyagina, I. G. Kolobov, E. A. Masalitin, V. D. Fil', Yu. V. Paderno, A. N. Bykov, V. N. Paderno, and V. I. Lyashenko; **28** (3), 190-3.
Characteristics of the electric field accompanying a longitudinal acoustic wave in a metal. Anomaly in the superconducting phase. — Yu. A. Avramenko, E. V. Bezuglyi, N. G. Burma, I. G. Kolobov, V. D. Fil', O. A. Shevchenko, and V. M. Gokhfeld; **28** (5), 328-36.

74.25.N Response to electromagnetic fields (nuclear magnetic resonance, surface impedance, etc.)

Reinforcement of pinning by surface magnetic microparticles in high-T_c superconductors. — P. N. Togulev, V. V. Bazarov, I. B. Khaĭbullin, and N. M. Suleĭmanov; **28** (4), 250-3.
Magnetic polarons in Y–Ba–Cu–O chains. — V. V. Eremenko, D. V. Lukashev, and B. L. Ponomarchuk; **28** (11), 830-41.

74.40 Fluctuations (noise, chaos, nonequilibrium superconductivity, localization, etc.)

Fluctuation conductivity in $YBa_2Cu_3O_{7-y}$ films with different oxygen content. I. Optimally and lightly doped YBCO films. — A. L. Solovjov, H.-U. Habermeier, and T. Haage; **28** (1), 17-24.
Fluctuation conductivity in $YBa_2Cu_3O_{7-y}$ films with different oxygen content. II. YBCO films with $T_c \approx 80$ K. — A. L. Solovjov, H.-U. Habermeier, and T. Haage; **28** (2), 99-108.
Manifestation of two-dimensional behavior of YBCO films in a study of their complex susceptibility. — A. V. Khokhlov, A. Yu. Prokhorov, V. F. Drobotko, G. G. Levchenko, and A. V. Klimov; **28** (6), 377-82.
Observation of stochastic resonance in percolative Josephson media. — A. M. Glukhov, A. G. Sivakov, and A. V. Ustinov; **28** (6), 383-6.
Excitation of oscillations of the magnetic induction in a Nb–Ti slab as a result of a thermomagnetic flux avalanche. — V. V. Chabanenko, V. F. Rusakov, V. A. Yampol'skiĭ, H. Szymczak, S. Piechota, S. Vasiliev, and A. Nabialek; **28** (6), 387-90.
Anomalies of the electronic heat capacity of thulium cuprates in the pseudogap phase region. — E. B. Amitin, K. R. Zhdanov, M. Yu. Kameneva, Yu. A. Kovalevskaya, L. P. Kozeeva, I. E. Paukov, and A. G. Blinov; **28** (8), 669-73.
Fluctuation conductivity in Y–Ba–Cu–O films with artificially produced defects. — A. L. Solovjov; **28** (11), 812-20.

74.50 Proximity effects, weak links, tunneling phenomena, and Josephson effects

Temperature-dependent resistance of a finite one-dimensional Josephson junction array. — K. Engström and J. M. Kinaret; **28** (1), 1-5.
Josephson effect in point contacts between ''*f*-wave'' superconductors. — R. Mahmoodi, S. N. Shevchenko, and Yu. A. Kolesnichenko; **28** (3), 184-9.
Direct evidence for the occurrence of superconductivity in the magnetic compound YFe_4Al_8. — V. M. Dmitriev, L. F. Rybaltchenko, P. Wyder, A. G. M. Jansen, N. N. Prentslau, and W. Suski; **28** (4), 260-2.
Observation of stochastic resonance in percolative Josephson media. — A. M. Glukhov, A. G. Sivakov, and A. V. Ustinov; **28** (6), 383-6.
Inelastic electron tunneling across magnetically active interfaces in cuprate and manganite heterostructures modified by electromigration processes. — M. A. Belogolovskiĭ, Yu. F. Revenko, A. Yu. Gerasimenko, V. M. Svistunov, E. Hatta, G. Plitnik, V. E. Shaternik, and E. M. Rudenko; **28** (6), 391-4.
Influence of dissipation on a low-voltage dc current in a long SNS junction. — S. I. Kulinich and R. I. Shekhter; **28** (7), 547-50.
Low-temperature electric conductivity of $Yba_2Cu_3O_{7-\delta}$ ceramic high-T_c superconductors with different oxygen concentrations. — V. A. Finkel; **28** (8), 687-90.

74.60 Type-II superconductivity

74.60.E Mixed state, critical fields, and surface sheath

Temperature-dependent resistance of a finite one-dimensional Josephson junction array. — K. Engström and J. M. Kinaret; **28** (1), 1-5.
Irreversible magnetostriction and magnetization of superconducting 2*H*-$NbSe_2$ single crystals in a peak-effect regime. — V. V. Eremenko, V. A. Sirenko, Yu. A. Shabakayeva, R. Schleser, and P. L. Gammel; **28** (1), 6-10.
Excitation of oscillations of the magnetic induction in a Nb–Ti slab as a result of a thermomagnetic flux avalanche. — V. V. Chabanenko, V. F. Rusakov, V. A. Yampol'skiĭ, H. Szymczak, S. Piechota, S. Vasiliev, and A. Nabialek; **28** (6), 387-90.
On the transverse magnetization of the anisotropic superconductor $2H$–$NbSe_2$. — V. A. Sirenko, N. I. Makedonska, Yu. A. Shabakayeva, and R. Schleser; **28** (7), 574-8.

74.60.G Flux pinning, flux creep, and flux-line lattice dynamics

Pinning of Abrikosov vortices on dislocations and the critical current in high-temperature superconductors. — É. A. Pashitskiĭ and V. I. Vakaryuk; **28** (1), 11-6.
Magnetic-field and temperature dependence of the critical current in thin epitaxial films of the high-temperature superconductor $YBa_2Cu_3O_{7-\delta}$. — Yu. V. Fedotov, S. M. Ryabchenko, É. A. Pashitskiĭ, A. V. Semenov, V. I. Vakaryuk, V. M. Pan, and V. S. Flis; **28** (3), 172-83.
MgB_2: Synthesis, sound velocity, and dynamics of the vortex phase. — T. V. Ignatova, G. A. Zvyagina, I. G. Kolobov, E. A. Masalitin, V. D. Fil', Yu. V. Paderno, A. N. Bykov, V. N. Paderno, and V. I. Lyashenko; **28** (3), 190-3.
Flux-line pinning by columnar magnetic defects in a type-II superconductor. — S. A. Krivenko and N. M. Suleĭmanov; **28** (4), 247-9.
Reinforcement of pinning by surface magnetic microparticles in high-T_c superconductors. — P. N. Togulev, V. V. Bazarov, I. B. Khaĭbullin, and N. M. Suleĭmanov; **28** (4), 250-3.
Anisotropy of the critical current and the guided motion of vortices in a stochastic model of bianisotropic pinning. I. Theoretical model. — V. A. Shklovskij and A. A. Soroka; **28** (4), 254-9.
Anisotropy of the critical current and the guided motion of vortices in a stochastic model of bianisotropic pinning. II. Observed effects. — V. A. Shklovskij and A. A. Soroka; **28** (5), 312-20.

74.60.J Critical currents

Pinning of Abrikosov vortices on dislocations and the critical current in high-temperature superconductors. — E. A. Pashitskiĭ and V. I. Vakaryuk; **28** (1), 11-6.
Magnetic-field and temperature dependence of the critical current in thin epitaxial films of the high-temperature superconductor $YBa_2Cu_3O_{7-\delta}$. — Yu. V. Fedotov, S. M. Ryabchenko, É. A. Pashitskiĭ, A. V. Semenov, V. I. Vakaryuk, V. M. Pan, and V. S. Flis; **28** (3), 172-83.
Anisotropy of the critical current and the guided motion of vortices in a stochastic model of bianisotropic pinning. I. Theoretical model. — V. A. Shklovskij and A. A. Soroka; **28** (4), 254-9.

Anisotropy of the critical current and the guided motion of vortices in a stochastic model of bianisotropic pinning. II. Observed effects. — V. A. Shklovskij and A. A. Soroka; **28** (5), 312-20.
Low-dose radiation effects in thin films of high-temperature superconducting $YBa_2Cu_3O_{7-x}$ irradiated by 1-MeV electrons. — Yu. V. Fedotov, B. A. Danilchenko, and I. S. Rogutskiĭ; **28** (10), 739-43.

74.62 Transition temperature variations

74.62.B Effects of material synthesis, crystal structure, and chemical composition

Fluctuation conductivity in $YBa_2Cu_3O_{7-y}$ films with different oxygen content. II. YBCO films with $T_c \approx 80$ K. — A. L. Solovjov, H.-U. Habermeier, and T. Haage; **28** (2), 99-108.

74.62.D Effects of crystal defects, doping and substitution

Reinforcement of pinning by surface magnetic microparticles in high-T_c superconductors. — P. N. Togulev, V. V. Bazarov, I. B. Khaĭbullin, and N. M. Suleĭmanov; **28** (4), 250-3.
Low-dose radiation effects in thin films of high-temperature superconducting $YBa_2Cu_3O_{7-x}$ irradiated by 1-MeV electrons. — Yu. V. Fedotov, B. A. Danilchenko, and I. S. Rogutskiĭ; **28** (10), 739-43.

74.62.F Pressure effects

On the criteria for superconductivity in $PrBa_2Cu_3O_{6.6}$. — F. A. Boyko, G. V. Bukin, V. A. Voloshin, and A. A. Gusev; **28** (2), 95-8.

74.62.Y Other effects

Characteristics of the electric field accompanying a longitudinal acoustic wave in a metal. Anomaly in the superconducting phase. — Yu. A. Avramenko, E. V. Bezuglyi, N. G. Burma, I. G. Kolobov, V. D. Fil', O. A. Shevchenko, and V. M. Gokhfeld; **28** (5), 328-36.

74.70 Superconducting materials (excluding high-T_c compounds)

74.70.A Metals; alloys and binary compounds (including A15, Laves phases, etc.)

MgB_2: Synthesis, sound velocity, and dynamics of the vortex phase. — T. V. Ignatova, G. A. Zvyagina, I. G. Kolobov, E. A. Masalitin, V. D. Fil', Yu. V. Paderno, A. N. Bykov, V. N. Paderno, and V. I. Lyashenko; **28** (3), 190-3.
Observation of stochastic resonance in percolative Josephson media. — A. M. Glukhov, A. G. Sivakov, and A. V. Ustinov; **28** (6), 383-6.
Excitation of oscillations of the magnetic induction in a Nb–Ti slab as a result of a thermomagnetic flux avalanche. — V. V. Chabanenko, V. F. Rusakov, V. A. Yampol'skiĭ, H. Szymczak, S. Piechota, S. Vasiliev, and A. Nabialek; **28** (6), 387-90.
On the transverse magnetization of the anisotropic superconductor $2H$–$NbSe_2$. — V. A. Sirenko, N. I. Makedonska, Yu. A. Shabakayeva, and R. Schleser; **28** (7), 574-8.
Heat capacity of mesoscopically disordered superconductors: implications for MgB_2. — A. M. Gabovich, A. I. Voitenko, Mai Suan Li, and H. Szymczak; **28** (11), 803-11.
Guided vortex motion in faceted niobium films. — A. K. Soroka and M. Huth; **28** (11), 842-4.

74.70.D Ternary, quaternary and multinary compounds (including Chevrel phases, borocarbides etc.)

Direct evidence for the occurrence of superconductivity in the magnetic compound YFe_4Al_8. — V. M. Dmitriev, L. F. Rybaltchenko, P. Wyder, A. G. M. Jansen, N. N. Prentslau, and W. Suski; **28** (4), 260-2.

74.70.W Fullerenes and related materials

On the role of Jahn–Teller vibrations in the mechanism of high-T_c superconductivity of intercalated C_{60} fullerite films with p-type conductivity. — V. M. Loktev and É. A. Pashitskiĭ; **28** (4), 295-7.
Key role of intramolecular Jahn–Teller vibrations and multivalley nature of the band spectrum in the mechanism of superconductivity in doped C_{60} fullerites. — V. M. Loktev, É. A. Pashitskiĭ, R. Shekhter, and M. Jonson; **28** (11), 821-9.

74.72 High-T_c compounds

Irreversible magnetostriction and magnetization of superconducting $2H$-$NbSe_2$ single crystals in a peak-effect regime. — V. V. Eremenko, V. A. Sirenko, Yu. A. Shabakayeva, R. Schleser, and P. L. Gammel; **28** (1), 6-10.
Pinning of Abrikosov vortices on dislocations and the critical current in high-temperature superconductors. — É. A. Pashitskiĭ and V. I. Vakaryuk; **28** (1), 11-6.
Superconductivity in impurity systems with a lower density of charge carriers and with strong electron correlations. — M. E. Palistrant; **28** (2), 109-16.
XIV international seminar on high-temperature superconductivity and school of applied superconductivity (Kurchatovets vacation base, Protvino, Russia, May 28–31, 2001). — M. A. Belogolovskiĭ, S. I. Bondarenko, and L. S. Shirshov; **28** (2), 143-5.

74.72.B Y-based cuprates

Fluctuation conductivity in $YBa_2Cu_3O_{7-y}$ films with different oxygen content. I. Optimally and lightly doped YBCO films. — A. L. Solovjov, H.-U. Habermeier, and T. Haage; **28** (1), 17-24.
Fluctuation conductivity in $YBa_2Cu_3O_{7-y}$ films with different oxygen content. II. YBCO films with $T_c \approx 80$ K. — A. L. Solovjov, H.-U. Habermeier, and T. Haage; **28** (2), 99-108.
Magnetic-field and temperature dependence of the critical current in thin epitaxial films of the high-temperature superconductor $YBa_2Cu_3O_{7-\delta}$. — Yu. V. Fedotov, S. M. Ryabchenko, É. A. Pashitskiĭ, A. V. Semenov, V. I. Vakaryuk, V. M. Pan, and V. S. Flis; **28** (3), 172-83.
Galvanomagnetic effects in the normal state of high-T_c metal oxides in a model two-band superconductor with a narrow band (level) near the Fermi boundary. — V. P. Galaĭko and E. N. Bratus'; **28** (5), 321-7.
Manifestation of two-dimensional behavior of YBCO films in a study of their complex susceptibility. — A. V. Khokhlov, A. Yu. Prokhorov, V. F. Drobotko, G. G. Levchenko, and A. V. Klimov; **28** (6), 377-82.
Optical spectroscopy of antiferromagnetic correlations and the stripe state in the superconductor $YBa_2Cu_3O_{6+x}$. — V. N. Samovarov, V. L. Vakula, M. Yu. Libin, S. A. Uyutnov, and G. G. Sergeeva; **28** (8), 674-86.
Low-temperature electric conductivity of $Yba_2Cu_3O_{7-\delta}$ ceramic high-T_c superconductors with different oxygen concentrations. — V. A. Finkel; **28** (8), 687-90.
Low-dose radiation effects in thin films of high-temperature superconducting $YBa_2Cu_3O_{7-x}$ irradiated by 1-MeV electrons. — Yu. V. Fedotov, B. A. Danilchenko, and I. S. Rogutskiĭ; **28** (10), 739-43.
Fluctuation conductivity in Y–Ba–Cu–O films with artificially produced defects. — A. L. Solovjov; **28** (11), 812-20.
Magnetic polarons in Y–Ba–Cu–O chains. — V. V. Eremenko, D. V. Lukashev, and B. L. Ponomarchuk; **28** (11), 830-41.

74.72.J Other cuprates

On the criteria for superconductivity in $PrBa_2Cu_3O_{6.6}$. — F. A. Boyko, G. V. Bukin, V. A. Voloshin, and A. A. Gusev; **28** (2), 95-8.
Optical study of $4f$ excitations in rare earth cuprates. — V. Nekvasil; **28** (7), 528-32.
Anomalies of the electronic heat capacity of thulium cuprates in the pseudogap phase region. — E. B. Amitin, K. R. Zhdanov, M. Yu. Kameneva, Yu. A. Kovalevskaya, L. P. Kozeeva, I. E. Paukov, and A. G. Blinov; **28** (8), 669-73.

74.76 Superconducting films

74.76.B High-T_c films

Pinning of Abrikosov vortices on dislocations and the critical current in high-temperature superconductors. — É. A. Pashitskiĭ and V. I. Vakaryuk; **28** (1), 11-6.
Fluctuation conductivity in $YBa_2Cu_3O_{7-y}$ films with different oxygen content. I. Optimally and lightly doped YBCO films. — A. L. Solovjov, H.-U. Habermeier, and T. Haage; **28** (1), 17-24.
Fluctuation conductivity in $YBa_2Cu_3O_{7-y}$ films with different oxygen content. II. YBCO films with $T_c \approx 80$ K. — A. L. Solovjov, H.-U. Habermeier, and T. Haage; **28** (2), 99-108.

Magnetic-field and temperature dependence of the critical current in thin epitaxial films of the high-temperature superconductor $YBa_2Cu_3O_{7-\delta}$. — Yu. V. Fedotov, S. M. Ryabchenko, É. A. Pashitskiĭ, A. V. Semenov, V. I. Vakaryuk, V. M. Pan, and V. S. Flis; **28** (3), 172-83.

Steady state diagram of current-carrying layered superconductors. — A. N. Artemov and Yu. V. Medvedev; **28** (4), 242-6.

Anisotropy of the critical current and the guided motion of vortices in a stochastic model of bianisotropic pinning. I. Theoretical model. — V. A. Shklovskij and A. A. Soroka; **28** (4), 254-9.

On the role of Jahn–Teller vibrations in the mechanism of high-T_c superconductivity of intercalated C_{60} fullerite films with *p*-type conductivity. — V. M. Loktev and É. A. Pashitskiĭ; **28** (4), 295-7.

Manifestation of two-dimensional behavior of YBCO films in a study of their complex susceptibility. — A. V. Khokhlov, A. Yu. Prokhorov, V. F. Drobotko, G. G. Levchenko, and A. V. Klimov; **28** (6), 377-82.

Optical spectroscopy of antiferromagnetic correlations and the stripe state in the superconductor $YBa_2Cu_3O_{6+x}$. — V. N. Samovarov, V. L. Vakula, M. Yu. Libin, S. A. Uyutnov, and G. G. Sergeeva; **28** (8), 674-86.

74.76.D Conventional superconducting films

Observation of stochastic resonance in percolative Josephson media. — A. M. Glukhov, A. G. Sivakov, and A. V. Ustinov; **28** (6), 383-6.

74.80 Spatially inhomogeneous structures

74.80.D Superconducting layer structures: superlattices, heterojunctions, and multilayers

Steady state diagram of current-carrying layered superconductors. — A. N. Artemov and Yu. V. Medvedev; **28** (4), 242-6.

74.80.F Point contacts; SN and SNS junctions

Josephson effect in point contacts between ''*f*-wave'' superconductors. — R. Mahmoodi, S. N. Shevchenko, and Yu. A. Kolesnichenko; **28** (3), 184-9.

Direct evidence for the occurrence of superconductivity in the magnetic compound YFe_4Al_8. — V. M. Dmitriev, L. F. Rybaltchenko, P. Wyder, A. G. M. Jansen, N. N. Prentslau, and W. Suski; **28** (4), 260-2.

75. Magnetic properties and materials

75.10 General theory and models of magnetic ordering

75.10.D Crystal-field theory and spin Hamiltonians

On the non-Heisenberg contribution to the spin–spin interaction of an antiferromagnet with $S = 3/2$. — V. M. Kalita and A. F. Lozenko; **28** (1), 66-8.

Mechanism for the changes with temperature of the EPR spectrum of the Fe^{3+} ion in polycrystalline materials containing complexes with a multiwell potential. — V. N. Vasyukov; **28** (3), 199-202.

Effects of chaotic local crystal fields in pseudobinary rare-earth intermetallides. — A. S. Ermolenko; **28** (10), 749-54.

Magnetic field induced phase transition in $KEr(MoO_4)_2$. Vibronic model. — A. A. Loginov; **28** (10), 755-61.

75.10.H Classical spin models

Resonance properties of the quasi-one-dimensional Ising magnet $[(CH_3)_3NH]CoCl_3 \cdot 2H_2O$ in the paramagnetic and magnetically ordered phases. — M. I. Kobets, E. N. Khatsko, V. A. Pashchenko, A. S. Chernyi, K. G. Dergachev, and V. G. Borisenko; **28** (12), 889-95.

75.10.J Quantized spin models

Specific heat study of magnetic excitations in a one-dimensional $S = 1$ Heisenberg magnet with strong planar anisotropy. — A. Feher, M. Orendáč, A. Orendáčová, and E. Čižmár; **28** (7), 551-5.

75.10.L Band and itinerant models

Metallic ferromagnetism in a generalized Hubbard model. — L. Didukh and O. Kramar; **28** (1), 30-6.

Electronic structure and magneto-optical Kerr effect in the compound $UCuP_2$. — O. Horpynyuk, V. V. Nemoshkalenko, V. N. Antonov, B. N. Harmon, and A. N. Yaresko; **28** (7), 533-8.

Specific heat study of magnetic excitations in a one-dimensional $S = 1$ Heisenberg magnet with strong planar anisotropy. — A. Feher, M. Orendáč, A. Orendáčová, and E. Čižmár; **28** (7), 551-5.

75.20 Diamagnetism, paramagnetism, and superparamagnetism

75.20.C Nonmetals

Resonance properties of the quasi-one-dimensional Ising magnet $[(CH_3)_3NH]CoCl_3 \cdot 2H_2O$ in the paramagnetic and magnetically ordered phases. — M. I. Kobets, E. N. Khatsko, V. A. Pashchenko, A. S. Chernyi, K. G. Dergachev, and V. G. Borisenko; **28** (12), 889-95.

75.20.H Local moment in compounds and alloys; Kondo effect, valence fluctuations, heavy fermions

Influence of Cr concentration on the structural and magnetic properties of the diluted magnetic semiconductor $Hg_{1-x}Cr_xSe$. — V. D. Prozorovskiĭ, I. Yu. Reshidova, A. I. Puzynya, S. Yu. Paranchych, and V. R. Romanyuk; **28** (12), 880-2.

Non-Fermi-liquid behavior: Exact results for ensembles of magnetic impurities. — A. A. Zvyagin; **28** (12), 907-20.

75.25 Spin arrangements in magnetically ordered materials (including neutron and spin-polarized electron studies, synchrotron-source x-ray scattering, etc.)

Features of the magnetization of an antiferromagnet with single-ion anisotropy of the easy-plane type and with ion spins $S = 1$. — V. M. Kalita, I. M. Ivanova, and V. M. Loktev; **28** (6), 475-7.

Recent progress in magneto-optics and research on its application (Review). — N. Kojima and K. Tsushima; **28** (7), 480-90.

Magnetic properties of copper metaborate CuB_2O_4. — G. A. Petrakovskiĭ, A. I. Pankrats, M. A. Popov, A. D. Balaev, D. A. Velikanov, A. M. Vorotynov, K. A. Sablina, B. Roessli, J. Schefer, A. Amato, U. Staub, M. Boehm, and B. Ouladdiaf; **28** (8), 606-12.

Noncollinear magnetic structures in an Fe/Si/Fe film with a ferromagnetic interlayer exchange interaction. — A. B. Chizhik, S. L. Gnatchenko, M. Baran, K. Fronc, R. Szymczak, and R. Zuberek; **28** (8), 639-41.

Features of the magnetic properties of rare-earth intermetallides RMn_2Ge_2 (Review). — N. P. Kolmakova, A. A. Sidorenko, and R. Z. Levitin; **28** (8), 653-68.

75.30 Intrinsic properties of magnetically ordered materials

75.30.C Saturation moments and magnetic susceptibilities

On the magnetic anisotropy of La_2CuO_4 above the Néel temperature. — V. M. Loktev; **28** (1), 69-71.

Insulating Van Vleck paramagnets at high magnetic fields (Review). — M. S. Tagirov and D. A. Tayurskiĭ; **28** (3), 147-64.

Features of the magnetic behavior of $Mn_{2-x}Cr_xSb$ alloys in the low-temperature state. — V. I. Val'kov, V. I. Kamenev, S. A. Buzhinsky, and N. A. Romanova; **28** (3), 194-8.

Magnetic properties of a lead-doped BKBO single crystal. — S. N. Barilo, V. I. Gatal'skaya, S. V. Shiryaev, T. V. Smirnova, H. Szymczak, R. Szymczak, and M. Baran; **28** (5), 349-53.

Purely antiferromagnetic spin waves (antimagnons) in tetragonal magnets and ways of exciting them. — E. A. Turov and I. F. Mirsaev; **28** (8), 592-600.

Nonmonotonic temperature dependence of the spontaneous magnetization of the antiferromagnetic crystal $LiCoPO_4$. — N. F. Kharchenko, V. A. Desnenko, Yu. N. Kharchenko, R. Szymczak, and M. Baran; **28** (8), 646-52.

Magnetic phases in $La_{0.66}Ba_{0.34}MnO_3$: effects of temperature and elastic strains. — A. B. Beznosov, V. V. Eremenko, E. L. Fertman, V. A. Desnenko, and D. D. Khalyavin; **28** (10), 762-6.

75.30.D Spin waves

Raman scattering in a $LiNiPO_4$ single crystal. — V. I. Fomin, V. P. Gnezdilov, V. S. Kurnosov, A. V. Peschanskii, A. V. Yeremenko, H. Schmid, J.-P. Rivera, and S. Gentil; **28** (3), 203-9.
Recent progress in magneto-optics and research on its application (Review). — N. Kojima and K. Tsushima; **28** (7), 480-90.
Elementary excitations in solid oxygen (Review). — Yu. A. Freiman and H. J. Jodl; **28** (7), 491-504.
Purely antiferromagnetic spin waves (antimagnons) in tetragonal magnets and ways of exciting them. — E. A. Turov and I. F. Mirsaev; **28** (8), 592-600.

75.30.E Exchange and superexchange interactions

Inhomogeneous states for small magnetic particles with exchange anisotropy. — B. A. Ivanov, A. Ya. Volk, and A. Yu. Merkulov; **28** (1), 25-9.
Metallic ferromagnetism in a generalized Hubbard model. — L. Didukh and O. Kramar; **28** (1), 30-6.
Magnetic phase diagram of the system of manganites $Nd_{0.6}Ca_{0.4}(Mn_{1-x}Cr_x)O_3$. — I. O. Troyanchuk, M. V. Bushinsky, V. V. Eremenko, V. A. Sirenko, and H. Szymczak; **28** (1), 45-8.
Exchange interaction and magnetoresistance in $La_{2/3}Ca_{1/3}MnO_3$: experiment and models. — A. B. Beznosov, B. I. Belevtsev, E. L. Fertman, V. A. Desnenko, D. G. Naugle, K. D. D. Rathnayaka, and A. Parasiris; **28** (7), 556-61.
Noncollinear magnetic structures in an Fe/Si/Fe film with a ferromagnetic interlayer exchange interaction. — A. B. Chizhik, S. L. Gnatchenko, M. Baran, K. Fronc, R. Szymczak, and R. Zuberek; **28** (8), 639-41.
Features of the magnetic properties of rare-earth intermetallides RMn_2Ge_2 (Review). — N. P. Kolmakova, A. A. Sidorenko, and R. Z. Levitin; **28** (8), 653-68.
On the theory of magnetic phase transitions in magnets with a large single-ion anisotropy. — V. M. Kalita and V. M. Loktev; **28** (12), 883-8.

75.30.G Magnetic anisotropy

Inhomogeneous states for small magnetic particles with exchange anisotropy. — B. A. Ivanov, A. Ya. Volk, and A. Yu. Merkulov; **28** (1), 25-9.
On the magnetic anisotropy of La_2CuO_4 above the Néel temperature. — V. M. Loktev; **28** (1), 69-71.
Magnetostriction of the antiferromagnet $NiCl_2$ in the homogeneous and multidomain states. — V. M. Kalita, A. F. Lozenko, and P. A. Trotsenko; **28** (4), 263-6.
Specific heat study of magnetic excitations in a one-dimensional $S = 1$ Heisenberg magnet with strong planar anisotropy. — A. Feher, M. Orendáč, A. Orendáčová, and E. Čižmár; **28** (7), 551-5.
Possibility of formation and reversible rearrangement of equilibrium domain structure in antiferromagnets. — E. V. Gomonay and V. M. Loktev; **28** (8), 621-9.
On the theory of magnetic phase transitions in magnets with a large single-ion anisotropy. — V. M. Kalita and V. M. Loktev; **28** (12), 883-8.

75.30.H Magnetic impurity interactions

Non-Fermi-liquid behavior: Exact results for ensembles of magnetic impurities. — A. A. Zvyagin; **28** (12), 907-20.

75.30.K Magnetic phase boundaries (including magnetic transitions, metamagnetism, etc.)

Metallic ferromagnetism in a generalized Hubbard model. — L. Didukh and O. Kramar; **28** (1), 30-6.
Effect of light illumination on antiferromagnet-metamagnet phase transitions in the garnet $Ca_3Mn_2Ge_3O_{12}$. — V. A. Bedarev, V. I. Gapon, S. L. Gnatchenko, M. Baran, R. Szymczak, J. M. Desvignes, and H. Le Gall; **28** (1), 37-44.
Magnetic phase diagram of the system of manganites $Nd_{0.6}Ca_{0.4}(Mn_{1-x}Cr_x)O_3$. — I. O. Troyanchuk, M. V. Bushinsky, V. V. Eremenko, V. A. Sirenko, and H. Szymczak; **28** (1), 45-8.
Features of the magnetic behavior of $Mn_{2-x}Cr_xSb$ alloys in the low-temperature state. — V. I. Val'kov, V. I. Kamenev, S. A. Buzhinsky, and N. A. Romanova; **28** (3), 194-8.
Features of the magnetization of an antiferromagnet with single-ion anisotropy of the easy-plane type and with ion spins $S = 1$. — V. M. Kalita, I. M. Ivanova, and V. M. Loktev; **28** (6), 475-7.
Spin–phonon interaction and mode softening in NiF_2. — D. J. Lockwood; **28** (7), 505-9.
Electronic Raman scattering through a stripe ordering transition in $La_{2-x}Sr_xNiO_4$. — V. P. Gnezdilov, A. V. Yeremenko, Yu. G. Pashkevich, P. Lemmens, G. Güntherodt, J. M. Tranquada, D. J. Buttrey, and K. Nakajima; **28** (7), 510-5.
Light scattering on phonons in quasi-one-dimensional antiferromagnet $CsFeCl_3 \cdot 2H_2O$ induced by magnetic ordering. — V. S. Kurnosov, A. V. Peschanskii, V. I. Fomin, A. V. Yeremenko, and Yu. G. Pashkevich; **28** (7), 516-22.
Magnetic phase transitions in the system $La_{1-x}Bi_xMnO_{3+\lambda}$. — I. O. Troyanchuk, O. S. Mantytskaja, H. Szymczak, and M. Yu. Shvedun; **28** (7), 569-73.
Features of the magnetic properties of rare-earth intermetallides RMn_2Ge_2 (Review). — N. P. Kolmakova, A. A. Sidorenko, and R. Z. Levitin; **28** (8), 653-68.
Magnetic phases in $La_{0.66}Ba_{0.34}MnO_3$: effects of temperature and elastic strains. — A. B. Beznosov, V. V. Eremenko, E. L. Fertman, V. A. Desnenko, and D. D. Khalyavin; **28** (10), 762-6.
Magnetic properties of a $LaMn_{0.46}Co_{0.54}O_3$ single crystal. — S. N. Barilo, V. I. Gatal'skaya, S. V. Shiryaev, L. A. Kurochkin, R. Shimchak, and M. Baran; **28** (11), 853-5.
On the theory of magnetic phase transitions in magnets with a large single-ion anisotropy. — V. M. Kalita and V. M. Loktev; **28** (12), 883-8.
Resonance properties of the quasi-one-dimensional Ising magnet $[(CH_3)_3NH]CoCl_3 \cdot 2H_2O$ in the paramagnetic and magnetically ordered phases. — M. I. Kobets, E. N. Khatsko, V. A. Pashchenko, A. S. Chernyi, K. G. Dergachev, and V. G. Borisenko; **28** (12), 889-95.

75.30.M Valence fluctuation, Kondo lattice, and heavy-fermion phenomena

Non-Fermi-liquid behavior: Exact results for ensembles of magnetic impurities. — A. A. Zvyagin; **28** (12), 907-20.

75.30.V Colossal magnetoresistance

Exchange interaction and magnetoresistance in $La_{2/3}Ca_{1/3}MnO_3$: experiment and models. — A. B. Beznosov, B. I. Belevtsev, E. L. Fertman, V. A. Desnenko, D. G. Naugle, K. D. D. Rathnayaka, and A. Parasiris; **28** (7), 556-61.
Anomalous magnetic and dynamic behavior in magnetoresistive compounds: origin of bulk colossal magnetoresistivity. — V. Chechersky and A. Nath; **28** (7), 562-8.
Elastic-strain mechanisms for the influence of temperature, magnetic field, and pressure on the resistive and magnetic properties of magnetic semiconductors. — P. I. Polyakov and S. S. Kucherenko; **28** (10), 744-8.

75.40 Critical-point effects, specific heats, short-range order

75.40.C Static properties (order parameter, static susceptibility, heat capacities, critical exponents, etc.)

Specific heat study of magnetic excitations in a one-dimensional $S = 1$ Heisenberg magnet with strong planar anisotropy. — A. Feher, M. Orendáč, A. Orendáčová, and E. Čižmár; **28** (7), 551-5.
Magnetic properties of copper metaborate CuB_2O_4. — G. A. Petrakovskiĭ, A. I. Pankrats, M. A. Popov, A. D. Balaev, D. A. Velikanov, A. M. Vorotynov, K. A. Sablina, B. Roessli, J. Schefer, A. Amato, U. Staub, M. Boehm, and B. Ouladdiaf; **28** (8), 606-12.
Magnetic properties of a $LaMn_{0.46}Co_{0.54}O_3$ single crystal. — S. N. Barilo, V. I. Gatal'skaya, S. V. Shiryaev, L. A. Kurochkin, R. Shimchak, and M. Baran; **28** (11), 853-5.
Non-Fermi-liquid behavior: Exact results for ensembles of magnetic impurities. — A. A. Zvyagin; **28** (12), 907-20.

75.40.G Dynamic properties (dynamic susceptibility, spin waves, spin diffusion, dynamic scaling, etc.)

Low-temperature domain-wall dynamics in weak ferromagnets. — A. P. Kuz'menko; **28** (5), 337-48.
Recent progress in magneto-optics and research on its application (Review). — N. Kojima and K. Tsushima; **28** (7), 480-90.

Electronic Raman scattering through a stripe ordering transition in $La_{2-x}Sr_xNiO_4$. — V. P. Gnezdilov, A. V. Yeremenko, Yu. G. Pashkevich, P. Lemmens, G. Güntherodt, J. M. Tranquada, D. J. Buttrey, and K. Nakajima; **28** (7), 510-5.
Purely antiferromagnetic spin waves (antimagnons) in tetragonal magnets and ways of exciting them. — E. A. Turov and I. F. Mirsaev; **28** (8), 592-600.
On the conditions for the existence of 1D magnetic solitons with frequency characteristics falling in the continuous spectrum. — A. M. Kosevich and V. I. Grishaev; **28** (8), 601-5.
Drift of domain walls of the ab type in weak ferromagnets. — V. S. Gerasimchuk and A. A. Shitov; **28** (12), 877-9.

75.50 Studies of specific magnetic materials

75.50.B Fe and its alloys

Investigation of interlayer coupling in $[Fe/Cr]_n$ magnetic multilayer structures by the ferromagnetic resonance method (Review). — N. M. Kreines; **28** (8), 581-91.
Noncollinear magnetic structures in an Fe/Si/Fe film with a ferromagnetic interlayer exchange interaction. — A. B. Chizhik, S. L. Gnatchenko, M. Baran, K. Fronc, R. Szymczak, and R. Zuberek; **28** (8), 639-41.

75.50.C Other ferromagnetic metals and alloys

Metallic ferromagnetism in a generalized Hubbard model. — L. Didukh and O. Kramar; **28** (1), 30-6.
Effects of chaotic local crystal fields in pseudobinary rare-earth intermetallides. — A. S. Ermolenko; **28** (10), 749-54.

75.50.D Nonmetallic ferromagnetic materials

Electronic structure and magneto-optical Kerr effect in the compound $UCuP_2$. — O. Horpynyuk, V. V. Nemoshkalenko, V. N. Antonov, B. N. Harmon, and A. N. Yaresko; **28** (7), 533-8.
Exchange interaction and magnetoresistance in $La_{2/3}Ca_{1/3}MnO_3$: experiment and models. — A. B. Beznosov, B. I. Belevtsev, E. L. Fertman, V. A. Desnenko, D. G. Naugle, K. D. D. Rathnayaka, and A. Parasiris; **28** (7), 556-61.
Anomalous magnetic and dynamic behavior in magnetoresistive compounds: origin of bulk colossal magnetoresistivity. — V. Chechersky and A. Nath; **28** (7), 562-8.
Magnetic phase transitions in the system $La_{1-x}Bi_xMnO_{3+\lambda}$. — I. O. Troyanchuk, O. S. Mantytskaja, H. Szymczak, and M. Yu. Shvedun; **28** (7), 569-73.
Magnetic phases in $La_{0.66}Ba_{0.34}MnO_3$: effects of temperature and elastic strains. — A. B. Beznosov, V. V. Eremenko, E. L. Fertman, V. A. Desnenko, and D. D. Khalyavin; **28** (10), 762-6.

75.50.E Antiferromagnetics

Effect of light illumination on antiferromagnet-metamagnet phase transitions in the garnet $Ca_3Mn_2Ge_3O_{12}$. — V. A. Bedarev, V. I. Gapon, S. L. Gnatchenko, M. Baran, R. Szymczak, J. M. Desvignes, and H. Le Gall; **28** (1), 37-44.
Magnetic phase diagram of the system of manganites $Nd_{0.6}Ca_{0.4}(Mn_{1-x}Cr_x)O_3$. — I. O. Troyanchuk, M. V. Bushinsky, V. V. Eremenko, V. A. Sirenko, and H. Szymczak; **28** (1), 45-8.
On the magnetic anisotropy of La_2CuO_4 above the Néel temperature. — V. M. Loktev; **28** (1), 69-71.
Raman scattering in a $LiNiPO_4$ single crystal. — V. I. Fomin, V. P. Gnezdilov, V. S. Kurnosov, A. V. Peschanskii, A. V. Yeremenko, H. Schmid, J.-P. Rivera, and S. Gentil; **28** (3), 203-9.
Magnetostriction of the antiferromagnet $NiCl_2$ in the homogeneous and multidomain states. — V. M. Kalita, A. F. Lozenko, and P. A. Trotsenko; **28** (4), 263-6.
Features of the magnetization of an antiferromagnet with single-ion anisotropy of the easy-plane type and with ion spins $S = 1$. — V. M. Kalita, I. M. Ivanova, and V. M. Loktev; **28** (6), 475-7.
Spin–phonon interaction and mode softening in NiF_2. — D. J. Lockwood; **28** (7), 505-9.
Light scattering on phonons in quasi-one-dimensional antiferromagnet $CsFeCl_3 \cdot 2H_2O$ induced by magnetic ordering. — V. S. Kurnosov, A. V. Peschanskii, V. I. Fomin, A. V. Yeremenko, and Yu. G. Pashkevich; **28** (7), 516-22.
Optical study of $4f$ excitations in rare earth cuprates. — V. Nekvasil; **28** (7), 528-32.
Magnetic phase transitions in the system $La_{1-x}Bi_xMnO_{3+\lambda}$. — I. O. Troyanchuk, O. S. Mantytskaja, H. Szymczak, and M. Yu. Shvedun; **28** (7), 569-73.
Nonmonotonic temperature dependence of the spontaneous magnetization of the antiferromagnetic crystal $LiCoPO_4$. — N. F. Kharchenko, V. A. Desnenko, Yu. N. Kharchenko, R. Szymczak, and M. Baran; **28** (8), 646-52.
Optical spectroscopy of antiferromagnetic correlations and the stripe state in the superconductor $YBa_2Cu_3O_{6+x}$. — V. N. Samovarov, V. L. Vakula, M. Yu. Libin, S. A. Uyutnov, and G. G. Sergeeva; **28** (8), 674-86.

75.50.G Ferrimagnetics

Effect of light illumination on antiferromagnet-metamagnet phase transitions in the garnet $Ca_3Mn_2Ge_3O_{12}$. — V. A. Bedarev, V. I. Gapon, S. L. Gnatchenko, M. Baran, R. Szymczak, J. M. Desvignes, and H. Le Gall; **28** (1), 37-44.
Features of the magnetic behavior of $Mn_{2-x}Cr_xSb$ alloys in the low-temperature state. — V. I. Val'kov, V. I. Kamenev, S. A. Buzhinsky, and N. A. Romanova; **28** (3), 194-8.
Photoinduced magnetic linear dichroism in a YIG:Co film. — O. V. Miloslavska, Yu. N. Kharchenko, N. F. Kharchenko, V. G. Yurko, A. Stupakiewicz, and A. Maziewski; **28** (4), 267-9.
Nonlinear optical spectroscopy of epitaxial magnetic garnet films. — V. V. Pavlov, R. V. Pisarev, M. Fiebig, and D. Fröhlich; **28** (7), 523-7.

75.50.K Amorphous and quasicrystalline magnetic materials

On the correlation of nonperturbative fluctuations of glass-forming liquids and magnetic glasses. — A. S. Bakaĭ; **28** (6), 415-22.

75.50.L Spin glasses and other random magnets

Magnetic phase transitions in the system $La_{1-x}Bi_xMnO_{3+\lambda}$. — I. O. Troyanchuk, O. S. Mantytskaja, H. Szymczak, and M. Yu. Shvedun; **28** (7), 569-73.
Influence of Cr concentration on the structural and magnetic properties of the diluted magnetic semiconductor $Hg_{1-x}Cr_xSe$. — V. D. Prozorovskiĭ, I. Yu. Reshidova, A. I. Puzynya, S. Yu. Paranchych, and V. R. Romanyuk; **28** (12), 880-2.

75.50.P Magnetic semiconductors

Elastic-strain mechanisms for the influence of temperature, magnetic field, and pressure on the resistive and magnetic properties of magnetic semiconductors. — P. I. Polyakov and S. S. Kucherenko; **28** (10), 744-8.
Influence of Cr concentration on the structural and magnetic properties of the diluted magnetic semiconductor $Hg_{1-x}Cr_xSe$. — V. D. Prozorovskiĭ, I. Yu. Reshidova, A. I. Puzynya, S. Yu. Paranchych, and V. R. Romanyuk; **28** (12), 880-2.

75.50.T Fine-particle systems; nanocrystalline materials

Inhomogeneous states for small magnetic particles with exchange anisotropy. — B. A. Ivanov, A. Ya. Volk, and A. Yu. Merkulov; **28** (1), 25-9.
Mechanism of vortex switching in magnetic nanodots under a circular magnetic field. I. Resonance action of the field on the nanodot eigenmodes. — A. S. Kovalev and J. E. Prilepsky; **28** (12), 921-9.

75.50.W Permanent magnets

Insulating Van Vleck paramagnets at high magnetic fields (Review). — M. S. Tagirov and D. A. Tayurskiĭ; **28** (3), 147-64.

75.60 Domain effects, magnetization curves, and hysteresis

75.60.C Domain walls and domain structure

Magnetostriction of the antiferromagnet $NiCl_2$ in the homogeneous and multidomain states. — V. M. Kalita, A. F. Lozenko, and P. A. Trotsenko; **28** (4), 263-6.
Low-temperature domain-wall dynamics in weak ferromagnets. — A. P. Kuz'menko; **28** (5), 337-48.
Possibility of formation and reversible rearrangement of equilibrium domain structure in antiferromagnets. — E. V. Gomonay and V. M. Loktev; **28** (8), 621-9.

Static properties and nonlinear dynamics of domain walls with a vortexlike internal structure in magnetic films (Review). — B. N. Filippov; **28** (10), 707-38.

Drift of domain walls of the ab type in weak ferromagnets. — V. S. Gerasimchuk and A. A. Shitov; **28** (12), 877-9.

75.60.E Magnetization curves, hysteresis, Barkhausen and related effects

Inhomogeneous states for small magnetic particles with exchange anisotropy. — B. A. Ivanov, A. Ya. Volk, and A. Yu. Merkulov; **28** (1), 25-9.

Magnetic phase diagram of the system of manganites $Nd_{0.6}Ca_{0.4}(Mn_{1-x}Cr_x)O_3$. — I. O. Troyanchuk, M. V. Bushinsky, V. V. Eremenko, V. A. Sirenko, and H. Szymczak; **28** (1), 45-8.

Magnetization dynamics of electron–impurity systems at paramagnetic resonance. — E. A. Ivanchenko; **28** (2), 117-22.

Low-temperature domain-wall dynamics in weak ferromagnets. — A. P. Kuz'menko; **28** (5), 337-48.

Features of the magnetization of an antiferromagnet with single-ion anisotropy of the easy-plane type and with ion spins $S = 1$. — V. M. Kalita, I. M. Ivanova, and V. M. Loktev; **28** (6), 475-7.

Features of the magnetic properties of rare-earth intermetallides RMn_2Ge_2 (Review). — N. P. Kolmakova, A. A. Sidorenko, and R. Z. Levitin; **28** (8), 653-68.

Effects of chaotic local crystal fields in pseudobinary rare-earth intermetallides. — A. S. Ermolenko; **28** (10), 749-54.

Magnetic phases in $La_{0.66}Ba_{0.34}MnO_3$: effects of temperature and elastic strains. — A. B. Beznosov, V. V. Eremenko, E. L. Fertman, V. A. Desnenko, and D. D. Khalyavin; **28** (10), 762-6.

Magnetic properties of a $LaMn_{0.46}Co_{0.54}O_3$ single crystal. — S. N. Barilo, V. I. Gatal'skaya, S. V. Shiryaev, L. A. Kurochkin, R. Shimchak, and M. Baran; **28** (11), 853-5.

Mechanism of vortex switching in magnetic nanodots under a circular magnetic field. I. Resonance action of the field on the nanodot eigenmodes. — A. S. Kovalev and J. E. Prilepsky; **28** (12), 921-9.

75.60.J Magnetization reversal mechanisms

Low-temperature domain-wall dynamics in weak ferromagnets. — A. P. Kuz'menko; **28** (5), 337-48.

75.70 Magnetic properties of thin films, surfaces, and interfaces

75.70.A Magnetic properties of monolayers and thin films

Photoinduced magnetic linear dichroism in a YIG:Co film. — O. V. Miloslavska, Yu. N. Kharchenko, N. F. Kharchenko, V. G. Yurko, A. Stupakiewicz, and A. Maziewski; **28** (4), 267-9.

Aging effect on the magnetic and transport properties of laser-deposited $La_{0.5}Sr_{0.5}CoO_{3-\delta}$ films. — V. G. Prokhorov, G. G. Kaminskiĭ, V. M. Ishchuk, I. N. Chukanova, Y. P. Lee, and K. W. Kim; **28** (5), 354-8.

Nonlinear optical spectroscopy of epitaxial magnetic garnet films. — V. V. Pavlov, R. V. Pisarev, M. Fiebig, and D. Fröhlich; **28** (7), 523-7.

Giant resistance switching effect in nano-scale twinned $La_{0.65}Ca_{0.35}MnO_3$ film. — V. G. Prokhorov, G. G. Kaminsky, V. A. Komashko, Y. P. Lee, A. I. Tovstolytkin, and A. N. Pogorily; **28** (11), 856-8.

75.70.C Interfacial magnetic properties (multilayers, superlattices)

Inelastic electron tunneling across magnetically active interfaces in cuprate and manganite heterostructures modified by electromigration processes. — M. A. Belogolovskiĭ, Yu. F. Revenko, A. Yu. Gerasimenko, V. M. Svistunov, E. Hatta, G. Plitnik, V. E. Shaternik, and E. M. Rudenko; **28** (6), 391-4.

Investigation of interlayer coupling in $[Fe/Cr]_n$ magnetic multilayer structures by the ferromagnetic resonance method (Review). — N. M. Kreines; **28** (8), 581-91.

Noncollinear magnetic structures in an Fe/Si/Fe film with a ferromagnetic interlayer exchange interaction. — A. B. Chizhik, S. L. Gnatchenko, M. Baran, K. Fronc, R. Szymczak, and R. Zuberek; **28** (8), 639-41.

75.70.K Domain structure (including magnetic bubbles)

Static properties and nonlinear dynamics of domain walls with a vortexlike internal structure in magnetic films (Review). — B. N. Filippov; **28** (10), 707-38.

75.75 Magnetic properties of nanostructures

Anomalous magnetic and dynamic behavior in magnetoresistive compounds: origin of bulk colossal magnetoresistivity. — V. Chechersky and A. Nath; **28** (7), 562-8.

Mechanism of vortex switching in magnetic nanodots under a circular magnetic field. I. Resonance action of the field on the nanodot eigenmodes. — A. S. Kovalev and J. E. Prilepsky; **28** (12), 921-9.

75.80 Magnetomechanical and magnetoelectric effects, magnetostriction

Effect of nonmagnetic impurities on the spontaneous magnetostriction in β-O_2 crystals. — A. I. Prokhvatilov, Yu. A. Freiman, N. N. Galtsov, and Yu. E. Stetsenko; **28** (1), 61-5.

Magnetostriction of the antiferromagnet $NiCl_2$ in the homogeneous and multidomain states. — V. M. Kalita, A. F. Lozenko, and P. A. Trotsenko; **28** (4), 263-6.

Purely antiferromagnetic spin waves (antimagnons) in tetragonal magnets and ways of exciting them. — E. A. Turov and I. F. Mirsaev; **28** (8), 592-600.

Possibility of formation and reversible rearrangement of equilibrium domain structure in antiferromagnets. — E. V. Gomonay and V. M. Loktev; **28** (8), 621-9.

Elastic-strain mechanisms for the influence of temperature, magnetic field, and pressure on the resistive and magnetic properties of magnetic semiconductors. — P. I. Polyakov and S. S. Kucherenko; **28** (10), 744-8.

Magnetoelastic waves in multisublattice systems. — I. R. Kyzyrgulov and M. Kh. Kharrasov; **28** (11), 875-6.

Drift of domain walls of the ab type in weak ferromagnets. — V. S. Gerasimchuk and A. A. Shitov; **28** (12), 877-9.

75.90 Other topics in magnetic properties and materials (restricted to new topics in section 75)

Effect of light illumination on antiferromagnet-metamagnet phase transitions in the garnet $Ca_3Mn_2Ge_3O_{12}$. — V. A. Bedarev, V. I. Gapon, S. L. Gnatchenko, M. Baran, R. Szymczak, J. M. Desvignes, and H. Le Gall; **28** (1), 37-44.

76. Magnetic resonances and relaxations in condensed matter, Mössbauer effect

76.30 Electron paramagnetic resonance and relaxation

Insulating Van Vleck paramagnets at high magnetic fields (Review). — M. S. Tagirov and D. A. Tayurskiĭ; **28** (3), 147-64.

Two-quantum electron spin–lattice relaxation in amorphous solids. — L. G. Zakharov, L. L. Chotorlishvili, and T. L. Buishvili; **28** (6), 412-4.

76.30.D Ions and impurities: general

Magnetization dynamics of electron–impurity systems at paramagnetic resonance. — E. A. Ivanchenko; **28** (2), 117-22.

76.30.F Iron group (3*d*) ions and impurities (Ti–Cu)

EPR spectrum of the Fe^{3+} ion in bromcresol green ($C_{21}H_{14}Br_4O_5S$) and features in the dynamics of the surrounding molecules. — V. V. Chabanenko, V. N. Vasyukov, R. O. Kochkanjan, M. M. Nechitailov, H. Szymczak, S. Piechota, and A. Nabialek; **28** (1), 49-53.

Mechanism for the changes with temperature of the EPR spectrum of the Fe^{3+} ion in polycrystalline materials containing complexes with a multiwell potential. — V. N. Vasyukov; **28** (3), 199-202.

Manifestation of the Jahn–Teller effect in the EPR spectrum of the metalorganic complex $[Cu(en)2H_2O]SO_4$. — A. G. Anders,

A. I. Kaplienko, O. V. Kravchina, V. S. Bondarenko, A. Feher, M. Orendáč, A. Orendáčová, M. Kajňaková, and J. Černák; **28** (8), 642-5.

76.30.K Rare-earth ions and impurities

Insulating Van Vleck paramagnets at high magnetic fields (Review). — M. S. Tagirov and D. A. Tayurskiĭ; **28** (3), 147-64.

76.50 Ferromagnetic, antiferromagnetic, and ferrimagnetic resonances; spin-wave resonance

Investigation of interlayer coupling in $[Fe/Cr]_n$ magnetic multilayer structures by the ferromagnetic resonance method (Review). — N. M. Kreines; **28** (8), 581-91.

Resonance properties of the quasi-one-dimensional Ising magnet $[(CH_3)_3NH]CoCl_3 \cdot 2H_2O$ in the paramagnetic and magnetically ordered phases. — M. I. Kobets, E. N. Khatsko, V. A. Pashchenko, A. S. Chernyi, K. G. Dergachev, and V. G. Borisenko; **28** (12), 889-95.

76.60 Nuclear magnetic resonance and relaxation

76.60.C Chemical and Knight shifts

Metallic properties of lead dioxide. Band structure and NMR of ^{207}Pb at low temperatures. — L. A. Boyarskiĭ, S. P. Gabuda, S. G. Kozlova, and R. N. Pletnev; **28** (8), 691-4.

76.75 Muon spin rotation and relaxation

Spectral function and character of the motion of a conduction electron in an orientationally disordered molecular cryocrystal. — V. M. Loktev, S. G. Sharapov, and H. Beck; **28** (3), 220-6.

Magnetic properties of copper metaborate CuB_2O_4. — G. A. Petrakovskiĭ, A. I. Pankrats, M. A. Popov, A. D. Balaev, D. A. Velikanov, A. M. Vorotynov, K. A. Sablina, B. Roessli, J. Schefer, A. Amato, U. Staub, M. Boehm, and B. Ouladdiaf; **28** (8), 606-12.

76.80 Mössbauer effect; other γ-ray spectroscopy

Anomalous magnetic and dynamic behavior in magnetoresistive compounds: origin of bulk colossal magnetoresistivity. — V. Chechersky and A. Nath; **28** (7), 562-8.

78. Optical properties, condensed-matter spectroscopy and other interactions of radiation and particles with condensed matter

78.20 Optical properties of bulk materials and thin films

78.20.L Magnetooptical effects

Photoinduced magnetic linear dichroism in a YIG:Co film. — O. V. Miloslavska, Yu. N. Kharchenko, N. F. Kharchenko, V. G. Yurko, A. Stupakiewicz, and A. Maziewski; **28** (4), 267-9.

Recent progress in magneto-optics and research on its application (Review). — N. Kojima and K. Tsushima; **28** (7), 480-90.

Electronic Raman scattering through a stripe ordering transition in $La_{2-x}Sr_xNiO_4$. — V. P. Gnezdilov, A. V. Yeremenko, Yu. G. Pashkevich, P. Lemmens, G. Güntherodt, J. M. Tranquada, D. J. Buttrey, and K. Nakajima; **28** (7), 510-5.

Nonlinear optical spectroscopy of epitaxial magnetic garnet films. — V. V. Pavlov, R. V. Pisarev, M. Fiebig, and D. Fröhlich; **28** (7), 523-7.

Electronic structure and magneto-optical Kerr effect in the compound $UCuP_2$. — O. Horpynyuk, V. V. Nemoshkalenko, V. N. Antonov, B. N. Harmon, and A. N. Yaresko; **28** (7), 533-8.

78.30 Infrared and Raman spectra

78.30.C Liquids

IR spectra of cryocondensates of an isotopic water mixture on thermocycling. — A. Aldijarov, A. S. Drobyshev, and S. S. Sarsembinov; **28** (4), 290-4.

78.30.H Other nonmetallic inorganics

Raman scattering in a $LiNiPO_4$ single crystal. — V. I. Fomin, V. P. Gnezdilov, V. S. Kurnosov, A. V. Peschanskii, A. V. Yeremenko, H. Schmid, J.-P. Rivera, and S. Gentil; **28** (3), 203-9.

Infrared spectra of thin films of cryocondensates of an isotopic water mixture. — A. Aldijarov, A. Drobyshev, and S. Sarsembinov; **28** (3), 210-4.

Electronic Raman scattering through a stripe ordering transition in $La_{2-x}Sr_xNiO_4$. — V. P. Gnezdilov, A. V. Yeremenko, Yu. G. Pashkevich, P. Lemmens, G. Güntherodt, J. M. Tranquada, D. J. Buttrey, and K. Nakajima; **28** (7), 510-5.

Light scattering on phonons in quasi-one-dimensional antiferromagnet $CsFeCl_3 \cdot 2H_2O$ induced by magnetic ordering. — V. S. Kurnosov, A. V. Peschanskii, V. I. Fomin, A. V. Yeremenko, and Yu. G. Pashkevich; **28** (7), 516-22.

78.40 Absorption and reflection spectra: visible and ultraviolet

78.40.H Other nonmetallic inorganics

Interaction of Pr^{3+} optical centers in the Y_2SiO_5 crystal. — Yu. V. Malyukin, P. N. Zhmurin, A. N. Lebedenko, M. A. Sholkina, B. V. Grinev, N. V. Znamenskiĭ, E. A. Manykin, Yu. V. Orlov, E. A. Petrenko, and T. G. Yukina; **28** (1), 54-7.

Excitons in the layered insulators ZnI_2 and CdI_2:Zn. — O. N. Yunakova, V. K. Miloslavsky, and E. N. Kovalenko; **28** (4), 284-9.

Optical spectroscopy of antiferromagnetic correlations and the stripe state in the superconductor $YBa_2Cu_3O_{6+x}$. — V. N. Samovarov, V. L. Vakula, M. Yu. Libin, S. A. Uyutnov, and G. G. Sergeeva; **28** (8), 674-86.

78.55 Photoluminescence

78.55.A Elemental semiconductors

Influence of structural inhomogeneity on the luminescence properties of silicon nanocrystallites. — I. V. Blonskiĭ, M. S. Brodyn, A. Yu. Vakhnin, A. Ya. Zhugayevych, V. M. Kadan, and A. K. Kadashchuk; **28** (8), 706-12.

78.55.H Other solid inorganic materials

Interaction of Pr^{3+} optical centers in the Y_2SiO_5 crystal. — Yu. V. Malyukin, P. N. Zhmurin, A. N. Lebedenko, M. A. Sholkina, B. V. Grinev, N. V. Znamenskiĭ, E. A. Manykin, Yu. V. Orlov, E. A. Petrenko, and T. G. Yukina; **28** (1), 54-7.

Microscopic nature of Pr^{3+} optical centers in Y_2SiO_5, Lu_2SiO_5, and Gd_2SiO_5 crystals. — Yu. V. Malyukin, P. N. Zhmurin, B. V. Grinev, V. P. Seminozhenko, N. V. Znamenskiĭ, E. A. Manykin, E. A. Petrenko, and T. G. Yukina; **28** (10), 774-9.

Structure and photoluminescence of helium-intercalated fullerite C_{60}. — I. V. Legchenkova, A. I. Prokhvatilov, Yu. E. Stetsenko, M. A. Strzhemechny, K. A. Yagotintsev, A. A. Avdeenko, V. V. Eremenko, P. V. Zinoviev, V. N. Zoryansky, N. B. Silaeva, and R. S. Ruoff; **28** (12), 942-4.

78.66 Optical properties of specific thin films

Infrared spectra of thin films of cryocondensates of an isotopic water mixture. — A. Aldijarov, A. Drobyshev, and S. Sarsembinov; **28** (3), 210-4.

78.66.N Insulators

Photoinduced magnetic linear dichroism in a YIG:Co film. — O. V. Miloslavska, Yu. N. Kharchenko, N. F. Kharchenko, V. G. Yurko, A. Stupakiewicz, and A. Maziewski; **28** (4), 267-9.

Excitons in the layered insulators ZnI_2 and CdI_2:Zn. — O. N. Yunakova, V. K. Miloslavsky, and E. N. Kovalenko; **28** (4), 284-9.

78.66.T Fullerenes and related materials

Structure and photoluminescence of helium-intercalated fullerite C_{60}. — I. V. Legchenkova, A. I. Prokhvatilov, Yu. E. Stetsenko, M. A. Strzhemechny, K. A. Yagotintsev, A. A. Avdeenko, V. V. Eremenko, P. V. Zinoviev, V. N. Zoryansky, N. B. Silaeva, and R. S. Ruoff; **28** (12), 942-4.

78.67 Optical properties of nanoscale materials and structures

78.67.B Nanocrystals and nanoparticles

Influence of structural inhomogeneity on the luminescence properties of silicon nanocrystallites. — I. V. Blonskiĭ, M. S. Brodyn, A. Yu. Vakhnin, A. Ya. Zhugayevych, V. M. Kadan, and A. K. Kadashchuk; **28** (8), 706-12.

78.70 Interactions of particles and radiation with matter

78.70.C X-ray scattering

Features of the low-temperature plasticity of Pb–In single crystals. — N. V. Isaev, V. S. Fomenko, V. V. Pustovalov, and I. S. Braude; **28** (5), 369-75.

81. Materials science

81.05 Specific materials: fabrication, treatment, testing and analysis

81.05.E III–V semiconductors

Thermal conductivity of a GaAs single crystal grown in microgravity. — A. I. Ivanov, A. N. Luk'yanov, B. A. Merisov, A. V. Sologubenko, and G. Ya. Khadjai; **28** (6), 462-4.

81.05.T Fullerenes and related materials

On the role of Jahn–Teller vibrations in the mechanism of high-T_c superconductivity of intercalated C_{60} fullerite films with *p*-type conductivity. — V. M. Loktev and E. A. Pashitskiĭ; **28** (4), 295-7.

81.10 Methods of crystal growth; physics of crystal growth

81.10.F Growth from melts; zone melting and refining

Thermal conductivity of a GaAs single crystal grown in microgravity. — A. I. Ivanov, A. N. Luk'yanov, B. A. Merisov, A. V. Sologubenko, and G. Ya. Khadjai; **28** (6), 462-4.

81.10.M Growth in microgravity environments

Thermal conductivity of a GaAs single crystal grown in microgravity. — A. I. Ivanov, A. N. Luk'yanov, B. A. Merisov, A. V. Sologubenko, and G. Ya. Khadjai; **28** (6), 462-4.

81.30 Phase diagrams and microstructures developed by solidification and solid–solid phase transformations

81.30.H Constant-composition solid–solid phase transformations: polymorphic, massive, and order–disorder

Kinetics of the low-temperature structural transformation in the In–4.3 at. % Cd solid solution. — S. V. Lubenets, V. D. Natsik, L. N. Pal-Val, P. P. Pal-Val, and L. S. Fomenko; **28** (6), 465-74.

81.40 Treatment of materials and its effects on microstructure and properties

81.40.E Cold working, work hardening; annealing, post-deformation annealing, quenching, tempering recovery, and crystallization

Staged work hardening of polycrystalline titanium at low temperatures and its relation to substructure evolution. — V. A. Moskalenko, A. R. Smirnov, V. N. Kovaleva, and V. D. Natsik; **28** (12), 935-41.

81.40.J Elasticity and anelasticity, stress-strain relations

Kinetics of the low-temperature structural transformation in the In–4.3 at. % Cd solid solution. — S. V. Lubenets, V. D. Natsik, L. N. Pal-Val, P. P. Pal-Val, and L. S. Fomenko; **28** (6), 465-74.

81.40.L Deformation, plasticity, and creep

Features of the low-temperature plasticity of Pb–In single crystals. — N. V. Isaev, V. S. Fomenko, V. V. Pustovalov, and I. S. Braude; **28** (5), 369-75.

Low-temperature deformation and fracture of bulk nanostructural titanium obtained by intense plastic deformation using equal channel angular pressing. — V. Z. Bengus, E. D. Tabachnikova, V. D. Natsik, I. Mishkuf, K. Chakh, V. V. Stolyarov, and R. Z. Valiev; **28** (11), 864-74.

Staged work hardening of polycrystalline titanium at low temperatures and its relation to substructure evolution. — V. A. Moskalenko, A. R. Smirnov, V. N. Kovaleva, and V. D. Natsik; **28** (12), 935-41.

81.40.N Fatigue, corrosion fatigue, embrittlement, cracking, fracture and failure

Low-temperature deformation and fracture of bulk nanostructural titanium obtained by intense plastic deformation using equal channel angular pressing. — V. Z. Bengus, E. D. Tabachnikova, V. D. Natsik, I. Mishkuf, K. Chakh, V. V. Stolyarov, and R. Z. Valiev; **28** (11), 864-74.

81.40.R Electrical and magnetic properties (related to treatment conditions)

Aging effect on the magnetic and transport properties of laser-deposited $La_{0.5}Sr_{0.5}CoO_{3-\delta}$ films. — V. G. Prokhorov, G. G. Kaminskiĭ, V. M. Ishchuk, I. N. Chukanova, Y. P. Lee, and K. W. Kim; **28** (5), 354-8.

85. Electronic and magnetic devices; microelectronics

85.25 Superconducting devices

XIV international seminar on high-temperature superconductivity and school of applied superconductivity (Kurchatovets vacation base, Protvino, Russia, May 28–31, 2001). — M. A. Belogolovskiĭ, S. I. Bondarenko, and L. S. Shirshov; **28** (2), 143-5.

85.25.C Josephson devices

Josephson effect in point contacts between ''*f*-wave'' superconductors. — R. Mahmoodi, S. N. Shevchenko, and Yu. A. Kolesnichenko; **28** (3), 184-9.

85.70 Magnetic devices

85.70.R Magnetic levitation, propulsion and control devices

Measurement of the densities of liquids and gases under pressure using magnetic levitation of a standard sample. — A. S. Panfilov and Yu. Ya. Pushkar'; **28** (10), 789-93.

AUTHOR INDEX TO VOLUME 28

Within each author listing papers are arranged in ascending page number order. This index is not a translation. It was produced by computer-aided photocomposition directly from the database of AIP's Current Physics Information system. Suggestions for improvements as well as other comments are welcome and should be addressed to the Translations and Special Publications Division Office.

A

Adamenko, I. N. — Asymmetry of relaxation processes and the creation of high-energy phonons in the anisotropic phonon systems of He II. — I. N. Adamenko, K. É. Nemchenko, and A. F. G. Wyatt; **28** (2), 85-94.

Aldijarov, A. — Infrared spectra of thin films of cryocondensates of an isotopic water mixture. — A. Aldijarov, A. Drobyshev, and S. Sarsembinov; **28** (3), 210-4.

— IR spectra of cryocondensates of an isotopic water mixture on thermocycling. — A. Aldijarov, A. S. Drobyshev, and S. S. Sarsembinov; **28** (4), 290-4.

Alekseeva, L. A. — Low-temperature unsteady creep of parahydrogen single crystals. — L. A. Alekseeva, A. V. Pustovalova, V. I. Khatuntsev, and Yu. V. Butenko; **28** (1), 58-60.

— Effect of impurity oxygen on the low-temperature plasticity of solid normal hydrogen. — L. A. Alekseeva and Yu. V. Butenko; **28** (2), 140-2.

Amato, A. — Magnetic properties of copper metaborate CuB_2O_4. — G. A. Petrakovskiĭ, A. I. Pankrats, M. A. Popov, A. D. Balaev, D. A. Velikanov, A. M. Vorotynov, K. A. Sablina, B. Roessli, J. Schefer, A. Amato, U. Staub, M. Boehm, and B. Ouladdiaf; **28** (8), 606-12.

Amitin, E. B. — Anomalies of the electronic heat capacity of thulium cuprates in the pseudogap phase region. — E. B. Amitin, K. R. Zhdanov, M. Yu. Kameneva, Yu. A. Kovalevskaya, L. P. Kozeeva, I. E. Paukov, and A. G. Blinov; **28** (8), 669-73.

Anders, A. G. — Manifestation of the Jahn–Teller effect in the EPR spectrum of the metalorganic complex $[Cu(en)2H_2O]SO_4$. — A. G. Anders, A. I. Kaplienko, O. V. Kravchina, V. S. Bondarenko, A. Feher, M. Orendáč, A. Orendáčová, M. Kajňaková, and J. Černák; **28** (8), 642-5.

Antonov, V. N. — Electronic structure and magneto-optical Kerr effect in the compound $UCuP_2$. — O. Horpynyuk, V. V. Nemoshkalenko, V. N. Antonov, B. N. Harmon, and A. N. Yaresko; **28** (7), 533-8.

Antsygina, T. N. — Lattice dynamics and heat capacity of a two-dimensional monoatomic crystal on a substrate. — T. N. Antsygina, I. I. Poltavsky, M. I. Poltavskaya, and K. A. Chishko; **28** (6), 442-51.

Artemov, A. N. — Steady state diagram of current-carrying layered superconductors. — A. N. Artemov and Yu. V. Medvedev; **28** (4), 242-6.

Avdeenko, A. A. — Structure and photoluminescence of helium-intercalated fullerite C_{60}. — I. V. Legchenkova, A. I. Prokhvatilov, Yu. E. Stetsenko, M. A. Strzhemechny, K. A. Yagotintsev, A. A. Avdeenko, V. V. Eremenko, P. V. Zinoviev, V. N. Zoryansky, N. B. Silaeva, and R. S. Ruoff; **28** (12), 942-4.

Avishai, Y. — Electronic excitations and correlations in quantum bars. — I. Kuzmenko, S. Gredeskul, K. Kikoin, and Y. Avishai; **28** (7), 539-46.

Avramenko, Yu. A. — Characteristics of the electric field accompanying a longitudinal acoustic wave in a metal. Anomaly in the superconducting phase. — Yu. A. Avramenko, E. V. Bezuglyi, N. G. Burma, I. G. Kolobov, V. D. Fil', O. A. Shevchenko, and V. M. Gokhfeld; **28** (5), 328-36.

B

Bakai, A. S. — On correlated heterogeneities of glass-forming liquids. — A. S. Bakai; **28** (12), 896-906.

Bakaĭ, A. S. — Field emission microscopy of the cluster and subcluster structure of a Zr–Ti–Cu–Ni–Be bulk metallic glass. — A. S. Bakaĭ, I. M. Mikhailovskij, T. I. Mazilova, and N. Wanderka; **28** (4), 279-83.

— On the correlation of nonperturbative fluctuations of glass-forming liquids and magnetic glasses. — A. S. Bakaĭ; **28** (6), 415-22.

Balaev, A. D. — Magnetic properties of copper metaborate CuB_2O_4. — G. A. Petrakovskiĭ, A. I. Pankrats, M. A. Popov, A. D. Balaev, D. A. Velikanov, A. M. Vorotynov, K. A. Sablina, B. Roessli, J. Schefer, A. Amato, U. Staub, M. Boehm, and B. Ouladdiaf; **28** (8), 606-12.

Baran, M. — Effect of light illumination on antiferromagnet-metamagnet phase transitions in the garnet $Ca_3Mn_2Ge_3O_{12}$. — V. A. Bedarev, V. I. Gapon, S. L. Gnatchenko, M. Baran, R. Szymczak, J. M. Desvignes, and H. Le Gall; **28** (1), 37-44.

— Magnetic properties of a lead-doped BKBO single crystal. — S. N. Barilo, V. I. Gatal'skaya, S. V. Shiryaev, T. V. Smirnova, H. Szymczak, R. Szymczak, and M. Baran; **28** (5), 349-53.

— Noncollinear magnetic structures in an Fe/Si/Fe film with a ferromagnetic interlayer exchange interaction. — A. B. Chizhik, S. L. Gnatchenko, M. Baran, K. Fronc, R. Szymczak, and R. Zuberek; **28** (8), 639-41.

— Nonmonotonic temperature dependence of the spontaneous magnetization of the antiferromagnetic crystal $LiCoPO_4$. — N. F. Kharchenko, V. A. Desnenko, Yu. N. Kharchenko, R. Szymczak, and M. Baran; **28** (8), 646-52.

— Magnetic properties of a $LaMn_{0.46}Co_{0.54}O_3$ single crystal. — S. N. Barilo, V. I. Gatal'skaya, S. V. Shiryaev, L. A. Kurochkin, R. Shimchak, and M. Baran; **28** (11), 853-5.

Barilo, S. N. — Magnetic properties of a lead-doped BKBO single crystal. — S. N. Barilo, V. I. Gatal'skaya, S. V. Shiryaev, T. V. Smirnova, H. Szymczak, R. Szymczak, and M. Baran; **28** (5), 349-53.

— Magnetic properties of a $LaMn_{0.46}Co_{0.54}O_3$ single crystal. — S. N. Barilo, V. I. Gatal'skaya, S. V. Shiryaev, L. A. Kurochkin, R. Shimchak, and M. Baran; **28** (11), 853-5.

Bazarov, V. V. — Reinforcement of pinning by surface magnetic microparticles in high-T_c superconductors. — P. N. Togulev, V. V. Bazarov, I. B. Khaĭbullin, and N. M. Suleĭmanov; **28** (4), 250-3.

Beck, H. — Spectral function and character of the motion of a conduction electron in an orientationally disordered molecular cryocrystal. — V. M. Loktev, S. G. Sharapov, and H. Beck; **28** (3), 220-6.

Bedarev, V. A. — Effect of light illumination on antiferromagnet-metamagnet phase transitions in the garnet $Ca_3Mn_2Ge_3O_{12}$. — V. A. Bedarev, V. I. Gapon, S. L. Gnatchenko, M. Baran, R. Szymczak, J. M. Desvignes, and H. Le Gall; **28** (1), 37-44.

Belevtsev, B. I. — Exchange interaction and magnetoresistance in $La_{2/3}Ca_{1/3}MnO_3$: experiment and models. — A. B. Beznosov, B. I. Belevtsev, E. L. Fertman, V. A. Desnenko, D. G. Naugle, K. D. D. Rathnayaka, and A. Parasiris; **28** (7), 556-61.

Belogolovskiĭ, M. A. — XIV international seminar on high-temperature superconductivity and school of applied superconductivity (Kurchatovets vacation base, Protvino, Russia, May 28–31, 2001). — M. A. Belogolovskiĭ, S. I. Bondarenko, and L. S. Shirshov; **28** (2), 143-5.

— Inelastic electron tunneling across magnetically active interfaces in cuprate and manganite heterostructures modified by electromigration processes. — M. A. Belogolovskiĭ, Yu. F. Revenko, A. Yu. Gerasimenko, V. M. Svistunov, E. Hatta, G. Plitnik, V. E. Shaternik, and E. M. Rudenko; **28** (6), 391-4.

Bengus, V. Z. — Low-temperature deformation and fracture of bulk nanostructural titanium obtained by intense plastic deformation using equal channel angular pressing. — V. Z. Bengus, E. D. Tabachnikova, V. D. Natsik, I. Mishkuf, K. Chakh, V. V. Stolyarov, and R. Z. Valiev; **28** (11), 864-74.

Beznosov, A. B. — Exchange interaction and magnetoresistance in $La_{2/3}Ca_{1/3}MnO_3$: experiment and models. — A. B. Beznosov, B. I. Belevtsev, E. L. Fertman, V. A. Desnenko, D. G. Naugle, K. D. D. Rathnayaka, and A. Parasiris; **28** (7), 556-61.

— Magnetic phases in $La_{0.66}Ba_{0.34}MnO_3$: effects of temperature and elastic strains. — A. B. Beznosov, V. V. Eremenko, E. L. Fertman, V. A. Desnenko, and D. D. Khalyavin; **28** (10), 762-6.

Bezuglyi, E. V. — Characteristics of the electric field accompanying a longitudinal acoustic wave in a metal. Anomaly in the

superconducting phase. — Yu. A. Avramenko, E. V. Bezuglyi, N. G. Burma, I. G. Kolobov, V. D. Fil', O. A. Shevchenko, and V. M. Gokhfeld; **28** (5), 328-36.

Blinov, A. G. — Anomalies of the electronic heat capacity of thulium cuprates in the pseudogap phase region. — E. B. Amitin, K. R. Zhdanov, M. Yu. Kameneva, Yu. A. Kovalevskaya, L. P. Kozeeva, I. E. Paukov, and A. G. Blinov; **28** (8), 669-73.

Blonskiĭ, I. V. — Influence of structural inhomogeneity on the luminescence properties of silicon nanocrystallites. — I. V. Blonskiĭ, M. S. Brodyn, A. Yu. Vakhnin, A. Ya. Zhugayevych, V. M. Kadan, and A. K. Kadashchuk; **28** (8), 706-12.

Boehm, M. — Magnetic properties of copper metaborate CuB_2O_4. — G. A. Petrakovskiĭ, A. I. Pankrats, M. A. Popov, A. D. Balaev, D. A. Velikanov, A. M. Vorotynov, K. A. Sablina, B. Roessli, J. Schefer, A. Amato, U. Staub, M. Boehm, and B. Ouladdiaf; **28** (8), 606-12.

Bondarenko, S. I. — XIV international seminar on high-temperature superconductivity and school of applied superconductivity (Kurchatovets vacation base, Protvino, Russia, May 28–31, 2001). — M. A. Belogolovskiĭ, S. I. Bondarenko, and L. S. Shirshov; **28** (2), 143-5.

Bondarenko, V. S. — Manifestation of the Jahn–Teller effect in the EPR spectrum of the metalorganic complex $[Cu(en)2H_2O]SO_4$. — A. G. Anders, A. I. Kaplienko, O. V. Kravchina, V. S. Bondarenko, A. Feher, M. Orendáč, A. Orendáčová, M. Kajňaková, and J. Černák; **28** (8), 642-5.

Borisenko, V. G. — Resonance properties of the quasi-one-dimensional Ising magnet $[(CH_3)_3NH]CoCl_3 \cdot 2H_2O$ in the paramagnetic and magnetically ordered phases. — M. I. Kobets, E. N. Khatsko, V. A. Pashchenko, A. S. Chernyi, K. G. Dergachev, and V. G. Borisenko; **28** (12), 889-95.

Boyarskiĭ, L. A. — Metallic properties of lead dioxide. Band structure and NMR of ^{207}Pb at low temperatures. — L. A. Boyarskiĭ, S. P. Gabuda, S. G. Kozlova, and R. N. Pletnev; **28** (8), 691-4.

Boyko, F. A. — On the criteria for superconductivity in $PrBa_2Cu_3O_{6.6}$. — F. A. Boyko, G. V. Bukin, V. A. Voloshin, and A. A. Gusev; **28** (2), 95-8.

Bratus', E. N. — Galvanomagnetic effects in the normal state of high-T_c metal oxides in a model two-band superconductor with a narrow band (level) near the Fermi boundary. — V. P. Galaĭko and E. N. Bratus'; **28** (5), 321-7.

Braude, I. S. — Features of the low-temperature plasticity of Pb–In single crystals. — N. V. Isaev, V. S. Fomenko, V. V. Pustovalov, and I. S. Braude; **28** (5), 369-75.

Brodyn, M. S. — Influence of structural inhomogeneity on the luminescence properties of silicon nanocrystallites. — I. V. Blonskiĭ, M. S. Brodyn, A. Yu. Vakhnin, A. Ya. Zhugayevych, V. M. Kadan, and A. K. Kadashchuk; **28** (8), 706-12.

Buishvili, T. L. — Two-quantum electron spin–lattice relaxation in amorphous solids. — L. G. Zakharov, L. L. Chotorlishvili, and T. L. Buishvili; **28** (6), 412-4.

Bukin, G. V. — On the criteria for superconductivity in $PrBa_2Cu_3O_{6.6}$. — F. A. Boyko, G. V. Bukin, V. A. Voloshin, and A. A. Gusev; **28** (2), 95-8.

Burma, N. G. — Characteristics of the electric field accompanying a longitudinal acoustic wave in a metal. Anomaly in the superconducting phase. — Yu. A. Avramenko, E. V. Bezuglyi, N. G. Burma, I. G. Kolobov, V. D. Fil', O. A. Shevchenko, and V. M. Gokhfeld; **28** (5), 328-36.

Bushinsky, M. V. — Magnetic phase diagram of the system of manganites $Nd_{0.6}Ca_{0.4}(Mn_{1-x}Cr_x)O_3$. — I. O. Troyanchuk, M. V. Bushinsky, V. V. Eremenko, V. A. Sirenko, and H. Szymczak; **28** (1), 45-8.

Butenko, Yu. V. — Low-temperature unsteady creep of parahydrogen single crystals. — L. A. Alekseeva, A. V. Pustovalova, V. I. Khatuntsev, and Yu. V. Butenko; **28** (1), 58-60.

— Effect of impurity oxygen on the low-temperature plasticity of solid normal hydrogen. — L. A. Alekseeva and Yu. V. Butenko; **28** (2), 140-2.

Buttrey, D. J. — Electronic Raman scattering through a stripe ordering transition in $La_{2-x}Sr_xNiO_4$. — V. P. Gnezdilov, A. V. Yeremenko, Yu. G. Pashkevich, P. Lemmens, G. Güntherodt, J. M. Tranquada, D. J. Buttrey, and K. Nakajima; **28** (7), 510-5.

Buzhinsky, S. A. — Features of the magnetic behavior of $Mn_{2-x}Cr_xSb$ alloys in the low-temperature state. — V. I. Val'kov, V. I. Kamenev, S. A. Buzhinsky, and N. A. Romanova; **28** (3), 194-8.

Bykov, A. N. — MgB_2: Synthesis, sound velocity, and dynamics of the vortex phase. — T. V. Ignatova, G. A. Zvyagina, I. G. Kolobov, E. A. Masalitin, V. D. Fil', Yu. V. Paderno, A. N. Bykov, V. N. Paderno, and V. I. Lyashenko; **28** (3), 190-3.

C

Černák, J. — Manifestation of the Jahn–Teller effect in the EPR spectrum of the metalorganic complex $[Cu(en)2H_2O]SO_4$. — A. G. Anders, A. I. Kaplienko, O. V. Kravchina, V. S. Bondarenko, A. Feher, M. Orendáč, A. Orendáčová, M. Kajňaková, and J. Černák; **28** (8), 642-5.

Chabanenko, V. V. — EPR spectrum of the Fe^{3+} ion in bromcresol green ($C_{21}H_{14}Br_4O_5S$) and features in the dynamics of the surrounding molecules. — V. V. Chabanenko, V. N. Vasyukov, R. O. Kochkanjan, M. M. Nechitailov, H. Szymczak, S. Piechota, and A. Nabialek; **28** (1), 49-53.

— Excitation of oscillations of the magnetic induction in a Nb–Ti slab as a result of a thermomagnetic flux avalanche. — V. V. Chabanenko, V. F. Rusakov, V. A. Yampol'skiĭ, H. Szymczak, S. Piechota, S. Vasiliev, and A. Nabialek; **28** (6), 387-90.

Chagovets, V. K. — Concentration dependence of the attenuation of first sound in supersaturated superfluid ^3He–^4He solutions under pressure. — A. A. Zadorozhko, T. V. Kalko, É. Ya. Rudavskiĭ, I. A. Usherov-Marshak, V. K. Chagovets, and G. A. Sheshin; **28** (2), 73-8.

Chakh, K. — Low-temperature deformation and fracture of bulk nanostructural titanium obtained by intense plastic deformation using equal channel angular pressing. — V. Z. Bengus, E. D. Tabachnikova, V. D. Natsik, I. Mishkuf, K. Chakh, V. V. Stolyarov, and R. Z. Valiev; **28** (11), 864-74.

Chechersky, V. — Anomalous magnetic and dynamic behavior in magnetoresistive compounds: origin of bulk colossal magnetoresistivity. — V. Chechersky and A. Nath; **28** (7), 562-8.

Chekanova, N. N. — On the classification of equilibrium superfluid states with scalar and tensor order parameters. — M. Yu. Kovalevsky, S. V. Peletminsky, and N. N. Chekanova; **28** (4), 227-34.

Chernyi, A. S. — Resonance properties of the quasi-one-dimensional Ising magnet $[(CH_3)_3NH]CoCl_3 \cdot 2H_2O$ in the paramagnetic and magnetically ordered phases. — M. I. Kobets, E. N. Khatsko, V. A. Pashchenko, A. S. Chernyi, K. G. Dergachev, and V. G. Borisenko; **28** (12), 889-95.

Chishko, K. A. — Lattice dynamics and heat capacity of a two-dimensional monoatomic crystal on a substrate. — T. N. Antsygina, I. I. Poltavsky, M. I. Poltavskaya, and K. A. Chishko; **28** (6), 442-51.

Chizhik, A. B. — Noncollinear magnetic structures in an Fe/Si/Fe film with a ferromagnetic interlayer exchange interaction. — A. B. Chizhik, S. L. Gnatchenko, M. Baran, K. Fronc, R. Szymczak, and R. Zuberek; **28** (8), 639-41.

Chkhaidze, N. D. — Sound propagation in a porous medium filled with superfluid helium. — Sh. E. Kekutiya and N. D. Chkhaidze; **28** (11), 795-802.

Chotorlishvili, L. L. — Two-quantum electron spin–lattice relaxation in amorphous solids. — L. G. Zakharov, L. L. Chotorlishvili, and T. L. Buishvili; **28** (6), 412-4.

Chukanova, I. N. — Aging effect on the magnetic and transport properties of laser-deposited $La_{0.5}Sr_{0.5}CoO_{3-\delta}$ films. — V. G. Prokhorov, G. G. Kaminskiĭ, V. M. Ishchuk, I. N. Chukanova, Y. P. Lee, and K. W. Kim; **28** (5), 354-8.

Čižmár, E. — Specific heat study of magnetic excitations in a one-dimensional $S = 1$ Heisenberg magnet with strong planar anisotropy. — A. Feher, M. Orendáč, A. Orendáčova, and E. Čižmár; **28** (7), 551-5.

D

Danilchenko, B. A. — Low-dose radiation effects in thin films of high-temperature superconducting $YBa_2Cu_3O_{7-x}$ irradiated by 1-MeV electrons. — Yu. V. Fedotov, B. A. Danilchenko, and I. S. Rogutskiĭ; **28** (10), 739-43.

Dergachev, K. G. — Resonance properties of the quasi-one-dimensional Ising magnet $[(CH_3)_3NH]CoCl_3 \cdot 2H_2O$ in the paramagnetic and magnetically ordered phases. — M. I. Kobets, E. N. Khatsko, V. A. Pashchenko, A. S. Chernyi, K. G. Dergachev, and V. G. Borisenko; **28** (12), 889-95.

Desnenko, V. A. — Exchange interaction and magnetoresistance in $La_{2/3}Ca_{1/3}MnO_3$: experiment and models. — A. B. Beznosov, B. I. Belevtsev, E. L. Fertman, V. A. Desnenko, D. G. Naugle, K. D. D. Rathnayaka, and A. Parasiris; **28** (7), 556-61.
— Nonmonotonic temperature dependence of the spontaneous magnetization of the antiferromagnetic crystal $LiCoPO_4$. — N. F. Kharchenko, V. A. Desnenko, Yu. N. Kharchenko, R. Szymczak, and M. Baran; **28** (8), 646-52.
— Magnetic phases in $La_{0.66}Ba_{0.34}MnO_3$: effects of temperature and elastic strains. — A. B. Beznosov, V. V. Eremenko, E. L. Fertman, V. A. Desnenko, and D. D. Khalyavin; **28** (10), 762-6.
Desvignes, J. M. — Effect of light illumination on antiferromagnet-metamagnet phase transitions in the garnet $Ca_3Mn_2Ge_3O_{12}$. — V. A. Bedarev, V. I. Gapon, S. L. Gnatchenko, M. Baran, R. Szymczak, J. M. Desvignes, and H. Le Gall; **28** (1), 37-44.
Didukh, L. — Metallic ferromagnetism in a generalized Hubbard model. — L. Didukh and O. Kramar; **28** (1), 30-6.
Dmitriev, V. M. — Direct evidence for the occurrence of superconductivity in the magnetic compound YFe_4Al_8. — V. M. Dmitriev, L. F. Rybaltchenko, P. Wyder, A. G. M. Jansen, N. N. Prentslau, and W. Suski; **28** (4), 260-2.
Drobotko, V. F. — Manifestation of two-dimensional behavior of YBCO films in a study of their complex susceptibility. — A. V. Khokhlov, A. Yu. Prokhorov, V. F. Drobotko, G. G. Levchenko, and A. V. Klimov; **28** (6), 377-82.
Drobyshev, A. — Infrared spectra of thin films of cryocondensates of an isotopic water mixture. — A. Aldijarov, A. Drobyshev, and S. Sarsembinov; **28** (3), 210-4.
Drobyshev, A. S. — IR spectra of cryocondensates of an isotopic water mixture on thermocycling. — A. Aldijarov, A. S. Drobyshev, and S. S. Sarsembinov; **28** (4), 290-4.
Dubrovskiĭ, I. M. — Exact solution of the problem of an electron in a magnetic field consisting of a uniform field and arbitrarily arranged magnetic strings parallel to the uniform field. — I. M. Dubrovskiĭ; **28** (11), 845-52.

E

Éckl', C. — Solitons in elastic plates. — A. S. Kovalev, E. S. Sokolova, A. P. Mayer, and C. Éckl'; **28** (10), 780-8.
Engström, K. — Temperature-dependent resistance of a finite one-dimensional Josephson junction array. — K. Engström and J. M. Kinaret; **28** (1), 1-5.
Eremenko, V. V. — Irreversible magnetostriction and magnetization of superconducting 2*H*-$NbSe_2$ single crystals in a peak-effect regime. — V. V. Eremenko, V. A. Sirenko, Yu. A. Shabakayeva, R. Schleser, and P. L. Gammel; **28** (1), 6-10.
— Magnetic phase diagram of the system of manganites $Nd_{0.6}Ca_{0.4}(Mn_{1-x}Cr_x)O_3$. — I. O. Troyanchuk, M. V. Bushinsky, V. V. Eremenko, V. A. Sirenko, and H. Szymczak; **28** (1), 45-8.
— Magnetic phases in $La_{0.66}Ba_{0.34}MnO_3$: effects of temperature and elastic strains. — A. B. Beznosov, V. V. Eremenko, E. L. Fertman, V. A. Desnenko, and D. D. Khalyavin; **28** (10), 762-6.
— Magnetic polarons in Y–Ba–Cu–O chains. — V. V. Eremenko, D. V. Lukashev, and B. L. Ponomarchuk; **28** (11), 830-41.
— Structure and photoluminescence of helium-intercalated fullerite C_{60}. — I. V. Legchenkova, A. I. Prokhvatilov, Yu. E. Stetsenko, M. A. Strzhemechny, K. A. Yagotintsev, A. A. Avdeenko, V. V. Eremenko, P. V. Zinoviev, V. N. Zoryansky, N. B. Silaeva, and R. S. Ruoff; **28** (12), 942-4.
Ermolenko, A. S. — Effects of chaotic local crystal fields in pseudobinary rare-earth intermetallides. — A. S. Ermolenko; **28** (10), 749-54.

F

Fedotov, Yu. V. — Magnetic-field and temperature dependence of the critical current in thin epitaxial films of the high-temperature superconductor $YBa_2Cu_3O_{7-\delta}$. — Yu. V. Fedotov, S. M. Ryabchenko, E. A. Pashitskiĭ, A. V. Semenov, V. I. Vakaryuk, V. M. Pan, and V. S. Flis; **28** (3), 172-83.
— Low-dose radiation effects in thin films of high-temperature superconducting $YBa_2Cu_3O_{7-x}$ irradiated by 1-MeV electrons. — Yu. V. Fedotov, B. A. Danilchenko, and I. S. Rogutskiĭ; **28** (10), 739-43.
Feher, A. — Specific heat study of magnetic excitations in a one-dimensional $S = 1$ Heisenberg magnet with strong planar anisotropy. — A. Feher, M. Orendáč, A. Orendáčová, and E. Cižmár; **28** (7), 551-5.
— Manifestation of the Jahn–Teller effect in the EPR spectrum of the metalorganic complex $[Cu(en)2H_2O]SO_4$. — A. G. Anders, A. I. Kaplienko, O. V. Kravchina, V. S. Bondarenko, A. Feher, M. Orendáč, A. Orendáčová, M. Kajňaková, and J. Černák; **28** (8), 642-5.
Fertman, E. L. — Exchange interaction and magnetoresistance in $La_{2/3}Ca_{1/3}MnO_3$: experiment and models. — A. B. Beznosov, B. I. Belevtsev, E. L. Fertman, V. A. Desnenko, D. G. Naugle, K. D. D. Rathnayaka, and A. Parasiris; **28** (7), 556-61.
— Magnetic phases in $La_{0.66}Ba_{0.34}MnO_3$: effects of temperature and elastic strains. — A. B. Beznosov, V. V. Eremenko, E. L. Fertman, V. A. Desnenko, and D. D. Khalyavin; **28** (10), 762-6.
Fiebig, M. — Nonlinear optical spectroscopy of epitaxial magnetic garnet films. — V. V. Pavlov, R. V. Pisarev, M. Fiebig, and D. Fröhlich; **28** (7), 523-7.
Fil', V. D. — MgB_2: Synthesis, sound velocity, and dynamics of the vortex phase. — T. V. Ignatova, G. A. Zvyagina, I. G. Kolobov, E. A. Masalitin, V. D. Fil', Yu. V. Paderno, A. N. Bykov, V. N. Paderno, and V. I. Lyashenko; **28** (3), 190-3.
— Characteristics of the electric field accompanying a longitudinal acoustic wave in a metal. Anomaly in the superconducting phase. — Yu. A. Avramenko, E. V. Bezuglyi, N. G. Burma, I. G. Kolobov, V. D. Fil', O. A. Shevchenko, and V. M. Gokhfeld; **28** (5), 328-36.
Filippov, B. N. — Static properties and nonlinear dynamics of domain walls with a vortexlike internal structure in magnetic films (Review). — B. N. Filippov; **28** (10), 707-38.
Finkel, V. A. — Low-temperature electric conductivity of $YBa_2Cu_3O_{7-\delta}$ ceramic high-T_c superconductors with different oxygen concentrations. — V. A. Finkel; **28** (8), 687-90.
Fishman, A. Ya. — Phase transformations of the decomposition type in systems with orbital degeneracy. — M. A. Ivanov, N. K. Tkachev, and A. Ya. Fishman; **28** (8), 613-20.
Fisun, V. V. — Point-contact studies of the Kondo size effect in the alloys CuMn, CuCr, and AuFe in a magnetic field. — V. V. Fisun, I. K. Yanson, J. M. van Ruitenbeek, and J. A. Mydosh; **28** (2), 123-7.
Flis, V. S. — Magnetic-field and temperature dependence of the critical current in thin epitaxial films of the high-temperature superconductor $YBa_2Cu_3O_{7-\delta}$. — Yu. V. Fedotov, S. M. Ryabchenko, E. A. Pashitskiĭ, A. V. Semenov, V. I. Vakaryuk, V. M. Pan, and V. S. Flis; **28** (3), 172-83.
Fomenko, L. S. — Kinetics of the low-temperature structural transformation in the In–4.3 at. % Cd solid solution. — S. V. Lubenets, V. D. Natsik, L. N. Pal-Val, P. P. Pal-Val, and L. S. Fomenko; **28** (6), 465-74.
Fomenko, V. S. — Features of the low-temperature plasticity of Pb–In single crystals. — N. V. Isaev, V. S. Fomenko, V. V. Pustovalov, and I. S. Braude; **28** (5), 369-75.
Fomin, V. I. — Raman scattering in a $LiNiPO_4$ single crystal. — V. I. Fomin, V. P. Gnezdilov, V. S. Kurnosov, A. V. Peschanskii, A. V. Yeremenko, H. Schmid, J.-P. Rivera, and S. Gentil; **28** (3), 203-9.
— Light scattering on phonons in quasi-one-dimensional antiferromagnet $CsFeCl_3 \cdot 2H_2O$ induced by magnetic ordering. — V. S. Kurnosov, A. V. Peschanskii, V. I. Fomin, A. V. Yeremenko, and Yu. G. Pashkevich; **28** (7), 516-22.
Freiman, Yu. A. — Effect of nonmagnetic impurities on the spontaneous magnetostriction in β-O_2 crystals. — A. I. Prokhvatilov, Yu. A. Freiman, N. N. Galtsov, and Yu. E. Stetsenko; **28** (1), 61-5.
— Elementary excitations in solid oxygen (Review). — Yu. A. Freiman and H. J. Jodl; **28** (7), 491-504.
Fröhlich, D. — Nonlinear optical spectroscopy of epitaxial magnetic garnet films. — V. V. Pavlov, R. V. Pisarev, M. Fiebig, and D. Fröhlich; **28** (7), 523-7.
Fronc, K. — Noncollinear magnetic structures in an Fe/Si/Fe film with a ferromagnetic interlayer exchange interaction. — A. B. Chizhik, S. L. Gnatchenko, M. Baran, K. Fronc, R. Szymczak, and R. Zuberek; **28** (8), 639-41.

G

G. Zakharov, L. — Two-quantum electron spin–lattice relaxation in amorphous solids. — L. G. Zakharov, L. L. Chotorlishvili, and T. L. Buishvili; **28** (6), 412-4.

Gabovich, A. M. — Heat capacity of mesoscopically disordered superconductors: implications for MgB_2. — A. M. Gabovich, A. I. Voitenko, Mai Suan Li, and H. Szymczak; **28** (11), 803-11.

Gabuda, S. P. — Metallic properties of lead dioxide. Band structure and NMR of ^{207}Pb at low temperatures. — L. A. Boyarskiĭ, S. P. Gabuda, S. G. Kozlova, and R. N. Pletnev; **28** (8), 691-4.

Galaĭko, V. P. — Galvanomagnetic effects in the normal state of high-T_c metal oxides in a model two-band superconductor with a narrow band (level) near the Fermi boundary. — V. P. Galaĭko and E. N. Bratus'; **28** (5), 321-7.

Galtsov, N. N. — Effect of nonmagnetic impurities on the spontaneous magnetostriction in β-O_2 crystals. — A. I. Prokhvatilov, Yu. A. Freiman, N. N. Galtsov, and Yu. E. Stetsenko; **28** (1), 61-5.

— Orientational order parameter in α-N_2 from x-ray data. — N. N. Galtsov, O. A. Klenova, and M. A. Strzhemechny; **28** (5), 365-8.

Gammel, P. L. — Irreversible magnetostriction and magnetization of superconducting 2*H*-$NbSe_2$ single crystals in a peak-effect regime. — V. V. Eremenko, V. A. Sirenko, Yu. A. Shabakayeva, R. Schleser, and P. L. Gammel; **28** (1), 6-10.

Gapon, V. I. — Effect of light illumination on antiferromagnet-metamagnet phase transitions in the garnet $Ca_3Mn_2Ge_3O_{12}$. — V. A. Bedarev, V. I. Gapon, S. L. Gnatchenko, M. Baran, R. Szymczak, J. M. Desvignes, and H. Le Gall; **28** (1), 37-44.

Gatal'skaya, V. I. — Magnetic properties of a lead-doped BKBO single crystal. — S. N. Barilo, V. I. Gatal'skaya, S. V. Shiryaev, T. V. Smirnova, H. Szymczak, R. Szymczak, and M. Baran; **28** (5), 349-53.

— Magnetic properties of a $LaMn_{0.46}Co_{0.54}O_3$ single crystal. — S. N. Barilo, V. I. Gatal'skaya, S. V. Shiryaev, L. A. Kurochkin, R. Shimchak, and M. Baran; **28** (11), 853-5.

Gentil, S. — Raman scattering in a $LiNiPO_4$ single crystal. — V. I. Fomin, V. P. Gnezdilov, V. S. Kurnosov, A. V. Peschanskii, A. V. Yeremenko, H. Schmid, J.-P. Rivera, and S. Gentil; **28** (3), 203-9.

Gerasimchuk, V. S. — Drift of domain walls of the ab type in weak ferromagnets. — V. S. Gerasimchuk and A. A. Shitov; **28** (12), 877-9.

Gerasimenko, A. Yu. — Inelastic electron tunneling across magnetically active interfaces in cuprate and manganite heterostructures modified by electromigration processes. — M. A. Belogolovskiĭ, Yu. F. Revenko, A. Yu. Gerasimenko, V. M. Svistunov, E. Hatta, G. Plitnik, V. E. Shaternik, and E. M. Rudenko; **28** (6), 391-4.

Gladchenko, S. P. — Magnetotransport in a quasi-one-dimensional electron system on superfluid helium. — B. A. Nikolaenko, Yu. Z. Kovdrya, and S. P. Gladchenko; **28** (11), 859-63.

Glukhov, A. M. — Observation of stochastic resonance in percolative Josephson media. — A. M. Glukhov, A. G. Sivakov, and A. V. Ustinov; **28** (6), 383-6.

Gnatchenko, E. V. — Features of the x-ray bremsstrahlung in the scattering of intermediate-energy electrons on atoms of inert elements. — É. T. Verkhovtseva and E. V. Gnatchenko; **28** (4), 270-8.

Gnatchenko, S. L. — Effect of light illumination on antiferromagnet-metamagnet phase transitions in the garnet $Ca_3Mn_2Ge_3O_{12}$. — V. A. Bedarev, V. I. Gapon, S. L. Gnatchenko, M. Baran, R. Szymczak, J. M. Desvignes, and H. Le Gall; **28** (1), 37-44.

— Noncollinear magnetic structures in an Fe/Si/Fe film with a ferromagnetic interlayer exchange interaction. — A. B. Chizhik, S. L. Gnatchenko, M. Baran, K. Fronc, R. Szymczak, and R. Zuberek; **28** (8), 639-41.

Gnezdilov, V. P. — Raman scattering in a $LiNiPO_4$ single crystal. — V. I. Fomin, V. P. Gnezdilov, V. S. Kurnosov, A. V. Peschanskii, A. V. Yeremenko, H. Schmid, J.-P. Rivera, and S. Gentil; **28** (3), 203-9.

— Electronic Raman scattering through a stripe ordering transition in $La_{2-x}Sr_xNiO_4$. — V. P. Gnezdilov, A. V. Yeremenko, Yu. G. Pashkevich, P. Lemmens, G. Güntherodt, J. M. Tranquada, D. J. Buttrey, and K. Nakajima; **28** (7), 510-5.

Gokhfeld, V. M. — Electromagnetic surface waves in layered conductors. — V. M. Gokhfeld; **28** (3), 215-9.

— Characteristics of the electric field accompanying a longitudinal acoustic wave in a metal. Anomaly in the superconducting phase. — Yu. A. Avramenko, E. V. Bezuglyi, N. G. Burma, I. G. Kolobov, V. D. Fil', O. A. Shevchenko, and V. M. Gokhfeld; **28** (5), 328-36.

Gomonay, E. V. — Possibility of formation and reversible rearrangement of equilibrium domain structure in antiferromagnets. — E. V. Gomonay and V. M. Loktev; **28** (8), 621-9.

Gorskyi, P. V. — Low-temperature inversion of the magnetoresistance in charge-ordered layered superstructures. — P. V. Gorskyi; **28** (10), 767-70.

Gredeskul, S. — Electronic excitations and correlations in quantum bars. — I. Kuzmenko, S. Gredeskul, K. Kikoin, and Y. Avishai; **28** (7), 539-46.

Grinev, B. V. — Interaction of Pr^{3+} optical centers in the Y_2SiO_5 crystal. — Yu. V. Malyukin, P. N. Zhmurin, A. N. Lebedenko, M. A. Sholkina, B. V. Grinev, N. V. Znamenskiĭ, É. A. Manykin, Yu. V. Orlov, E. A. Petrenko, and T. G. Yukina; **28** (1), 54-7.

— Microscopic nature of Pr^{3+} optical centers in Y_2SiO_5, Lu_2SiO_5, and Gd_2SiO_5 crystals. — Yu. V. Malyukin, P. N. Zhmurin, B. V. Grinev, V. P. Seminozhenko, N. V. Znamenskiĭ, É. A. Manykin, E. A. Petrenko, and T. G. Yukina; **28** (10), 774-9.

Grishaev, V. I. — On the conditions for the existence of 1D magnetic solitons with frequency characteristics falling in the continuous spectrum. — A. M. Kosevich and V. I. Grishaev; **28** (8), 601-5.

Güntherodt, G. — Electronic Raman scattering through a stripe ordering transition in $La_{2-x}Sr_xNiO_4$. — V. P. Gnezdilov, A. V. Yeremenko, Yu. G. Pashkevich, P. Lemmens, G. Güntherodt, J. M. Tranquada, D. J. Buttrey, and K. Nakajima; **28** (7), 510-5.

Gusev, A. A. — On the criteria for superconductivity in $PrBa_2Cu_3O_{6.6}$. — F. A. Boyko, G. V. Bukin, V. A. Voloshin, and A. A. Gusev; **28** (2), 95-8.

H

Haage, T. — Fluctuation conductivity in $YBa_2Cu_3O_{7-y}$ films with different oxygen content. I. Optimally and lightly doped YBCO films. — A. L. Solovjov, H.-U. Habermeier, and T. Haage; **28** (1), 17-24.

— Fluctuation conductivity in $YBa_2Cu_3O_{7-y}$ films with different oxygen content. II. YBCO films with $T_c \approx 80$ K. — A. L. Solovjov, H.-U. Habermeier, and T. Haage; **28** (2), 99-108.

Habermeier, H.-U. — Fluctuation conductivity in $YBa_2Cu_3O_{7-y}$ films with different oxygen content. I. Optimally and lightly doped YBCO films. — A. L. Solovjov, H.-U. Habermeier, and T. Haage; **28** (1), 17-24.

— Fluctuation conductivity in $YBa_2Cu_3O_{7-y}$ films with different oxygen content. II. YBCO films with $T_c \approx 80$ K. — A. L. Solovjov, H.-U. Habermeier, and T. Haage; **28** (2), 99-108.

Harmon, B. N. — Electronic structure and magneto-optical Kerr effect in the compound $UCuP_2$. — O. Horpynyuk, V. V. Nemoshkalenko, V. N. Antonov, B. N. Harmon, and A. N. Yaresko; **28** (7), 533-8.

Hatta, E. — Inelastic electron tunneling across magnetically active interfaces in cuprate and manganite heterostructures modified by electromigration processes. — M. A. Belogolovskiĭ, Yu. F. Revenko, A. Yu. Gerasimenko, V. M. Svistunov, E. Hatta, G. Plitnik, V. E. Shaternik, and E. M. Rudenko; **28** (6), 391-4.

Horpynyuk, O. — Electronic structure and magneto-optical Kerr effect in the compound $UCuP_2$. — O. Horpynyuk, V. V. Nemoshkalenko, V. N. Antonov, B. N. Harmon, and A. N. Yaresko; **28** (7), 533-8.

Huth, M. — Guided vortex motion in faceted niobium films. — A. K. Soroka and M. Huth; **28** (11), 842-4.

I

Ignatova, T. V. — MgB_2: Synthesis, sound velocity, and dynamics of the vortex phase. — T. V. Ignatova, G. A. Zvyagina, I. G. Kolobov, E. A. Masalitin, V. D. Fil', Yu. V. Paderno, A. N. Bykov, V. N. Paderno, and V. I. Lyashenko; **28** (3), 190-3.

Ignatyeva, T. A. — Features of the thermopower of Mo–Re and Mo–Re–Nb alloys and the electronic–topological transition in these systems. — T. A. Ignatyeva and A. N. Velikodny; **28** (6), 403-11.

Isaev, N. V. — Features of the low-temperature plasticity of Pb–In single crystals. — N. V. Isaev, V. S. Fomenko, V. V. Pustovalov, and I. S. Braude; **28** (5), 369-75.

Ishchuk, V. M. — Aging effect on the magnetic and transport properties of laser-deposited $La_{0.5}Sr_{0.5}CoO_{3-\delta}$ films. — V. G. Prokhorov, G. G. Kaminskiĭ, V. M. Ishchuk, I. N. Chukanova, Y. P. Lee, and K. W. Kim; **28** (5), 354-8.

Ivanchenko, E. A. — Magnetization dynamics of electron–impurity systems at paramagnetic resonance. — E. A. Ivanchenko; **28** (2), 117-22.

Ivanov, A. I. — Thermal conductivity of a GaAs single crystal grown in microgravity. — A. I. Ivanov, A. N. Luk'yanov, B. A. Merisov, A. V. Sologubenko, and G. Ya. Khadjai; **28** (6), 462-4.
Ivanov, B. A. — Inhomogeneous states for small magnetic particles with exchange anisotropy. — B. A. Ivanov, A. Ya. Volk, and A. Yu. Merkulov; **28** (1), 25-9.
Ivanov, M. A. — Phase transformations of the decomposition type in systems with orbital degeneracy. — M. A. Ivanov, N. K. Tkachev, and A. Ya. Fishman; **28** (8), 613-20.
Ivanova, I. M. — Features of the magnetization of an antiferromagnet with single-ion anisotropy of the easy-plane type and with ion spins $S = 1$. — V. M. Kalita, I. M. Ivanova, and V. M. Loktev; **28** (6), 475-7.

J

Jansen, A. G. M. — Direct evidence for the occurrence of superconductivity in the magnetic compound YFe_4Al_8. — V. M. Dmitriev, L. F. Rybaltchenko, P. Wyder, A. G. M. Jansen, N. N. Prentslau, and W. Suski; **28** (4), 260-2.
Jodl, H. J. — Elementary excitations in solid oxygen (Review). — Yu. A. Freiman and H. J. Jodl; **28** (7), 491-504.
Jonson, M. — Key role of intramolecular Jahn–Teller vibrations and multivalley nature of the band spectrum in the mechanism of superconductivity in doped C_{60} fullerites. — V. M. Loktev, É. A. Pashitskiĭ, R. Shekhter, and M. Jonson; **28** (11), 821-9.

K

Kadan, V. M. — Influence of structural inhomogeneity on the luminescence properties of silicon nanocrystallites. — I. V. Blonskiĭ, M. S. Brodyn, A. Yu. Vakhnin, A. Ya. Zhugayevych, V. M. Kadan, and A. K. Kadashchuk; **28** (8), 706-12.
Kadashchuk, A. K. — Influence of structural inhomogeneity on the luminescence properties of silicon nanocrystallites. — I. V. Blonskiĭ, M. S. Brodyn, A. Yu. Vakhnin, A. Ya. Zhugayevych, V. M. Kadan, and A. K. Kadashchuk; **28** (8), 706-12.
Kajňaková, M. — Manifestation of the Jahn–Teller effect in the EPR spectrum of the metalorganic complex $[Cu(en)2H_2O]SO_4$. — A. G. Anders, A. I. Kaplienko, O. V. Kravchina, V. S. Bondarenko, A. Feher, M. Orendáč, A. Orendáčová, M. Kajňaková, and J. Černák; **28** (8), 642-5.
Kalita, V. M. — On the non-Heisenberg contribution to the spin–spin interaction of an antiferromagnet with $S = 3/2$. — V. M. Kalita and A. F. Lozenko; **28** (1), 66-8.
— Magnetostriction of the antiferromagnet $NiCl_2$ in the homogeneous and multidomain states. — V. M. Kalita, A. F. Lozenko, and P. A. Trotsenko; **28** (4), 263-6.
— Features of the magnetization of an antiferromagnet with single-ion anisotropy of the easy-plane type and with ion spins $S = 1$. — V. M. Kalita, I. M. Ivanova, and V. M. Loktev; **28** (6), 475-7.
— On the theory of magnetic phase transitions in magnets with a large single-ion anisotropy. — V. M. Kalita and V. M. Loktev; **28** (12), 883-8.
Kalko, T. V. — Concentration dependence of the attenuation of first sound in supersaturated superfluid ^3He–^4He solutions under pressure. — A. A. Zadorozhko, T. V. Kalko, E. Ya. Rudavskiĭ, I. A. Usherov-Marshak, V. K. Chagovets, and G. A. Sheshin; **28** (2), 73-8.
Kamenev, V. I. — Features of the magnetic behavior of $Mn_{2-x}Cr_xSb$ alloys in the low-temperature state. — V. I. Val'kov, V. I. Kamenev, S. A. Buzhinsky, and N. A. Romanova; **28** (3), 194-8.
Kameneva, M. Yu. — Anomalies of the electronic heat capacity of thulium cuprates in the pseudogap phase region. — E. B. Amitin, K. R. Zhdanov, M. Yu. Kameneva, Yu. A. Kovalevskaya, L. P. Kozeeva, I. E. Paukov, and A. G. Blinov; **28** (8), 669-73.
Kaminskiĭ, G. G. — Aging effect on the magnetic and transport properties of laser-deposited $La_{0.5}Sr_{0.5}CoO_{3-\delta}$ films. — V. G. Prokhorov, G. G. Kaminskiĭ, V. M. Ishchuk, I. N. Chukanova, Y. P. Lee, and K. W. Kim; **28** (5), 354-8.
Kaminsky, G. G. — Giant resistance switching effect in nano-scale twinned $La_{0.65}Ca_{0.35}MnO_3$ film. — V. G. Prokhorov, G. G. Kaminsky, V. A. Komashko, Y. P. Lee, A. I. Tovstolytkin, and A. N. Pogorily; **28** (11), 856-8.
Kaplienko, A. I. — Manifestation of the Jahn–Teller effect in the EPR spectrum of the metalorganic complex $[Cu(en)2H_2O]SO_4$. — A. G. Anders, A. I. Kaplienko, O. V. Kravchina, V. S. Bondarenko, A. Feher, M. Orendáč, A. Orendáčová, M. Kajňaková, and J. Černák; **28** (8), 642-5.
Karnatsevich, L. V. — Equation of state of an equimolar ^3He–^4He mixture. — L. V. Karnatsevich, R. M. Sibileva, M. A. Khazhmuradov, I. N. Shapoval, and A. V. Meriuz; **28** (4), 235-8.
Kekutiya, Sh. E. — Sound propagation in a porous medium filled with superfluid helium. — Sh. E. Kekutiya and N. D. Chkhaidze; **28** (11), 795-802.
Khadjai, G. Ya. — Thermal conductivity of a GaAs single crystal grown in microgravity. — A. I. Ivanov, A. N. Luk'yanov, B. A. Merisov, A. V. Sologubenko, and G. Ya. Khadjai; **28** (6), 462-4.
Khaĭbullin, I. B. — Reinforcement of pinning by surface magnetic microparticles in high-T_c superconductors. — P. N. Togulev, V. V. Bazarov, I. B. Khaĭbullin, and N. M. Suleĭmanov; **28** (4), 250-3.
Khalyavin, D. D. — Magnetic phases in $La_{0.66}Ba_{0.34}MnO_3$: effects of temperature and elastic strains. — A. B. Beznosov, V. V. Eremenko, E. L. Fertman, V. A. Desnenko, and D. D. Khalyavin; **28** (10), 762-6.
Kharchenko, N. F. — Photoinduced magnetic linear dichroism in a YIG:Co film. — O. V. Miloslavska, Yu. N. Kharchenko, N. F. Kharchenko, V. G. Yurko, A. Stupakiewicz, and A. Maziewski; **28** (4), 267-9.
— Nonmonotonic temperature dependence of the spontaneous magnetization of the antiferromagnetic crystal $LiCoPO_4$. — N. F. Kharchenko, V. A. Desnenko, Yu. N. Kharchenko, R. Szymczak, and M. Baran; **28** (8), 646-52.
Kharchenko, Yu. N. — Photoinduced magnetic linear dichroism in a YIG:Co film. — O. V. Miloslavska, Yu. N. Kharchenko, N. F. Kharchenko, V. G. Yurko, A. Stupakiewicz, and A. Maziewski; **28** (4), 267-9.
— Nonmonotonic temperature dependence of the spontaneous magnetization of the antiferromagnetic crystal $LiCoPO_4$. — N. F. Kharchenko, V. A. Desnenko, Yu. N. Kharchenko, R. Szymczak, and M. Baran; **28** (8), 646-52.
Kharrasov, M. Kh. — Magnetoelastic waves in multisublattice systems. — I. R. Kyzyrgulov and M. Kh. Kharrasov; **28** (11), 875-6.
Khatsko, E. N. — Resonance properties of the quasi-one-dimensional Ising magnet $[(CH_3)_3NH]CoCl_3 \cdot 2H_2O$ in the paramagnetic and magnetically ordered phases. — M. I. Kobets, E. N. Khatsko, V. A. Pashchenko, A. S. Chernyi, K. G. Dergachev, and V. G. Borisenko; **28** (12), 889-95.
Khatuntsev, V. I. — Low-temperature unsteady creep of parahydrogen single crystals. — L. A. Alekseeva, A. V. Pustovalova, V. I. Khatuntsev, and Yu. V. Butenko; **28** (1), 58-60.
Khazhmuradov, M. A. — Equation of state of an equimolar ^3He–^4He mixture. — L. V. Karnatsevich, R. M. Sibileva, M. A. Khazhmuradov, I. N. Shapoval, and A. V. Meriuz; **28** (4), 235-8.
Khokhlov, A. V. — Manifestation of two-dimensional behavior of YBCO films in a study of their complex susceptibility. — A. V. Khokhlov, A. Yu. Prokhorov, V. F. Drobotko, G. G. Levchenko, and A. V. Klimov; **28** (6), 377-82.
Kikoin, K. — Electronic excitations and correlations in quantum bars. — I. Kuzmenko, S. Gredeskul, K. Kikoin, and Y. Avishai; **28** (7), 539-46.
Kim, K. W. — Aging effect on the magnetic and transport properties of laser-deposited $La_{0.5}Sr_{0.5}CoO_{3-\delta}$ films. — V. G. Prokhorov, G. G. Kaminskiĭ, V. M. Ishchuk, I. N. Chukanova, Y. P. Lee, and K. W. Kim; **28** (5), 354-8.
Kinaret, J. M. — Temperature-dependent resistance of a finite one-dimensional Josephson junction array. — K. Engström and J. M. Kinaret; **28** (1), 1-5.
Kirichenko, O. V. — Low-frequency quantum oscillations of the impedance of layered conductors at high magnetic field. — O. V. Kirichenko and I. V. Kozlov; **28** (5), 359-64.
Klenova, O. A. — Orientational order parameter in α-N_2 from x-ray data. — N. N. Galtsov, O. A. Klenova, and M. A. Strzhemechny; **28** (5), 365-8.
Klimov, A. V. — Manifestation of two-dimensional behavior of YBCO films in a study of their complex susceptibility. — A. V. Khokhlov, A. Yu. Prokhorov, V. F. Drobotko, G. G. Levchenko, and A. V. Klimov; **28** (6), 377-82.
Klymenko, Yu. O. — Manifestation of Coulomb blockade effects at an arbitrary degeneracy of the levels of a molecular contact. — Yu. O. Klymenko; **28** (6), 395-402.

Kobets, M. I. — Resonance properties of the quasi-one-dimensional Ising magnet $[(CH_3)_3NH]CoCl_3 \cdot 2H_2O$ in the paramagnetic and magnetically ordered phases. — M. I. Kobets, E. N. Khatsko, V. A. Pashchenko, A. S. Chernyi, K. G. Dergachev, and V. G. Borisenko; **28** (12), 889-95.

Kochkanjan, R. O. — EPR spectrum of the Fe^{3+} ion in bromcresol green ($C_{21}H_{14}Br_4O_5S$) and features in the dynamics of the surrounding molecules. — V. V. Chabanenko, V. N. Vasyukov, R. O. Kochkanjan, M. M. Nechitailov, H. Szymczak, S. Piechota, and A. Nabialek; **28** (1), 49-53.

Kojima, N. — Recent progress in magneto-optics and research on its application (Review). — N. Kojima and K. Tsushima; **28** (7), 480-90.

Kokotin, A. M. — Watergel—a new form of water condensed in liquid ^{4}He. — A. M. Kokotin and L. P. Mezhov-Deglin; **28** (3), 165-71.

Kolesnichenko, Yu. A. — Josephson effect in point contacts between "*f*-wave" superconductors. — R. Mahmoodi, S. N. Shevchenko, and Yu. A. Kolesnichenko; **28** (3), 184-9.

Kolmakova, N. P. — Features of the magnetic properties of rare-earth intermetallides RMn_2Ge_2 (Review). — N. P. Kolmakova, A. A. Sidorenko, and R. Z. Levitin; **28** (8), 653-68.

Kolobov, I. G. — MgB_2: Synthesis, sound velocity, and dynamics of the vortex phase. — T. V. Ignatova, G. A. Zvyagina, I. G. Kolobov, E. A. Masalitin, V. D. Fil', Yu. V. Paderno, A. N. Bykov, V. N. Paderno, and V. I. Lyashenko; **28** (3), 190-3.

— Characteristics of the electric field accompanying a longitudinal acoustic wave in a metal. Anomaly in the superconducting phase. — Yu. A. Avramenko, E. V. Bezuglyi, N. G. Burma, I. G. Kolobov, V. D. Fil', O. A. Shevchenko, and V. M. Gokhfeld; **28** (5), 328-36.

Komashko, V. A. — Giant resistance switching effect in nano-scale twinned $La_{0.65}Ca_{0.35}MnO_3$ film. — V. G. Prokhorov, G. G. Kaminsky, V. A. Komashko, Y. P. Lee, A. I. Tovstolytkin, and A. N. Pogorily; **28** (11), 856-8.

Konstantinov, V. A. — Molar volume dependence of the thermal conductivity in mixed cryocrystals. — V. A. Konstantinov, E. S. Orel, and V. P. Revyakin; **28** (2), 136-9.

Kopeliovich, A. I. — On the deviations from Matthiessen's rule in quasi-one-dimensional conductors. — A. I. Kopeliovich, A. A. Mamalui, L. G. Petrenko, and T. N. Shelest; **28** (10), 771-3.

Kosevich, A. M. — On the conditions for the existence of 1D magnetic solitons with frequency characteristics falling in the continuous spectrum. — A. M. Kosevich and V. I. Grishaev; **28** (8), 601-5.

Koshkin, V. M. — Instability zones and short-lived defects in the physics of crystals. — V. M. Koshkin; **28** (8), 695-705.

Kovalenko, E. N. — Excitons in the layered insulators ZnI_2 and CdI_2:Zn. — O. N. Yunakova, V. K. Miloslavsky, and E. N. Kovalenko; **28** (4), 284-9.

Kovalev, A. S. — Dynamical chaos and low-temperature surface diffusion of small adatom clusters. — A. S. Kovalev and A. I. Landau; **28** (6), 423-8.

— Multidimensional and surface solitons in a nonlinear elastic medium. — A. S. Kovalev, E. S. Syrkin, and J. A. Maugin; **28** (6), 452-61.

— Solitons in elastic plates. — A. S. Kovalev, E. S. Sokolova, A. P. Mayer, and C. Eckl'; **28** (10), 780-8.

— Mechanism of vortex switching in magnetic nanodots under a circular magnetic field. I. Resonance action of the field on the nanodot eigenmodes. — A. S. Kovalev and J. E. Prilepsky; **28** (12), 921-9.

Kovaleva, V. N. — Staged work hardening of polycrystalline titanium at low temperatures and its relation to substructure evolution. — V. A. Moskalenko, A. R. Smirnov, V. N. Kovaleva, and V. D. Natsik; **28** (12), 935-41.

Kovalevskaya, Yu. A. — Anomalies of the electronic heat capacity of thulium cuprates in the pseudogap phase region. — E. B. Amitin, K. R. Zhdanov, M. Yu. Kameneva, Yu. A. Kovalevskaya, L. P. Kozeeva, I. E. Paukov, and A. G. Blinov; **28** (8), 669-73.

Kovalevsky, M. Yu. — On the classification of equilibrium superfluid states with scalar and tensor order parameters. — M. Yu. Kovalevsky, S. V. Peletminsky, and N. N. Chekanova; **28** (4), 227-34.

Kovdrya, Yu. Z. — Magnetotransport in a quasi-one-dimensional electron system on superfluid helium. — B. A. Nikolaenko, Yu. Z. Kovdrya, and S. P. Gladchenko; **28** (11), 859-63.

Kovtun, H. A. — Wigner-like crystallization of Anderson-localized electron systems with low electron densities. — A. A. Slutskin, H. A. Kovtun, and M. Pepper; **28** (12), 930-4.

Kozeeva, L. P. — Anomalies of the electronic heat capacity of thulium cuprates in the pseudogap phase region. — E. B. Amitin, K. R. Zhdanov, M. Yu. Kameneva, Yu. A. Kovalevskaya, L. P. Kozeeva, I. E. Paukov, and A. G. Blinov; **28** (8), 669-73.

Kozlov, I. V. — Low-frequency quantum oscillations of the impedance of layered conductors at high magnetic field. — O. V. Kirichenko and I. V. Kozlov; **28** (5), 359-64.

Kozlova, S. G. — Metallic properties of lead dioxide. Band structure and NMR of ^{207}Pb at low temperatures. — L. A. Boyarskiĭ, S. P. Gabuda, S. G. Kozlova, and R. N. Pletnev; **28** (8), 691-4.

Kramar, O. — Metallic ferromagnetism in a generalized Hubbard model. — L. Didukh and O. Kramar; **28** (1), 30-6.

Kravchina, O. V. — Manifestation of the Jahn–Teller effect in the EPR spectrum of the metalorganic complex $[Cu(en)2H_2O]SO_4$. — A. G. Anders, A. I. Kaplienko, O. V. Kravchina, V. S. Bondarenko, A. Feher, M. Orendáč, A. Orendáčová, M. Kajňaková, and J. Černák; **28** (8), 642-5.

Kreines, N. M. — Investigation of interlayer coupling in $[Fe/Cr]_n$ magnetic multilayer structures by the ferromagnetic resonance method (Review). — N. M. Kreines; **28** (8), 581-91.

Krivenko, S. A. — Flux-line pinning by columnar magnetic defects in a type-II superconductor. — S. A. Krivenko and N. M. Suleĭmanov; **28** (4), 247-9.

Kucherenko, S. S. — Elastic-strain mechanisms for the influence of temperature, magnetic field, and pressure on the resistive and magnetic properties of magnetic semiconductors. — P. I. Polyakov and S. S. Kucherenko; **28** (10), 744-8.

Kulinich, S. I. — Influence of dissipation on a low-voltage dc current in a long SNS junction. — S. I. Kulinich and R. I. Shekhter; **28** (7), 547-50.

Kurnosov, V. S. — Raman scattering in a $LiNiPO_4$ single crystal. — V. I. Fomin, V. P. Gnezdilov, V. S. Kurnosov, A. V. Peschanskii, A. V. Yeremenko, H. Schmid, J.-P. Rivera, and S. Gentil; **28** (3), 203-9.

— Light scattering on phonons in quasi-one-dimensional antiferromagnet $CsFeCl_3 \cdot 2H_2O$ induced by magnetic ordering. — V. S. Kurnosov, A. V. Peschanskii, V. I. Fomin, A. V. Yeremenko, and Yu. G. Pashkevich; **28** (7), 516-22.

Kurochkin, L. A. — Magnetic properties of a $LaMn_{0.46}Co_{0.54}O_3$ single crystal. — S. N. Barilo, V. I. Gatal'skaya, S. V. Shiryaev, L. A. Kurochkin, R. Shimchak, and M. Baran; **28** (11), 853-5.

Kuz'menko, A. P. — Low-temperature domain-wall dynamics in weak ferromagnets. — A. P. Kuz'menko; **28** (5), 337-48.

Kuzmenko, I. — Electronic excitations and correlations in quantum bars. — I. Kuzmenko, S. Gredeskul, K. Kikoin, and Y. Avishai; **28** (7), 539-46.

Kyzyrgulov, I. R. — Magnetoelastic waves in multisublattice systems. — I. R. Kyzyrgulov and M. Kh. Kharrasov; **28** (11), 875-6.

L

Landau, A. I. — Dynamical chaos and low-temperature surface diffusion of small adatom clusters. — A. S. Kovalev and A. I. Landau; **28** (6), 423-8.

Lebedenko, A. N. — Interaction of Pr^{3+} optical centers in the Y_2SiO_5 crystal. — Yu. V. Malyukin, P. N. Zhmurin, A. N. Lebedenko, M. A. Sholkina, B. V. Grinev, N. V. Znamenskiĭ, E. A. Manykin, Yu. V. Orlov, E. A. Petrenko, and T. G. Yukina; **28** (1), 54-7.

Lee, Y. P. — Aging effect on the magnetic and transport properties of laser-deposited $La_{0.5}Sr_{0.5}CoO_{3-\delta}$ films. — V. G. Prokhorov, G. G. Kaminskiĭ, V. M. Ishchuk, I. N. Chukanova, Y. P. Lee, and K. W. Kim; **28** (5), 354-8.

— Giant resistance switching effect in nano-scale twinned $La_{0.65}Ca_{0.35}MnO_3$ film. — V. G. Prokhorov, G. G. Kaminsky, V. A. Komashko, Y. P. Lee, A. I. Tovstolytkin, and A. N. Pogorily; **28** (11), 856-8.

Le Gall, H. — Effect of light illumination on antiferromagnet-metamagnet phase transitions in the garnet $Ca_3Mn_2Ge_3O_{12}$. — V. A. Bedarev, V. I. Gapon, S. L. Gnatchenko, M. Baran, R. Szymczak, J. M. Desvignes, and H. Le Gall; **28** (1), 37-44.

Legchenkova, I. V. — Structure and photoluminescence of helium-intercalated fullerite C_{60}. — I. V. Legchenkova, A. I. Prokhvatilov, Yu. E. Stetsenko, M. A. Strzhemechny, K. A. Yagotintsev, A. A. Avdeenko, V. V. Eremenko, P. V. Zinoviev, V. N. Zoryansky, N. B. Silaeva, and R. S. Ruoff; **28** (12), 942-4.

Lemmens, P. — Electronic Raman scattering through a stripe ordering transition in $La_{2-x}Sr_xNiO_4$. — V. P. Gnezdilov, A. V. Yeremenko, Yu. G. Pashkevich, P. Lemmens, G. Güntherodt, J. M. Tranquada, D. J. Buttrey, and K. Nakajima; **28** (7), 510-5.

Levchenko, G. G. — Manifestation of two-dimensional behavior of YBCO films in a study of their complex susceptibility. — A. V. Khokhlov, A. Yu. Prokhorov, V. F. Drobotko, G. G. Levchenko, and A. V. Klimov; **28** (6), 377-82.

Levitin, R. Z. — Features of the magnetic properties of rare-earth intermetallides RMn_2Ge_2 (Review). — N. P. Kolmakova, A. A. Sidorenko, and R. Z. Levitin; **28** (8), 653-68.

Li, Mai Suan — Heat capacity of mesoscopically disordered superconductors: implications for MgB_2. — A. M. Gabovich, A. I. Voitenko, Mai Suan Li, and H. Szymczak; **28** (11), 803-11.

Libin, M. Yu. — Optical spectroscopy of antiferromagnetic correlations and the stripe state in the superconductor $YBa_2Cu_3O_{6+x}$. — V. N. Samovarov, V. L. Vakula, M. Yu. Libin, S. A. Uyutnov, and G. G. Sergeeva; **28** (8), 674-86.

Lockwood, D. J. — Spin–phonon interaction and mode softening in NiF_2. — D. J. Lockwood; **28** (7), 505-9.

Loginov, A. A. — Magnetic field induced phase transition in $KEr(MoO_4)_2$. Vibronic model. — A. A. Loginov; **28** (10), 755-61.

Loktev, V. M. — On the magnetic anisotropy of La_2CuO_4 above the Néel temperature. — V. M. Loktev; **28** (1), 69-71.

— Spectral function and character of the motion of a conduction electron in an orientationally disordered molecular cryocrystal. — V. M. Loktev, S. G. Sharapov, and H. Beck; **28** (3), 220-6.

— On the role of Jahn–Teller vibrations in the mechanism of high-T_c superconductivity of intercalated C_{60} fullerite films with *p*-type conductivity. — V. M. Loktev and E. A. Pashitskiĭ; **28** (4), 295-7.

— Features of the magnetization of an antiferromagnet with single-ion anisotropy of the easy-plane type and with ion spins $S = 1$. — V. M. Kalita, I. M. Ivanova, and V. M. Loktev; **28** (6), 475-7.

— Possibility of formation and reversible rearrangement of equilibrium domain structure in antiferromagnets. — E. V. Gomonay and V. M. Loktev; **28** (8), 621-9.

— Key role of intramolecular Jahn–Teller vibrations and multivalley nature of the band spectrum in the mechanism of superconductivity in doped C_{60} fullerites. — V. M. Loktev, É. A. Pashitskiĭ, R. Shekhter, and M. Jonson; **28** (11), 821-9.

— On the theory of magnetic phase transitions in magnets with a large single-ion anisotropy. — V. M. Kalita and V. M. Loktev; **28** (12), 883-8.

Lozenko, A. F. — On the non-Heisenberg contribution to the spin–spin interaction of an antiferromagnet with $S = 3/2$. — V. M. Kalita and A. F. Lozenko; **28** (1), 66-8.

— Magnetostriction of the antiferromagnet $NiCl_2$ in the homogeneous and multidomain states. — V. M. Kalita, A. F. Lozenko, and P. A. Trotsenko; **28** (4), 263-6.

Lubenets, S. V. — Kinetics of the low-temperature structural transformation in the In–4.3 at. % Cd solid solution. — S. V. Lubenets, V. D. Natsik, L. N. Pal-Val, P. P. Pal-Val, and L. S. Fomenko; **28** (6), 465-74.

Lukashev, D. V. — Magnetic polarons in Y–Ba–Cu–O chains. — V. V. Eremenko, D. V. Lukashev, and B. L. Ponomarchuk; **28** (11), 830-41.

Luk'yanov, A. N. — Thermal conductivity of a GaAs single crystal grown in microgravity. — A. I. Ivanov, A. N. Luk'yanov, B. A. Merisov, A. V. Sologubenko, and G. Ya. Khadjai; **28** (6), 462-4.

Lyashenko, V. I. — MgB_2: Synthesis, sound velocity, and dynamics of the vortex phase. — T. V. Ignatova, G. A. Zvyagina, I. G. Kolobov, E. A. Masalitin, V. D. Fil', Yu. V. Paderno, A. N. Bykov, V. N. Paderno, and V. I. Lyashenko; **28** (3), 190-3.

M

Mahmoodi, R. — Josephson effect in point contacts between "*f*-wave" superconductors. — R. Mahmoodi, S. N. Shevchenko, and Yu. A. Kolesnichenko; **28** (3), 184-9.

Maidanov, V. A. — Spin–lattice relaxation in the bcc phase of phase-separated ^{3}He–^{4}He solid mixtures. — N. P. Mikhin, V. A. Maidanov, and A. V. Polev; **28** (4), 239-41.

Makedonska, N. I. — On the transverse magnetization of the anisotropic superconductor $2H$–$NbSe_2$. — V. A. Sirenko, N. I. Makedonska, Yu. A. Shabakayeva, and R. Schleser; **28** (7), 574-8.

Malyukin, Yu. V. — Interaction of Pr^{3+} optical centers in the Y_2SiO_5 crystal. — Yu. V. Malyukin, P. N. Zhmurin, A. N. Lebedenko, M. A. Sholkina, B. V. Grinev, N. V. Znamenskiĭ, É. A. Manykin, Yu. V. Orlov, E. A. Petrenko, and T. G. Yukina; **28** (1), 54-7.

— Microscopic nature of Pr^{3+} optical centers in Y_2SiO_5, Lu_2SiO_5, and Gd_2SiO_5 crystals. — Yu. V. Malyukin, P. N. Zhmurin, B. V. Grinev, V. P. Seminozhenko, N. V. Znamenskiĭ, É. A. Manykin, E. A. Petrenko, and T. G. Yukina; **28** (10), 774-9.

Mamalui, A. A. — On the deviations from Matthiessen's rule in quasi-one-dimensional conductors. — A. I. Kopeliovich, A. A. Mamalui, L. G. Petrenko, and T. N. Shelest; **28** (10), 771-3.

Mantytskaja, O. S. — Magnetic phase transitions in the system $La_{1-x}Bi_xMnO_{3+\lambda}$. — I. O. Troyanchuk, O. S. Mantytskaja, H. Szymczak, and M. Yu. Shvedun; **28** (7), 569-73.

Manykin, É. A. — Interaction of Pr^{3+} optical centers in the Y_2SiO_5 crystal. — Yu. V. Malyukin, P. N. Zhmurin, A. N. Lebedenko, M. A. Sholkina, B. V. Grinev, N. V. Znamenskiĭ, É. A. Manykin, Yu. V. Orlov, E. A. Petrenko, and T. G. Yukina; **28** (1), 54-7.

— Microscopic nature of Pr^{3+} optical centers in Y_2SiO_5, Lu_2SiO_5, and Gd_2SiO_5 crystals. — Yu. V. Malyukin, P. N. Zhmurin, B. V. Grinev, V. P. Seminozhenko, N. V. Znamenskiĭ, É. A. Manykin, E. A. Petrenko, and T. G. Yukina; **28** (10), 774-9.

Masalitin, E. A. — MgB_2: Synthesis, sound velocity, and dynamics of the vortex phase. — T. V. Ignatova, G. A. Zvyagina, I. G. Kolobov, E. A. Masalitin, V. D. Fil', Yu. V. Paderno, A. N. Bykov, V. N. Paderno, and V. I. Lyashenko; **28** (3), 190-3.

Mashkevich, S. V. — Self-consistent calculation of the spectrum of quasiparticles in a superfluid Bose liquid with a quenched Bose–Einstein condensate. — É. A. Pashitskiĭ, S. I. Vilchinsky, and S. V. Mashkevich; **28** (2), 79-84.

Maugin, J. A. — Multidimensional and surface solitons in a nonlinear elastic medium. — A. S. Kovalev, E. S. Syrkin, and J. A. Maugin; **28** (6), 452-61.

Mayer, A. P. — Solitons in elastic plates. — A. S. Kovalev, E. S. Sokolova, A. P. Mayer, and C. Eckl'; **28** (10), 780-8.

Maziewski, A. — Photoinduced magnetic linear dichroism in a YIG:Co film. — O. V. Miloslavska, Yu. N. Kharchenko, N. F. Kharchenko, V. G. Yurko, A. Stupakiewicz, and A. Maziewski; **28** (4), 267-9.

Mazilova, T. I. — Field emission microscopy of the cluster and subcluster structure of a Zr–Ti–Cu–Ni–Be bulk metallic glass. — A. S. Bakaĭ, I. M. Mikhailovskij, T. I. Mazilova, and N. Wanderka; **28** (4), 279-83.

Medvedev, Yu. V. — Steady state diagram of current-carrying layered superconductors. — A. N. Artemov and Yu. V. Medvedev; **28** (4), 242-6.

Merisov, B. A. — Thermal conductivity of a GaAs single crystal grown in microgravity. — A. I. Ivanov, A. N. Luk'yanov, B. A. Merisov, A. V. Sologubenko, and G. Ya. Khadjai; **28** (6), 462-4.

Meriuz, A. V. — Equation of state of an equimolar ^{3}He–^{4}He mixture. — L. V. Karnatsevich, R. M. Sibileva, M. A. Khazhmuradov, I. N. Shapoval, and A. V. Meriuz; **28** (4), 235-8.

Merkulov, A. Yu. — Inhomogeneous states for small magnetic particles with exchange anisotropy. — B. A. Ivanov, A. Ya. Volk, and A. Yu. Merkulov; **28** (1), 25-9.

Mezhov-Deglin, L. P. — Watergel—a new form of water condensed in liquid ^{4}He. — A. M. Kokotin and L. P. Mezhov-Deglin; **28** (3), 165-71.

Mikhailovskij, I. M. — Field emission microscopy of the cluster and subcluster structure of a Zr–Ti–Cu–Ni–Be bulk metallic glass. — A. S. Bakaĭ, I. M. Mikhailovskij, T. I. Mazilova, and N. Wanderka; **28** (4), 279-83.

Mikhin, N. P. — Spin–lattice relaxation in the bcc phase of phase-separated ^{3}He–^{4}He solid mixtures. — N. P. Mikhin, V. A. Maidanov, and A. V. Polev; **28** (4), 239-41.

Miloslavska, O. V. — Photoinduced magnetic linear dichroism in a YIG:Co film. — O. V. Miloslavska, Yu. N. Kharchenko, N. F. Kharchenko, V. G. Yurko, A. Stupakiewicz, and A. Maziewski; **28** (4), 267-9.

Miloslavsky, V. K. — Excitons in the layered insulators ZnI_2 and CdI_2:Zn. — O. N. Yunakova, V. K. Miloslavsky, and E. N. Kovalenko; **28** (4), 284-9.

Mirsaev, I. F. — Purely antiferromagnetic spin waves (antimagnons) in tetragonal magnets and ways of exciting them. — E. A. Turov and I. F. Mirsaev; **28** (8), 592-600.

Mishkuf, Ĭ. — Low-temperature deformation and fracture of bulk nanostructural titanium obtained by intense plastic deformation using equal channel angular pressing. — V. Z. Bengus, E. D. Tabachnikova, V. D. Natsik, Ĭ. Mishkuf, K. Chakh, V. V. Stolyarov, and R. Z. Valiev; **28** (11), 864-74.

Moskalenko, V. A. — Staged work hardening of polycrystalline titanium at low temperatures and its relation to substructure evolution. — V. A. Moskalenko, A. R. Smirnov, V. N. Kovaleva, and V. D. Natsik; **28** (12), 935-41.

Mydosh, J. A. — Point-contact studies of the Kondo size effect in the alloys CuMn, CuCr, and AuFe in a magnetic field. — V. V. Fisun, I. K. Yanson, J. M. van Ruitenbeek, and J. A. Mydosh; **28** (2), 123-7.

N

Nabialek, A. — EPR spectrum of the Fe^{3+} ion in bromcresol green ($C_{21}H_{14}Br_4O_5S$) and features in the dynamics of the surrounding molecules. — V. V. Chabanenko, V. N. Vasyukov, R. O. Kochkanjan, M. M. Nechitailov, H. Szymczak, S. Piechota, and A. Nabialek; **28** (1), 49-53.

— Excitation of oscillations of the magnetic induction in a Nb–Ti slab as a result of a thermomagnetic flux avalanche. — V. V. Chabanenko, V. F. Rusakov, V. A. Yampol'skiĭ, H. Szymczak, S. Piechota, S. Vasiliev, and A. Nabialek; **28** (6), 387-90.

Nakajima, K. — Electronic Raman scattering through a stripe ordering transition in $La_{2-x}Sr_xNiO_4$. — V. P. Gnezdilov, A. V. Yeremenko, Yu. G. Pashkevich, P. Lemmens, G. Güntherodt, J. M. Tranquada, D. J. Buttrey, and K. Nakajima; **28** (7), 510-5.

Naletov, V. V. — Magnetic coupling between liquid ^{3}He and solid insulators (Review). — V. V. Naletov, M. S. Tagirov, and D. A. Tayurskiĭ; **28** (5), 299-311.

Nath, A. — Anomalous magnetic and dynamic behavior in magnetoresistive compounds: origin of bulk colossal magnetoresistivity. — V. Chechersky and A. Nath; **28** (7), 562-8.

Natsik, V. D. — Kinetics of the low-temperature structural transformation in the In–4.3 at. % Cd solid solution. — S. V. Lubenets, V. D. Natsik, L. N. Pal-Val, P. P. Pal-Val, and L. S. Fomenko; **28** (6), 465-74.

— Low-temperature deformation and fracture of bulk nanostructural titanium obtained by intense plastic deformation using equal channel angular pressing. — V. Z. Bengus, E. D. Tabachnikova, V. D. Natsik, Ĭ. Mishkuf, K. Chakh, V. V. Stolyarov, and R. Z. Valiev; **28** (11), 864-74.

— Staged work hardening of polycrystalline titanium at low temperatures and its relation to substructure evolution. — V. A. Moskalenko, A. R. Smirnov, V. N. Kovaleva, and V. D. Natsik; **28** (12), 935-41.

Naugle, D. G. — Exchange interaction and magnetoresistance in $La_{2/3}Ca_{1/3}MnO_3$: experiment and models. — A. B. Beznosov, B. I. Belevtsev, E. L. Fertman, V. A. Desnenko, D. G. Naugle, K. D. D. Rathnayaka, and A. Parasiris; **28** (7), 556-61.

Nechitailov, M. M. — EPR spectrum of the Fe^{3+} ion in bromcresol green ($C_{21}H_{14}Br_4O_5S$) and features in the dynamics of the surrounding molecules. — V. V. Chabanenko, V. N. Vasyukov, R. O. Kochkanjan, M. M. Nechitailov, H. Szymczak, S. Piechota, and A. Nabialek; **28** (1), 49-53.

Nekvasil, V. — Optical study of $4f$ excitations in rare earth cuprates. — V. Nekvasil; **28** (7), 528-32.

Nemchenko, K. É. — Asymmetry of relaxation processes and the creation of high-energy phonons in the anisotropic phonon systems of He II. — I. N. Adamenko, K. É. Nemchenko, and A. F. G. Wyatt; **28** (2), 85-94.

Nemoshkalenko, V. V. — Electronic structure and magneto-optical Kerr effect in the compound $UCuP_2$. — O. Horpynyuk, V. V. Nemoshkalenko, V. N. Antonov, B. N. Harmon, and A. N. Yaresko; **28** (7), 533-8.

Nikolaenko, B. A. — Magnetotransport in a quasi-one-dimensional electron system on superfluid helium. — B. A. Nikolaenko, Yu. Z. Kovdrya, and S. P. Gladchenko; **28** (11), 859-63.

O

Orel, E. S. — Molar volume dependence of the thermal conductivity in mixed cryocrystals. — V. A. Konstantinov, E. S. Orel, and V. P. Revyakin; **28** (2), 136-9.

Orendáč, M. — Specific heat study of magnetic excitations in a one-dimensional $S = 1$ Heisenberg magnet with strong planar anisotropy. — A. Feher, M. Orendáč, A. Orendáčová, and E. Čižmár; **28** (7), 551-5.

— Manifestation of the Jahn–Teller effect in the EPR spectrum of the metalorganic complex $[Cu(en)2H_2O]SO_4$. — A. G. Anders, A. I. Kaplienko, O. V. Kravchina, V. S. Boďarenko, A. Feher, M. Orendáč, A. Orendáčová, M. Kajňaková, and J. Černák; **28** (8), 642-5.

Orendáčová, A. — Specific heat study of magnetic excitations in a one-dimensional $S = 1$ Heisenberg magnet with strong planar anisotropy. — A. Feher, M. Orendáč, A. Orendáčová, and E. Čižmár; **28** (7), 551-5.

— Manifestation of the Jahn–Teller effect in the EPR spectrum of the metalorganic complex $[Cu(en)2H_2O]SO_4$. — A. G. Anders, A. I. Kaplienko, O. V. Kravchina, V. S. Boďarenko, A. Feher, M. Orendáč, A. Orendáčová, M. Kajňaková, and J. Černák; **28** (8), 642-5.

Orlov, Yu. V. — Interaction of Pr^{3+} optical centers in the Y_2SiO_5 crystal. — Yu. V. Malyukin, P. N. Zhmurin, A. N. Lebedenko, M. A. Sholkina, B. V. Grinev, N. V. Znamenskiĭ, É. A. Manykin, Yu. V. Orlov, E. A. Petrenko, and T. G. Yukina; **28** (1), 54-7.

Ouladdiaf, B. — Magnetic properties of copper metaborate CuB_2O_4. — G. A. Petrakovskiĭ, A. I. Pankrats, M. A. Popov, A. D. Balaev, D. A. Velikanov, A. M. Vorotynov, K. A. Sablina, B. Roessli, J. Schefer, A. Amato, U. Staub, M. Boehm, and B. Ouladdiaf; **28** (8), 606-12.

P

Paderno, V. N. — MgB_2: Synthesis, sound velocity, and dynamics of the vortex phase. — T. V. Ignatova, G. A. Zvyagina, I. G. Kolobov, E. A. Masalitin, V. D. Fil', Yu. V. Paderno, A. N. Bykov, V. N. Paderno, and V. I. Lyashenko; **28** (3), 190-3.

Paderno, Yu. V. — MgB_2: Synthesis, sound velocity, and dynamics of the vortex phase. — T. V. Ignatova, G. A. Zvyagina, I. G. Kolobov, E. A. Masalitin, V. D. Fil', Yu. V. Paderno, A. N. Bykov, V. N. Paderno, and V. I. Lyashenko; **28** (3), 190-3.

Palistrant, M. E. — Superconductivity in impurity systems with a lower density of charge carriers and with strong electron correlations. — M. E. Palistrant; **28** (2), 109-16.

Pal-Val, L. N. — Kinetics of the low-temperature structural transformation in the In–4.3 at. % Cd solid solution. — S. V. Lubenets, V. D. Natsik, L. N. Pal-Val, P. P. Pal-Val, and L. S. Fomenko; **28** (6), 465-74.

Pal-Val, P. P. — Kinetics of the low-temperature structural transformation in the In–4.3 at. % Cd solid solution. — S. V. Lubenets, V. D. Natsik, L. N. Pal-Val, P. P. Pal-Val, and L. S. Fomenko; **28** (6), 465-74.

Pan, V. M. — Magnetic-field and temperature dependence of the critical current in thin epitaxial films of the high-temperature superconductor $YBa_2Cu_3O_{7-\delta}$. — Yu. V. Fedotov, S. M. Ryabchenko, É. A. Pashitskiĭ, A. V. Semenov, V. I. Vakaryuk, V. M. Pan, and V. S. Flis; **28** (3), 172-83.

Panfilov, A. S. — Measurement of the densities of liquids and gases under pressure using magnetic levitation of a standard sample. — A. S. Panfilov and Yu. Ya. Pushkar'; **28** (10), 789-93.

Pankrats, A. I. — Magnetic properties of copper metaborate CuB_2O_4. — G. A. Petrakovskiĭ, A. I. Pankrats, M. A. Popov, A. D. Balaev, D. A. Velikanov, A. M. Vorotynov, K. A. Sablina, B. Roessli, J. Schefer, A. Amato, U. Staub, M. Boehm, and B. Ouladdiaf; **28** (8), 606-12.

Paranchych, S. Yu. — Influence of Cr concentration on the structural and magnetic properties of the diluted magnetic semiconductor $Hg_{1-x}Cr_xSe$. — V. D. Prozorovskiĭ, I. Yu. Reshidova, A. I. Puzynya, S. Yu. Paranchych, and V. R. Romanyuk; **28** (12), 880-2.

Parasiris, A. — Exchange interaction and magnetoresistance in $La_{2/3}Ca_{1/3}MnO_3$: experiment and models. — A. B. Beznosov, B. I. Belevtsev, E. L. Fertman, V. A. Desnenko, D. G. Naugle, K. D. D. Rathnayaka, and A. Parasiris; **28** (7), 556-61.

Pashchenko, V. A. — Resonance properties of the quasi-one-dimensional Ising magnet $[(CH_3)_3NH]CoCl_3 \cdot 2H_2O$ in the paramagnetic and magnetically ordered phases. — M. I. Kobets, E. N. Khatsko, V. A. Pashchenko, A. S. Chernyi, K. G. Dergachev, and V. G. Borisenko; **28** (12), 889-95.

Pashitskiĭ, E. A. — Pinning of Abrikosov vortices on dislocations and the critical current in high-temperature superconductors. — É. A. Pashitskiĭ and V. I. Vakaryuk; **28** (1), 11-6.

— Self-consistent calculation of the spectrum of quasiparticles in a superfluid Bose liquid with a quenched Bose–Einstein condensate. — É. A. Pashitskiĭ, S. I. Vilchinsky, and S. V. Mashkevich; **28** (2), 79-84.
— Magnetic-field and temperature dependence of the critical current in thin epitaxial films of the high-temperature superconductor $YBa_2Cu_3O_{7-\delta}$. — Yu. V. Fedotov, S. M. Ryabchenko, É. A. Pashitskiĭ, A. V. Semenov, V. I. Vakaryuk, V. M. Pan, and V. S. Flis; **28** (3), 172-83.
— On the role of Jahn–Teller vibrations in the mechanism of high-T_c superconductivity of intercalated C_{60} fullerite films with *p*-type conductivity. — V. M. Loktev and É. A. Pashitskiĭ; **28** (4), 295-7.
— Key role of intramolecular Jahn–Teller vibrations and multivalley nature of the band spectrum in the mechanism of superconductivity in doped C_{60} fullerites. — V. M. Loktev, É. A. Pashitskiĭ, R. Shekhter, and M. Jonson; **28** (11), 821-9.
Pashkevich, Yu. G. — Electronic Raman scattering through a stripe ordering transition in $La_{2-x}Sr_xNiO_4$. — V. P. Gnezdilov, A. V. Yeremenko, Yu. G. Pashkevich, P. Lemmens, G. Güntherodt, J. M. Tranquada, D. J. Buttrey, and K. Nakajima; **28** (7), 510-5.
— Light scattering on phonons in quasi-one-dimensional antiferromagnet $CsFeCl_3 \cdot 2H_2O$ induced by magnetic ordering. — V. S. Kurnosov, A. V. Peschanskii, V. I. Fomin, A. V. Yeremenko, and Yu. G. Pashkevich; **28** (7), 516-22.
Paukov, I. E. — Anomalies of the electronic heat capacity of thulium cuprates in the pseudogap phase region. — E. B. Amitin, K. R. Zhdanov, M. Yu. Kameneva, Yu. A. Kovalevskaya, L. P. Kozeeva, I. E. Paukov, and A. G. Blinov; **28** (8), 669-73.
Pavlov, V. V. — Nonlinear optical spectroscopy of epitaxial magnetic garnet films. — V. V. Pavlov, R. V. Pisarev, M. Fiebig, and D. Fröhlich; **28** (7), 523-7.
Peletminsky, S. V. — On the classification of equilibrium superfluid states with scalar and tensor order parameters. — M. Yu. Kovalevsky, S. V. Peletminsky, and N. N. Chekanova; **28** (4), 227-34.
Pepper, M. — Wigner-like crystallization of Anderson-localized electron systems with low electron densities. — A. A. Slutskin, H. A. Kovtun, and M. Pepper; **28** (12), 930-4.
Peschanskii, A. V. — Raman scattering in a $LiNiPO_4$ single crystal. — V. I. Fomin, V. P. Gnezdilov, V. S. Kurnosov, A. V. Peschanskii, A. V. Yeremenko, H. Schmid, J.-P. Rivera, and S. Gentil; **28** (3), 203-9.
— Light scattering on phonons in quasi-one-dimensional antiferromagnet $CsFeCl_3 \cdot 2H_2O$ induced by magnetic ordering. — V. S. Kurnosov, A. V. Peschanskii, V. I. Fomin, A. V. Yeremenko, and Yu. G. Pashkevich; **28** (7), 516-22.
Petrakovskiĭ, G. A. — Magnetic properties of copper metaborate CuB_2O_4. — G. A. Petrakovskiĭ, A. I. Pankrats, M. A. Popov, A. D. Balaev, D. A. Velikanov, A. M. Vorotynov, K. A. Sablina, B. Roessli, J. Schefer, A. Amato, U. Staub, M. Boehm, and B. Ouladdiaf; **28** (8), 606-12.
Petrenko, E. A. — Interaction of Pr^{3+} optical centers in the Y_2SiO_5 crystal. — Yu. V. Malyukin, P. N. Zhmurin, A. N. Lebedenko, M. A. Sholkina, B. V. Grinev, N. V. Znamenskiĭ, É. A. Manykin, Yu. V. Orlov, E. A. Petrenko, and T. G. Yukina; **28** (1), 54-7.
— Microscopic nature of Pr^{3+} optical centers in Y_2SiO_5, Lu_2SiO_5, and Gd_2SiO_5 crystals. — Yu. V. Malyukin, P. N. Zhmurin, B. V. Grinev, V. P. Seminozhenko, N. V. Znamenskiĭ, É. A. Manykin, E. A. Petrenko, and T. G. Yukina; **28** (10), 774-9.
Petrenko, L. G. — On the deviations from Matthiessen's rule in quasi-one-dimensional conductors. — A. I. Kopeliovich, A. A. Mamalui, L. G. Petrenko, and T. N. Shelest; **28** (10), 771-3.
Petrov, É. G. — Role of paramagnetic ions in the formation of the low-temperature current through a molecular wire. — É. G. Petrov; **28** (8), 630-8.
Piechota, S. — EPR spectrum of the Fe^{3+} ion in bromcresol green ($C_{21}H_{14}Br_4O_5S$) and features in the dynamics of the surrounding molecules. — V. V. Chabanenko, V. N. Vasyukov, R. O. Kochkanjan, M. M. Nechitailov, H. Szymczak, S. Piechota, and A. Nabialek; **28** (1), 49-53.
— Excitation of oscillations of the magnetic induction in a Nb–Ti slab as a result of a thermomagnetic flux avalanche. — V. V. Chabanenko, V. F. Rusakov, V. A. Yampol'skiĭ, H. Szymczak, S. Piechota, S. Vasiliev, and A. Nabialek; **28** (6), 387-90.
Pisarev, R. V. — Nonlinear optical spectroscopy of epitaxial magnetic garnet films. — V. V. Pavlov, R. V. Pisarev, M. Fiebig, and D. Fröhlich; **28** (7), 523-7.
Pletnev, R. N. — Metallic properties of lead dioxide. Band structure and NMR of ^{207}Pb at low temperatures. — L. A. Boyarskiĭ, S. P. Gabuda, S. G. Kozlova, and R. N. Pletnev; **28** (8), 691-4.
Plitnik, G. — Inelastic electron tunneling across magnetically active interfaces in cuprate and manganite heterostructures modified by electromigration processes. — M. A. Belogolovskiĭ, Yu. F. Revenko, A. Yu. Gerasimenko, V. M. Svistunov, E. Hatta, G. Plitnik, V. E. Shaternik, and E. M. Rudenko; **28** (6), 391-4.
Pogorily, A. N. — Giant resistance switching effect in nano-scale twinned $La_{0.65}Ca_{0.35}MnO_3$ film. — V. G. Prokhorov, G. G. Kaminsky, V. A. Komashko, Y. P. Lee, A. I. Tovstolytkin, and A. N. Pogorily; **28** (11), 856-8.
Polev, A. V. — Spin–lattice relaxation in the bcc phase of phase-separated ^3He–^4He solid mixtures. — N. P. Mikhin, V. A. Maidanov, and A. V. Polev; **28** (4), 239-41.
Poltavskaya, M. I. — Lattice dynamics and heat capacity of a two-dimensional monoatomic crystal on a substrate. — T. N. Antsygina, I. I. Poltavsky, M. I. Poltavskaya, and K. A. Chishko; **28** (6), 442-51.
Poltavsky, I. I. — Lattice dynamics and heat capacity of a two-dimensional monoatomic crystal on a substrate. — T. N. Antsygina, I. I. Poltavsky, M. I. Poltavskaya, and K. A. Chishko; **28** (6), 442-51.
Poluéktov, Yu. M. — Self-consistent field model for spatially inhomogeneous Bose systems. — Yu. M. Poluéktov; **28** (6), 429-41.
Polyakov, P. I. — Elastic-strain mechanisms for the influence of temperature, magnetic field, and pressure on the resistive and magnetic properties of magnetic semiconductors. — P. I. Polyakov and S. S. Kucherenko; **28** (10), 744-8.
Ponomarchuk, B. L. — Magnetic polarons in Y–Ba–Cu–O chains. — V. V. Eremenko, D. V. Lukashev, and B. L. Ponomarchuk; **28** (11), 830-41.
Popov, M. A. — Magnetic properties of copper metaborate CuB_2O_4. — G. A. Petrakovskiĭ, A. I. Pankrats, M. A. Popov, A. D. Balaev, D. A. Velikanov, A. M. Vorotynov, K. A. Sablina, B. Roessli, J. Schefer, A. Amato, U. Staub, M. Boehm, and B. Ouladdiaf; **28** (8), 606-12.
Prentslau, N. N. — Direct evidence for the occurrence of superconductivity in the magnetic compound YFe_4Al_8. — V. M. Dmitriev, L. F. Rybaltchenko, P. Wyder, A. G. M. Jansen, N. N. Prentslau, and W. Suski; **28** (4), 260-2.
Prilepsky, J. E. — Mechanism of vortex switching in magnetic nanodots under a circular magnetic field. I. Resonance action of the field on the nanodot eigenmodes. — A. S. Kovalev and J. E. Prilepsky; **28** (12), 921-9.
Prokhorov, A. Yu. — Manifestation of two-dimensional behavior of YBCO films in a study of their complex susceptibility. — A. V. Khokhlov, A. Yu. Prokhorov, V. F. Drobotko, G. G. Levchenko, and A. V. Klimov; **28** (6), 377-82.
Prokhorov, V. G. — Aging effect on the magnetic and transport properties of laser-deposited $La_{0.5}Sr_{0.5}CoO_{3-\delta}$ films. — V. G. Prokhorov, G. G. Kaminskiĭ, V. M. Ishchuk, I. N. Chukanova, Y. P. Lee, and K. W. Kim; **28** (5), 354-8.
— Giant resistance switching effect in nano-scale twinned $La_{0.65}Ca_{0.35}MnO_3$ film. — V. G. Prokhorov, G. G. Kaminsky, V. A. Komashko, Y. P. Lee, A. I. Tovstolytkin, and A. N. Pogorily; **28** (11), 856-8.
Prokhvatilov, A. I. — Effect of nonmagnetic impurities on the spontaneous magnetostriction in β-O_2 crystals. — A. I. Prokhvatilov, Yu. A. Freiman, N. N. Galtsov, and Yu. E. Stetsenko; **28** (1), 61-5.
— Structure and photoluminescence of helium-intercalated fullerite C_{60}. — I. V. Legchenkova, A. I. Prokhvatilov, Yu. E. Stetsenko, M. A. Strzhemechny, K. A. Yagotintsev, A. A. Avdeenko, V. V. Eremenko, P. V. Zinoviev, V. N. Zoryansky, N. B. Silaeva, and R. S. Ruoff; **28** (12), 942-4.
Prozorovskiĭ, V. D. — Influence of Cr concentration on the structural and magnetic properties of the diluted magnetic semiconductor $Hg_{1-x}Cr_xSe$. — V. D. Prozorovskiĭ, I. Yu. Reshidova, A. I. Puzynya, S. Yu. Paranchych, and V. R. Romanyuk; **28** (12), 880-2.
Pushkar', Yu. Ya. — Measurement of the densities of liquids and gases under pressure using magnetic levitation of a standard sample. — A. S. Panfilov and Yu. Ya. Pushkar'; **28** (10), 789-93.
Pustovalov, V. V. — Features of the low-temperature plasticity of Pb–In single crystals. — N. V. Isaev, V. S. Fomenko, V. V. Pustovalov, and I. S. Braude; **28** (5), 369-75.

Pustovalova, A. V. — Low-temperature unsteady creep of parahydrogen single crystals. — L. A. Alekseeva, A. V. Pustovalova, V. I. Khatuntsev, and Yu. V. Butenko; **28** (1), 58-60.

Puzynya, A. I. — Influence of Cr concentration on the structural and magnetic properties of the diluted magnetic semiconductor $Hg_{1-x}Cr_xSe$. — V. D. Prozorovskiĭ, I. Yu. Reshidova, A. I. Puzynya, S. Yu. Paranchych, and V. R. Romanyuk; **28** (12), 880-2.

R

Rathnayaka, K. D. D. — Exchange interaction and magnetoresistance in $La_{2/3}Ca_{1/3}MnO_3$: experiment and models. — A. B. Beznosov, B. I. Belevtsev, E. L. Fertman, V. A. Desnenko, D. G. Naugle, K. D. D. Rathnayaka, and A. Parasiris; **28** (7), 556-61.

Reshidova, I. Yu. — Influence of Cr concentration on the structural and magnetic properties of the diluted magnetic semiconductor $Hg_{1-x}Cr_xSe$. — V. D. Prozorovskiĭ, I. Yu. Reshidova, A. I. Puzynya, S. Yu. Paranchych, and V. R. Romanyuk; **28** (12), 880-2.

Revenko, Yu. F. — Inelastic electron tunneling across magnetically active interfaces in cuprate and manganite heterostructures modified by electromigration processes. — M. A. Belogolovskiĭ, Yu. F. Revenko, A. Yu. Gerasimenko, V. M. Svistunov, E. Hatta, G. Plitnik, V. E. Shaternik, and E. M. Rudenko; **28** (6), 391-4.

Revyakin, V. P. — Molar volume dependence of the thermal conductivity in mixed cryocrystals. — V. A. Konstantinov, E. S. Orel, and V. P. Revyakin; **28** (2), 136-9.

Rivera, J.-P. — Raman scattering in a $LiNiPO_4$ single crystal. — V. I. Fomin, V. P. Gnezdilov, V. S. Kurnosov, A. V. Peschanskii, A. V. Yeremenko, H. Schmid, J.-P. Rivera, and S. Gentil; **28** (3), 203-9.

Roessli, B. — Magnetic properties of copper metaborate CuB_2O_4. — G. A. Petrakovskiĭ, A. I. Pankrats, M. A. Popov, A. D. Balaev, D. A. Velikanov, A. M. Vorotynov, K. A. Sablina, B. Roessli, J. Schefer, A. Amato, U. Staub, M. Boehm, and B. Ouladdiaf; **28** (8), 606-12.

Rogutskiĭ, I. S. — Low-dose radiation effects in thin films of high-temperature superconducting $YBa_2Cu_3O_{7-x}$ irradiated by 1-MeV electrons. — Yu. V. Fedotov, B. A. Danilchenko, and I. S. Rogutskiĭ; **28** (10), 739-43.

Romanova, N. A. — Features of the magnetic behavior of $Mn_{2-x}Cr_xSb$ alloys in the low-temperature state. — V. I. Val'kov, V. I. Kamenev, S. A. Buzhinsky, and N. A. Romanova; **28** (3), 194-8.

Romanyuk, V. R. — Influence of Cr concentration on the structural and magnetic properties of the diluted magnetic semiconductor $Hg_{1-x}Cr_xSe$. — V. D. Prozorovskiĭ, I. Yu. Reshidova, A. I. Puzynya, S. Yu. Paranchych, and V. R. Romanyuk; **28** (12), 880-2.

Rudavskiĭ, É. Ya. — Concentration dependence of the attenuation of first sound in supersaturated superfluid $^3He-^4He$ solutions under pressure. — A. A. Zadorozhko, T. V. Kalko, É. Ya. Rudavskiĭ, I. A. Usherov-Marshak, V. K. Chagovets, and G. A. Sheshin; **28** (2), 73-8.

Rudenko, E. M. — Inelastic electron tunneling across magnetically active interfaces in cuprate and manganite heterostructures modified by electromigration processes. — M. A. Belogolovskiĭ, Yu. F. Revenko, A. Yu. Gerasimenko, V. M. Svistunov, E. Hatta, G. Plitnik, V. E. Shaternik, and E. M. Rudenko; **28** (6), 391-4.

Ruoff, R. S. — Structure and photoluminescence of helium-intercalated fullerite C_{60}. — I. V. Legchenkova, A. I. Prokhvatilov, Yu. E. Stetsenko, M. A. Strzhemechny, K. A. Yagotintsev, A. A. Avdeenko, V. V. Eremenko, P. V. Zinoviev, V. N. Zoryansky, N. B. Silaeva, and R. S. Ruoff; **28** (12), 942-4.

Rusakov, V. F. — Excitation of oscillations of the magnetic induction in a Nb–Ti slab as a result of a thermomagnetic flux avalanche. — V. V. Chabanenko, V. F. Rusakov, V. A. Yampol'skiĭ, H. Szymczak, S. Piechota, S. Vasiliev, and A. Nabialek; **28** (6), 387-90.

Ryabchenko, S. M. — Magnetic-field and temperature dependence of the critical current in thin epitaxial films of the high-temperature superconductor $YBa_2Cu_3O_{7-\delta}$. — Yu. V. Fedotov, S. M. Ryabchenko, É. A. Pashitskiĭ, A. V. Semenov, V. I. Vakaryuk, V. M. Pan, and V. S. Flis; **28** (3), 172-83.

Rybaltchenko, L. F. — Direct evidence for the occurrence of superconductivity in the magnetic compound YFe_4Al_8. — V. M. Dmitriev, L. F. Rybaltchenko, P. Wyder, A. G. M. Jansen, N. N. Prentslau, and W. Suski; **28** (4), 260-2.

S

Sablina, K. A. — Magnetic properties of copper metaborate CuB_2O_4. — G. A. Petrakovskiĭ, A. I. Pankrats, M. A. Popov, A. D. Balaev, D. A. Velikanov, A. M. Vorotynov, K. A. Sablina, B. Roessli, J. Schefer, A. Amato, U. Staub, M. Boehm, and B. Ouladdiaf; **28** (8), 606-12.

Samovarov, V. N. — Optical spectroscopy of antiferromagnetic correlations and the stripe state in the superconductor $YBa_2Cu_3O_{6+x}$. — V. N. Samovarov, V. L. Vakula, M. Yu. Libin, S. A. Uyutnov, and G. G. Sergeeva; **28** (8), 674-86.

Sarsembinov, S. — Infrared spectra of thin films of cryocondensates of an isotopic water mixture. — A. Aldijarov, A. Drobyshev, and S. Sarsembinov; **28** (3), 210-4.

Sarsembinov, S. S. — IR spectra of cryocondensates of an isotopic water mixture on thermocycling. — A. Aldijarov, A. S. Drobyshev, and S. S. Sarsembinov; **28** (4), 290-4.

Schefer, J. — Magnetic properties of copper metaborate CuB_2O_4. — G. A. Petrakovskiĭ, A. I. Pankrats, M. A. Popov, A. D. Balaev, D. A. Velikanov, A. M. Vorotynov, K. A. Sablina, B. Roessli, J. Schefer, A. Amato, U. Staub, M. Boehm, and B. Ouladdiaf; **28** (8), 606-12.

Schleser, R. — Irreversible magnetostriction and magnetization of superconducting $2H$-$NbSe_2$ single crystals in a peak-effect regime. — V. V. Eremenko, V. A. Sirenko, Yu. A. Shabakayeva, R. Schleser, and P. L. Gammel; **28** (1), 6-10.

— On the transverse magnetization of the anisotropic superconductor $2H-NbSe_2$. — V. A. Sirenko, N. I. Makedonska, Yu. A. Shabakayeva, and R. Schleser; **28** (7), 574-8.

Schmid, H. — Raman scattering in a $LiNiPO_4$ single crystal. — V. I. Fomin, V. P. Gnezdilov, V. S. Kurnosov, A. V. Peschanskii, A. V. Yeremenko, H. Schmid, J.-P. Rivera, and S. Gentil; **28** (3), 203-9.

Semenov, A. V. — Magnetic-field and temperature dependence of the critical current in thin epitaxial films of the high-temperature superconductor $YBa_2Cu_3O_{7-\delta}$. — Yu. V. Fedotov, S. M. Ryabchenko, É. A. Pashitskiĭ, A. V. Semenov, V. I. Vakaryuk, V. M. Pan, and V. S. Flis; **28** (3), 172-83.

Seminozhenko, V. P. — Microscopic nature of Pr^{3+} optical centers in Y_2SiO_5, Lu_2SiO_5, and Gd_2SiO_5 crystals. — Yu. V. Malyukin, P. N. Zhmurin, B. V. Grinev, V. P. Seminozhenko, N. V. Znamenskiĭ, É. A. Manykin, E. A. Petrenko, and T. G. Yukina; **28** (10), 774-9.

Sergeeva, G. G. — Optical spectroscopy of antiferromagnetic correlations and the stripe state in the superconductor $YBa_2Cu_3O_{6+x}$. — V. N. Samovarov, V. L. Vakula, M. Yu. Libin, S. A. Uyutnov, and G. G. Sergeeva; **28** (8), 674-86.

Shabakayeva, Yu. A. — Irreversible magnetostriction and magnetization of superconducting $2H$-$NbSe_2$ single crystals in a peak-effect regime. — V. V. Eremenko, V. A. Sirenko, Yu. A. Shabakayeva, R. Schleser, and P. L. Gammel; **28** (1), 6-10.

— On the transverse magnetization of the anisotropic superconductor $2H-NbSe_2$. — V. A. Sirenko, N. I. Makedonska, Yu. A. Shabakayeva, and R. Schleser; **28** (7), 574-8.

Shapoval, I. N. — Equation of state of an equimolar $^3He-^4He$ mixture. — L. V. Karnatsevich, R. M. Sibileva, M. A. Khazhmuradov, I. N. Shapoval, and A. V. Meriuz; **28** (4), 235-8.

Sharapov, S. G. — Spectral function and character of the motion of a conduction electron in an orientationally disordered molecular cryocrystal. — V. M. Loktev, S. G. Sharapov, and H. Beck; **28** (3), 220-6.

Shaternik, V. E. — Inelastic electron tunneling across magnetically active interfaces in cuprate and manganite heterostructures modified by electromigration processes. — M. A. Belogolovskiĭ, Yu. F. Revenko, A. Yu. Gerasimenko, V. M. Svistunov, E. Hatta, G. Plitnik, V. E. Shaternik, and E. M. Rudenko; **28** (6), 391-4.

Shekhter, R. — Key role of intramolecular Jahn–Teller vibrations and multivalley nature of the band spectrum in the mechanism of superconductivity in doped C_{60} fullerites. — V. M. Loktev, É. A. Pashitskiĭ, R. Shekhter, and M. Jonson; **28** (11), 821-9.

Shekhter, R. I. — Influence of dissipation on a low-voltage dc current in a long SNS junction. — S. I. Kulinich and R. I. Shekhter; **28** (7), 547-50.

Shelest, T. N. — On the deviations from Matthiessen's rule in quasi-one-dimensional conductors. — A. I. Kopeliovich, A. A. Mamalui, L. G. Petrenko, and T. N. Shelest; **28** (10), 771-3.

Sheshin, G. A. — Concentration dependence of the attenuation of first sound in supersaturated superfluid $^3He-^4He$ solutions under pressure. — A. A. Zadorozhko, T. V. Kalko, É. Ya. Rudavskiĭ, I. A. Usherov-Marshak, V. K. Chagovets, and G. A. Sheshin; **28** (2), 73-8.

Shevchenko, O. A. — Characteristics of the electric field accompanying a longitudinal acoustic wave in a metal. Anomaly in the superconducting phase. — Yu. A. Avramenko, E. V. Bezuglyi, N. G. Burma, I. G. Kolobov, V. D. Fil', O. A. Shevchenko, and V. M. Gokhfeld; **28** (5), 328-36.

Shevchenko, S. N. — Josephson effect in point contacts between "*f*-wave" superconductors. — R. Mahmoodi, S. N. Shevchenko, and Yu. A. Kolesnichenko; **28** (3), 184-9.

Shimchak, R. — Magnetic properties of a $LaMn_{0.46}Co_{0.54}O_3$ single crystal. — S. N. Barilo, V. I. Gatal'skaya, S. V. Shiryaev, L. A. Kurochkin, R. Shimchak, and M. Baran; **28** (11), 853-5.

Shirshov, L. S. — XIV international seminar on high-temperature superconductivity and school of applied superconductivity (Kurchatovets vacation base, Protvino, Russia, May 28–31, 2001). — M. A. Belogolovskiĭ, S. I. Bondarenko, and L. S. Shirshov; **28** (2), 143-5.

Shiryaev, S. V. — Magnetic properties of a lead-doped BKBO single crystal. — S. N. Barilo, V. I. Gatal'skaya, S. V. Shiryaev, T. V. Smirnova, H. Szymczak, R. Szymczak, and M. Baran; **28** (5), 349-53.

— Magnetic properties of a $LaMn_{0.46}Co_{0.54}O_3$ single crystal. — S. N. Barilo, V. I. Gatal'skaya, S. V. Shiryaev, L. A. Kurochkin, R. Shimchak, and M. Baran; **28** (11), 853-5.

Shitov, A. A. — Drift of domain walls of the ab type in weak ferromagnets. — V. S. Gerasimchuk and A. A. Shitov; **28** (12), 877-9.

Shklovskij, V. A. — Anisotropy of the critical current and the guided motion of vortices in a stochastic model of bianisotropic pinning. I. Theoretical model. — V. A. Shklovskij and A. A. Soroka; **28** (4), 254-9.

— Anisotropy of the critical current and the guided motion of vortices in a stochastic model of bianisotropic pinning. II. Observed effects. — V. A. Shklovskij and A. A. Soroka; **28** (5), 312-20.

Sholkina, M. A. — Interaction of Pr^{3+} optical centers in the Y_2SiO_5 crystal. — Yu. V. Malyukin, P. N. Zhmurin, A. N. Lebedenko, M. A. Sholkina, B. V. Grinev, N. V. Znamenskiĭ, E. A. Manykin, Yu. V. Orlov, E. A. Petrenko, and T. G. Yukina; **28** (1), 54-7.

Shvedun, M. Yu. — Magnetic phase transitions in the system $La_{1-x}Bi_xMnO_{3+\lambda}$. — I. O. Troyanchuk, O. S. Mantytskaja, H. Szymczak, and M. Yu. Shvedun; **28** (7), 569-73.

Sibileva, R. M. — Equation of state of an equimolar ^3He–^4He mixture. — L. V. Karnatsevich, R. M. Sibileva, M. A. Khazhmuradov, I. N. Shapoval, and A. V. Meriuz; **28** (4), 235-8.

Sidorenko, A. A. — Features of the magnetic properties of rare-earth intermetallides RMn_2Ge_2 (Review). — N. P. Kolmakova, A. A. Sidorenko, and R. Z. Levitin; **28** (8), 653-68.

Silaeva, N. B. — Structure and photoluminescence of helium-intercalated fullerite C_{60}. — I. V. Legchenkova, A. I. Prokhvatilov, Yu. E. Stetsenko, M. A. Strzhemechny, K. A. Yagotintsev, A. A. Avdeenko, V. V. Eremenko, P. V. Zinoviev, V. N. Zoryansky, N. B. Silaeva, and R. S. Ruoff; **28** (12), 942-4.

Sirenko, V. A. — Irreversible magnetostriction and magnetization of superconducting $2H$-$NbSe_2$ single crystals in a peak-effect regime. — V. V. Eremenko, V. A. Sirenko, Yu. A. Shabakayeva, R. Schleser, and P. L. Gammel; **28** (1), 6-10.

— Magnetic phase diagram of the system of manganites $Nd_{0.6}Ca_{0.4}(Mn_{1-x}Cr_x)O_3$. — I. O. Troyanchuk, M. V. Bushinsky, V. V. Eremenko, V. A. Sirenko, and H. Szymczak; **28** (1), 45-8.

— On the transverse magnetization of the anisotropic superconductor $2H$–$NbSe_2$. — V. A. Sirenko, N. I. Makedonska, Yu. A. Shabakayeva, and R. Schleser; **28** (7), 574-8.

Sivakov, A. G. — Observation of stochastic resonance in percolative Josephson media. — A. M. Glukhov, A. G. Sivakov, and A. V. Ustinov; **28** (6), 383-6.

Slutskin, A. A. — Wigner-like crystallization of Anderson-localized electron systems with low electron densities. — A. A. Slutskin, H. A. Kovtun, and M. Pepper; **28** (12), 930-4.

Smirnov, A. R. — Staged work hardening of polycrystalline titanium at low temperatures and its relation to substructure evolution. — V. A. Moskalenko, A. R. Smirnov, V. N. Kovaleva, and V. D. Natsik; **28** (12), 935-41.

Smirnova, T. V. — Magnetic properties of a lead-doped BKBO single crystal. — S. N. Barilo, V. I. Gatal'skaya, S. V. Shiryaev, T. V. Smirnova, H. Szymczak, R. Szymczak, and M. Baran; **28** (5), 349-53.

Sokolova, E. S. — Solitons in elastic plates. — A. S. Kovalev, E. S. Sokolova, A. P. Mayer, and C. Éckl'; **28** (10), 780-8.

Sologubenko, A. V. — Thermal conductivity of a GaAs single crystal grown in microgravity. — A. I. Ivanov, A. N. Luk'yanov, B. A. Merisov, A. V. Sologubenko, and G. Ya. Khadjai; **28** (6), 462-4.

Solovjov, A. L. — Fluctuation conductivity in $YBa_2Cu_3O_{7-y}$ films with different oxygen content. I. Optimally and lightly doped YBCO films. — A. L. Solovjov, H.-U. Habermeier, and T. Haage; **28** (1), 17-24.

— Fluctuation conductivity in $YBa_2Cu_3O_{7-y}$ films with different oxygen content. II. YBCO films with $T_c \approx 80$ K. — A. L. Solovjov, H.-U. Habermeier, and T. Haage; **28** (2), 99-108.

— Fluctuation conductivity in Y–Ba–Cu–O films with artificially produced defects. — A. L. Solovjov; **28** (11), 812-20.

Soroka, A. A. — Anisotropy of the critical current and the guided motion of vortices in a stochastic model of bianisotropic pinning. I. Theoretical model. — V. A. Shklovskij and A. A. Soroka; **28** (4), 254-9.

— Anisotropy of the critical current and the guided motion of vortices in a stochastic model of bianisotropic pinning. II. Observed effects. — V. A. Shklovskij and A. A. Soroka; **28** (5), 312-20.

Soroka, A. K. — Guided vortex motion in faceted niobium films. — A. K. Soroka and M. Huth; **28** (11), 842-4.

Staub, U. — Magnetic properties of copper metaborate CuB_2O_4. — G. A. Petrakovskiĭ, A. I. Pankrats, M. A. Popov, A. D. Balaev, D. A. Velikanov, A. M. Vorotynov, K. A. Sablina, B. Roessli, J. Schefer, A. Amato, U. Staub, M. Boehm, and B. Ouladdiaf; **28** (8), 606-12.

Stetsenko, Yu. E. — Effect of nonmagnetic impurities on the spontaneous magnetostriction in β-O_2 crystals. — A. I. Prokhvatilov, Yu. A. Freiman, N. N. Galtsov, and Yu. E. Stetsenko; **28** (1), 61-5.

— Structure and photoluminescence of helium-intercalated fullerite C_{60}. — I. V. Legchenkova, A. I. Prokhvatilov, Yu. E. Stetsenko, M. A. Strzhemechny, K. A. Yagotintsev, A. A. Avdeenko, V. V. Eremenko, P. V. Zinoviev, V. N. Zoryansky, N. B. Silaeva, and R. S. Ruoff; **28** (12), 942-4.

Stolyarov, V. V. — Low-temperature deformation and fracture of bulk nanostructural titanium obtained by intense plastic deformation using equal channel angular pressing. — V. Z. Bengus, E. D. Tabachnikova, V. D. Natsik, I. Mishkuf, K. Chakh, V. V. Stolyarov, and R. Z. Valiev; **28** (11), 864-74.

Strzhemechny, M. A. — Orientational order parameter in α-N_2 from x-ray data. — N. N. Galtsov, O. A. Klenova, and M. A. Strzhemechny; **28** (5), 365-8.

— Structure and photoluminescence of helium-intercalated fullerite C_{60}. — I. V. Legchenkova, A. I. Prokhvatilov, Yu. E. Stetsenko, M. A. Strzhemechny, K. A. Yagotintsev, A. A. Avdeenko, V. V. Eremenko, P. V. Zinoviev, V. N. Zoryansky, N. B. Silaeva, and R. S. Ruoff; **28** (12), 942-4.

Stupakiewicz, A. — Photoinduced magnetic linear dichroism in a YIG:Co film. — O. V. Miloslavska, Yu. N. Kharchenko, N. F. Kharchenko, V. G. Yurko, A. Stupakiewicz, and A. Maziewski; **28** (4), 267-9.

Suleĭmanov, N. M. — Flux-line pinning by columnar magnetic defects in a type-II superconductor. — S. A. Krivenko and N. M. Suleĭmanov; **28** (4), 247-9.

— Reinforcement of pinning by surface magnetic microparticles in high-T_c superconductors. — P. N. Togulev, V. V. Bazarov, I. B. Khaĭbullin, and N. M. Suleĭmanov; **28** (4), 250-3.

Suski, W. — Direct evidence for the occurrence of superconductivity in the magnetic compound YFe_4Al_8. — V. M. Dmitriev, L. F. Rybaltchenko, P. Wyder, A. G. M. Jansen, N. N. Prentslau, and W. Suski; **28** (4), 260-2.

Svistunov, V. M. — Inelastic electron tunneling across magnetically active interfaces in cuprate and manganite heterostructures modified by electromigration processes. — M. A. Belogolovskiĭ, Yu. F. Revenko, A. Yu. Gerasimenko, V. M. Svistunov, E. Hatta, G. Plitnik, V. E. Shaternik, and E. M. Rudenko; **28** (6), 391-4.

Syrkin, E. S. — Multidimensional and surface solitons in a nonlinear elastic medium. — A. S. Kovalev, E. S. Syrkin, and J. A. Maugin; **28** (6), 452-61.

Szymczak, H. — Magnetic phase diagram of the system of manganites $Nd_{0.6}Ca_{0.4}(Mn_{1-x}Cr_x)O_3$. — I. O. Troyanchuk, M. V. Bushinsky, V. V. Eremenko, V. A. Sirenko, and H. Szymczak; **28** (1), 45-8.

— EPR spectrum of the Fe^{3+} ion in bromcresol green ($C_{21}H_{14}Br_4O_5S$) and features in the dynamics of the surrounding molecules. — V. V. Chabanenko, V. N. Vasyukov, R. O. Kochkanjan, M. M. Nechitailov, H. Szymczak, S. Piechota, and A. Nabialek; **28** (1), 49-53.

— Magnetic properties of a lead-doped BKBO single crystal. — S. N. Barilo, V. I. Gatal'skaya, S. V. Shiryaev, T. V. Smirnova, H. Szymczak, R. Szymczak, and M. Baran; **28** (5), 349-53.
— Excitation of oscillations of the magnetic induction in a Nb–Ti slab as a result of a thermomagnetic flux avalanche. — V. V. Chabanenko, V. F. Rusakov, V. A. Yampol'skiĭ, H. Szymczak, S. Piechota, S. Vasiliev, and A. Nabialek; **28** (6), 387-90.
— Magnetic phase transitions in the system $La_{1-x}Bi_xMnO_{3+\lambda}$. — I. O. Troyanchuk, O. S. Mantytskaja, H. Szymczak, and M. Yu. Shvedun; **28** (7), 569-73.
— Heat capacity of mesoscopically disordered superconductors: implications for MgB_2. — A. M. Gabovich, A. I. Voitenko, Mai Suan Li, and H. Szymczak; **28** (11), 803-11.
Szymczak, R. — Effect of light illumination on antiferromagnet-metamagnet phase transitions in the garnet $Ca_3Mn_2Ge_3O_{12}$. — V. A. Bedarev, V. I. Gapon, S. L. Gnatchenko, M. Baran, R. Szymczak, J. M. Desvignes, and H. Le Gall; **28** (1), 37-44.
— Magnetic properties of a lead-doped BKBO single crystal. — S. N. Barilo, V. I. Gatal'skaya, S. V. Shiryaev, T. V. Smirnova, H. Szymczak, R. Szymczak, and M. Baran; **28** (5), 349-53.
— Noncollinear magnetic structures in an Fe/Si/Fe film with a ferromagnetic interlayer exchange interaction. — A. B. Chizhik, S. L. Gnatchenko, M. Baran, K. Fronc, R. Szymczak, and R. Zuberek; **28** (8), 639-41.
— Nonmonotonic temperature dependence of the spontaneous magnetization of the antiferromagnetic crystal $LiCoPO_4$. — N. F. Kharchenko, V. A. Desnenko, Yu. N. Kharchenko, R. Szymczak, and M. Baran; **28** (8), 646-52.

T

Tabachnikova, E. D. — Low-temperature deformation and fracture of bulk nanostructural titanium obtained by intense plastic deformation using equal channel angular pressing. — V. Z. Bengus, E. D. Tabachnikova, V. D. Natsik, I. Mishkuf, K. Chakh, V. V. Stolyarov, and R. Z. Valiev; **28** (11), 864-74.
Tagirov, M. S. — Insulating Van Vleck paramagnets at high magnetic fields (Review). — M. S. Tagirov and D. A. Tayurskiĭ; **28** (3), 147-64.
— Magnetic coupling between liquid ^{3}He and solid insulators (Review). — V. V. Naletov, M. S. Tagirov, and D. A. Tayurskiĭ; **28** (5), 299-311.
Tayurskiĭ, D. A. — Magnetic coupling between liquid ^{3}He and solid insulators (Review). — V. V. Naletov, M. S. Tagirov, and D. A. Tayurskiĭ; **28** (5), 299-311.
Tayurskiĭ, D. A. — Insulating Van Vleck paramagnets at high magnetic fields (Review). — M. S. Tagirov and D. A. Tayurskiĭ; **28** (3), 147-64.
Tkachev, N. K. — Phase transformations of the decomposition type in systems with orbital degeneracy. — M. A. Ivanov, N. K. Tkachev, and A. Ya. Fishman; **28** (8), 613-20.
Togulev, P. N. — Reinforcement of pinning by surface magnetic microparticles in high-T_c superconductors. — P. N. Togulev, V. V. Bazarov, I. B. Khaĭbullin, and N. M. Suleĭmanov; **28** (4), 250-3.
Tovstolytkin, A. I. — Giant resistance switching effect in nano-scale twinned $La_{0.65}Ca_{0.35}MnO_3$ film. — V. G. Prokhorov, G. G. Kaminsky, V. A. Komashko, Y. P. Lee, A. I. Tovstolytkin, and A. N. Pogorily; **28** (11), 856-8.
Tranquada, J. M. — Electronic Raman scattering through a stripe ordering transition in $La_{2-x}Sr_xNiO_4$. — V. P. Gnezdilov, A. V. Yeremenko, Yu. G. Pashkevich, P. Lemmens, G. Güntherodt, J. M. Tranquada, D. J. Buttrey, and K. Nakajima; **28** (7), 510-5.
Trotsenko, P. A. — Magnetostriction of the antiferromagnet $NiCl_2$ in the homogeneous and multidomain states. — V. M. Kalita, A. F. Lozenko, and P. A. Trotsenko; **28** (4), 263-6.
Troyanchuk, I. O. — Magnetic phase diagram of the system of manganites $Nd_{0.6}Ca_{0.4}(Mn_{1-x}Cr_x)O_3$. — I. O. Troyanchuk, M. V. Bushinsky, V. V. Eremenko, V. A. Sirenko, and H. Szymczak; **28** (1), 45-8.
— Magnetic phase transitions in the system $La_{1-x}Bi_xMnO_{3+\lambda}$. — I. O. Troyanchuk, O. S. Mantytskaja, H. Szymczak, and M. Yu. Shvedun; **28** (7), 569-73.
Tsushima, K. — Recent progress in magneto-optics and research on its application (Review). — N. Kojima and K. Tsushima; **28** (7), 480-90.
Turov, E. A. — Purely antiferromagnetic spin waves (antimagnons) in tetragonal magnets and ways of exciting them. — E. A. Turov and I. F. Mirsaev; **28** (8), 592-600.

U

Usherov-Marshak, I. A. — Concentration dependence of the attenuation of first sound in supersaturated superfluid ^{3}He–^{4}He solutions under pressure. — A. A. Zadorozhko, T. V. Kalko, É. Ya. Rudavskiĭ, I. A. Usherov-Marshak, V. K. Chagovets, and G. A. Sheshin; **28** (2), 73-8.
Ustinov, A. V. — Observation of stochastic resonance in percolative Josephson media. — A. M. Glukhov, A. G. Sivakov, and A. V. Ustinov; **28** (6), 383-6.
Uyutnov, S. A. — Optical spectroscopy of antiferromagnetic correlations and the stripe state in the superconductor $YBa_2Cu_3O_{6+x}$. — V. N. Samovarov, V. L. Vakula, M. Yu. Libin, S. A. Uyutnov, and G. G. Sergeeva; **28** (8), 674-86.

V

Vakaryuk, V. I. — Pinning of Abrikosov vortices on dislocations and the critical current in high-temperature superconductors. — É. A. Pashitskiĭ and V. I. Vakaryuk; **28** (1), 11-6.
— Magnetic-field and temperature dependence of the critical current in thin epitaxial films of the high-temperature superconductor $YBa_2Cu_3O_{7-\delta}$. — Yu. V. Fedotov, S. M. Ryabchenko, É. A. Pashitskiĭ, A. V. Semenov, V. I. Vakaryuk, V. M. Pan, and V. S. Flis; **28** (3), 172-83.
Vakhnin, A. Yu. — Influence of structural inhomogeneity on the luminescence properties of silicon nanocrystallites. — I. V. Blonskiĭ, M. S. Brodyn, A. Yu. Vakhnin, A. Ya. Zhugayevych, V. M. Kadan, and A. K. Kadashchuk; **28** (8), 706-12.
Vakula, V. L. — Optical spectroscopy of antiferromagnetic correlations and the stripe state in the superconductor $YBa_2Cu_3O_{6+x}$. — V. N. Samovarov, V. L. Vakula, M. Yu. Libin, S. A. Uyutnov, and G. G. Sergeeva; **28** (8), 674-86.
Valiev, R. Z. — Low-temperature deformation and fracture of bulk nanostructural titanium obtained by intense plastic deformation using equal channel angular pressing. — V. Z. Bengus, E. D. Tabachnikova, V. D. Natsik, I. Mishkuf, K. Chakh, V. V. Stolyarov, and R. Z. Valiev; **28** (11), 864-74.
Val'kov, V. I. — Features of the magnetic behavior of $Mn_{2-x}Cr_xSb$ alloys in the low-temperature state. — V. I. Val'kov, V. I. Kamenev, S. A. Buzhinsky, and N. A. Romanova; **28** (3), 194-8.
van Ruitenbeek, J. M. — Point-contact studies of the Kondo size effect in the alloys CuMn, CuCr, and AuFe in a magnetic field. — V. V. Fisun, I. K. Yanson, J. M. van Ruitenbeek, and J. A. Mydosh; **28** (2), 123-7.
Vasiliev, S. — Excitation of oscillations of the magnetic induction in a Nb–Ti slab as a result of a thermomagnetic flux avalanche. — V. V. Chabanenko, V. F. Rusakov, V. A. Yampol'skiĭ, H. Szymczak, S. Piechota, S. Vasiliev, and A. Nabialek; **28** (6), 387-90.
Vasyukov, V. N. — EPR spectrum of the Fe^{3+} ion in bromcresol green ($C_{21}H_{14}Br_4O_5S$) and features in the dynamics of the surrounding molecules. — V. V. Chabanenko, V. N. Vasyukov, R. O. Kochkanjan, M. M. Nechitailov, H. Szymczak, S. Piechota, and A. Nabialek; **28** (1), 49-53.
— Mechanism for the changes with temperature of the EPR spectrum of the Fe^{3+} ion in polycrystalline materials containing complexes with a multiwell potential. — V. N. Vasyukov; **28** (3), 199-202.
Velikanov, D. A. — Magnetic properties of copper metaborate CuB_2O_4. — G. A. Petrakovskiĭ, A. I. Pankrats, M. A. Popov, A. D. Balaev, D. A. Velikanov, A. M. Vorotynov, K. A. Sablina, B. Roessli, J. Schefer, A. Amato, U. Staub, M. Boehm, and B. Ouladdiaf; **28** (8), 606-12.
Velikodny, A. N. — Features of the thermopower of Mo–Re and Mo–Re–Nb alloys and the electronic–topological transition in these systems. — T. A. Ignatyeva and A. N. Velikodny; **28** (6), 403-11.
Verkhovtseva, É. T. — Features of the x-ray bremsstrahlung in the scattering of intermediate-energy electrons on atoms of inert elements. — É. T. Verkhovtseva and E. V. Gnatchenko; **28** (4), 270-8.
Vilchinsky, S. I. — Self-consistent calculation of the spectrum of quasiparticles in a superfluid Bose liquid with a quenched Bose–Einstein condensate. — É. A. Pashitskiĭ, S. I. Vilchinsky, and S. V. Mashkevich; **28** (2), 79-84.

Voitenko, A. I. — Heat capacity of mesoscopically disordered superconductors: implications for MgB_2. — A. M. Gabovich, A. I. Voitenko, Mai Suan Li, and H. Szymczak; **28** (11), 803-11.

Volk, A. Ya. — Inhomogeneous states for small magnetic particles with exchange anisotropy. — B. A. Ivanov, A. Ya. Volk, and A. Yu. Merkulov; **28** (1), 25-9.

Voloshin, V. A. — On the criteria for superconductivity in $PrBa_2Cu_3O_{6.6}$. — F. A. Boyko, G. V. Bukin, V. A. Voloshin, and A. A. Gusev; **28** (2), 95-8.

Vorotynov, A. M. — Magnetic properties of copper metaborate CuB_2O_4. — G. A. Petrakovskiĭ, A. I. Pankrats, M. A. Popov, A. D. Balaev, D. A. Velikanov, A. M. Vorotynov, K. A. Sablina, B. Roessli, J. Schefer, A. Amato, U. Staub, M. Boehm, and B. Ouladdiaf; **28** (8), 606-12.

W

Wanderka, N. — Field emission microscopy of the cluster and subcluster structure of a Zr–Ti–Cu–Ni–Be bulk metallic glass. — A. S. Bakaĭ, I. M. Mikhailovskij, T. I. Mazilova, and N. Wanderka; **28** (4), 279-83.

Wyatt, A. F. G. — Asymmetry of relaxation processes and the creation of high-energy phonons in the anisotropic phonon systems of He II. — I. N. Adamenko, K. É. Nemchenko, and A. F. G. Wyatt; **28** (2), 85-94.

Wyder, P. — Direct evidence for the occurrence of superconductivity in the magnetic compound YFe_4Al_8. — V. M. Dmitriev, L. F. Rybaltchenko, P. Wyder, A. G. M. Jansen, N. N. Prentslau, and W. Suski; **28** (4), 260-2.

Y

Yagotintsev, K. A. — Structure and photoluminescence of helium-intercalated fullerite C_{60}. — I. V. Legchenkova, A. I. Prokhvatilov, Yu. E. Stetsenko, M. A. Strzhemechny, K. A. Yagotintsev, A. A. Avdeenko, V. V. Eremenko, P. V. Zinoviev, V. N. Zoryansky, N. B. Silaeva, and R. S. Ruoff; **28** (12), 942-4.

Yampol'skiĭ, V. A. — Excitation of oscillations of the magnetic induction in a Nb–Ti slab as a result of a thermomagnetic flux avalanche. — V. V. Chabanenko, V. F. Rusakov, V. A. Yampol'skiĭ, H. Szymczak, S. Piechota, S. Vasiliev, and A. Nabialek; **28** (6), 387-90.

Yanson, I. K. — Point-contact studies of the Kondo size effect in the alloys CuMn, CuCr, and AuFe in a magnetic field. — V. V. Fisun, I. K. Yanson, J. M. van Ruitenbeek, and J. A. Mydosh; **28** (2), 123-7.

Yaresko, A. N. — Electronic structure and magneto-optical Kerr effect in the compound $UCuP_2$. — O. Horpynyuk, V. V. Nemoshkalenko, V. N. Antonov, B. N. Harmon, and A. N. Yaresko; **28** (7), 533-8.

Yeremenko, A. V. — Raman scattering in a $LiNiPO_4$ single crystal. — V. I. Fomin, V. P. Gnezdilov, V. S. Kurnosov, A. V. Peschanskii, A. V. Yeremenko, H. Schmid, J.-P. Rivera, and S. Gentil; **28** (3), 203-9.

— Electronic Raman scattering through a stripe ordering transition in $La_{2-x}Sr_xNiO_4$. — V. P. Gnezdilov, A. V. Yeremenko, Yu. G. Pashkevich, P. Lemmens, G. Güntherodt, J. M. Tranquada, D. J. Buttrey, and K. Nakajima; **28** (7), 510-5.

— Light scattering on phonons in quasi-one-dimensional antiferromagnet $CsFeCl_3 \cdot 2H_2O$ induced by magnetic ordering. — V. S. Kurnosov, A. V. Peschanskii, V. I. Fomin, A. V. Yeremenko, and Yu. G. Pashkevich; **28** (7), 516-22.

Yukina, T. G. — Interaction of Pr^{3+} optical centers in the Y_2SiO_5 crystal. — Yu. V. Malyukin, P. N. Zhmurin, A. N. Lebedenko, M. A. Sholkina, B. V. Grinev, N. V. Znamenskiĭ, É. A. Manykin, Yu. V. Orlov, E. A. Petrenko, and T. G. Yukina; **28** (1), 54-7.

— Microscopic nature of Pr^{3+} optical centers in Y_2SiO_5, Lu_2SiO_5, and Gd_2SiO_5 crystals. — Yu. V. Malyukin, P. N. Zhmurin, B. V. Grinev, V. P. Seminozhenko, N. V. Znamenskiĭ, É. A. Manykin, E. A. Petrenko, and T. G. Yukina; **28** (10), 774-9.

Yunakova, O. N. — Excitons in the layered insulators ZnI_2 and CdI_2:Zn. — O. N. Yunakova, V. K. Miloslavsky, and E. N. Kovalenko; **28** (4), 284-9.

Yurko, V. G. — Photoinduced magnetic linear dichroism in a YIG:Co film. — O. V. Miloslavska, Yu. N. Kharchenko, N. F. Kharchenko, V. G. Yurko, A. Stupakiewicz, and A. Maziewski; **28** (4), 267-9.

Z

Zadorozhko, A. A. — Concentration dependence of the attenuation of first sound in supersaturated superfluid ^3He–^4He solutions under pressure. — A. A. Zadorozhko, T. V. Kalko, É. Ya. Rudavskiĭ, I. A. Usherov-Marshak, V. K. Chagovets, and G. A. Sheshin; **28** (2), 73-8.

Zhdanov, K. R. — Anomalies of the electronic heat capacity of thulium cuprates in the pseudogap phase region. — E. B. Amitin, K. R. Zhdanov, M. Yu. Kameneva, Yu. A. Kovalevskaya, L. P. Kozeeva, I. E. Paukov, and A. G. Blinov; **28** (8), 669-73.

Zhenov, A. P. — Dependence of semiconductor energy bands on the isotopic composition. A universal relation for monoatomic crystals. — A. P. Zhenov; **28** (2), 128-35.

Zhmurin, P. N. — Interaction of Pr^{3+} optical centers in the Y_2SiO_5 crystal. — Yu. V. Malyukin, P. N. Zhmurin, A. N. Lebedenko, M. A. Sholkina, B. V. Grinev, N. V. Znamenskiĭ, É. A. Manykin, Yu. V. Orlov, E. A. Petrenko, and T. G. Yukina; **28** (1), 54-7.

— Microscopic nature of Pr^{3+} optical centers in Y_2SiO_5, Lu_2SiO_5, and Gd_2SiO_5 crystals. — Yu. V. Malyukin, P. N. Zhmurin, B. V. Grinev, V. P. Seminozhenko, N. V. Znamenskiĭ, É. A. Manykin, E. A. Petrenko, and T. G. Yukina; **28** (10), 774-9.

Zhugayevych, A. Ya. — Influence of structural inhomogeneity on the luminescence properties of silicon nanocrystallites. — I. V. Blonskiĭ, M. S. Brodyn, A. Yu. Vakhnin, A. Ya. Zhugayevych, V. M. Kadan, and A. K. Kadashchuk; **28** (8), 706-12.

Zinoviev, P. V. — Structure and photoluminescence of helium-intercalated fullerite C_{60}. — I. V. Legchenkova, A. I. Prokhvatilov, Yu. E. Stetsenko, M. A. Strzhemechny, K. A. Yagotintsev, A. A. Avdeenko, V. V. Eremenko, P. V. Zinoviev, V. N. Zoryansky, N. B. Silaeva, and R. S. Ruoff; **28** (12), 942-4.

Znamenskiĭ, N. V. — Interaction of Pr^{3+} optical centers in the Y_2SiO_5 crystal. — Yu. V. Malyukin, P. N. Zhmurin, A. N. Lebedenko, M. A. Sholkina, B. V. Grinev, N. V. Znamenskiĭ, É. A. Manykin, Yu. V. Orlov, E. A. Petrenko, and T. G. Yukina; **28** (1), 54-7.

— Microscopic nature of Pr^{3+} optical centers in Y_2SiO_5, Lu_2SiO_5, and Gd_2SiO_5 crystals. — Yu. V. Malyukin, P. N. Zhmurin, B. V. Grinev, V. P. Seminozhenko, N. V. Znamenskiĭ, É. A. Manykin, E. A. Petrenko, and T. G. Yukina; **28** (10), 774-9.

Zoryansky, V. N. — Structure and photoluminescence of helium-intercalated fullerite C_{60}. — I. V. Legchenkova, A. I. Prokhvatilov, Yu. E. Stetsenko, M. A. Strzhemechny, K. A. Yagotintsev, A. A. Avdeenko, V. V. Eremenko, P. V. Zinoviev, V. N. Zoryansky, N. B. Silaeva, and R. S. Ruoff; **28** (12), 942-4.

Zuberek, R. — Noncollinear magnetic structures in an Fe/Si/Fe film with a ferromagnetic interlayer exchange interaction. — A. B. Chizhik, S. L. Gnatchenko, M. Baran, K. Fronc, R. Szymczak, and R. Zuberek; **28** (8), 639-41.

Zvyagin, A. A. — Non-Fermi-liquid behavior: Exact results for ensembles of magnetic impurities. — A. A. Zvyagin; **28** (12), 907-20.

Zvyagina, G. A. — MgB_2: Synthesis, sound velocity, and dynamics of the vortex phase. — T. V. Ignatova, G. A. Zvyagina, I. G. Kolobov, E. A. Masalitin, V. D. Fil', Yu. V. Paderno, A. N. Bykov, V. N. Paderno, and V. I. Lyashenko; **28** (3), 190-3.